

Northumbria Research Link

Citation: Roynarin, Wirachai (2004) Optimisation of vertical axis wind turbines. Doctoral thesis, Northumbria University.

This version was downloaded from Northumbria Research Link:
<http://nrl.northumbria.ac.uk/id/eprint/1655/>

Northumbria University has developed Northumbria Research Link (NRL) to enable users to access the University's research output. Copyright © and moral rights for items on NRL are retained by the individual author(s) and/or other copyright owners. Single copies of full items can be reproduced, displayed or performed, and given to third parties in any format or medium for personal research or study, educational, or not-for-profit purposes without prior permission or charge, provided the authors, title and full bibliographic details are given, as well as a hyperlink and/or URL to the original metadata page. The content must not be changed in any way. Full items must not be sold commercially in any format or medium without formal permission of the copyright holder. The full policy is available online: <http://nrl.northumbria.ac.uk/policies.html>

Some theses deposited to NRL up to and including 2006 were digitised by the British Library and made available online through the [EThOS e-thesis online service](#). These records were added to NRL to maintain a central record of the University's research theses, as well as still appearing through the British Library's service. For more information about Northumbria University research theses, please visit [University Library Online](#).

OPTIMISATION OF VERTICAL AXIS WIND TURBINES

Wirachai Roynarin B.Eng., M.Sc.

**A thesis submitted in partial fulfilment of the requirements for
the degree of Doctor of Philosophy**

Funded by RIT

School of Engineering and Technology

Northumbria University

March 2004

Dedicated To:

Parents and Friends

*The Awakened Ones can but point the way; we must make
the effort ourselves. (Dhp. v. 2 76)*

Abstract

A practical Vertical Axis Wind Turbine (VAWTs) based on a *Darrieus* rotor has been designed and tested and found to be capable of self-starting at wind speeds above 4 m/s. The self-start feature has been achieved by replacing the usual symmetrical aerofoil blade in the VAWT rotor and by using a concentric Savonius rotor or semi-cylinder turbine.

A computer program was produced to compute the power coefficient versus tip speed ratio characteristics of a selected aerofoil profile employed in a VAWT. The program accounts for chord length, pitch angle, number of blades, and rotor radius at any wind speed. The published data from 40 aerofoil sections were assessed, taking into account the two main criteria - self-starting and efficiency.

Computational fluid dynamics software (ANSYS, Flotran) has been used to the lift and drag performance of a NACA 66-212 and NACA 4421 aerofoils in order to check the computer program predictions. Excellent agreement was obtained for the static aerofoil assessment, but only after special ICEM Computational Fluid Dynamics (CFD) meshing interface routines were utilised. However, agreement between the theoretical and published results was not good for the rotating aerofoils in a VAWT. Thus, further CFD work was not pursued and in preference, an experimental route was initiated.

In the first series of wind tunnel tests involving three candidate profiles, good agreement was found between the experimental results and the mathematical models. The aerofoils chosen were the NACA 661-212, the S1223 and the Clark-Y standard aerofoils. A number of prototype VANVTs were fabricated and tested for the influence of the blade pitch angle, the chord length ratio, with 2 or 3 blades. The aerofoil surfaces were made from aluminium sheet with a standard surface finish. The prototype designs were tested in the Northumbria University low speed wind tunnel facility - the models were 0.4 m high with a 0.4 m diameter. The torque versus Wind speed characteristics were recorded and analysed. The S1223 profile was found to be self-starting with high

efficiency. This model generated a high power coefficient of about 0.3 at a tip speed ratio of 1:2.

The second series of tests were carried out in field sites in the UK with a 2 m diameter straight-bladed Darrieus rotor prototype with 3 blades using the S1223 blade section. Three field trials were undertaken in the UK to produce realistic performance characteristics for wind conditions of 4-10 m/s. The maximum power coefficient of this machine was found to be 0.18 at a tip speed ratio of 1.2.

In addition, an alternative semi-cylinder turbine combined with a Darrieus rotor was fabricated and tested in the UK. It demonstrated the advantage that it could self-start at lower wind speeds, that is 3 m/s but delivers approximately 50% less power than that obtained from the first proposed design.

A final phase of testing was carried out with an enlarged and modified 3m diameter prototype installed at a shrimp farm in Thailand to demonstrate how the unit could be used to replace an equivalent 2 HP 2-stroke diesel engine and hence eliminate its inherent emission pollution problems. A Savonius rotor was fitted to the prototype to improve self-start capabilities at a wind speed of 4 m/s for a practical application which by its nature required a high starting torque.

The designs are easy to fabricate, low cost, pollution free and have been demonstrated to be ideal for applications in developing countries where there are sufficient wind resources.

Table of Contents

Abstract.....	I
Table of Contents.....	III
List of Tables.....	IX
List of Figures.....	XI
Acknowledgement.....	XX
Declaration.....	XXI
Darrieus Rotor Vertical Axis Wind Turbine Nomenclature.....	XXII
Chapter 1 Introduction.....	1
1.1 Type of wind machines.....	1
1.1.1 The Horizontal Axis Wind Turbines (HAWTs).....	1
1.1.2 Vertical Axis Wind Turbines (VAWTs).....	2
1.2 Why and How to Optimise the VAWTs.....	2
1.3 The aims of this study: the need for renewable decentralised energy supplies with optimised Vertical Axis Wind Turbines...	5
Chapter 2 Literature Review.....	7
2.1 A brief history of wind turbines.....	7
2.2 Wind Turbine Applications.....	12
2.3 Advantages and Disadvantages of VAWTs compared to HAWTs.....	15
2.3.1 Advantages of VAWTs.....	15
2.3.2 Disadvantages of VAWTs.....	16
2.4 Aerodynamics of wind turbines.....	17
2.4.1 One-Dimensional Momentum Theory.....	17
2.4.2 Betz theory (Betz Limit).....	20
2.5 Review of Darrieus wind machine (D-rotor).....	23
2.5.1 Performance analysis.....	23

2.5.2	Survey of the study of the Darrieus rotor.....	25
2.6	Review of the Savonius Wind machine (S-Rotor).....	31
2.6.1	The power coefficient C_p analysis.....	31
2.6.2	The survey of the study of the Savonius wind machine...	34
2.7	Combined Wind machine (D+S Rotor).....	38
Chapter 3 Analytical Method.....		41
3.1	The theory for analytical models.....	41
3.2	Procedures adopted in MATLAB program.....	45
3.3	The analytical models.....	46
3.4	The procedures to operate the analytical models.....	48
3.5	Darrieus VAWTs Design Parameters and MATLAB results.....	53
3.5.1	The aerofoils section.....	54
3.5.1.1	High Reynolds number aerofoils.....	55
3.5.1.2	Low Reynolds number aerofoils.....	57
3.5.2	Number of blades.....	58
3.5.3	The Reynolds number Re effects.....	60
3.5.4	The effects of chord ratio ($\frac{c}{r}$) and the Results.....	62
3.5.5	The Blade pitch angle α	64
3.6	Observations and Conclusions of analytical method.....	65
Chapter 4 Computational Fluid Dynamics (CFD).....		68
4.1	Introduction.....	68
4.2	The Cartesian coordination of CFD to investigate lift and drag coefficient.....	68
4.2.1	Problem descriptions.....	68
4.2.2	The procedures to use the ANSYS CFD.....	70
4.2.2.1	Pre-processing (Turbulent models).....	70

4.2.2.2	Solution (Turbulent model).....	75
4.2.2.3	Post processing.....	77
4.2.3	Lift and Drag Coefficient Results.....	79
4.2.3.1	NACA 661-212.....	80
4.2.3.2	NACA 4424.....	82
4.3	The Polar co-ordinate CFD to investigate the torque on the rotor of wind machine.....	85
4.3.1	Problem descriptions.....	86
4.3.2	The procedures.....	87
4.4	The solution using ANSYS Flotran CFD.....	91
4.4.1	ICEM CFD.....	91
4.4.2	Apply ICEM CFD to the model.....	93
4.4.3	Mesh creations and results investigation.....	97
4.4.3.1	ANSYS Flotran CFD.....	97
4.4.3.2	ICEM CFD.....	98
4.4.4	Results and Observations.....	98
4.5	Conclusion of CFD technique.....	102
Chapter 5 Experimental Testing.....		103
5.1	Introduction.....	103
5.1.1	Aims of the experimental testing.....	103
5.2	Wind Turbine Design.....	104
5.2.1	The rotor construction.....	105
5.3	Experimental Methodology.....	109
5.4	The Experimental Results.....	113
5.4.1	The experimental study of the three aerofoils sections employed in the D-rotor.....	113
5.4.1.1	Aerofoil: Clark-Y.....	114

5.4.1.2	Aerofoil: NACA 661-212.....	117
5.4.1.3	Aerofoil: S1223.....	119
5.4.1.4	The discussion on the aerofoils shape effects.....	121
5.4.2	The study of chord ratio effect ($\frac{C}{r}$).....	126
5.4.2.1	Aerofoil: NACA 661-212.....	127
5.4.2.2	Aerofoil: Clark-Y.....	129
5.4.2.3	Aerofoil: S1223.....	130
5.4.2.4	The discussion of chord length ratio effect.....	132
5.4.3	The study of number of blade (b) effect.....	133
5.4.3.1	Aerofoil: NACA661-212.....	133
5.4.3.2	Aerofoil: Clark-Y.....	135
5.4.3.4	Aerofoil: S1223.....	138
5.4.3.5	The Discussion of number of blade (b) effect....	140
5.4.4	The study of combination of aerofoils for Darrieus rotor	141
5.4.4.1	Observation results of combination of aerofoils on D-Rotor.....	143
5.5	The conclusion from experimental testing.....	144
Chapter 6 Wind Turbine Field Test.....		145
6.1	Introduction.....	145
6.2	The stand-alone 3 bladed Vertical Axis Wind Turbines.....	145
6.2.1	Design and construction of the wind machine.....	145
6.2.1.1	The rotor blades.....	147
6.2.1.2	The main shaft and the supporting frame.....	149
6.2.1.3	The wind turbine base.....	150
6.2.2	The instruments used for the field test.....	151
6.2.3	Generator and control loads.....	151

6.2.4	Torque Transducer and Visual Interface Software.....	152
6.2.5	The anemometer and its interface software.....	153
6.2.6	Field Test set up and observation results.....	154
6.2.6.1	The first test at St. Mary's Island, Whitley Bay..	154
6.2.6.2	Wind turbine site testing at Amble Caravan Park, Northumberland.....	158
6.2.6.3	The final test at NaRec, Blyth Northumberland..	165
6.3	The novel wind machine for shrimp farm aeration process.....	170
6.3.1	General information about the shrimp farm.....	170
6.3.2	Aeration process.....	173
6.3.3	The test site.....	174
6.3.4	The wind machine design.....	176
6.3.5	The wind machine manufacturing.....	178
6.3.6	The results and the observation.....	179
6.4	Discussion of the Results.....	181
Chapter 7 Discussions.....		182
7.1	The analytical method of the aerofoils employed to Darrieus wind machine.....	182
7.2	CFD analysis.....	183
7.3	The wind tunnel test for small models.....	183
7.4	The field test of 3-bladed prototype in the UK.....	184
7.5	Thailand test of combined wind machine.....	186
Chapter 8 Conclusions.....		188
Chapter 9 Suggestions for Further Work.....		190
References.....		191
Publications.....		197

Appendix A	Enhancing the performance of straight blade Darrieus Rotor Wind Turbines.....	198
Appendix B	The performance of a Vertical Darrieus machine with modern high lift aerofoils.....	199
Appendix C	Using wind turbine machine to reduce carbon dioxide emission in shrimp farm aeration process.....	200
Appendix D	Wind Machine for Shrimp Farm Aeration Process.....	201
Appendix E	The investigation of aerofoil characteristics using CFD techniques.....	202
Appendix F	Matlab program to predict C_p vs Tip Speed Ratio.....	203
Appendix G	Matlab program to predict torque vs Tip Speed Ratio.....	206
Appendix H	The Predicted Power Coefficients of 10 High Reynolds number aerofoils vs Tip Speed Ratio.....	208
Appendix I	The Predicted Power Coefficients of 30 Low Re aerofoils vs Tip Speed Ratio.....	213
Appendix J	The Predicted Power Coefficient of NACA 661-212 with different number of blades.....	228
Appendix K	The Predicted Power Coefficients of Eppler E374 aerofoil with different Reynolds numbers.....	232
Appendix L	The Predicted Power Coefficients of NACA 661-212 with different blade pitch angles.....	234
Appendix M	The wind speed and weather conditions at amble caravan site.....	238
Appendix N	The wind turbine field-test data of S1223 rotor blade at NaRec.....	239
Appendix O	The wind turbine field-test data of S1223+SCT at NaRec Blyth.....	243
Appendix P	Two alternative schemes for further development for the shrimp farm industry.....	247

List of Tables

Table 4.1	Model specifications for NACA661-212 aerofoil.....	69
Table 4.2	Comparison results of CFD and NACA data.....	81
Table 4.3	Model specifications for NACA 4424 aerofoil.....	83
Table 4.4	Comparison of results of NACA 4424 lift and drag coefficients...	83
Table 4.5	The model specification.....	87
Table 4.6	Results of the investigation using CFD to compute the torque.....	90
Table 4.7	The results of the investigation.....	99
Table 5.1	NACA 661 -212 Co-ordinations.....	106
Table 5.2	S1223 Co-ordinations.....	107
Table 5.3	Clark-Y Co-ordinations.....	108
Table 5.4	Torque transducer specifications.....	111
Table 5.5	Clark-Y at wind velocity, $V=12$ m/sec.....	114
Table 5.6	Clark-Y at Wind velocity, $V=14$ m/sec.....	114
Table 5.7	Clark-Y at wind velocity, $V=16$ m/sec.....	114
Table 5.8	Clark-Y at wind velocity, $V=18$ m/sec.....	115
Table 5.9	NACA 661-212 at wind velocity, $V=12$ m/sec.....	117
Table 5.10	NACA 661-212 at wind velocity, $V=14$ m/sec.....	117
Table 5.11	NACA 661-212 at wind velocity, $V=16$ m/sec.....	117
Table 5.12	NACA 661-212 at wind velocity, $V=18$ m/sec.....	117
Table 5.13	S1223 at wind velocity, $V=10$ m/sec.....	119
Table 5.14	S1223 at wind velocity, $V=12$ m/sec.....	119
Table 5.15	Evaluation of the errors on Clark-Y experimental results.....	125
Table 5.16	Evaluation of the errors on NACA 661-212 experimental results.	125
Table 5.17	Evaluation of the efforts on S 1223 experimental.....	125

Table 5.18	NACA661-212 at wind velocity, $V=12$ m/sec.....	127
Table 5.19	NACA661-212 at wind velocity, $V= 16$ m/sec.....	127
Table 5.20	Clark-Y at wind velocity, $V=12$ m/sec.....	129
Table 5.21	Clark-Y at wind velocity, $V=16$ m/sec.....	129
Table 5.22	S1223 at wind velocity, $V=12$ m/sec.....	130
Table 5.23	S1223 at wind velocity, $V= 16$ m/sec.....	130
Table 5.24	NACA 661-212 at wind velocity, $V= 14$ m/sec.....	133
Table 5.25	NACA 661-212 at wind velocity $V= 16$ m/sec.....	134
Table 5.26	Clark -Y at Wind velocity, $V= 14$ m/sec.....	136
Table 5.27	Clark -Y at Wind velocity, $V= 16$ m/sec.....	136
Table 5.28	S1223 at wind velocity, $V= 10$ m/sec.....	138
Table 5.29	S1223 at wind velocity, $V= 12$ m/sec.....	138
Table 5.30	S1223 at wind velocity, $V= 12$ m/sec.....	139
Table 5.31	Three aerofoil sections at wind velocity, $V= 10$ m/sec.....	142
Table 5.32	Three aerofoil sections at wind velocity, $V= 12$ m/sec.....	142
Table 5.33	Three aerofoil sections at wind velocity, $V= 14$ m/sec.....	142
Table 5.34	Three aerofoil sections at wind velocity, $V= 16$ m/sec.....	142
Table 6.1	E300/RWTI-2 specifications.....	153
Table 6.2	Physical speciation of the Kestrel 4000.....	154
Table 6.3	The investigation results of pitch angle on S1223 using CFD.....	156
Table 6.4	The variable cost in selected shrimp farm (Unit baht/rai).....	172
Table 6.5	The specifications of designed VAWTs for shrimp farm process.	178
Table 6.6	Observation of site testing.....	180

List of Figures

Fig. 1.1	Key parts of Horizontal Axis Wind Turbines [4].....	2
Fig. 1.2	Savonius wind turbine for pumping water and its configurations [5].....	3
Fig. 1.3	(a) C-shaped VAWTs ([6]) and (b) Straight blade VAWTs [7].....	4
Fig. 1.4	The combined rotor vertical axis wind turbine [3].....	4
Fig. 2.1	Early Persian windmill [9].....	8
Fig. 2.2	Other type of vertical axis wind machine [9].....	8
Fig. 2.3	Some other types of horizontal axis wind machine [9].....	9
Fig. 2.4	The largest HAWTs offshore wind farm at Horn Rev. Denmark [10].....	10
Fig. 2.5	The damaged 2 MW wind machine which is located at Tjaereborg in Denmark [15].....	11
Fig. 2.6	(a) The old model of biggest 3 MW wind machine which was dismantled and replaced with modern 2 MW Wind machine (b) [16].....	11
Fig. 2.7	Chinook 2000 vertical axis wind turbine [19].....	12
Fig. 2.8	The idea of producing heat from VAWTs [20].....	13
Fig. 2.9	The Various applications of wind machines [25].....	14
Fig. 2.10	Flow pattern of actuator disc theory [27].....	17
Fig. 2.11	The stream tube [3].....	21
Fig. 2.12	C_p versus V_2/V_1 in Betz' limit.....	22
Fig. 2.13	The ideal windmill and various models of power coefficient modified from [25].....	23
Fig. 2.14	Sandia 17-m VAWTs and its performance predictions [32].....	24
Fig. 2.15	Various of torques and power coefficients versus tip speed ratios for different value of solidities from [34].....	25
Fig. 2.16	NACA 661-212 lift coefficients at 0-360 degree blade position.....	26
Fig. 2.17	S1223 lift coefficient at 0-360 degree blade position.....	26

Fig. 2.18	Schematic representation of a stabilised self-acting pitch control system [38].....	27
Fig. 2.19	The effect of solidity on the low speed torque coefficient of fixed pitch turbine [38].....	28
Fig. 2.20	The schematic representation of pivoting blade arrangement and turbine design model from [39].....	28
Fig. 2.21	A diagram illustration of the cyclogiro wind turbine [42].....	30
Fig. 2.22	(a) Experimental prototype and (b) effect of the rotor solidity on the wind machine performance [43].....	31
Fig. 2.23	The Savonius rotor configurations.....	32
Fig. 2.24	S-Rotor in the wind tunnel test.....	33
Fig. 2.25	The performance of a Savonius rotor as a function of ratio e/d [3]..	34
Fig. 2.26	The Savonius rotor and bucket geometry (a-g) from [44].....	36
Fig. 2.27	(a) The sketch of experimental set up and (b) the results from [47].	37
Fig. 2.28	The sketch definitions of the study of the combined wind machine [49].....	39
Fig. 2.29	The starting torque of S and D rotor and (b) the combined machine [49].....	39
Fig. 2.30	The concept of power characteristics for hybrid wind turbine [50]..	40
Fig. 2.31	The comparison results of hybrid and straight-blade Darrieus wind machine [50].....	40
Fig. 3.1	(a) Schematic diagram for D-rotor when the wind pass through the rotor, (b) 2-D model for 2 blades of D-rotor.....	41
Fig. 3.2	Angle of attack (θ) and position of blade (γ) of D-rotor.....	42
Fig. 3.3	Schematic diagram for analytical analysis.....	47
Fig. 3.4	(a) Lift coefficient and (b) drag coefficient of NACA4421 [51].....	48
Fig. 3.5	First step, M file for input C_l and C_d to the analytical model.....	49
Fig. 3.6	The run command in Matlab tool.....	49
Fig. 3.7	The power_coef M file function using to compute the performance of Darrieus wind machine.....	50

Fig. 3.8	Find_clcd M file sub program for lift and drag coefficient database	51
Fig. 3.9	The main program to predict the performance of D-rotor using C_l and C_d data of a selected aerofoil.....	51
Fig. 3.10	The wait bar showing progress of the prediction.....	52
Fig. 3.11	The power coefficient versus tip speed ratio of NACA 4421 for straight-bladed Darrieus Wind machine.....	52
Fig. 3.12	Example of the generated torque using NACA661-212 aerofoil characteristics.....	53
Fig. 3.13	Example of cambered aerofoils for VAWTs rotor blades [56].....	54
Fig. 3.14	Example of symmetrical aerofoils from [51].....	55
Fig. 3.15	Performance prediction results of 4 aerofoil sections on D-rotor....	56
Fig. 3.16	Performance results of first set 10 low Re aerofoils on D-rotor.....	57
Fig. 3.17	Comparison of performance results of other 10 low Re aerofoils employed to D-rotor.....	58
Fig. 3.18	Effects of number of blades on the performance of D-rotor.....	60
Fig. 3.19	Summary results of Re effects to the performance of D-rotor.....	61
Fig. 3.20	Chord ratio effects on the performance of D-rotor (c constant).....	62
Fig. 3.21	Chord ratio effects on the performance of D-rotor (r constant).....	63
Fig. 3.22	Comparison graph between two methods.....	64
Fig. 3.23	Effect of blade pitch angle to the power coefficients on D-rotor....	65
Fig. 4.1	Model description of the CFD analysis.....	69
Fig. 4.2	The preference selection in Pre-processing of CFD.....	70
Fig. 4.3	Define element type in CFD.....	71
Fig. 4.4	Create the Rectangle wind tunnel.....	71
Fig. 4.5	Line connect to the created key points to form the profiles.....	72
Fig. 4.6	Aerofoil and the wind tunnel is subtracted ready to create the mesh and element.....	72
Fig. 4.7	Mesh generated around aerofoil by ANSYS CFD package.....	73

Fig. 4.8	Boundary conditions applied to the CFD model (Cartesian mode)..	74
Fig. 4.9	Air properties apply to the CFD model.....	75
Fig. 4.10	The Flotran solution option apply to the model.....	76
Fig. 4.11	Execution control set up for the model.....	76
Fig. 4.12	The vision monitoring while running the execution.....	77
Fig. 4.13	The velocity (a) and Pressure (b) plot results by Post Processing command in ANSYS CFD.....	78
Fig. 4.14	Integration of pressure around aerofoil from CFD.....	78
Fig. 4.15	The lift, drag and moment developed at zero degree wind attack on NACA661-212 by CFD.....	79
Fig. 4.16	Lift coefficients between CFD and NACA results.....	82
Fig. 4.17	Comparison of drag coefficient between CFD and NACA results...	82
Fig. 4.18	Displays the comparison of NAC4421 aerofoils characteristics (C_l , C_d) results between CFD method and the published data.....	84
Fig. 4.19	Comparison of results: Drag Coefficients.....	85
Fig. 4.20	Comparison of results: Lift Coefficients.....	85
Fig. 4.21	Schematic drawing showing the rotating and non-rotating part of the present model study (Polar mode).....	86
Fig. 4.22	Mesh generated using ANSYS mesh creator to the model.....	88
Fig. 4.23	Boundary conditions on the investigation model in CFD (Polar Mode).....	88
Fig. 4.24	Changing of Flotran coordinate system.....	89
Fig. 4.25	Example of vector contour plot on the model at 1000 Iteration number and angular velocity of 50.....	89
Fig. 4.26	(a) Contour plot of the wind velocity on aerofoil and (b) the pressure computed by CFD on the rotor blade of Darrieus wind machine.....	89
Fig. 4.27	The schematic diagram of ICEM CFD interface with ANSYS 6.1 (modified from [70]).....	91
Fig. 4.28	Available formats using in ICEM CFD package [70].....	92

Fig. 4.29	NACA 661-211 and wind tunnel was create by CAD program.....	93
Fig. 4.30	Export CAD model to IGES format.....	93
Fig. 4.31	ICEM CFD package at import geometry state transfer to tetin format.....	94
Fig. 4.32	State of hexagonal mesh creation in ICEM CFD.....	94
Fig. 4.33	Model after finishing the Projection command.....	95
Fig. 4.34	Edge meshing parameters window to create the Relative Point Density of the mesh.....	95
Fig. 4.35	Display windows in CEM CFD mesh editor.....	96
Fig. 4.36	Final unstructured mesh generated by the ICEM CFD.....	96
Fig. 4.37	The final mesh generated around aerofoil loaded from the ICEM CFD to ANSYS.....	97
Fig. 4.38	Elements around the aerofoil generated using ANASYS Flotran....	98
Fig. 4.39	Mesh and elements created using ICEM CFD package.....	98
Fig. 4.40	Example of new result of the CFD investigation using mesh created by ICEM CFD.....	99
Fig. 4.41	Comparison of results of drag coefficient between previous investigation and new results using mesh creation package.....	100
Fig. 4.42	Comparison of results of lift coefficient between previous investigation and new results using mesh creation package.....	100
Fig. 4.43	(a) the model in polar coordination (b) the failure of the solution...	101
Fig. 4.44	Performance comparison using the analytical models.....	102
Fig. 5.1	3-D model of two-bladed D-Rotor for wind tunnel testing.....	104
Fig. 5.2	Band Saw, the power tool used for cutting the aerofoil cross sections.....	105
Fig. 5.3	NACA 661-212 model which was created by AutoCAD software...	106
Fig. 5.4	S1223 model which was created by AutoCAD Software.....	107
Fig. 5.5	Clark-Y model which was created by AutoCAD.....	108

Fig. 5.6	(a) Photograph of an example aerofoil structure made by MDF material (b) The aluminium sheet covered the aerofoil section making the aerofoil prototype.....	109
Fig. 5.7	Three completed rotor blades for wind tunnel testing of D-Rotor...	109
Fig. 5.8	Photograph of wind tunnel experimental set up.....	110
Fig. 5.9	Display and Control panel of the wind tunnel.....	110
Fig. 5.10	Working section area of the wind tunnel experimental set up.....	111
Fig. 5.11	Strain gauge torque transducer.....	112
Fig. 5.12	Summary of the experimental data and average line at wind velocity from 12-18 m/sec of Clark-Y aerofoil section.....	115
Fig. 5.13	The analytical prediction of Clark-Y on the D-Rotor.....	116
Fig. 5.14	Comparison of results of Clark-Y between analytical prediction and experimental results.....	116
Fig. 5.15	Experimental data and the average line on wind velocity from 12-18 m/sec of NACA 661-212 aerofoil.....	118
Fig. 5.16	Analytical model prediction results of NACA661-212 aerofoil.....	118
Fig. 5.17	Comparison of results of NACA661-212 between analytical and experimental studies.....	119
Fig. 5.18	Average line of the experimental results of wind velocity 10-14 m/sec of S1223 aerofoil.....	120
Fig. 5.19	Analytical model prediction of S1223 aerofoil on D-Rotor.....	121
Fig. 5.20	Comparison results of the power coefficient Vs tip speed ratio of S1223 aerofoil.....	121
Fig. 5.21	Result from the experimental models.....	122
Fig. 5.22	Result from the analytical models prediction.....	122
Fig. 5.23	Full range of prediction results from analytical models.....	123
Fig. 5.24	Comparison results between analytical and experimental models of Clark-Y aerofoil.....	123
Fig. 5.25	Comparison results between analytical and experimental model of NACA661-212 aerofoil.....	124

Fig. 5.26	Comparison results between analytical and experimental model of S1223 aerofoil.....	124
Fig. 5.27	Experimental results for NACA 661-212.....	128
Fig. 5.28	Comparison between analytical and experimental results.....	128
Fig. 5.29	Experimental and the average line for Clark-Y aerofoil.....	129
Fig. 5.30	Comparison between analytical and experimental results on Clark-Y aerofoil.....	130
Fig. 5.31	Experimental results and average line of S 1223 on Darrieus turbine.....	131
Fig. 5.32	Comparison between the analytical and the experimental results of S1223.....	131
Fig. 5.33	Performance comparison results of three experiments for 2 blade Darrieus rotor at chord length of 0.15 m.....	132
Fig. 5.34	Experimental set up of three blades NACA 661-212.....	133
Fig. 5.35	Experimental results and average line of three bladed NACA661-212 on Darrieus wind machine.....	134
Fig. 5.36	Comparison of experimental and analytical prediction of NACA 661-212 on Darrieus wind machine.....	134
Fig. 5.37	Comparison results of the experimental testing between two and three blades of NACA 661-212.....	135
Fig. 5.38	The experimental set up of three blades Clark-Y.....	135
Fig. 5.39	Experimental results and average line of three blades Clark-Y.....	136
Fig. 5.40	Comparison of 3 blades machine's analytical and experimental results.....	137
Fig. 5.41	Experimental results of two and three blade Clark-Y.....	137
Fig. 5.42	Experimental set up of three blades S1223 machine.....	138
Fig. 5.43	Experimental results and average line of three bladed S1223.....	139
Fig. 5.44	Experimental results and average line of three bladed S1223.....	139
Fig. 5.45	The experimental results of two and three blade of S1223.....	140
Fig. 5.46	Summarised experimental results of 3 blades D-Rotor.....	140

Fig. 5.47	The wind turbine model set up for rotor blade combination.....	141
Fig. 5.48	Power coefficients of three aerofoils combined on D-Rotor.....	143
Fig. 6.1	3-D modelling prototype of the straight-bladed Darrieus Vertical Axis Wind Turbine.....	147
Fig. 6.2	The process of fine finish surface of a rotor blade.....	148
Fig. 6.3	The painting of the rotor blades.....	148
Fig. 6.4	Completed set of S 1223 rotor blades ready to use for VAWTs.....	149
Fig. 6.5	Shaft and Shaft supporter on pre-assembling the wind machine.....	149
Fig. 6.6	Welding process to construct the tower and the base of the prototype.....	150
Fig. 6.7	Test-assembly of the prototype.....	150
Fig. 6.8	The permanent magnet induction generator Rutland FM 1803.....	151
Fig. 6.9	The control loads box used to control output of the prototype.....	152
Fig. 6.10	E300/RWTI -2 Torque Transducer and Torque view software.....	152
Fig. 6.11	The Kestrel 4000 digital anemometer.....	153
Fig. 6.12	The site before wind machine instillation at St Mary's Island.....	155
Fig. 6.13	The wind machine at St Mary's Island, Whitley Bay.....	155
Fig. 6.14	(a-c) Velocity contours plot of S1223 aerofoil rotor blade at various pitch angles.....	157
Fig. 6.15	The anemometer distance recommended from [72].....	159
Fig. 6.16	Full set-up wind machine at Amble Caravan Park.....	160
Fig. 6.17	The Semi Cylinder Turbine (SCT) as the starting aids device.....	160
Fig. 6.18	The wind flow fluctuation on Amble Caravan Park.....	161
Fig. 6.19	The RPM of stand-alone of three S1223 rotors versus wind speed at Amble Caravan Park site testing.....	162
Fig. 6.20	VAWTs combined with 0.16 m SCT at 0.2 m.....	163
Fig. 6.21	VAWTs combined with 0.16 m SCT at 0.4 m.....	163
Fig. 6.22	VAWTs combined with 0.16 m S CT at 0.6 m.....	163

Fig. 6.23	VAWTs combined with 0.16 m S CT at 0.8 m.....	164
Fig. 6.24	Folk lift used for assembling the rotor to the structure.....	166
Fig. 6.25	The control and instrumentations unit.....	166
Fig. 6.26	Schematic diagram of the wind turbine field test.....	167
Fig. 6.27	The completed set up with 1:3 stepping up gear unit of D-Rotor VAWTs at Nares, Blyth, Northumberland.....	167
Fig. 6.28	Power coefficient versus tip speed ratio of Straight-Bladed VAWTs from site test and compared with Matlab prediction (inset).....	168
Fig. 6.29	The SCT attached to D-rotor at 0.4 m radius of VAWTs.....	169
Fig. 6.30	Power Coefficient versus Tip Speed ratio of SCT with D-Rotor.....	169
Fig. 6.31	The typical tiger shrimp farm in southern Thailand.....	171
Fig. 6.32	Pie chart displaying the contribution of each value to a total cost in a selected farm.....	172
Fig. 6.33	Two-stroke diesel engine for conventional water treatment.....	173
Fig. 6.34	Electrical motor used for water treatment in shrimp farm.....	174
Fig. 6.35	The author with portable anemometer at shrimp farm.....	174
Fig. 6.36	The wind energy resource atlas in Thailand and some neighbour countries [76].....	175
Fig. 6.37	Wind resource at test point in southern Thailand [76].....	175
Fig. 6.38	Aerators used for the test in a shrimp farm aeration system.....	176
Fig. 6.39	The wind turbine specification for shrimp farm aeration process...	177
Fig. 6.40	External side welding to the end plate for S-Rotor.....	178
Fig. 6.41	Final welding and pre-assembling combined VAWTs.....	179
Fig. 6.42	Illustrates the completed set of the combined wind turbine at the selected shrimp farm.....	180

Acknowledgement

The author would like to express his sincere gratitude and appreciation to everyone who have been involved in this project.

I gratefully acknowledge:

Principle Supervisor: **Dr. Ken Leung** for his sound advice and understanding in all knowledge throughout this research.

Second supervisor: **Prof. P.K Datta** for all his support and advise.

All **friends and technicians**: Thanks for your help and friendly assistance during the process of this work.

My institute: Rajamangala Institute of Technology (**RIT**) for its financial support throughout my study for a doctoral degree in England

In addition, the most of all, sincere acknowledgement to **My Family**: father, mother and all sisters and brothers for their love and support throughout life.

Declaration

I hereby declare that:

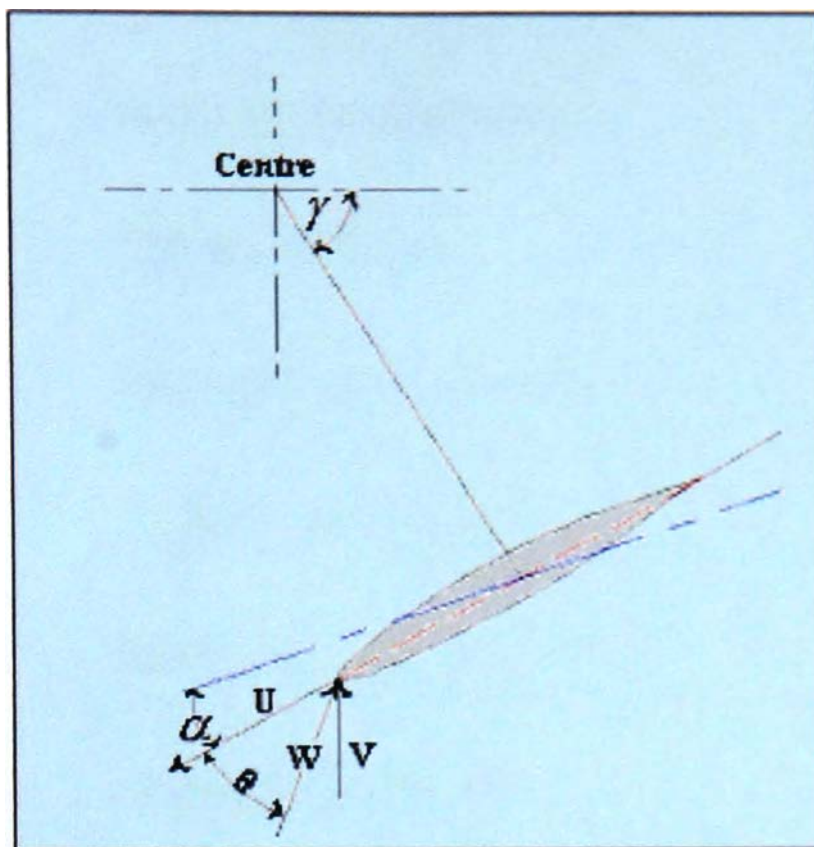
During the period I have been registered for the degree of Ph.D. for which the thesis is submitted, I have not been a registered candidate for any other award of a University.

Furthermore, that I have published relevant papers and attended relevant seminars within the Northumbria University, and annual conferences for the European wind energy in Paris and Madrid.

Wirachai Roynarin

March 2004

Darrieus Rotor Vertical Axis Wind Turbine Nomenclature



General Parameters

A	=	Turbine rotor area (m^2)
B, b	=	Number of blades
C, C	=	Chord length (m)
D	=	Drag force (N)
d	=	Rotor diameter (m)
G	=	Interference factor
H	=	Rotor height (m)
L	=	Lift force (N)
P	=	Output power (W)
R, r	=	Rotor radius (m)
S	=	Blade area (m^2)

T	=	Torque (N.m)
U	=	Wind blade velocity (m/sec)
V	=	Absolute wind velocity at the rotor blade (m/sec)
W	=	Relative wind velocity (m/sec)
C_p	=	Rotor power coefficient
C_t	=	Thrust coefficient
C_n	=	Normal force coefficient
C_l	=	Coefficient of lift force
C_d	=	Coefficient of drag force
P_a	=	Available power (W)
P_w	=	Power extracted by rotor (W)
P_{max}	=	Maximum power (W)
T_a	=	Thrust (N)
Re	=	Reynolds number
X	=	Tip Speed Ratio

Greek

σ	=	Solidity	=	$\frac{bc}{D}$
θ	=	Angle attack of the wind (Degree)		
α	=	Blade pitch angle (Degree)		
ρ	=	Density of the air (kg/m ³)		
ω	=	Angular velocity of the rotor (rad/s)		
γ	=	The blade position (Degree)		
Ω	=	Angular velocity of the experimental models (rad/s)		

Chapter 1

Introduction

The power from the wind will never cease while the sun is still rising and the earth is revolving. Wind exists everywhere on the earth, and in some places with considerable energy density. This thesis aims to study this renewable energy, which will remain a useful power source until the end of this world. Wind has been used in the past to generate mechanical power. Nowadays wind power has become a promising source to generate electricity because wind power is clean, quiet and efficient. It reduces acid rain, smog and pollutants to the atmosphere. Renewable energy has become popular in recent years, due to the need for the utilisation of more environmentally friendly energy sources. In generating wind power, both the Vertical Axis Wind Turbine (VAWTs) and the Horizontal Axis Wind Turbines (HAWTs) play a significant role.

1.1 Type of wind machines

There are many concepts to describe the type of wind machines which are used. All of the wind machines fall into two types depending on whether the turbine blade rotates about a horizontal-axis or a vertical-axis.

1.1.1 The Horizontal Axis Wind Turbines (HAWTs)

This wind machine has a maximum theoretical power coefficient C_p of approximately 0.45 [1-3]. However, in reality this wind machine can only achieve an average power coefficient of approximately 0.3. Fig. 1.1 describes the main components for modern propeller type HAWTs. The main advantage of this machine is its high power coefficient compared to the other types. Nevertheless, the disadvantages of HAWTs include their operation at high starting wind velocity, low starting torque, the requirement of a yaw mechanism to turn the rotor toward the wind and the power loss when the rotors are tracking the wind directions. These are the poor features of the HAWTs, which are difficult to be solved. More details of this wind machine can be seen in Chapter 2.

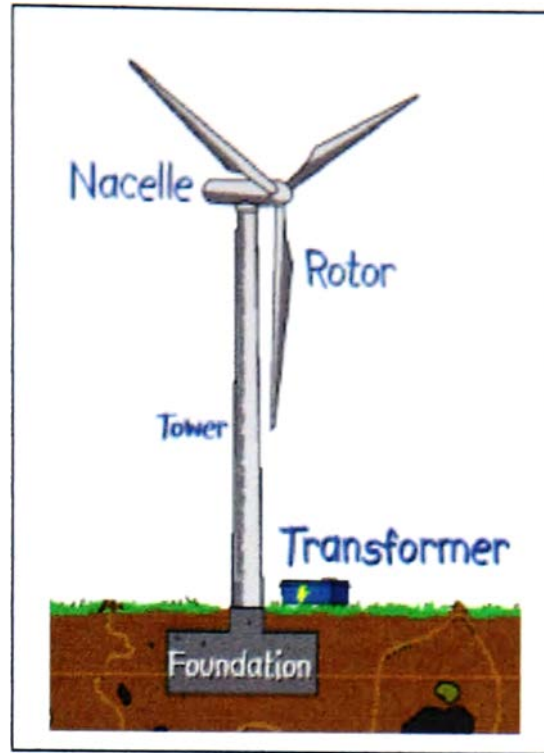


Fig. 1.1 Key parts of Horizontal Axis Wind Turbines [4]

1.1.2 Vertical Axis Wind Turbines (VAWTs)

This type of Wind machine is the main focus of this research. The rotor of this wind machine rotates perpendicular to the direction of the wind. It has some advantages over the RAWTs, these include its simple construction, its ability to catch the wind from any direction and high starting torque (Savonius rotor). However, this machine has also some disadvantages such as low power coefficient compared to that of the HAWTs, and poor starting torque (Darrieus rotor) (more details are given in Chapter 2). Normally VAWTs can be divided into three main types:

- ❖ Savonius rotor or S-rotor
- ❖ Darrieus rotor or D-rotor
- ❖ Combined rotor between S and D rotor

1. The Savonius rotor is the simplest form of vertical axis wind machines. It is economical for the small power requirements, and it generates a high starting torque but has a lower power coefficient of about 0.25 [1,3]. At its most basic level, an S-rotor comprises two half cylinders displaced so that one convex face and one concave face are presented to the wind (Fig. 1.2). The difference in drag on two sides produces a torque for most, but not all, orientations to the wind. Therefore, at least two rotors at different angles are required to

ensure self-starting. Although they are simple to build, they are very large and heavy compared with other wind turbines of similar power output. The Savonius rotor is not the main focus of this study, except that this wind machine is used as a starting device for high starting torque requirements.

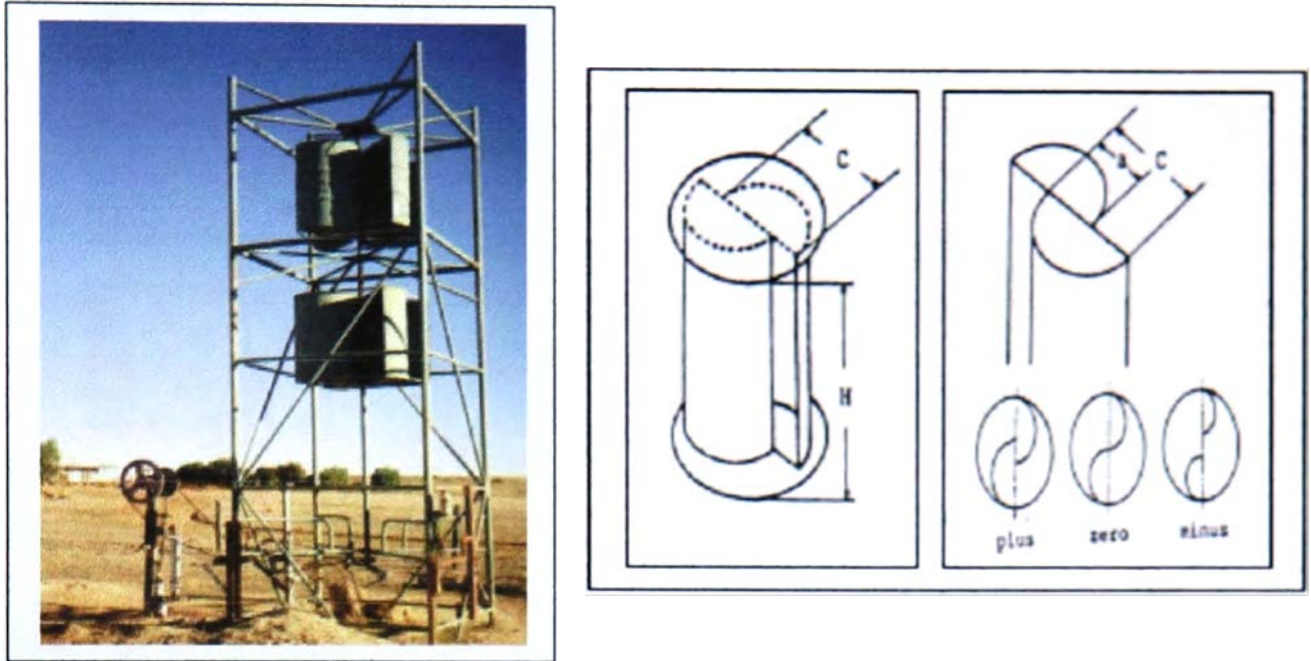


Fig. 1.2 Savonius wind turbine for pumping water and its configurations [5]

2. The Darrieus rotor is named after the French engineer Georges Darrieus who patented the design in 1931. This Wind machine was manufactured by the US Company, FloWind. This Wind machine employs aerodynamics lift surface to generate useful torque. The Darrieus machine is characterised by its C-shaped rotor blades, which make it look a bit like an eggbeater. It is normally built with two or three blades. This Wind machine has been studied and investigated for preliminary designs by Wilson and Lissaman [1] and others [3,4,8]. This type of machine (Fig. 1.3 (a), (b)) can produce the maximum power coefficient about 0.35, which is higher than that obtained from the S-rotor. But whether the blades of this wind machine are curved or straight, typically it develops little or no torque at low speed (very hard to start rotor itself), and so must be motored up to speed, making it unsuitable for stand-alone operation. However, there are several ways to overcome these disadvantages, which are the focus for this research.

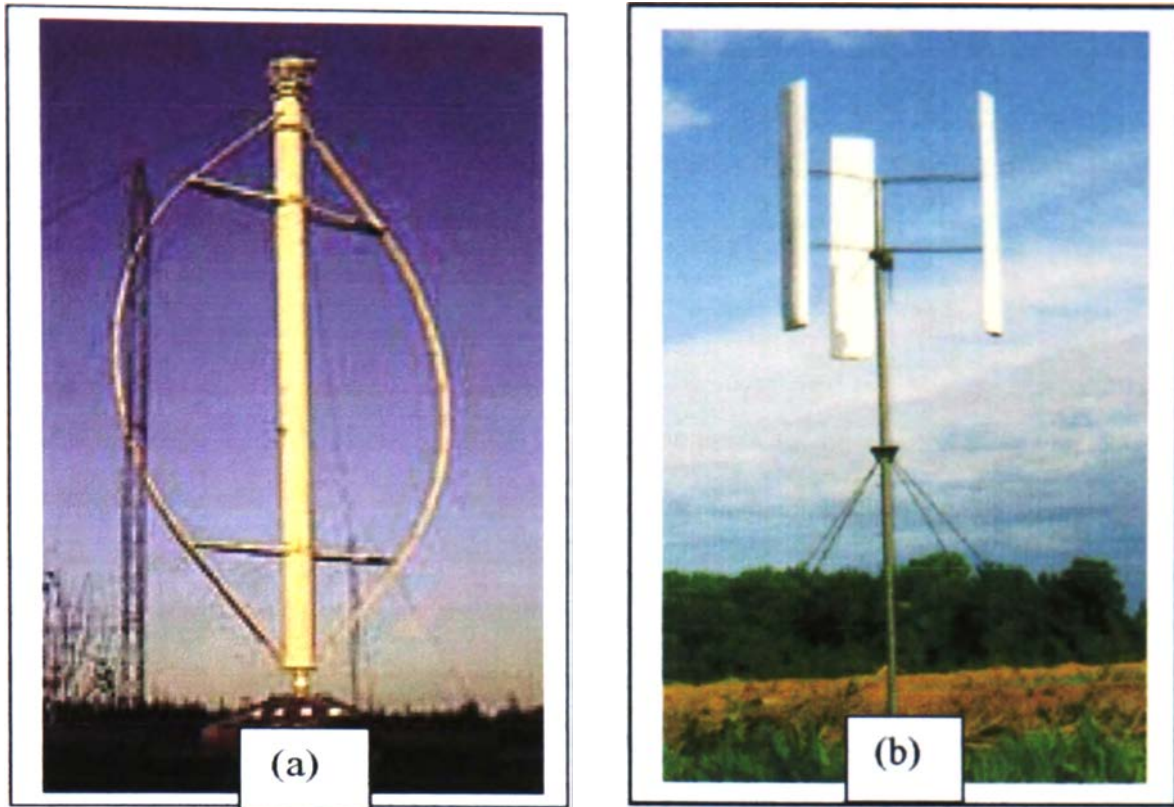


Fig. 1.3 (a) C-shaped VAWTs Q61) and (b) Straight blade VAWTs 171

3. Combined rotor is generally one of the many ways to optimise and overcome the problems of low starting torque on Darrieus wind machine. Although the S-rotor has a lower power coefficient than the D-rotor, its useful characteristic is its high starting torque and self-starting at low tip speed ratio. It is equally possible to start the D-rotor with the aid of an S-rotor. Fig. 1.4 shows the combined idea rotors (from Ref 3). It works by producing a large starting torque from the S-rotor but at higher tip speed ratio operated by D-rotor. Further details are given in the literature review (Chapter 2).

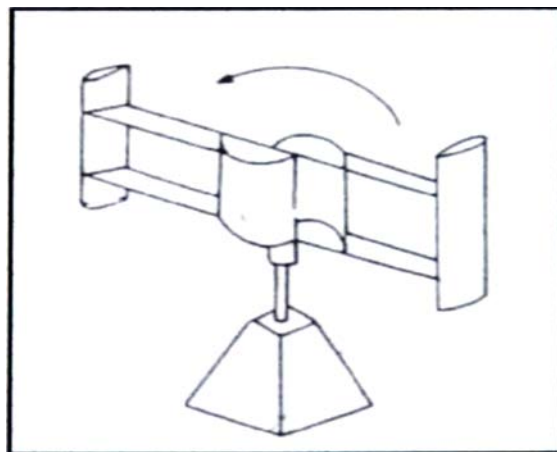


Fig. 1.4 The combined rotor vertical axis wind turbine [3]

1.2 Why and How to Optimise the VAWTs

This study has a major focus on the straight-bladed Darrieus wind turbine (Fig. 1.3 b) with normally lower performance than the horizontal machine. However, this is not the only consideration for undertaking research on this. Other characteristics are that this wind machine can be simply built and is suitable to some specific applications, which cannot be achieved with other types of wind machines. However, the self-starting problem of this wind machine still remains unsolved and this is why the straight-bladed Darrieus wind turbine will never be competitive with HAWTs. If this problem can be solved, this wind machine will become more attractive again.

Most rotors of the straight-bladed Darrieus wind machine, which have been investigated and studied in the past, were made by only a few symmetrical aerofoil profiles [8]. There are such as NACA 0012, NACA 0005 or NACA 0016. Nevertheless, only few aerofoil profiles can be rotor blades for this type of wind machine. Therefore, this study considers further candidate aerofoil profiles employed for the rotor of the Darrieus wind machine. The aerofoils characteristics from the literature survey which giving lift and drag coefficient (C_l , C_d) were taken to analyse their performance on the Darrieus wind machine using the analytical method. The most promising aerofoil sections showing good performance in the analytical method have been further studied using different approaches including Computational Fluid Dynamics (CFD), small model testing in the wind tunnel and also by assessing wind machine prototypes in field tests. It is believed that with careful research and by using the optimised aerofoil section, the main problems and some disadvantages of the Darrieus Wind machine can be solved. In addition, a novel application of the combined VAWTs has been considered. This study has a major focus on two main criteria to optimise VAWTs - self-starting and efficiency.

1.3 The aims of this study: the need for renewable decentralised energy supplies with optimised Vertical Axis Wind Turbines

Most of the energy used today comes from fossil fuel - coal, oil, and natural gas. These fuels take a long time to form before they become fossil fuels [1]. Additionally, fossil fuels are continuously being consumed. There are many sources of renewable energy such as solar, wind and geothermal etc. This study focuses on the power from the wind to generate useful energy. Wind power is one of the most promising renewable energy sources and its use has

seen a fast growth rate in the last 10 years. The kinetic energy of moving air may be converted to rotational energy by the rotor of the wind turbine, which in turn may be converted to electrical energy by the wind turbine generator. This research focuses on 'the optimisation of Vertical Axis Wind Turbines'. The aims of the investigation are:

- To study the characteristics of different turbine blade models
- To develop and to improve the performance of the VAWTs
- To apply the VAWTs (Fig. 1.2-1.4) to suitable applications
- To try to overcome the main disadvantage associated with the problem of self-starting for VAWTs
- To investigate the performance of using VAWTs for the shrimp farm applications

The results of this study are expected to improve the performance of VAWTs, The thesis is presented in 9 chapters. The second chapter presents a critical review of the literature relevant to this work. Focusing on vertical axis wind machine, the analytical models of a straight-bladed Darrieus wind machine are given in Chapter 3. Computational Fluid Dynamics (CFD) studies for selected aerofoils, chosen from the analytical study, are presented in Chapter 4. Wind tunnel testing is described in Chapter 5. Chapter 6 deals with the field-testing of a small prototype VAWTs. Results are discussed in Chapter 7. Chapter 8 lists a series of conclusions and suggestions. Further works are given in Chapter 9.

Chapter 2

Literature Review

This chapter presents a review of the historical development focusing on three main types of VAWTs. Their advantages and disadvantages relative to HAWTs are discussed and evaluated. The various parameters considered in VAWTs design are discussed with particular reference to self-starting capability, which is an important consideration for all stand-alone power supplies. Literature on research, development issues and the applications of VAWTs are reviewed.

2.1 A brief history of wind turbines

Wind turbines have been used as a source of useful power for centuries. Records of ancient history indicate that the first wind machines were built by the Persians in approximately 900 AD. [9]. This wind machine (Fig. 2.1) had a vertical axis and it worked by drag force pushing the turbine blades to generate the useful power. The use of these vertical wind machines subsequently spread throughout the Islamic world.

In Europe, wind energy made its appearance in the 11th century A. D. These wind machines were introduced from the Middle East. They were all horizontal axis machines. These wind machines were used for many mechanical tasks, including pumping water, grinding mill, sawing wood and powering tools. By the 14th century, the Dutch took the lead in improving wind machines and used them widely thereafter for draining the marshes and lakes of the Rhine River delta.

Fig. 2.2 and Fig 2.3 illustrate different types of VAWTs and HAWTs. However, some of these wind machines presented remain as concepts.

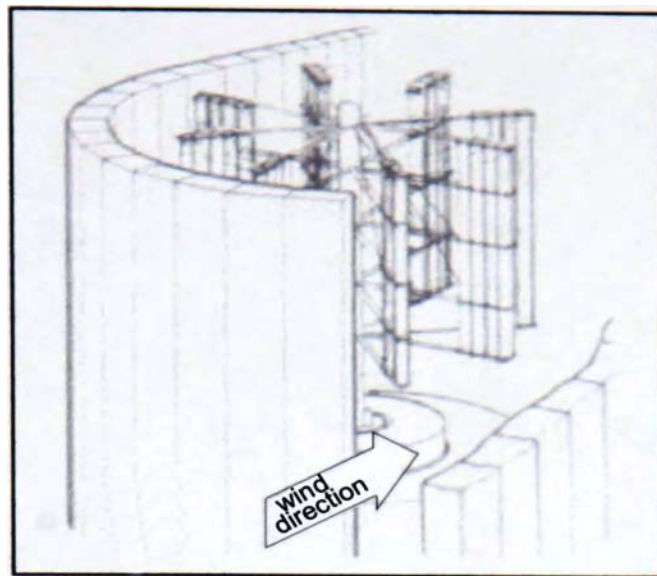


Fig. 2.1 Early Persian windmill [9]

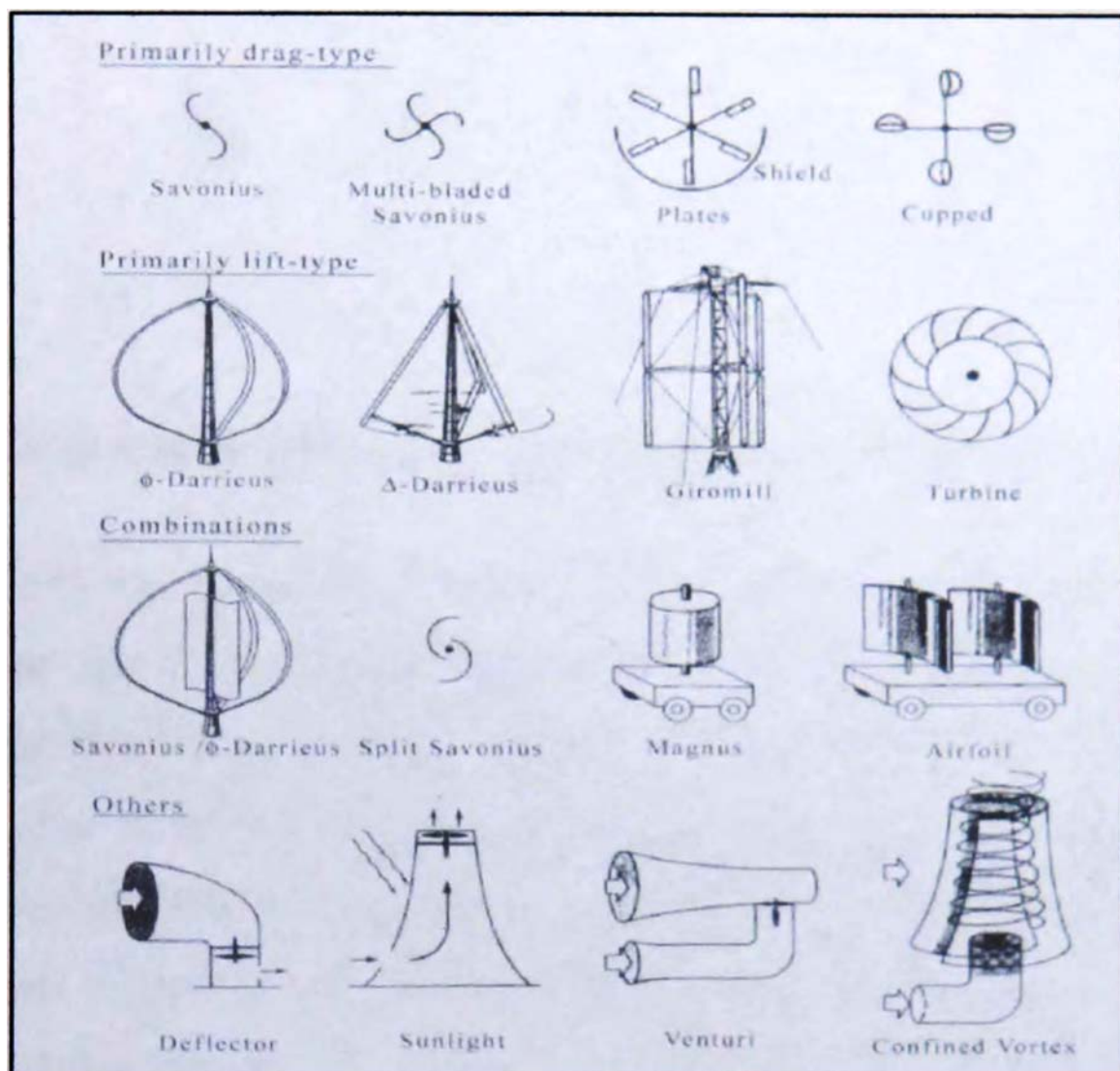


Fig. 2.2 Other types of vertical axis wind machine [9]

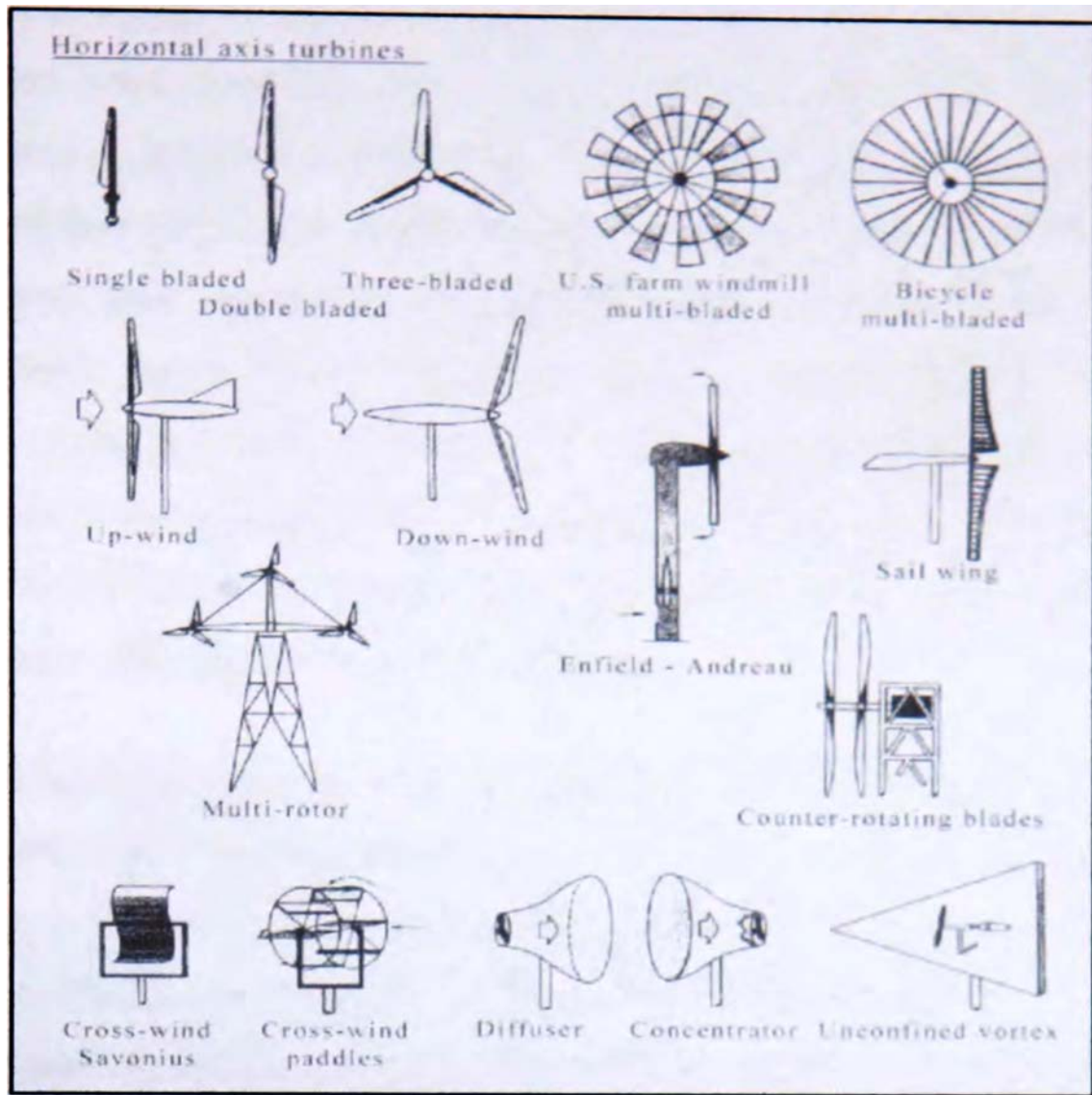


Fig. 2.3 Some other types of horizontal axis wind machine [9]

The performance of the wind turbine is our main concern in the design stage. It is argued that vertical axis wind turbines with improved self-starting capabilities could play a significant part in the provision of stand-alone power supplies. Most of the modern wind machines nowadays are used to generate electricity connected to the power grid line. However, generally wind turbines can be used as a source of energy; some wind turbines produce useful torque used for irrigation and aeration system replacing diesel engines or motors, consequently reducing pollutants such as carbon dioxide being released into the atmosphere.

However, in high wind places around the world wind turbines are normally used for electricity supply to the grid line. Horizontal Axis Wind turbines of the propeller blade shaped type are the most popular compared with other wind machines. In the last 10 years this types of wind machine have been generating a large number of Megawatts (MW) of electricity around the world. In addition, many commercial companies based

on HAWTs are trying to produce larger megawatt wind turbines. For example in the world's largest wind farm [10], Horn Rev, which consists of 80 HAWTs, each turbine produces a power output of 2 MW (Fig. 2.4). The first wind machine was connected to the power grid line on 29 July 2002. However, gearbox and blade failures have occurred in recent times and research and development on HAWTs are continuing. On 4 November 2002, an accident occurred with a Vestas V80-2.0 NIW (see Fig. 2.5) offshore test turbine, which is located at Tjaereborg in Denmark; the accident caused serious turbine rotor damage [11]. The reported failure was due to the control system allowing the turbine to over-speed. This is just one of many problems that still remain for the engineers and researchers to investigate.

Nowadays most horizontal axis wind machines are similar in geometry. The UK had one of the oldest and largest HAWTs in the world. It is the three megawatt two bladed model, which was developed by Wind Energy Group. This wind turbine was located at Burgar Hill in Orkney; it used to be the largest of its kind when it was inaugurated in 1987 as an experimental machine [12]. Now the turbine, which cost £17m to build, has been brought to the ground and replaced with the modern 2 blades, 2 MW wind machine (See Fig. 2.6). There are more details of wind turbine design and economics which can be seen in [13, 14].



Fig. 2.4 The largest HAWTs offshore wind farm at Horn Rev, Denmark [10]



Fig. 2.5 The damaged 2 MW wind machine which is located at Tjaereborg in Denmark [15]

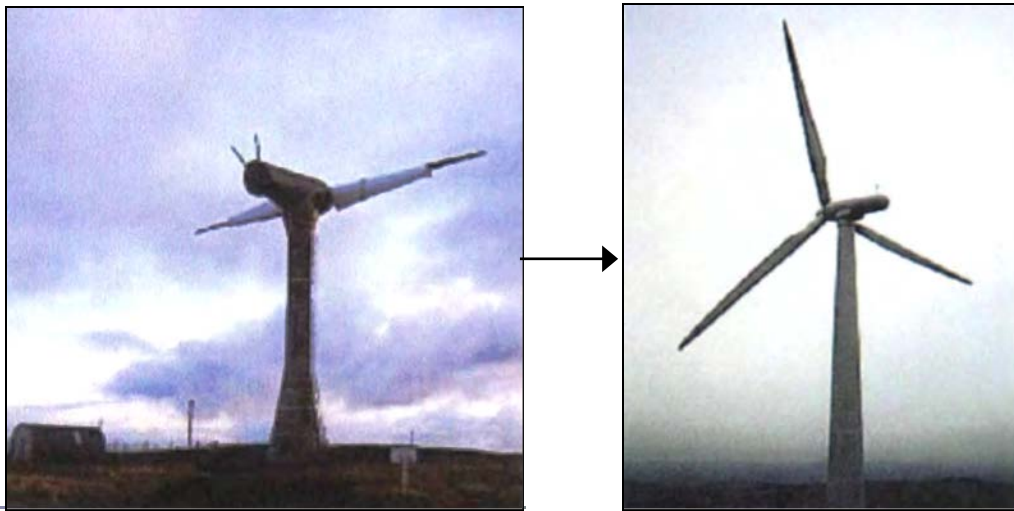


Fig. 2.6 (a) The old model of biggest 3 MW wind machine which was dismantled and replaced with modern 2 MW wind machine (b) [16]

A vertical wind machine was developed by Sandia National Laboratories, shaped like 'egg beater' and producing a large amount of electricity [17]. The wind energy group of Sandia National Laboratories, which is located in Albuquerque, New Mexico, has done a lot of research on Darrieus type wind machine. SAND80-2469 provides a comparison of field and wind tunnel tests on Darrieus wind turbine. Additionally straight-bladed VAWTs were explored by the National Wind Technology Centre at NREL [18]. However, VAWTs was not well recognised compared to HAWTs because as mentioned earlier that the machine is not self-starting for stand-alone application and performs at a low power coefficient if located at a ground level. In the summer of 1997, the last U.S. Company dealing with Darrieus VAWTs named FloWind went bankrupt.

However, advantages of this wind machine are being redeveloped. The latest version of vertical axis wind machine that produces large number of megawatts named 'Chinook 2000' (Fig. 2.7) which was designed by Geramanischer Ltd. Each wind machine generates high rated power of 250 kW at a wind speed of 17m/s.

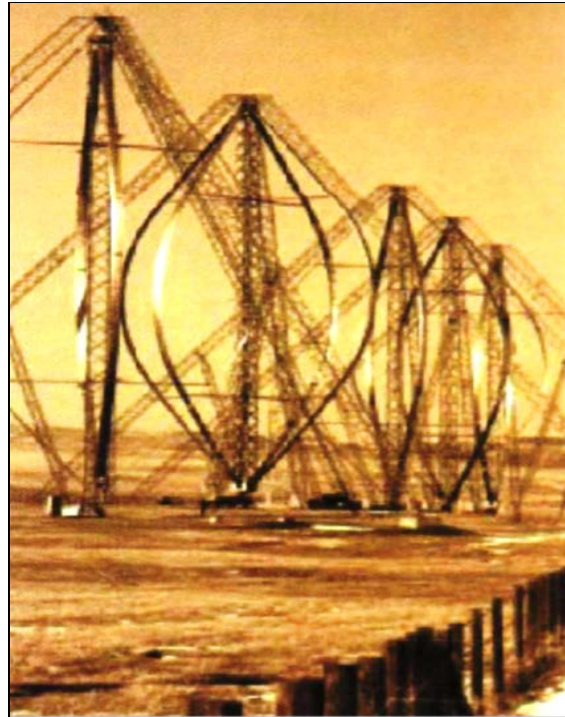


Fig. 2.7 Chinook 2000 vertical axis wind turbine [19]

2.2 Wind Turbine Applications

As mentioned earlier, most of wind turbine machines are used for producing electricity and are connected to the power grid. Additionally, because of the versatility of electrical energy grids and liquid fuels, these two forms of energy supply have dominated energy policy in recent years. However, some decentralised applications on the direct use of mechanical shaft power from a wind machine may be simpler and more economical.

These applications, which use wind turbines as a power source, include

- ❖ Pumping water
- ❖ Desalinating saline or brackish water
- ❖ Aerating water, reservoirs and aquaculture ponds farm
- ❖ Circulating potable wastewater
- ❖ Heating water by fluid turbulence

Frantsi et al. [20] studied and investigated the use of the VAWTs to generate heat. They designed and developed aerodynamic models for vertical NNInd machines used in commercial greenhouses. These are based upon the straight-bladed Darrieus wind turbine using a Savonius starter (Fig. 2.8). This wind machine converts wind energy into hydraulic pressure energy. Then the pressure energy is converted into thermal energy. Their prediction showed that the wind machine with rotor blade diameter of 6 metres and length of 2 meters would generate the useful power at a power coefficient C_p of 0.2. Additionally, this wind machine can be used as a source of energy in some rural areas in developing countries.

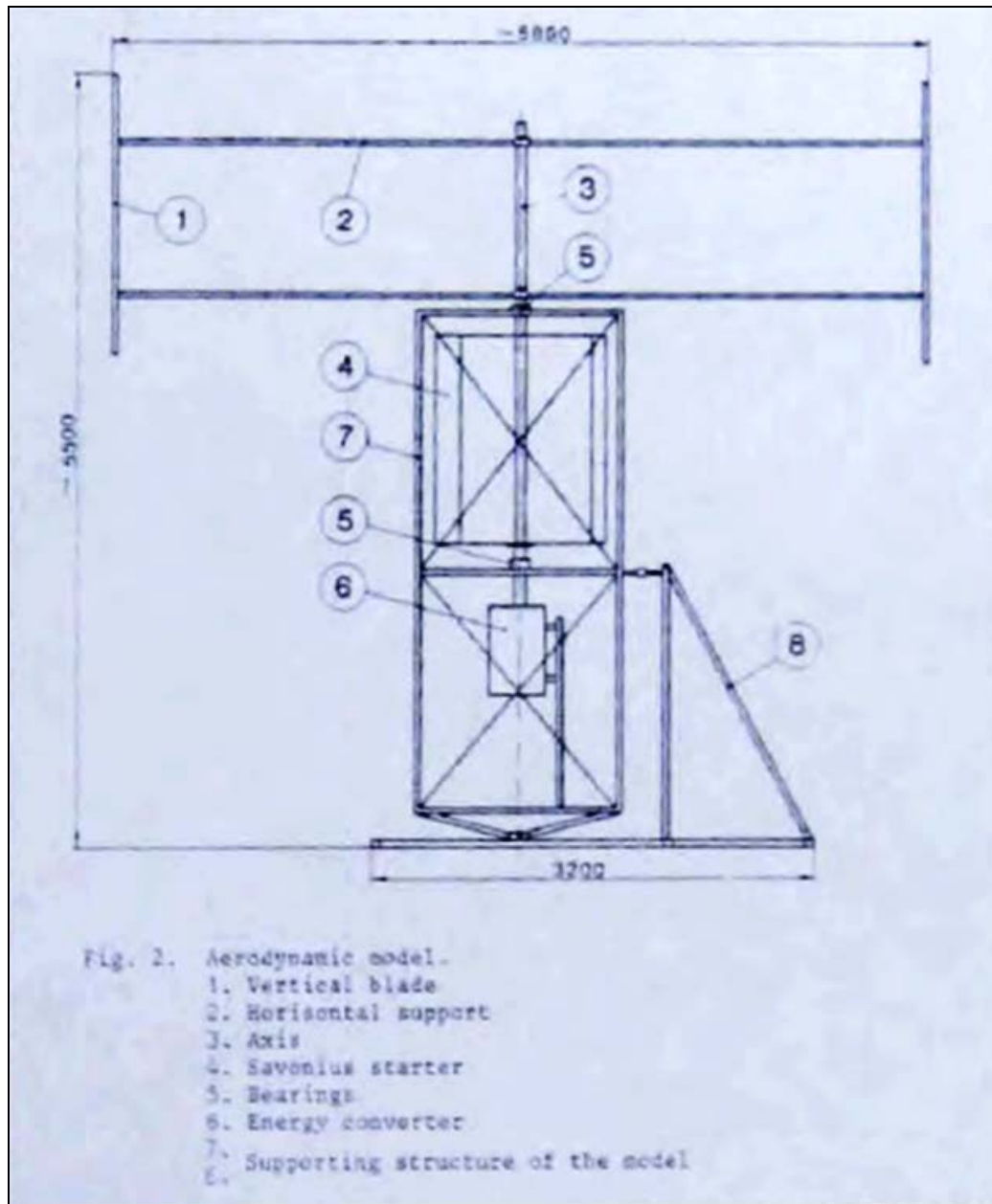


Fig. 2.8 The idea of producing heat from VAWTs [20]

Smulders and Folling [21] have developed and proposed the idea of using a wind machine to drive a cooling machine to store food such as meat, fish, milk and vegetables. They showed

from the modelling investigation the possibility of building an autonomous wind machine to drive a cooling system. The results of their studies indicate that the application of wind energy driven cooling systems can be economically justified. D. J. Hilton [22] proposed initially very useful applications of vertical axis wind machines for farm use. His wind machine was designed and considered for water pumping. This straight blade Darrieus wind machine was a simple design, giving a low cost machine, and makes it suitable to rotary borehole pumps. There are many studies [23-25] which considered applications of the wind machines. The summary of the applications of this wind machine in other fields can be seen in Eldridge 1251. Fig. 2.9 gives a summary of the applications for both vertical or horizontal axis wind machine.

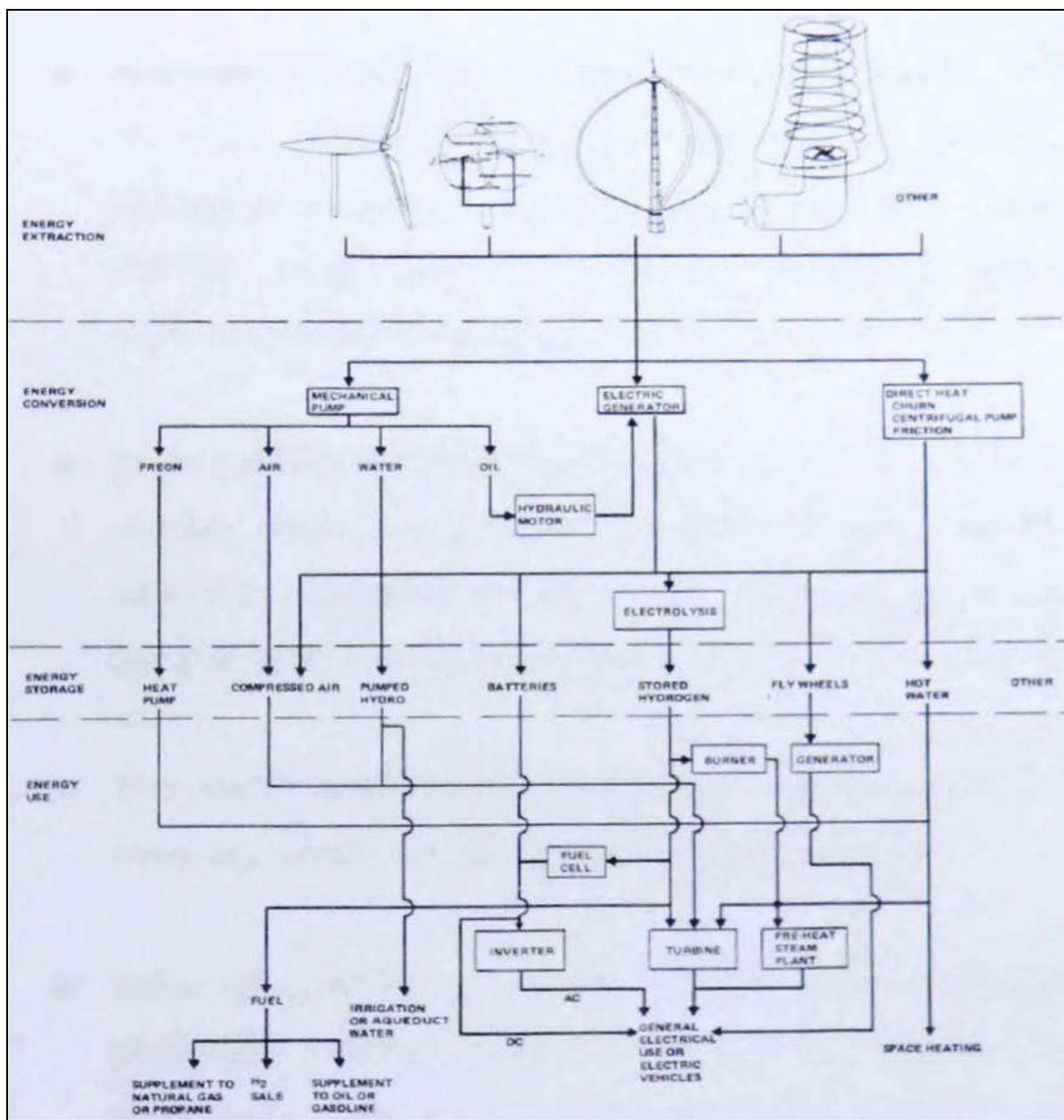


Fig. 2.9 The Various applications of wind machines [25]

However, the applications of wind machines are not the major consideration of this study. The application that will be considered in this thesis will be the use of the wind machine for farm aeration process, in particular the application of wind machines for shrimp farm aeration process.

2.3 Advantages and Disadvantages of VAWTs compared to HAWTs

The relative advantages and disadvantages of VAWTs and HAWTs are presented below:

2.3.1 Advantages of VAWTs

- Normally VAWTs are an omni-directional machine. This wind machine does not require orientation of the rotor toward the wind directions. Therefore, complex yaw mechanism, which is used in conventional upwind HAWTs, is not required in VAWTs. Consequently, there is no power loss while the rotor turns toward wind direction (yaw error).
- Most VAWTs are placed at the ground level while the HAWTs are mounted on high column tower. Thus for VAWTs the heavy transmission system and gears box, generator and control box may be easily situated at the ground level allowing easy operation and accessibility for maintenance.
- The overall height of HAWTs is higher than that of the VAWTs resulting in more acceptable visual impact to the surroundings.
- Some of VAWTs are simple to build such as Savonius wind machine producing sufficient torque for certain applications. Therefore, in some applications, which require low cost, VAWTs should be considered.
- VAWTs are normally designed in such a way that centrifugal loads are balanced. But in HAWTs, the rotor blades are additionally subject to cantilever loads resulting in bending moment at the blade roots.

- VAWTs are well equipped to rotor blade lightning protection because the main shaft of VAWTs is not directly connected with the generator. This is not easy to achieve for HAWTs, as the rotor blades are always placed higher than the tower, resulting in the blade tip being close to the lightning during thunderstorms. Lightning protected rotor blades of HAWTs are extremely expensive compared to VAWTs rotors.

2.3.2 Disadvantages of VAWTs

- Generally, VAWTs have lower performances than the modern propeller HAWTs resulting in less power output for the same wind speed.
- VAWTs are generally not self-starting (except by well-designed mechanisms). However, the Savonius rotor is an exception but it has fairly low efficiency.
- Since VAWTs are placed and constructed close to the ground level, they are subject to less wind speed and more turbulence. Therefore, for the same rotor size (swept area) and weight, the power output of VAWTs is less than that of the comparable HAWTs.
- Because VAWTs work under centrifugal loads and the rotor blades are sited on the tower, guy cables are required to hold it.
- Torque and power output generated by VAWTs fluctuate in a cyclic manner during each revolution as the blades move in and out of the wind, whereas in HAWTs, the torque and power output are fairly steady.
- Generally, VAWTs work in cyclic manner which causes variation in torque. This wind machine has many natural frequencies of vibration, which need to be considered during development. For fast running of the machine, the control mechanism may result in serious vibration, damaging the rotor. A well-designed HAWT has no such vibration problems.

The comparison of variable geometry VAWTs and HAWTs can be seen in [13,26].

2.4 Aerodynamics of wind turbines

This section describes the main theories of wind turbine aerodynamics. In fact, wind turbines operate on the basis of the principles of the fluid dynamic engineering. The essential theorems of the Horizontal Axis Wind Turbines (HAWTs) and also the Vertical Axis Wind Turbines (VAWTs) are given below:

2.4.1 One-Dimensional Momentum Theory

This theory considers the turbine blades as the actuator discs. The assumption of this theory are based on:

1. Steady, homogeneous wind
2. No obstruction to wind flow either upstream or downstream
3. Uniform flow velocity at the rotor disc
4. Wind flow passing through the rotor can be defined a boundary
5. Incompressible wind flow
6. No rotation of the flow produced by disc

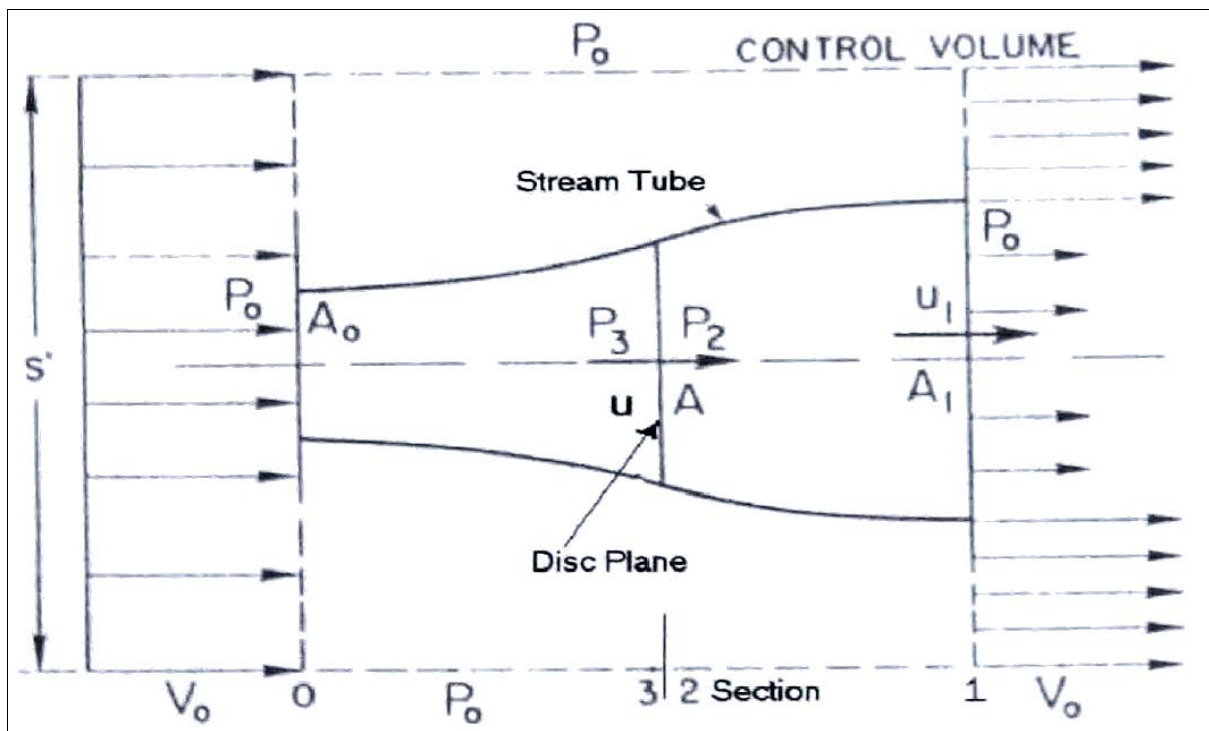


Fig. 2.10 Flow pattern of actuator disc theory [27]

Fig. 2.10 shows a diagram for a flow pattern of the air through the actuator disk. The parameters include

S = cross section area of control volume (m)

V_0 = wind velocity at inlet and outlet of control volume (m/sec)

u = upstream wind velocity to rotor disc (m/sec)

u_1 = downstream wind velocity from the rotor disc (m/sec)

P_0 = ambient atmospheric pressure (N/m²)

P_2 = downstream pressure from rotor disc (N/m²)

P_3 = upstream pressure to rotor disc (N/m²)

A_0 = the area of inlet cross section of stream tube (m)

A = area of the rotor disc (m)

A_1 = area of outlet cross section of stream tube (M)

Q = flow rate (m³/sec)

v = induced wind velocity = $V_0 - u$ (m/sec)

For normal atmospheric pressure at 15 Celsius, the density ρ of the air is 1.225 kg/m³ [27]. The flow rate of the wind within the stream tube (wind tunnel) is the same, therefore the continuity equation for the flow rate is required, when $Q = AV$, then $V_0 A_0 = uA = u_1 A_1$. From Bernoulli theorem, considering in term of pressure along the section 0 to section 3 and section 2 to section 1 we have

$$\frac{1}{2}\rho V_0^2 + P_0 = \frac{1}{2}\rho u^2 + P_3 \quad (1)$$

$$\frac{1}{2}\rho u^2 + P_2 = \frac{1}{2}\rho u_1^2 + P_0 \quad (2)$$

The thrust T_a on the rotor is then

$$T_a = A(P_3 - P_2) \quad (3)$$

$$T_a = \rho A(V_0^2 - u_1^2)/2 \quad (4)$$

$$\text{as } Au = A_1 u_1, \text{ then we find that } u = (V_0 + u_1)/2 \quad (5)$$

Defining an axial interference factor, a , as the fractional decrease in wind velocity between the free stream and the rotor plane represented by $a = \frac{v}{V_0}$, if $v = V - u$, then by analysing this equation by substituting $v = V_0 - u$ into $a = \frac{v}{V_0}$,

then eventually a becomes $\frac{V_0 - u}{V_0} = 1 - \frac{u}{V_0}$; and gives

$$u = V_0(1 - a) \quad (6)$$

Substituting u to Eq. (5). downstream wind velocity from the rotor disc, u_1 is obtained as

$$u_1 = V_0(1 - 2a) \quad (7)$$

If $a = 0$, it means that wind is not disturbed by any factors and the power is obtained minimum value, whereas for $a \neq 0$, the wind is retarded and without the presence of flow, and at $a = 1$ no power is generated by the wind rotors. In this theory, the obtained energy removed by rotor per unit time, P_w is

$$P_w = \frac{1}{2}\rho V_0^2 A u - \frac{1}{2}\rho u_1^2 A u; \text{ and substituting } u \text{ and } u_1 \text{ in terms of } a \text{ gives}$$

$$P_w = \frac{1}{2}\rho A V_0^3 4a(1 - a)^2 \quad (8)$$

The amount of power available, P_a , in freely flowing in cross section area, A , for this theory is

$$P_a = (\text{volumetric flow rate}) \times (\text{kinetic energy per unit volume})$$

$$P_a = (AV_0) \times \frac{1}{2}\rho V_0^2 = \frac{1}{2}\rho A V_0^3$$

Then define a power coefficient, C_p , as:

$$C_p = \frac{P_w}{P_a} = \frac{\frac{1}{2}\rho A V_0^3 4a(1 - a)^2}{\frac{\rho A V_0^3}{2}} \quad (9)$$

$$\text{So that } C_p = 4a(1 - a)^2 \quad (10)$$

Obtaining a maximum C_p as function of a gives $a = 1/3$. The following section explains the solution and how to obtain a value by the differentiate method.

From Eq. 10 C_p becomes:

$$C_p = 4a - 8a^2 + 4a^3$$

$$\frac{dC_p}{da} = 4 - 16a + 12a^2$$

Defined $\frac{dC_p}{da} = 0$ gives:

$$12a^2 - 16a + 4 = 0$$

$$3a^2 - 4a + 1 = 0$$

$$a = \frac{4 \pm \sqrt{(-4)^2 - 4 \times 3 \times 1}}{2 \times 3}, \quad a = \frac{4 \pm \sqrt{4}}{6}$$

$$a = \frac{2}{3} \pm \frac{1}{3}, \quad a = 1 \text{ or } a = \frac{1}{3}$$

In reality, it is impossible to get a value equal to 1, because this situation will happen only where the wind will not pass through the rotor blade. Only one practical case can occur with an axial interference factor $a = 1/3$. Substituting $a = 1/3$ to equation (10) gives $C_{p_{\max}} = 0.59259$. Therefore, for the wind turbine of the best rotor design, it is evidently not possible to extract more than about 60 percent of the kinetic wind energy.

Also substituting $a = 1/3$ in Eq. (6) and (7) gives, $u = \frac{2}{3}V_0$ and $u_1 = \frac{1}{3}V_0$

Additional data that can be derived from this model include the thrust loading on the rotor. The thrust on the turbine rotor is:

$$T_a = \frac{1}{2} \rho V_0^2 A [4a(1 - a)] = qA [4a(1 - a)] \quad (11)$$

Where q is the dynamic pressure $= \frac{1}{2} \rho V^2$ and a thrust coefficient is defined as:

$$C_t = \frac{T_a}{qA} \quad (12)$$

2.4.2 Betz theory (Betz Limit)

This first global theory to analyse the wind machine was established by A. Betz of the Institute of Gottingen (1926). Fig. 2.11 illustrates the imaginary tube, so called the stream tube. This figure is used for proving Betz' theorem. According to Betz theory, the wind

speed slows down gradually behind the rotor, until the speed of the wind becomes almost constant. The reasonable assumption is that the average wind speed through the rotor area is the average of the undisturbed wind speed before the wind reaches the rotor, V_1 and after the wind passes through rotor V_2 . The average wind speed through the rotor area is $\frac{(V_1+V_2)}{2}$.

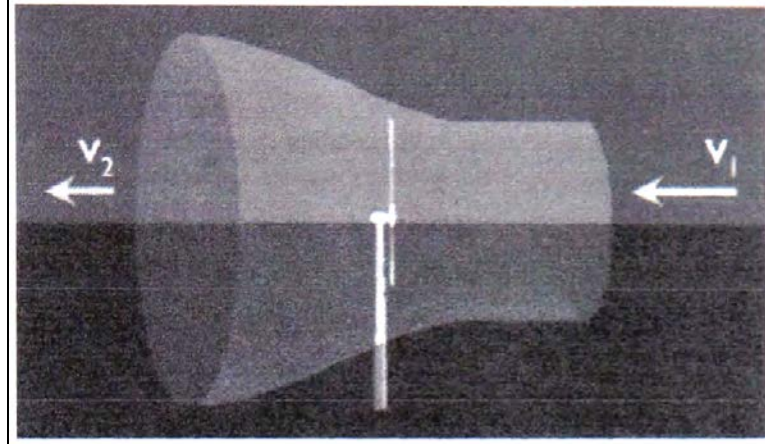


Fig. 2.11 The stream tube [3]

The mass of the air flow passing through the rotor area per second is given by

$$m = \frac{\rho A(V_1 + V_2)}{2}$$

where A is the swept rotor area.

The power extracted from the wind by rotor, P is equal to the mass times the drop in the wind speed squared. According to the kinetic energy, $KE = \frac{1}{2}mV^2$

Therefore the power extracted, $P = \frac{1}{2}\rho A(V_1^2 - V_2^2)$

Then, if substituted mass, $m = \frac{\rho A(V_1+V_2)}{2}$ in the power extracted, P equation the actual power extracted from the wind, P_w is then obtained as follows

$$P_w = \frac{\rho}{4}(V_1^2 - V_2^2)(V_1 + V_2)A \quad (13)$$

Thus P_w is calculated from equation 13.

The actual available power P_a for wind speed V_1 is as follows

$$P_a = \frac{1}{2}mV_1^2 \text{ when } m = \rho AV_1 \text{ then } P_a = \frac{1}{2}\rho AV_1^3 \quad (14)$$

The ratio between the power extracted from the wind, P_w and the actual power available P_a is then shown as a power coefficient C_p .

$$\frac{P_w}{P_a} = C_p \quad (15)$$

From this equation it can be seen that C_p is a function of V_2/V_1 , as given in Figure 2.12.

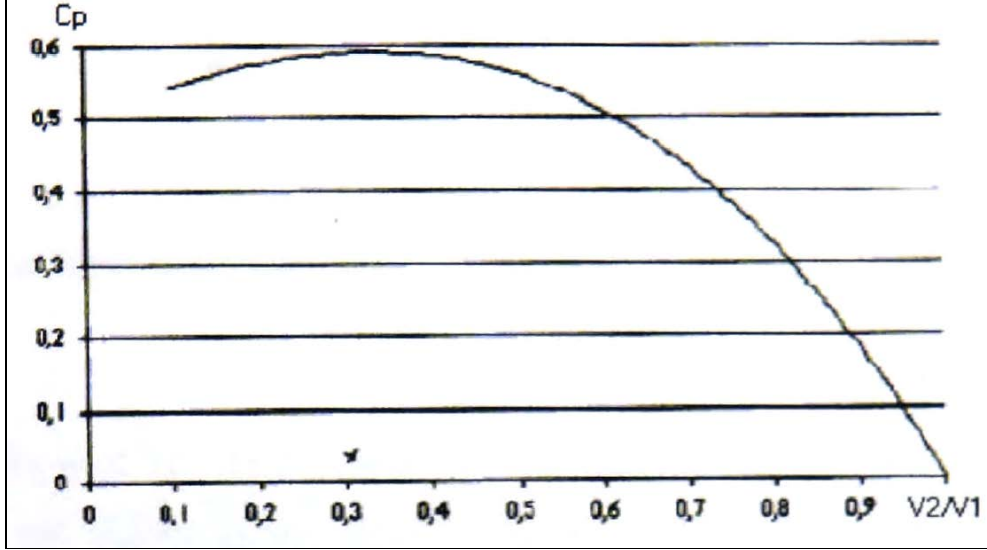


Fig. 2.12 C_p versus V_2/V_1 in Betz' limit

Fig. 2.12 shows that the function reaches its maximum at $V_2/V_1 = 1/3$ generating the maximum power coefficient, C_p of the wind machine.

The theorem suggests that $C_p \text{ max} = 16 / 27 \approx 0.59259$ when $V_2/V_1 = 1/3$ (See Fig. 2.13)

(Betz limited)

However, the differentiation of Eq. 15 by assuming that the upstream velocity V_1 is known then $\frac{dP_w}{dV_2}$ can be calculated

$$\frac{dP_w}{dV_2} = \frac{1}{4} \rho S (V_1^2 - 2V_1V_2 - 3V_2^2)$$

The $\frac{dP_w}{dV_2} = 0$ can be true in two solutions:

1. $V_2 = -V_1$ which has no physical meaning in stream tube
2. $V_2 = \frac{V_1}{3}$ which corresponds to the maximum power

Fig. 2.13 shows the typical performance characteristics wind machines.

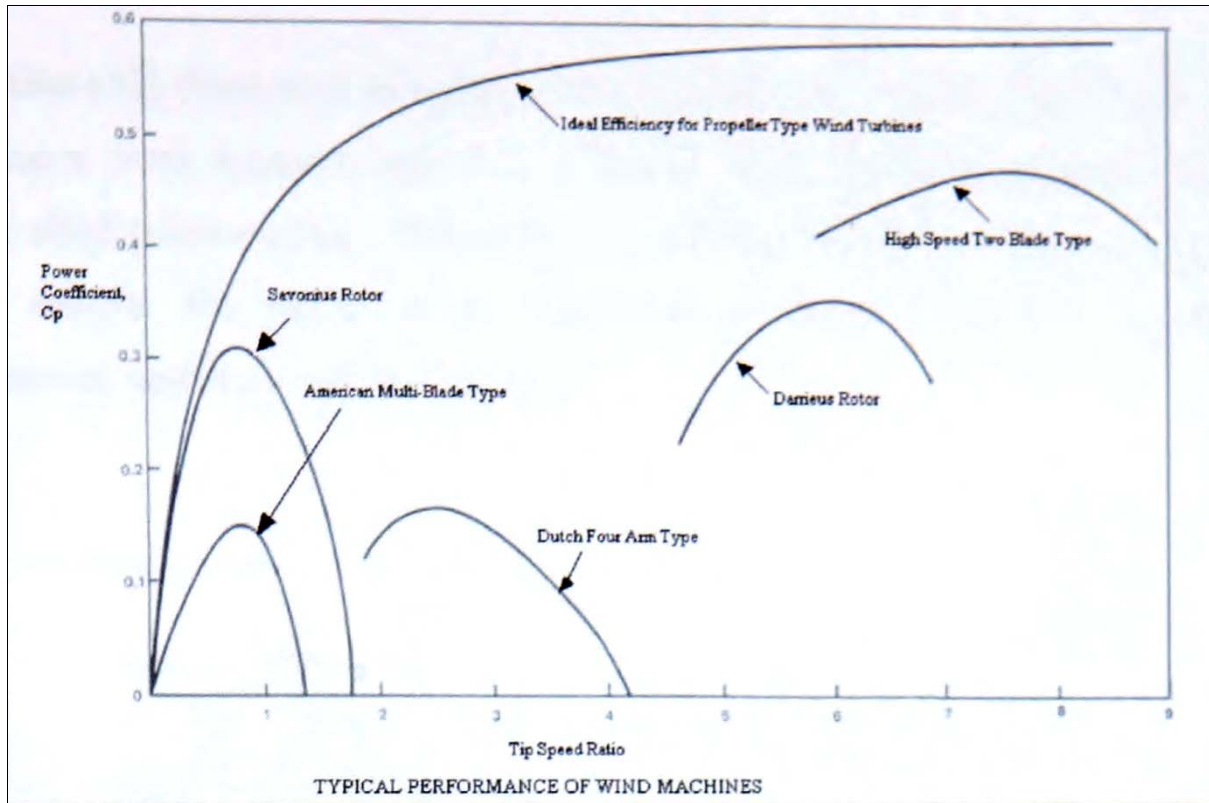


Fig. 2.13 The ideal windmill and various models of power coefficient modified from [25]

This thesis focuses on optimisation of VAWTs, therefore, the main investigation and observation will relate to this type of machine. HAWTs are of course not the main interest in this thesis. The following section presents a review of various types of VAWTs.

2.5 Review of Darrieus wind machine (D-rotor)

2.5.1 Performance analysis

The aeroelastic analysis of the blades of Darrieus wind machine is fairly complicated. In reality the flow about this wind machine is three-dimensional, viscous, and unsteady. Its direct simulation is very complicated because: (1) the flow fields vary with the turbine blade angle, (2) the turbine blade will need to go through the wake path of the previous blade, and (3) the blades are curved. In 1979 De Vries [28] classified the vertical axis wind turbines theorems into the following groups:

- (1) Multi-stream tube method, which is attributed to Strickland [29]
- (2) Momentum theory, which is a modification of Glauert's method [30]
- (3) Vortex method, which is attributed to Holmes [31]

A. Allet [32] developed computer codes to predict the performance of the curved blade Darrieus wind machine (see Fig. 2.14) by applying the momentum equations to a controlled volume of air. This study also includes viscous, stochastic wind and dynamic stall effects. The results of the investigation shown in Fig. 2.14 demonstrate good agreement with the experimental data.

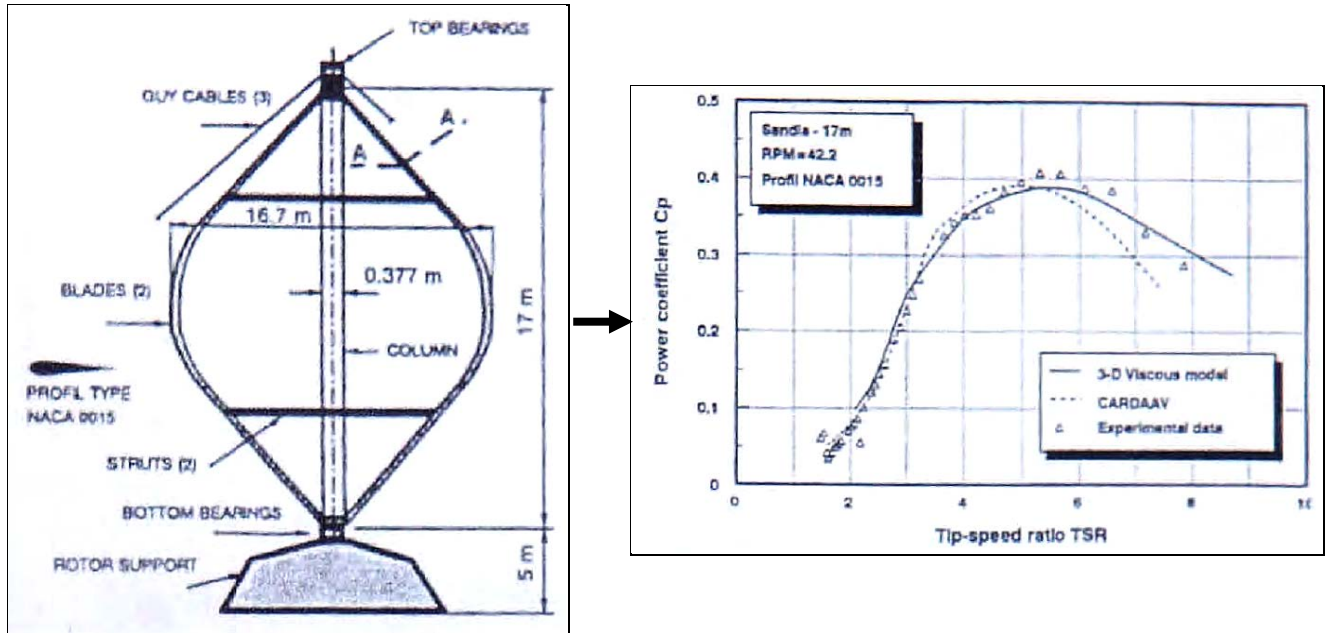


Fig. 2.14 Sandia 17-m VAWTs and its performance predictions [32]

Flow curvature and dynamic stall simulated with an aerodynamic-free vortex model for VAWT has been investigated by Jose L. Cardona [331]. The study modified the vortex model, which is described in Strickland [29]. This modified model included the dynamic stall condition and the camber of profile. The computer code corresponding to this study was written in Fortran IV language. The predictions of the instantaneous aerodynamic forces upon the vertical axis straight-blade wind turbine are notably improved.

M. N. Nahas [34] proposed a new design concept to improve the performance of the vertical axis wind turbine using momentum theory and modification of Glauert method [30]. I-Es machine was a straight blade Darrieus wind machine. This new design makes the wind machine generate torque and power at low rotational speed. Additionally, the effect of the geometry on performance was also analysed. The results of this study indicated that the solidity σ , affected the performance of Wind machine (see Fig. 2-15). The result indicated that as the value of solidity increased from 0.06 to 0.14, the maximum power coefficient is increased from 0.273 to 0.335. Additionally, as the solidity increased above 0.14, the maximum power coefficient is reduced.

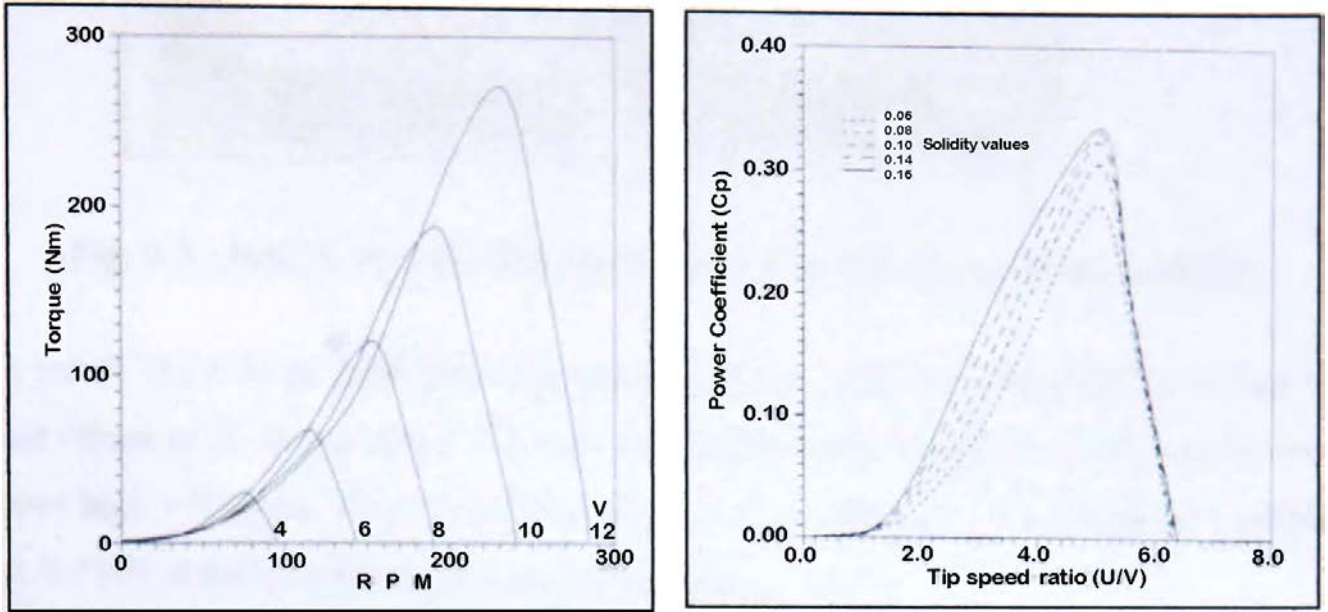


Fig. 2.15 Various of torques and power coefficients versus tip speed ratios for different value of solidities from [34]

More information on the research and development of the prediction models for VAWTs can be seen in ref. [35-37].

2.5.2 Survey of the study of the Darrieus rotor

The Darrieus forms of VAWT are potentially far more efficient and economical than Savonius rotors but typically suffer from one serious drawback. The Darrieus rotors have poor performance at low values of the tip speed ratio X due to the cyclic variation in angle of wind attack resulting in low lift force and generate low torque during starting operations. Fig. 2.16 shows how lift coefficients of NACA 661-212 section vanes with rotor blade position (γ) (0-360 degree) at some certain rotor revolutions (rpm).

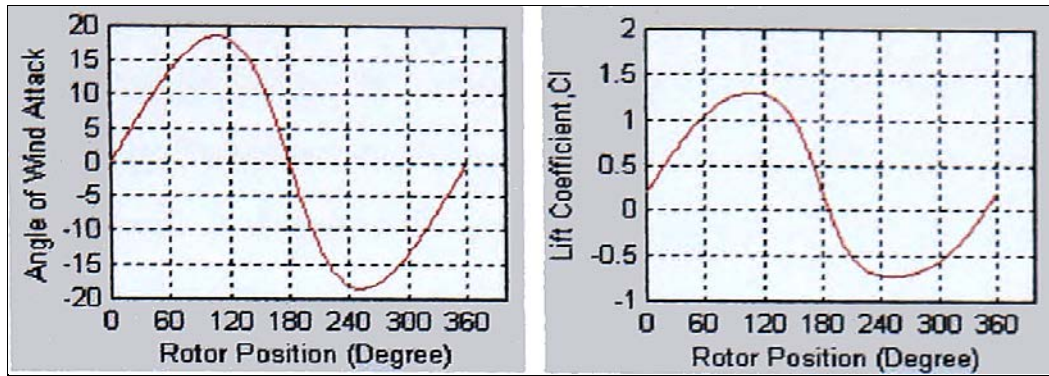


Fig. 2.16 NACA 661-212 lift coefficients at 0-360 degree blade position

As a result, most fixed pitch Darrieus turbines do not reliably self-start and it is only at higher values of X , above about 2-3, that the blades remain unstalled and the turbine can achieve high efficiency. Even Kentfield, who developed a form of self-starting variable pitch VAWT states in a recent publication (Kentfield, 1996).

"The Darrieus turbine... is inherently non self-starting"

This is true of typical fixed pitch Darrieus machines but not of the variable pitch machines based on the Darrieus principle. Fig. 2.16 and 2.17 illustrates the lift coefficient generated by different aerofoil profiles.

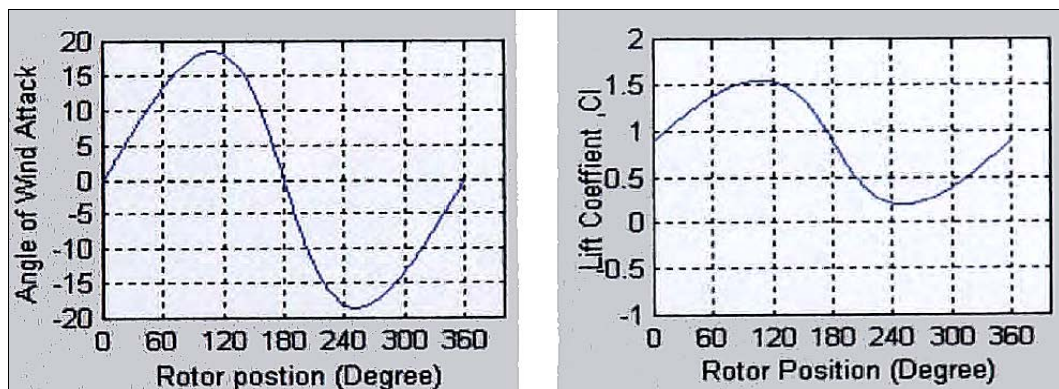


Fig. 2.17 S1223 lift coefficient at 0-360 degree blade position

Fig. 2.16 presents the lift coefficient for rotor position (γ) 0-360 degree of symmetrical aerofoil NACA 661-212. The graphs show that at rotor position over 180-degree the lift coefficient becomes a negative value, which is not preferred for wind turbine design for stand-alone application. Fig. 2.17 illustrates that using camber blade high lift aerofoil S1223 the self-starting problem could be overcome. It shows the positive lift coefficients along the whole range of rotor blade position, which is due to the fact that the turbine generates enough torque to start the rotor without any auxiliary devices.

B. K. Kirke and L. Lazauskas [38] (1991) indicated that using their studies of variable pitch system, starting problem may be overcome by means of a simple and Inexpensive variable pitch system in which the blade pitch is self-adjusting. This self-adjusting pitch control concept which is determined by the interplay of two opposing moments on each blade: (1) Pitching moments generated by aerodynamic forces on the rotor blade which tend to reduce the angle of Wind attack and (2) Stabilising moments generated by inertial forces which tend to maintain each blade at zero pitch. These arrangements are shown schematically in Fig. 2.18. However, only mathematical modelling prediction was presented with positive results. And, this study also showed that the wind machine with fixed-blade could start rotor itself at high value of solidity (see Fig. 2.19).

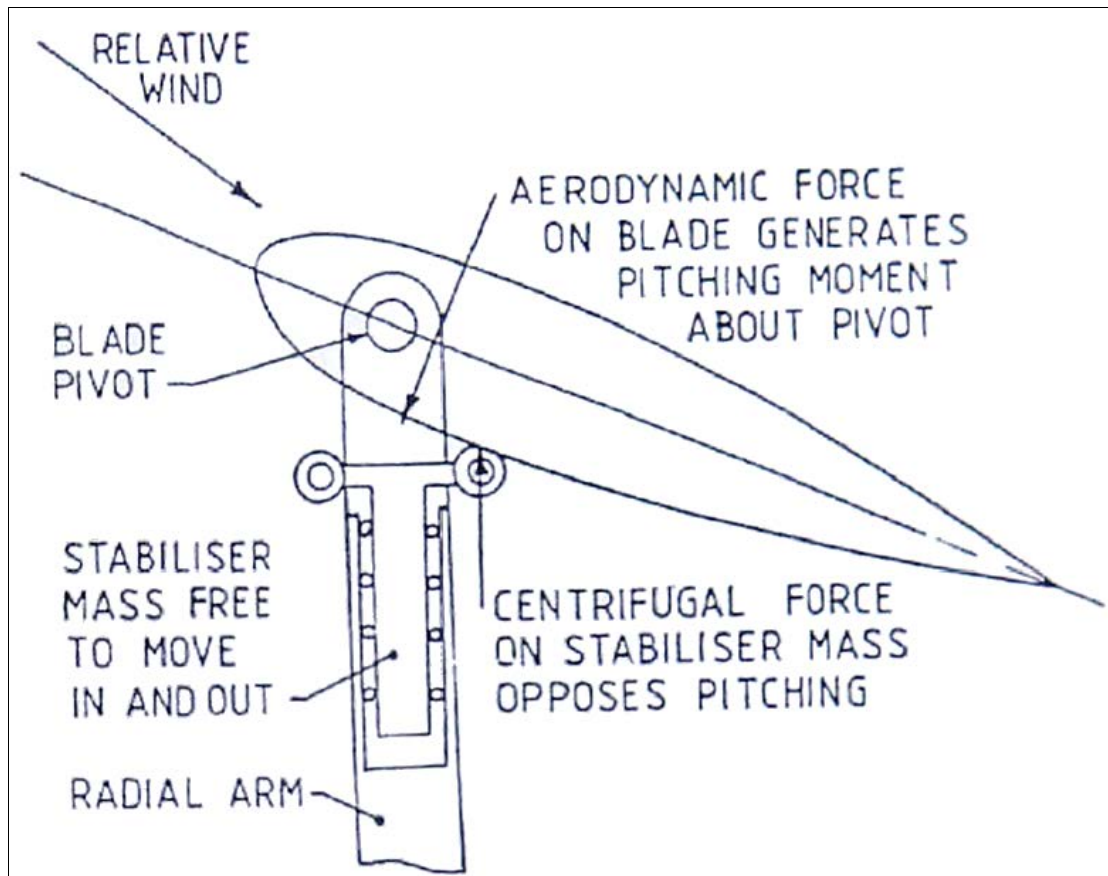


Fig. 2.18 Schematic representation of a stabilised self-acting pitch control system [38]

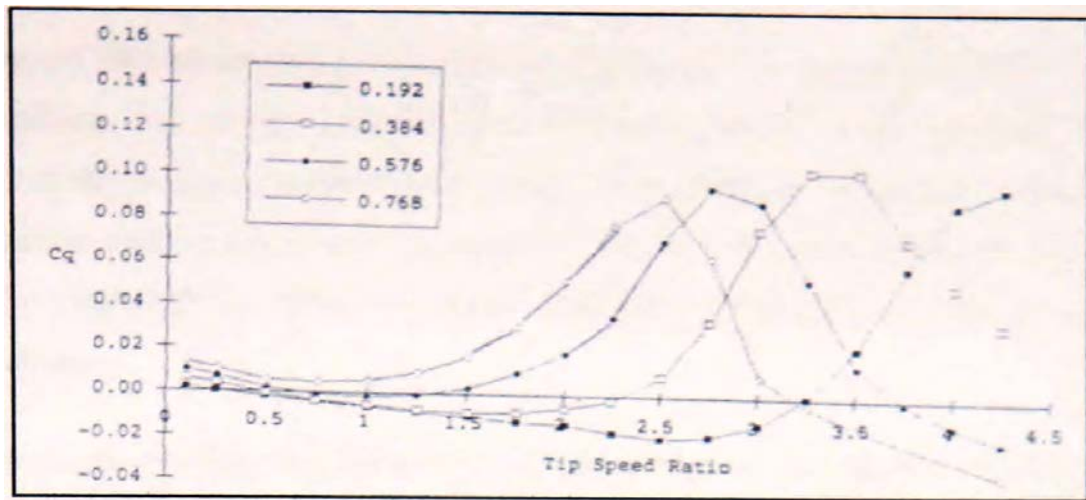


Fig. 2.19 The effect of solidity on the low speed torque coefficient of fixed pitch turbine [38]

Nevertheless, even the variable pitch control could be applied to the Darrieus wind machine. It was concluded that an ideal pitch control system could theoretically yield some further improvements in performance, and it would be much more complex, and expensive to achieve in reality. The evaluation of a variable pitch VAWTs has been also presented in the investigation by N. C. K. Pawsey and A. J. Barratt [39]. Their design concept is shown in Fig. 2.20; this principle of design is to attach a flyweight to the blade so that the centre of mass of assembly lies on a radius extended from the turbine central axis. The results of this design concept leads to the rotor blade seeking a zero pitch position under the influence of the inertia force during the turbine rotation. The blade pitch is used to reduce the angle of wind attack to the optimum value, at high tip speed ratios.

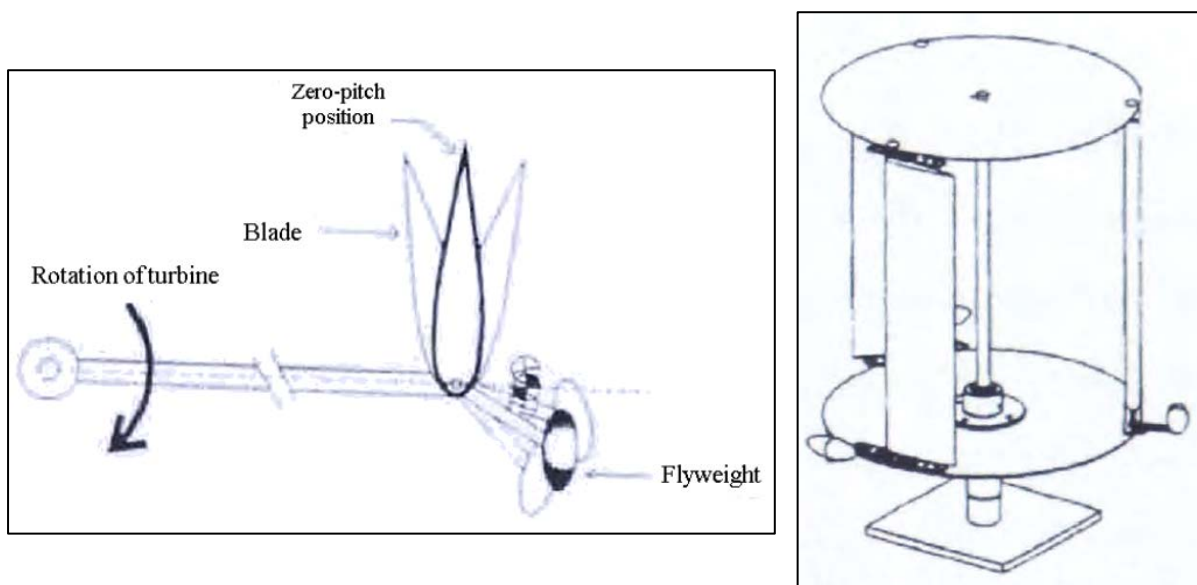


Fig. 2.20 The schematic representation of pivoting blade arrangement and turbine design model from [39]

The conclusion of the study of a turbine of diameter 2.4 m and solidity 0.36 showed that the power coefficients at tip speed ratio lower than 3.5 are greater than those of the fixed blades VAWTs. It is concluded that their design of passive pitching mechanism would be suitable with a micro or a small Darrieus Wind machine only. Therefore, this design is not compatible with a bigger machine because of the complication of the mechanism system.

Self-starting process of the Darrieus wind turbine also has been studied and investigated by S. Rajaoferson and R. Comolet [40]. They built a small scale Darrieus wind machine and predicted that with some mechanical care the auxiliary, motor is unnecessary. However, their machine failed to start itself but showed that at solidity $\sigma > 2$ the machine had the best self-starting condition. The friction of the bearing and the inertia of the wind machine were found to be the major obstructions to self-starting. P. Vittecoq and A. Laneville [41] constructed a small scale wind machine, the radius and height of the rotor were respectively 0.3 m and 0.6 m with 2 rotor blades. Their wind machine rotor blades were made from balsa wood using the symmetrical aerofoil NACA 0018 with the solidity $\frac{c}{r}$ of 0.2. The results of their investigation showed that the wind machine would not self-start with a dynamic stall condition at tip speed ratio $X < 3.5$.

In 1981, a vertical axis cyclogiro type of vertical axis wind machine was presented with good results by D. Bayly and J. A. Kentfield [42]. They designed and constructed a straight blade Darrieus With freely-hinged blades. This wind machine was constructed and tested in the open air to provide experimental verification. The machine was a high blade solidity of 0.2 with 4.57 meter diameter in order to minimise the blade stress problem. The turbine rotor blades were made from the NACA 643-018 aerofoil section. The blades were of build-up construction using a rectangular, cross-section main spar, pressed aluminium ribs and a sheet aluminium skin. The prototype (Fig. 2.21) was tested which achieved the power coefficient of 0.37 at tip speed ratio about 3.6. This wind machine showed a better performance than the curved blade Darrieus wind machine. This wind machine was found to self-start easily at high wind speed about 7 m/sec. However, this machine did not become attractive in building a scaled-up version.

Martino Marini et. al [43] states in the publication in 1989 that “the fluid dynamic aspects of vertical axis wind turbine can be investigated in a fruitful way by interfacing experimental measurements and theoretical studies”.

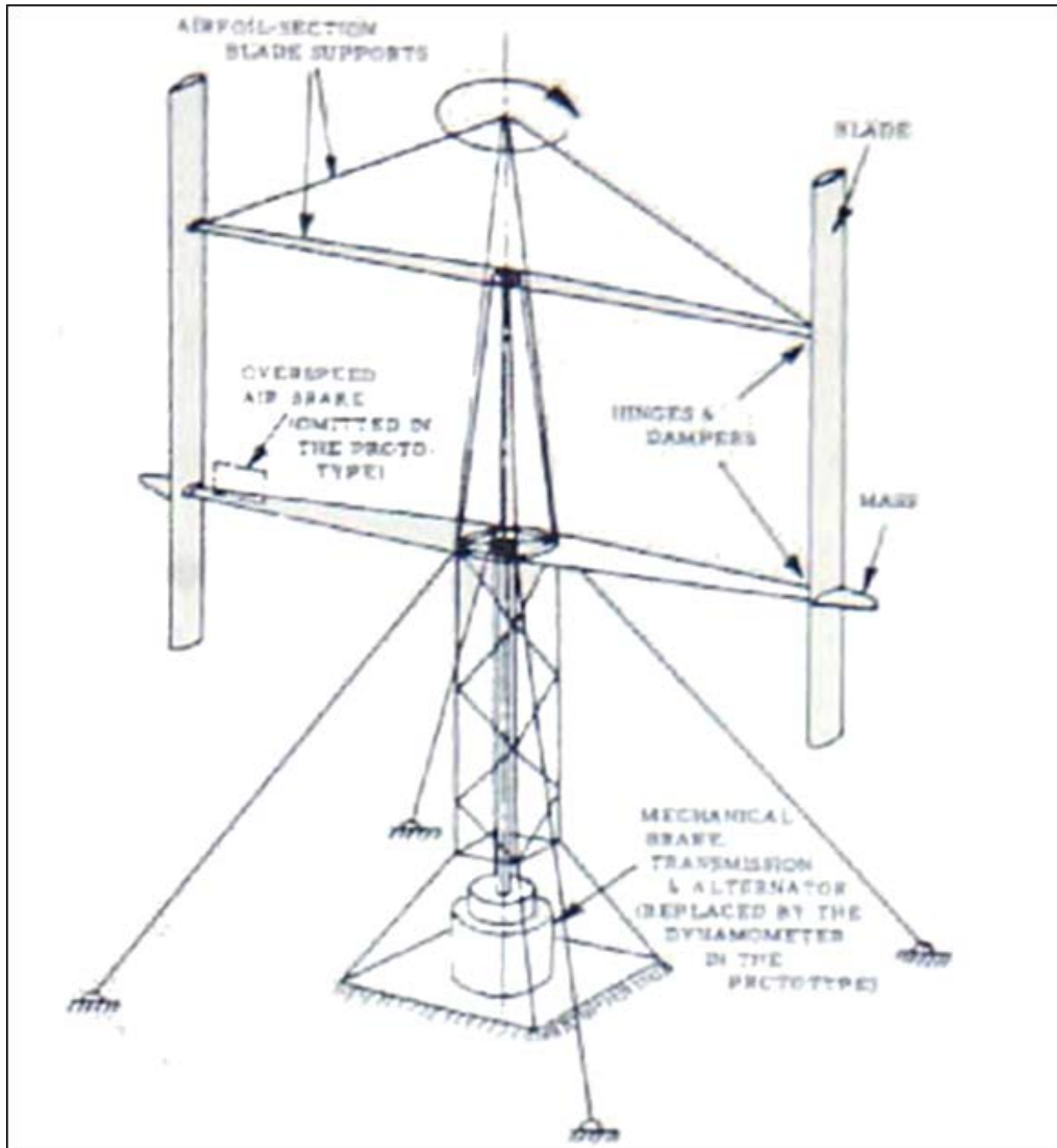


Fig. 2.21 A diagram illustration of the cyclogiro wind turbine [42]

A wind turbine with 3 blades of 6-meter diameter (see Fig. 2.22 (a)) was constructed to compare experiment results with the analytical analysis. The rotor for this wind machine was made by using the NACA 0012 profile section at a solidity of 0.15. The results of this study showed that the Wind machine solidity (σ) is a very important consideration in order to make the turbine self-start and retain the high power coefficient (Fig 2.22(b)). Additionally, they concluded that the experimental results agreed with the analytical results and also indicated that the information on air wakes is useful in arranging a group of wind machine near each other to estimate the environmental impact on a large scale.

Original Darrieus wind turbine designs had curved blades (See Fig. 2.14). This form of VAWT is sometimes referred to as the "eggbeater". The reason for adopting this shape is to minimise the bending moments in the blades caused by centripetal acceleration so that the blades need to only resist tensile forces and can be made very slender, thereby reducing costs. However this shape cannot entirely eliminate the bending moments [32] caused by the varying combinations of aerodynamic, gravitational and inertial forces encountered in service. Darrieus rotors can also be built with straight blades fixed to the radial arms (used in this thesis). Nevertheless, most research indicates that whether the blades are curved or straight, if they are of fixed pitch the VAWT typically develops little or no torque at low speeds and so must be motored up to speed, making it unsuitable for stand-alone operation with non-electrical loads. The objective of this study is to optimise the vertical axis wind turbine, which will minimise cost of construction, allow easy building and show good performance with self-start. Several ways to overcome this problem have been suggested in the literature as described in previous parts. And the investigations of suitable aerofoil shapes need to overcome the main disadvantages for vertical axis wind machine.

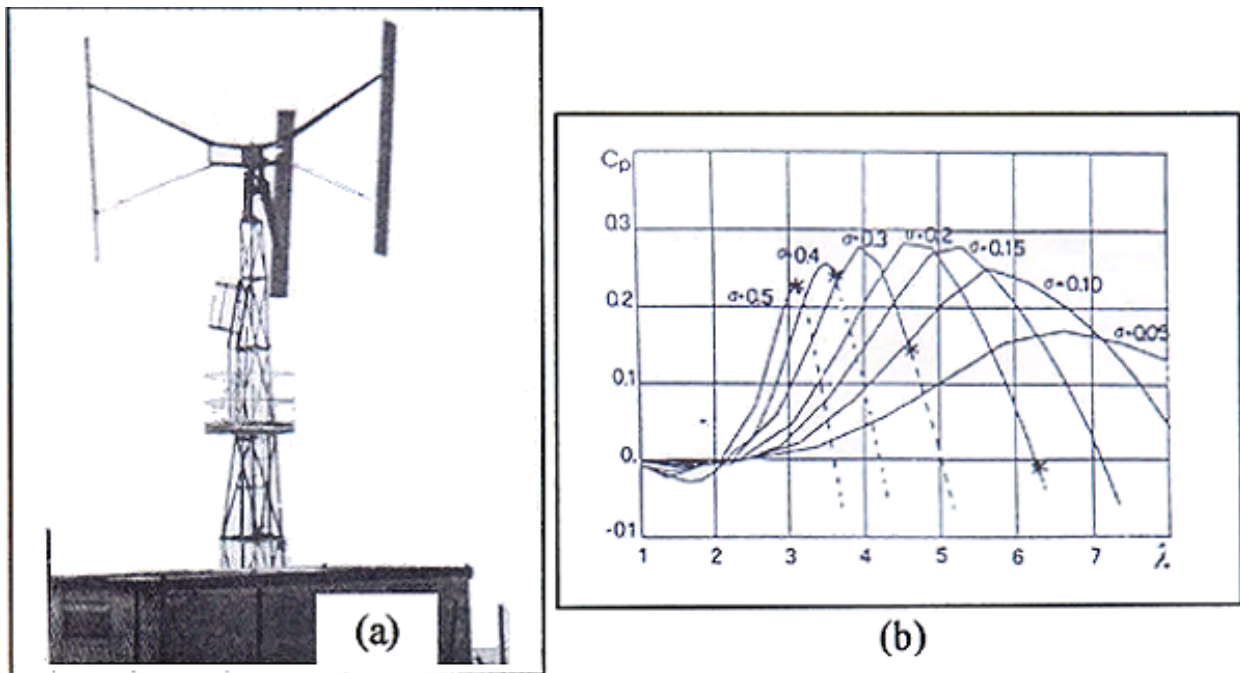


Fig. 2.22 (a) Experimental prototype and (b) effect of the rotor solidity on the wind machine performance [43]

2.6 Review of the Savonius Wind machine (S-Rotor)

2.6.1 The power coefficient C_p analysis

The relation between the power coefficient C_p and the wind speed can express the basic theory of this wind machine. Basically the power that the rotor can extract from the wind P , is less than the actual available from the wind power P_a . In order to calculate the performance

of this wind machine, the configuration of this wind machine which can be seen in Fig. 2.23 is essentially important. Practically, when the turbine is placed in a wind tunnel (Fig. 2.24), the power can be extracted from the wind and can be found by the following steps:

- Find the average of wind speed through the rotor area is $\frac{(V_1 + V_2)}{2}$ where V_1 and V_2 are the inlet and outlet wind speed in m/sec respectively.
- Define the mass of the airflows passing through the S-rotor area, A per second in stream tube by $m = \frac{\rho A(V_1 + V_2)}{2}$.
- And according to the kinetic energy, $KE = \frac{1}{2}mV^2$
- Therefore the power extracted, $P = \frac{1}{2}\rho A(V_1^2 - V_2^2)$. Then substituting the mass of air to this formula the power that rotor can be extracted from the wind is

$$P_w = \frac{\rho}{4}(V_1^2 - V_2^2)(V_1 + V_2)A, \text{ when swept area } A = h(2d - e) = h \times D, \text{ m}^2$$

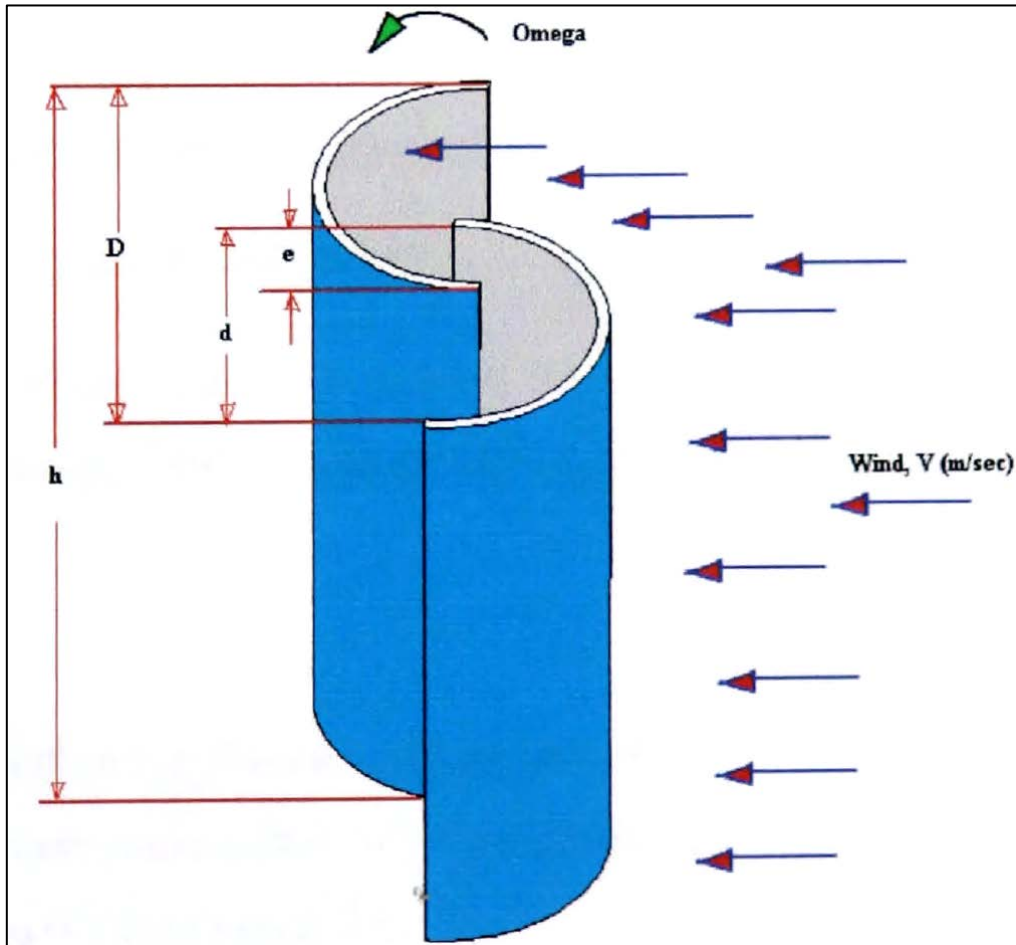


Fig. 2.23 The Savonius rotor configurations

Similarly, if the S-rotor generates the electricity, the power that the rotor can extract from the wind is $P_w = E \times I$ (Watt). The available power, P_a from the wind is

$$P_a = \frac{1}{2} m V_1^2 = \frac{1}{2} \rho A V_0^3 \text{ when } m = \rho A V_1; \text{ therefore } P_a = \frac{1}{2} \rho A V_1^3.$$

The power coefficient C_p is given by

$$C_p = \frac{P_w}{P_a}$$



Fig. 2.24 S-Rotor in the wind tunnel test

The power coefficient C_p and the torque coefficient C_m are related to each other. The power coefficient C_p can be calculated by the equation $C_p = C_m X$. Where $X = \frac{R\omega}{V}$, where R = radius of rotor (m), V = average wind velocity (m/s), ω = circumferential velocity of the rotor (radian/sec) and the driving torque M is given by

$$M = \frac{1}{2} \rho C_m R A V^2$$

According to Canadian experiments [3] the best results for the torque and power are obtained for the rotor constructed with a parameter $e/d = 1/6$ and the maximum power coefficient reaches 0.3 (see Fig. 2.25).

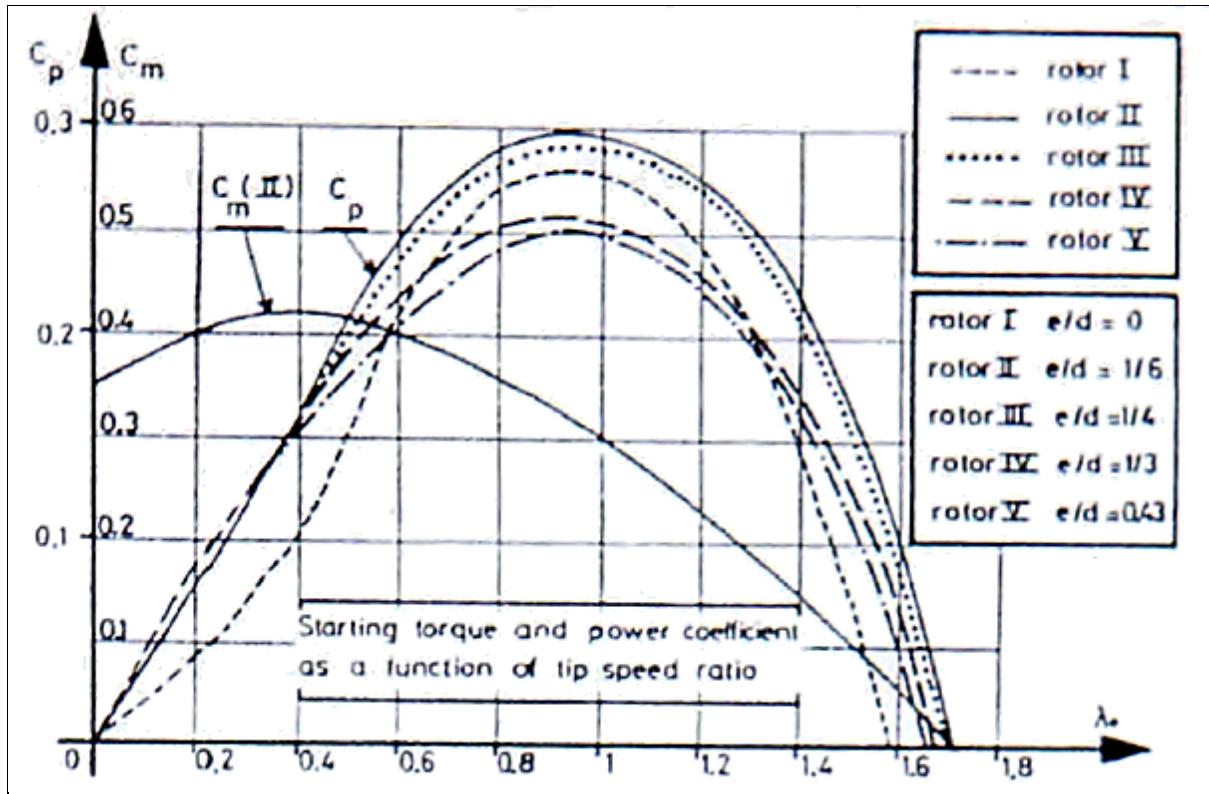


Fig. 2.25 The performance of a Savonius rotor as a function of ratio e/d [3]

2.6.2 The survey of the study of the Savonius wind machine

The Finish engineer Sigur Savonius invented this wind machine in 1924 and it was patented in 1929 [3] Fig. 2.26. This machine is based on drag force and similar to principle of a paddle propelling a vehicle through water. Therefore, if there is no slip between the paddle and water, the maximum speed attained will be same as the tangential speed of the paddle. Similarly in a drag force based wind machine, the speed at the tip of the turbine blades can seldom exceed the speed of the wind. Generally, this wind machine has not been widely developed commercially due to its low rotation speed and efficiency. In general however, it is simplest of vertical axis wind machine and economical for small power generation [44]. This machine also works on the same principle as a cup anemometer.

Basically, it consists of two half cylinders whose axes are offset relative to one another (see Fig. 2.26). The Savonius rotor produces torque by the pressure difference between the concave and convex surface. The maximum of power coefficient of this wind is approximately 31 %. And it requires about 30 times more surface for the same power output as a conventional Wind rotor. The following section presents the advantages and disadvantages of this wind machine. Advantage points: simple structure and construction, economical for small power generation, high starting torque, self-starting at low wind speed.

Disadvantage points: low power efficiency and not suitable for high-speed wind turbine. From its characteristics, this machine is very useful for applications such as pumping water for irrigation, agitating water for aeration of ponds, small scale household wind turbines and starting up Darrieus wind rotors because of its high starting torque and low cut-in speed wind velocity operation.

Izumi Ushiyama and Hiroshi Nagai [44] showed how to optimise the design configuration for this machine. This study investigated seven parameters effects on the aerodynamic performance of the rotor. There are Aspect Ratio AR, Overlap Ratio O_L , Separation Gap ratio G_P , Profile of bucket cross section, Number of buckets, Bucket endplates and Bucket stacking (see all theses parameters in Fig. 2.26). In addition, this study investigates the flow around the rotor by flow visualization. This study examined all these parameters to clarify their effects on the performance of the Savonius rotors. The experiment prototypes were made form a thin steel sheet of 0.4 mm and fixed with end plates 1.0 mm. thick. From this study the following conclusions were presented:

- (1) Aspect ratio AR of 0.42 gives the best results in torque and power coefficients.
- (2) For the buckets of semi-circular cross section, the appropriate overlap O_L , is 20-30 percent.
- (3) The batch type is superior to the semi-circular type in both torque and performance at low tip speed ratio range.
- (4) The two-bucket type is generally more appropriate compared with three-bucket rotor which is inferior.
- (5) The double-stack rotor is slightly superior to corresponding single-stack rotor.
- (6) The Savonius rotor with endplate support shows greater performance compared to the rotor without endplate.

The optimum parameter for this study showed that the Savonious rotor achieved the maximum power coefficient of 0.23 at tip speed ratio of 0.8.

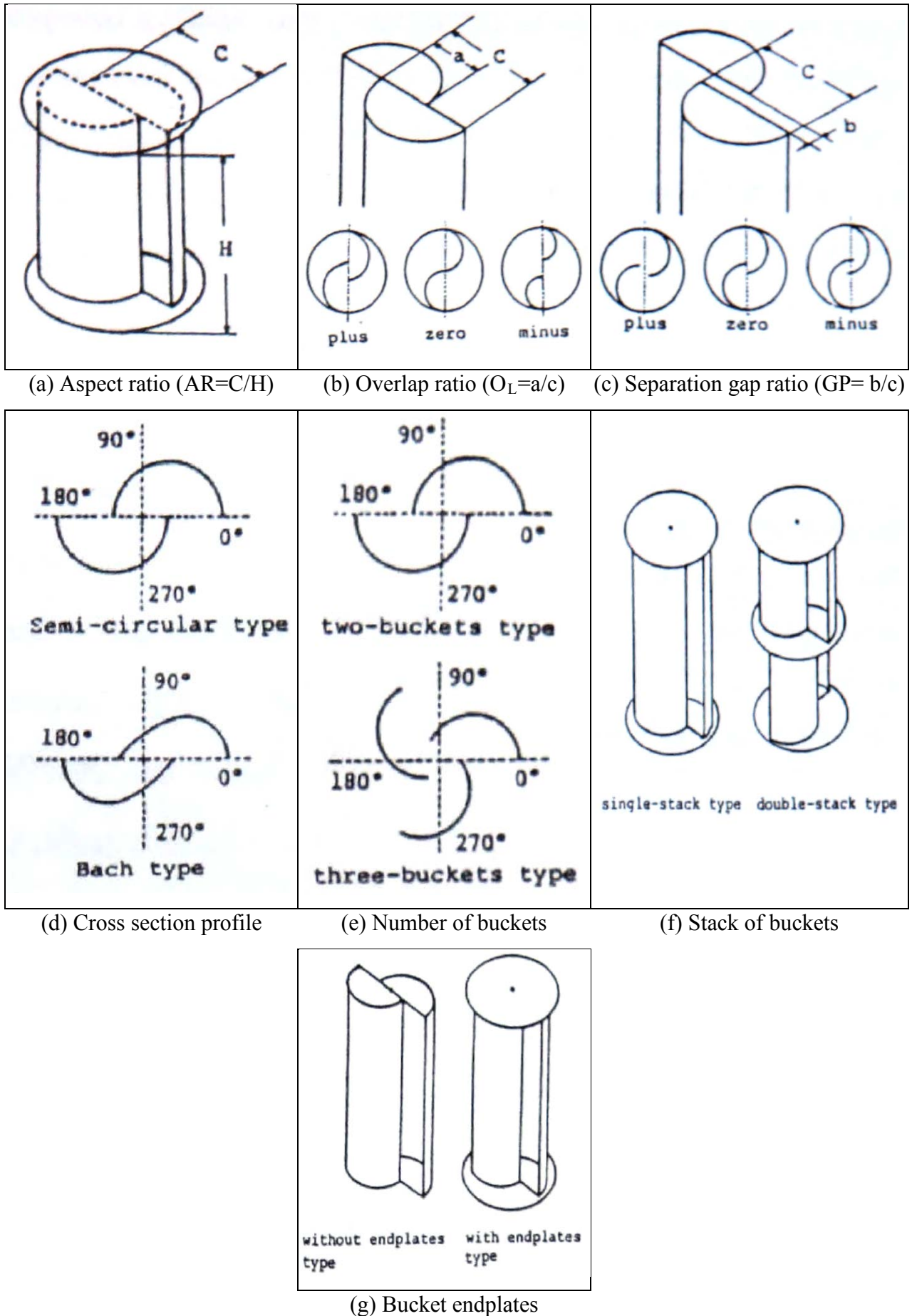


Fig. 2.26 The Savonius rotor and bucket geometry (a-g) from [44]

The blade configuration of this wind machine was also investigated by A. Savers [45]. He proposed a cheap and easily manufactured alternative prototype. This wind machine was constructed by cutting a 44-gallon (210 litre) oil drum longitudinally in halves and mounting the two halves on a vertical shaft to form an S shape of Savonius rotor. This model prototype was tested in the wind tunnel, the power and performance coefficients were determined in order to find the optimum point of the machine. The maximum power coefficient was 0.132 at overlapped ratios $0.23 < O_L < 0.29$. He also mentioned that S-rotor with end plate support generated higher performance compared with without end plate. S.J. Savomus [46] who is the originally designer for this wind machine however mentioned that the highest actual power output could reach 40 %.

In 1993, A.K.M. Sadrul [47] studied the aerodynamic characteristics of a stationary Savonius rotor. In this study, the static torques and drag coefficients of this wind machine were investigated by measuring the pressure distribution on the blade surface for various angles. The experiment (Fig. 2.27 (a)) and the predicted power coefficient for different tip speed ratios are shown in Fig. 2.27 (b) along with the measured data of others researchers.

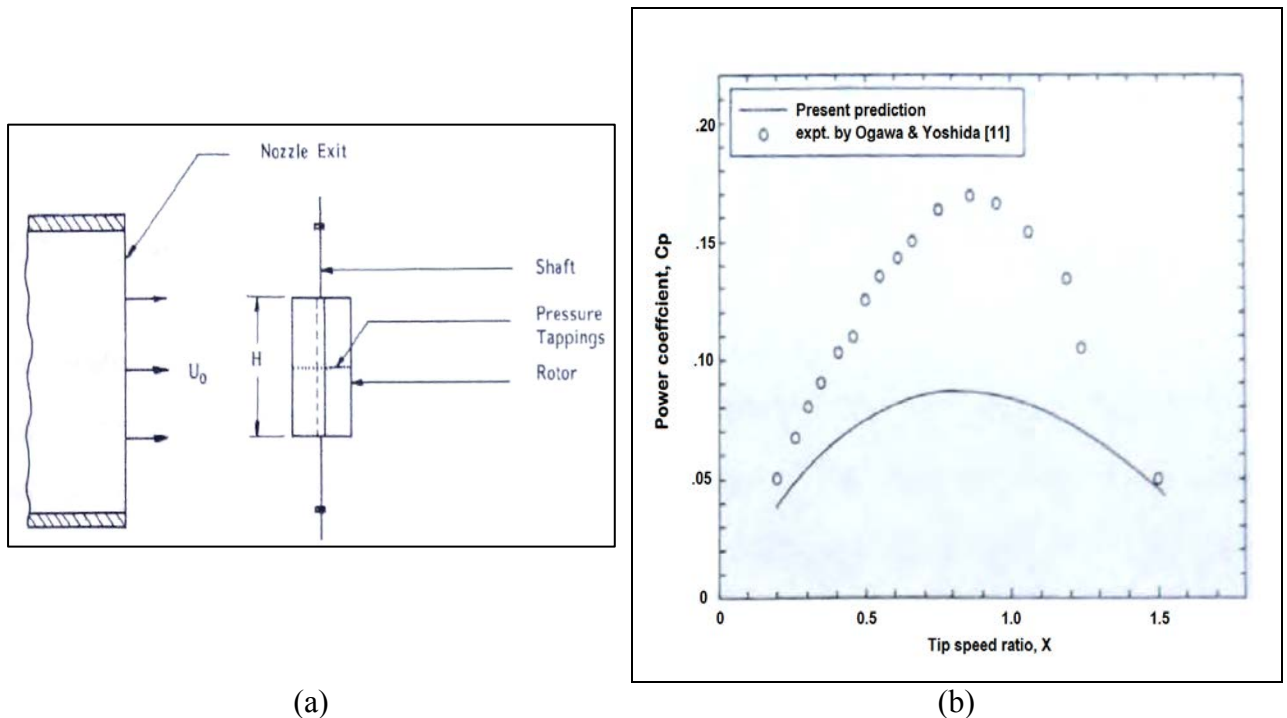


Fig. 2.27 (a) The sketch of experimental set up and (b) the results from [47]

In this technique, the pressure distribution and the torque with overlap ratio of 0.2 have been investigated experimentally. The results are summarised:

- (1) The difference in pressure on the concave and convex surfaces produces drag coefficients, C_n and C_t in the normal and tangential directions of the chord. These coefficients are functions of the rotor angle. Their resultant reaches a maximum value at rotor angle of 120 degree and minimum value at 0 degree.
- (2) The maximum static torque occurs at rotor angle about 45 degree and becomes negative in the range of 150-180 degrees rotor angle.

Nobuyuki [48] investigated the flow field in and around the Savonius rotor using the numerical analysis technique. The results showed that the measurement and numerical calculation for the rotors at various overlap ratio 0, 0.15, 0.3 or 0.35 and the tip speed ratio $X = 0.9$, the turbine produced the maximum power output. Additionally, the study suggesting that although numerical calculation can predict the basic features of flow field with the rotor angle, the flow field of a stationary rotor, especially at small rotor angles, is not well reproduced in the calculations. Therefore, the assumptions of flow separation at the tips of the blades and the two dimensionality of the flow are invalid. The wind tunnel and essentially the field test are still really important to investigate the performance of wind machines.

2.7 Combined Wind machine (D+S Rotor)

Generally, there has been limited work in this area, J. Masson and F. Diaz [49] studied this type of machine experimentally. Their experiments were carried out in a low turbulence open jet. The S-rotor was made of two half cylinders of diameter 7 cm and 20 cm height. The gap ratio e/d of 1/6 was selected [3]. The Darrieus (D rotor) was made with two symmetrical aerofoil sections of NACA 0012 type with a 0 degree attack angle. Fig. 2.28 shows the sketch definition in this study. This research indicated that the S-rotor was only positive in the starting process or when the machine runs at low rotation velocities and that its contribution was negative when the rotation velocity increased. Additionally, the study also suggested that if wind machines can self-start without S rotor, they will perform more efficiently than the Darrieus + Savonius wind machine. This project also was a balance between the centrifugal force action and the spring recovery force to adjust the Savonius rotor when the tip speed ratio increases beyond a prefixed value. Although, this wind machine gave impressive results (Fig. 2.29) by obtaining a maximum power coefficient of 0.35, the model was too complicated to make.

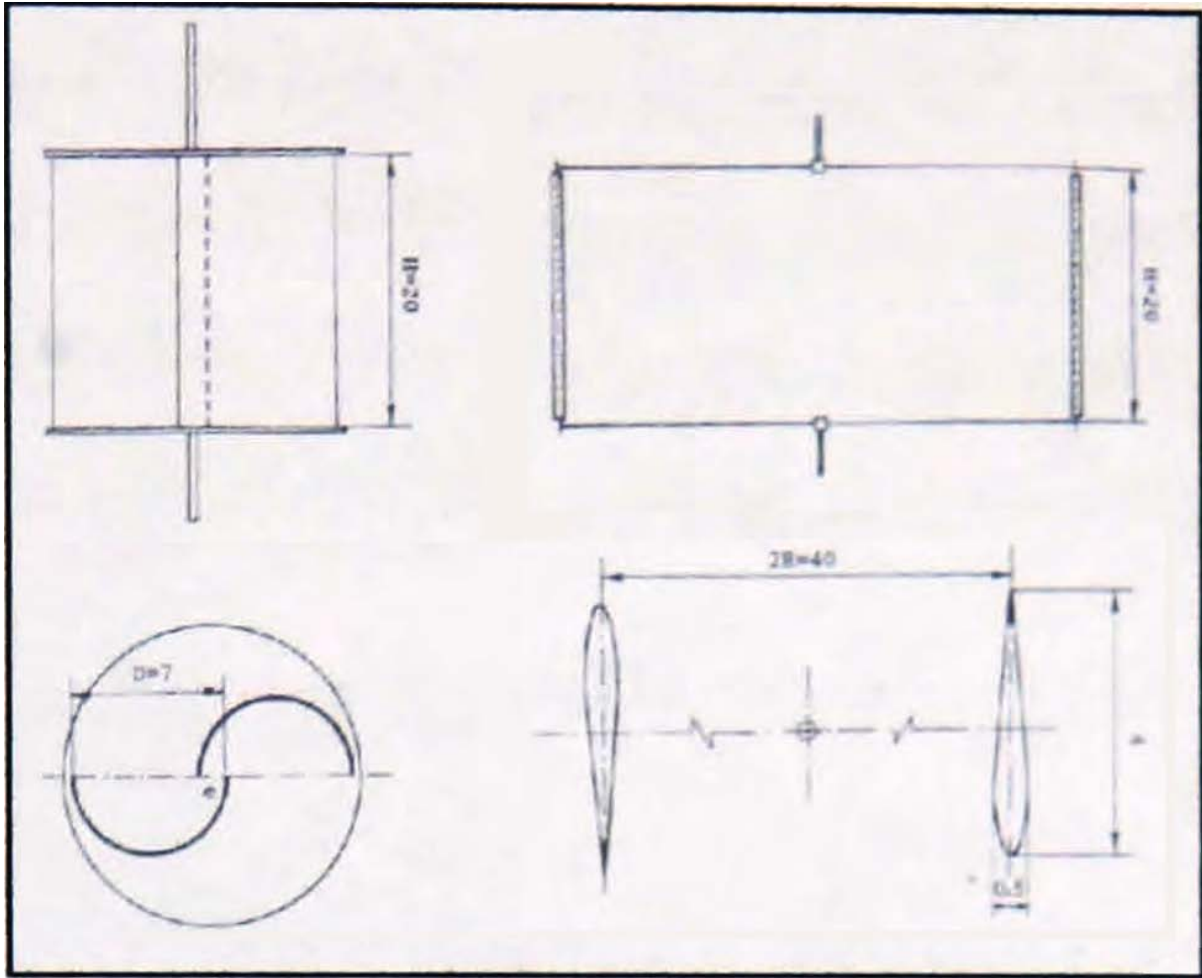


Fig. 2.28 The sketch definitions of the study of the combined wind machine [49]

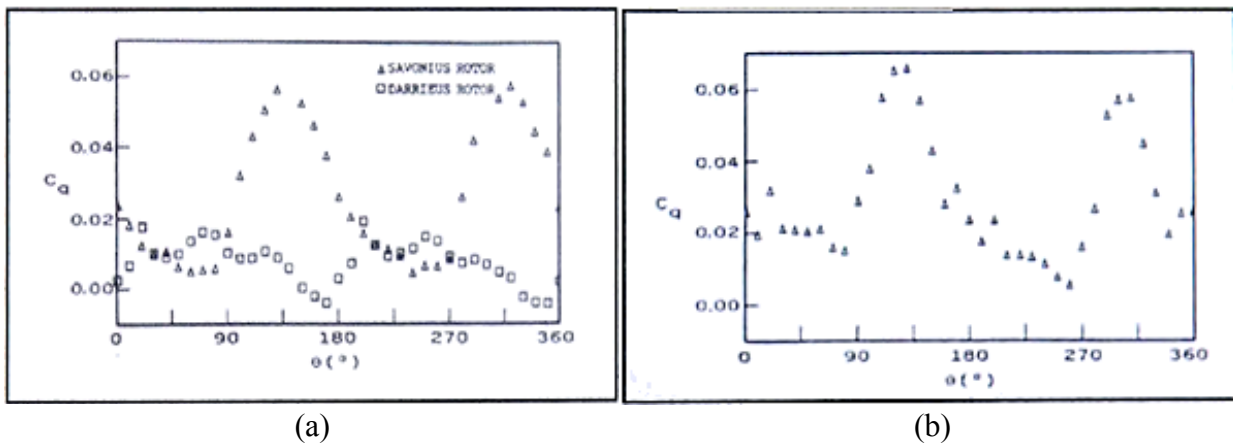


Fig. 2.29 The starting torque of S and D rotor and (b) the combined machine [49]

The combination Darrieus and Savonius wind machines was also investigated experimentally by Nobuhiro [50]. This project considered the practical application of small-scale hybrid vertical axis wind turbine. The small hybrid wind machine consisting of two vertical coaxial wind turbines; a straight blade Darrieus type (diameter and height of 720

mm) and Savonius type (diameter and height of 340, 505 mm respectively) was constructed. The Darrieus blades were made using NACA 0018 profile and the Savonius rotor is made of Bach-type buckets. In this study, the model was constructed and tested in a wind tunnel. This study investigated and confirmed the self-starting characteristics for the combined vertical wind machine. Fig. 2.30 displays the concept of power characteristics for the combined wind machine. The results of the study mentioned that at low rotational speed range, the performances for hybrid rotors were higher than those of stand-alone Darrieus rotor. However, at a higher rotational speed ranges the performances of the Darrieus rotor were higher than that for hybrid rotor. Fig. 2.31 shows the comparison of the output powers for both hybrid and Darrieus stand-alone vertical axis wind turbine.

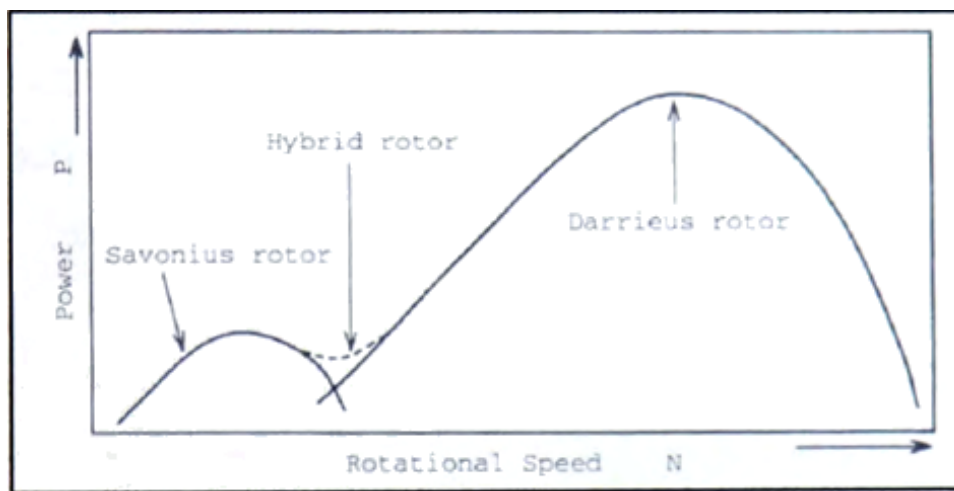


Fig. 2.30 The concept of power characteristics for hybrid wind turbine [50]

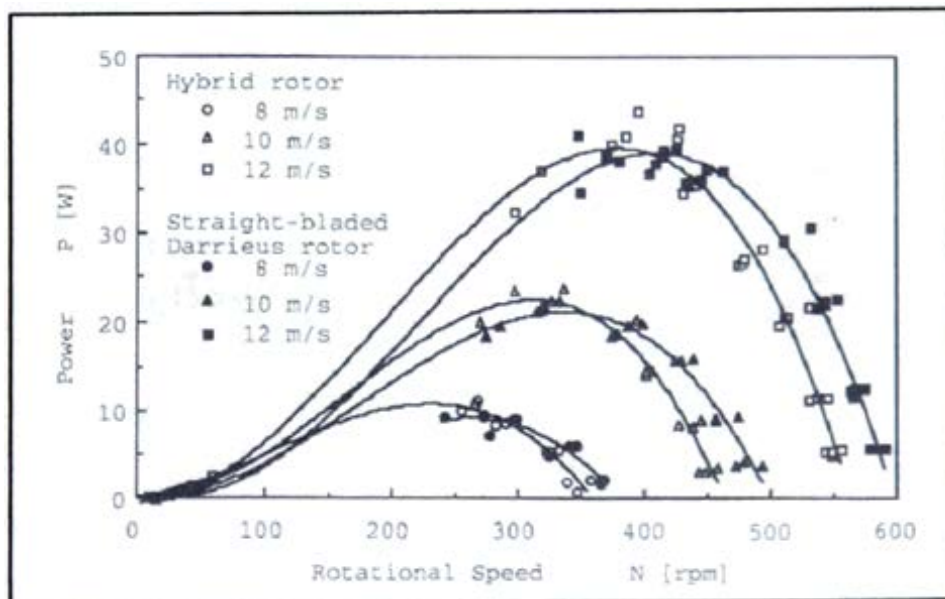


Fig. 2.31 The comparison results of hybrid and straight-blade Darrieus wind machine [50]

Chapter 3

Analytical Method

3.1 The theory for analytical models

This section presents the theory used for the prediction of the performance of the Darrieus wind machine (D-rotor). The D-rotor is rotated by the lift and drag force aerofoils characteristics. The lift and drag forces are developed when the wind passes across the aerofoil shape. Since the wind flow passes through the different flow volumes,, the velocity will change. It passes more rapidly over the longer (upper) side of the aerofoil (see Fig. 3.1), creating a lower-pressure area above the aerofoil. The pressure differential between top and bottom surfaces results in a force, called aerodynamic lift. Since the rotor blades of this Wind machine are constrained and can move in a plane with the connected link to the hub as its centre, the lift force causes the rotor blades to rotate about the axis. The shape of the aerofoil section and its angle to the wind flow stream cause the wind turbine rotors to rotate and develop the power output. In addition to the lift force, there is a drag force, which is perpendicular to the lift force. Therefore, a required design objective is the aerofoil profile rotor blades to have a relatively high lift-to-drag ratio.

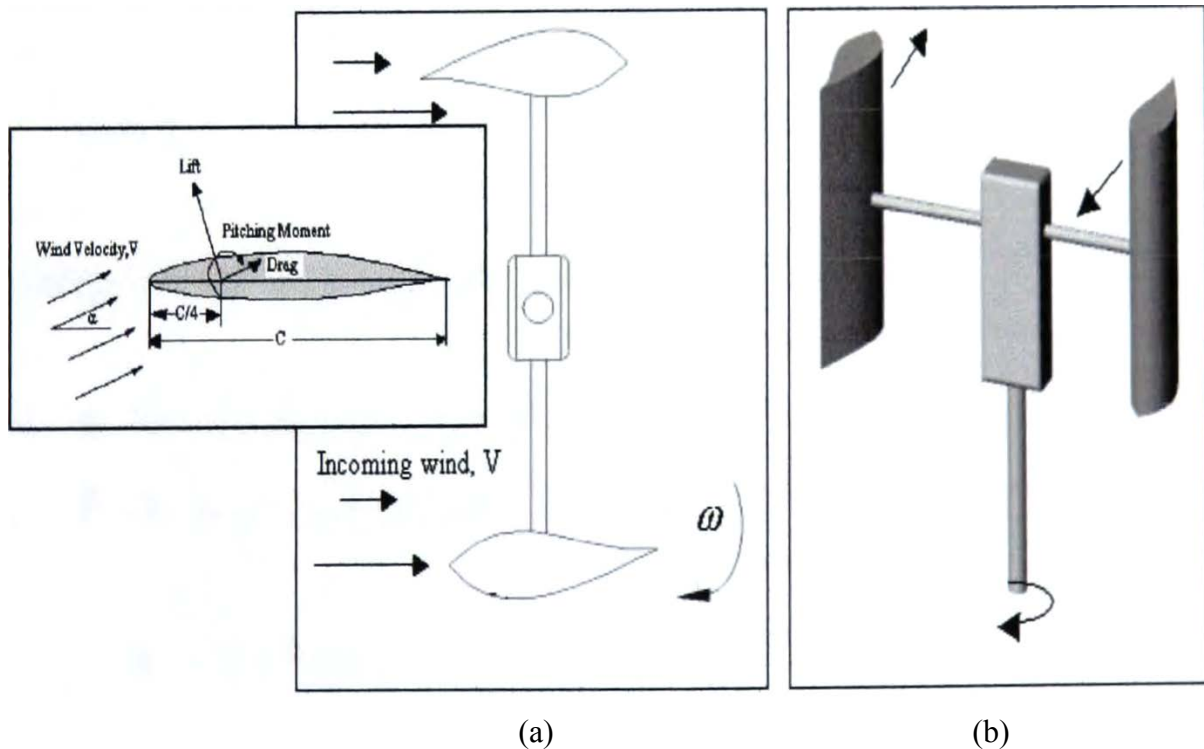


Fig. 3.1 (a) Schematic diagram for D-rotor when the wind pass through the rotor, (b) 2-D model for 2 blades of D-rotor

For a good aerofoil, the lift force should be maintained for a long period at a high angle of attack (θ) of the wind. As the D-rotor rotates, the lift force will generate a torque and maintain the rotation. Generally, the D-rotor can use curved or straight blades. This study is focused on the straight-blades D-rotor. Fig. 3.2 displays the velocity diagram and the sign conventions used for analysing the performance of Darrieus wind machine.

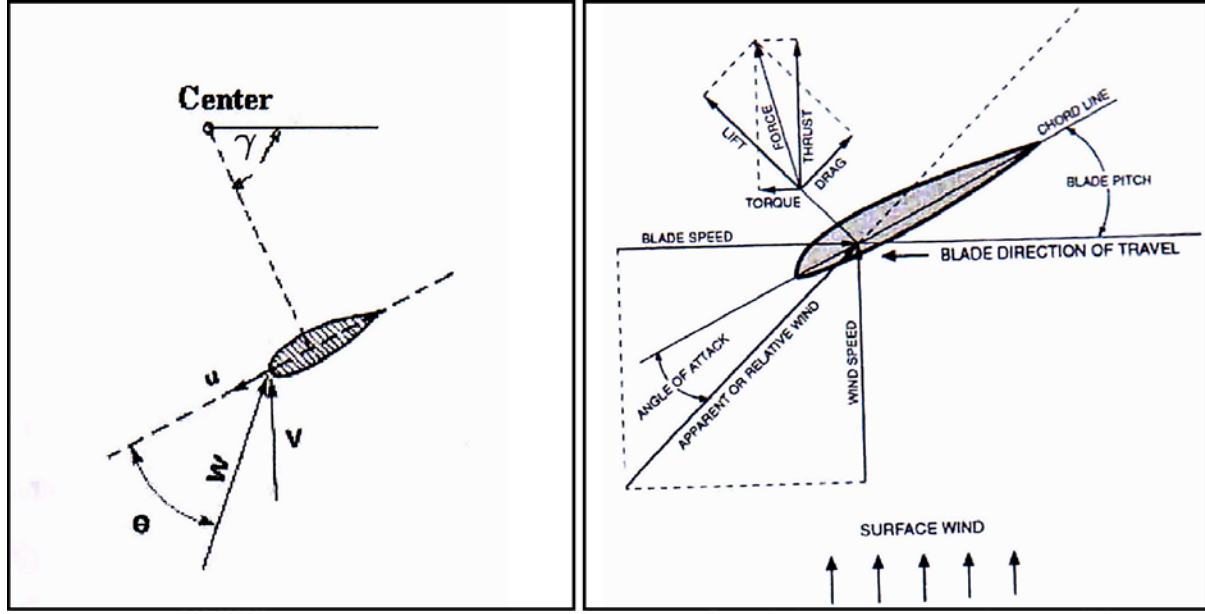


Fig. 3.2 Angle of attack (θ) and position of blade (γ) of D-rotor

From Fig. 3.2, the relative velocity W is related to the blade velocity U and the absolute wind velocity of the rotor V , by the following vector equation:

$$W = V - U \quad (16)$$

The components of W can be found in two directions:

- ❖ The chordwise direction W_c
- ❖ The perpendicular direction to the chord W_n and they are found by:

$$W_c = U + V \cos \gamma \quad (17)$$

$$W_n = V \sin \gamma \quad (18)$$

From the speed of relative velocity W then

$$W = \sqrt{W_c^2 - W_n^2} \quad (19)$$

The angle of attack for an un-pitched blade becomes:

$$\tan \theta = \frac{W_n}{W_c}, \text{ and then } \theta = \tan^{-1} \frac{V \sin \gamma}{\omega R + V \cos \gamma}$$

For a pitched blade, the angle of attack (θ) is

$$\theta = \tan^{-1} \frac{V \sin \gamma}{\omega R + V \cos \gamma} - \alpha \quad (20)$$

If the lift coefficient C_l and drag coefficient C_d are obtained. then a chordwise thrust coefficient C_t and a normal force coefficient C_n can be calculated by the following equations:

$$C_t = C_l \sin (\theta + \alpha) - C_d \cos (\theta + \alpha) \quad (21)$$

$$C_n = C_l \cos (\theta + \alpha) - C_d \sin (\theta + \alpha) \quad (22)$$

If C is the blade chord and H is the blade span, then we can calculate the area S of the blade by $S = C \times H$.

Therefore, the instantaneous torque is $T_l = C_t \frac{1}{2} \rho W^2 SR$.

For the complete rotor with ' b ' blades, the torque becomes:

$$T = \frac{0.5 \rho S R b}{2\pi} \int_0^{2\pi} C_t W^2 d\gamma \quad (23)$$

Then we can calculate the produced power P by the following equations.

$$P = T\omega = \frac{0.5\rho SRb\omega}{2\pi} \int_0^{2\pi} C_t W^2 d\gamma \quad (23)$$

The power coefficient, which is the parameter of the performance, is the ratio of the produced power to the maximum available power. The maximum available power is the power that the rotor can extract from the wind. The maximum power coefficient can be found by using the following equation.

$$P_{max} = \frac{1}{2} \rho A V_1^3 \quad (25)$$

For the D-rotor, the area A is the swept area of rotor rotation. It can be found by, the following equation.

$$A = 2 \times R \times H \quad (26)$$

The force in the direction of the absolute wind velocity V exerted on a blade is

$$F_1 = \frac{1}{2} \rho W^2 S (C_n \sin \gamma - C_t \cos \gamma) \quad (27)$$

For the complete force exerted of b rotor can be calculated by

$$F = \frac{0.5\rho SRb}{2\pi} \int_0^{2\pi} W^2 (C_n \sin \gamma - C_t \cos \gamma) d\gamma \quad (28)$$

However, consider the absolute velocity, V of the wind through the rotor area is the average of the undisturbed wind speed of the upwind V_1 , and wind passed through rotor V_2 is

$$V = \frac{1}{2} (V_1 + V_2)$$

And the force that is given by Betz [3] as

$$F = \frac{1}{2} \rho A (V_1^2 - V_2^2) \quad (29)$$

Setting $V_2 = kV_1$ then $V = \frac{1}{2} V_1 (1+k)$

The force F is then can be calculated by

$$F = 2\rho AV^2 G \quad (30)$$

Where $G = \frac{(1-k)}{(1+k)}$ and G can also be found by

$$G = \frac{Sb}{8\pi A} \frac{1}{V^2} \int_0^{2\pi} W^2 (C_n \sin \gamma - C_t \cos \gamma) d\gamma \quad (31)$$

Hence, the incoming undisturbed wind velocity $V_1 = V(1 + G)$

Therefore the power coefficient of the D-rotor is

$$C_P = \frac{P}{0.5\rho AV^3(1+G)^3} \quad (32)$$

The above are the 2 dimensional analysis of straight-bladed Darrieus wind machine. These equations were used to code the analytical models to calculate the performance of a variety of wind machine designs.

3.2 Procedures adopted in MATLAB program

The input data comprise the specifications of the Darrieus rotor, the rotor diameter D , the rotor height H and chord length c of a chosen aerofoil profile. Assuming incoming wind velocity V , and turbine revolution N in rpm, then the following steps are followed:

1. Select the aerofoil model and look up the table of lift and drag coefficients from the provided data (such as NACA 0009 aerofoil profile)
2. Define the angular position of rotor (γ) from 0 to 2π
3. Calculate the angle of wind attack θ by the following equation

$$\theta = \tan^{-1} \frac{V \sin \gamma}{\omega R + V \cos \gamma} - \alpha \text{ (In case no pitch angle, ignore the } \alpha \text{ sign)}$$

4. Find the relative wind velocity by $W = \sqrt{W_c^2 + W_n^2}$
5. Calculate C_n and C_t
6. Determine the produced power for selected rotor model using:

$$P = T\omega = \frac{0.5\rho SRb\omega}{2\pi} \int_0^{2\pi} C_t W^2 d\gamma$$

7. Calculate the interference factor G using the following equation:

$$G = \frac{Sb}{8\pi A} \frac{1}{V^2} \int_0^{2\pi} W^2 (C_n \sin \gamma - C_t \cos \gamma) d\gamma$$

8. Find the power coefficient C_p

$$C_p = \frac{P}{0.5\rho AV^3(1+G)^3}$$

Full details of the program model are shown in Appendix F. The calculation time depends on how many points of the results of power coefficient are requested. The models can be adjusted increasing or decreasing the number of blade interval position (θ).

3.3 The analytical models

The schematic diagrams for analytical models, which were developed in this study, are shown in Figure 3.3. The analytical models developed investigate the design parameters for the straight-blade Darrieus wind machine only. The models are not capable of predicting the parameters for curved-bladed Darrieus wind machine. In order to find out which aerofoil profile characteristics are suitable for D-rotor. The following assumption of the turbine specifications are required- Rotor height $H = 8\text{m}$, rotor diameter $D = 8\text{m}$, chord length $C = 0.24\text{ m}$., number of blade $b = 2$, wind velocity V of 10 m/sec with blade solidity $\sigma = \frac{bc}{D}$ of 0.06 .

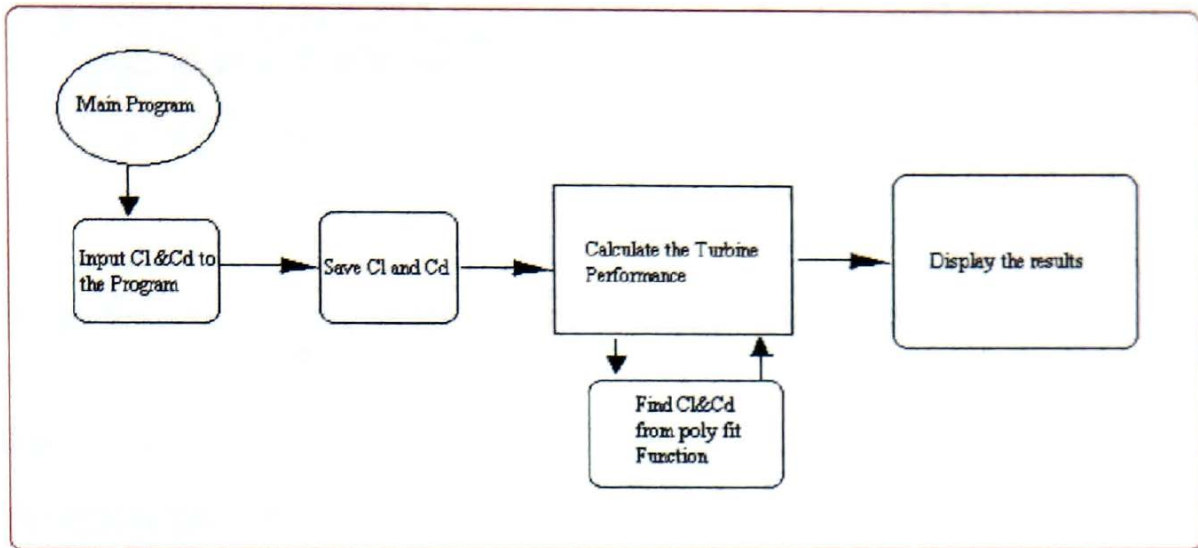
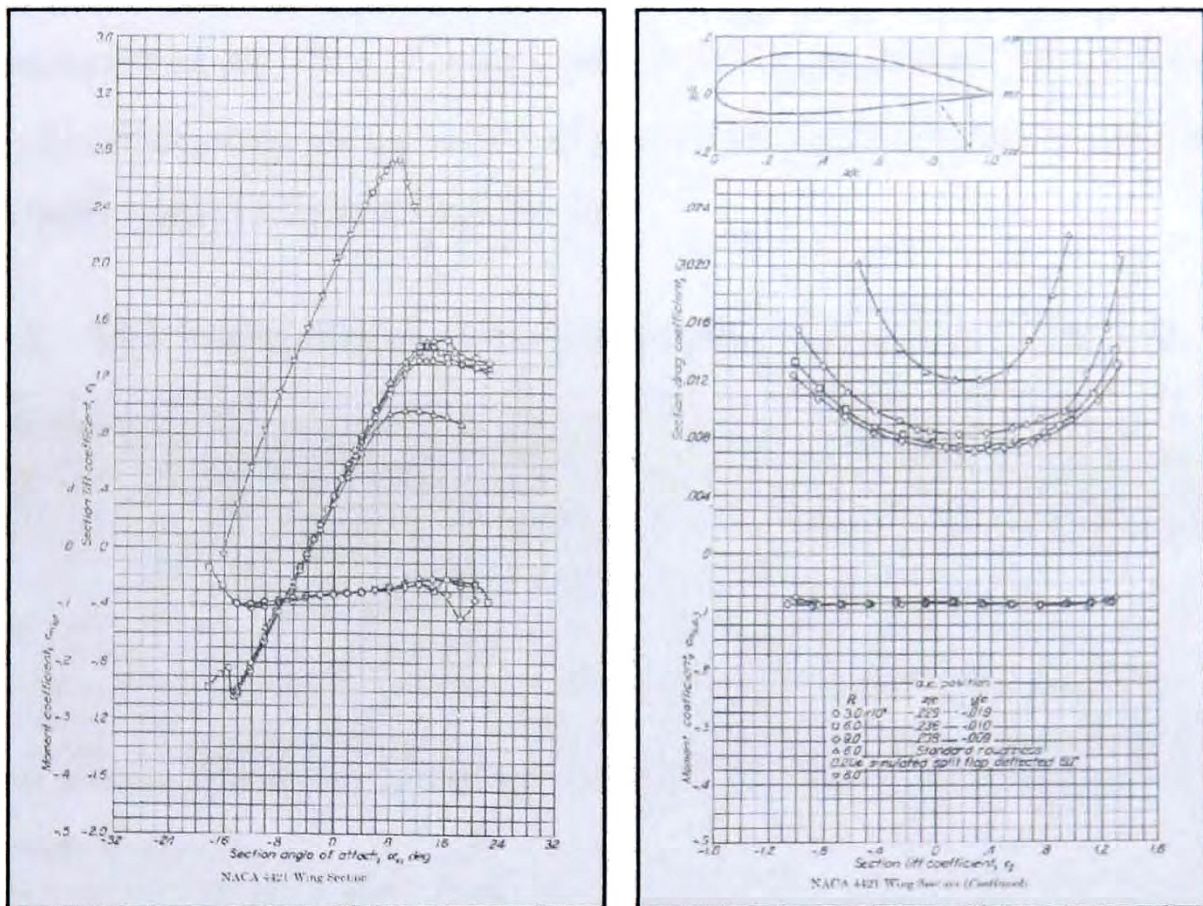


Fig. 3.3 Schematic diagram for analytical analysis

The analytical models, which have been written and coded, in this study use the following designations:

Matlab	Designation
<i>A</i>	A: Rotor swept area
<i>B</i>	b: Number of blade
<i>C</i>	c: Chord length
<i>G</i>	G: Interference factor
<i>H</i>	H: Rotor Height
<i>P</i>	P: Produced power from the model
<i>S</i>	S: Blade area
<i>V</i>	V: Wind velocity passing the rotor
<i>U</i>	U: Blade velocity
<i>X</i>	X: Tip speed ratio of rotor
<i>W</i>	W: Absolute wind velocity
<i>gamma</i>	γ : Angular position of the blade
<i>omega</i>	ω : Angular velocity of the blade
<i>theta</i>	θ : The angle of attack of the wind
<i>Cl</i>	C_l : Lift coefficient
<i>Cd</i>	C_d : Drag coefficient
<i>Ct</i>	C_t : Thrust coefficient
<i>Cn</i>	C_n : Normal force coefficient

This section describes how to use the analytical models (as described in previous section) to investigate the power coefficient of straight-blade Darrieus wind machine. NACA 4421 is an example profile used for the purpose. Firstly, the lift and drag coefficients of this aerofoil were taken from the provided source [51]. Fig. 3.4(a) and (b) illustrates the lift and drag coefficient of NACA4421 aerofoil profile.



At every angle of wind attack, C_l and C_d of this aerofoil from (-14) to (+16) degree were manually taken to M file function subprogram named *createclcd* (Fig. 3.4). The following 3 major steps are detailed about these analytical models to predict the power coefficient C_p versus the tip speed ratio X of NACA 4412 aerofoil characteristics employed to the straight-bladed Darrieus wind machine.

1. C_l and C_d characteristic data from Fig. 3.4 were taken to M file function subprogram named *createclcd* (Fig. 3.5).

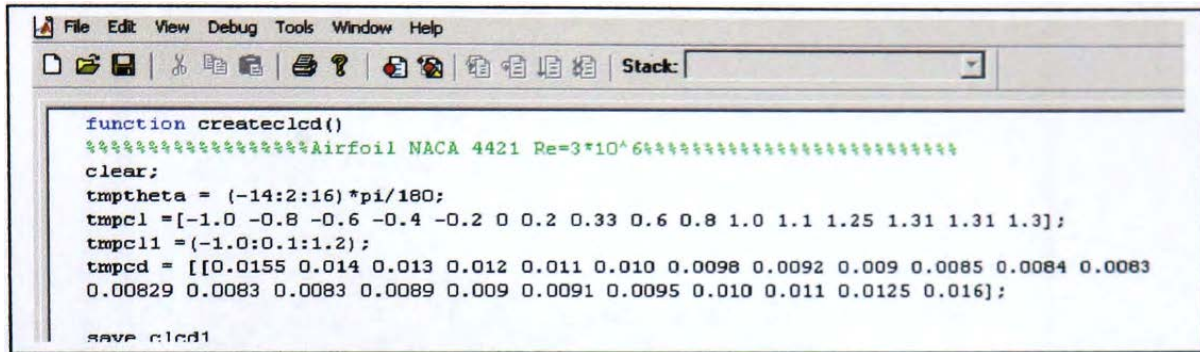


Fig. 3.5 First step, M file for input C_l and C_d to the analytical model

The accuracies of the lift and drag coefficients will affect the results. This subprogram named *createclcd* uses as the main database of aerofoils characteristics to calculate the turbine performance of any parameter designs.

2. This M file function was compiled using run command tool (Fig. 3.6).

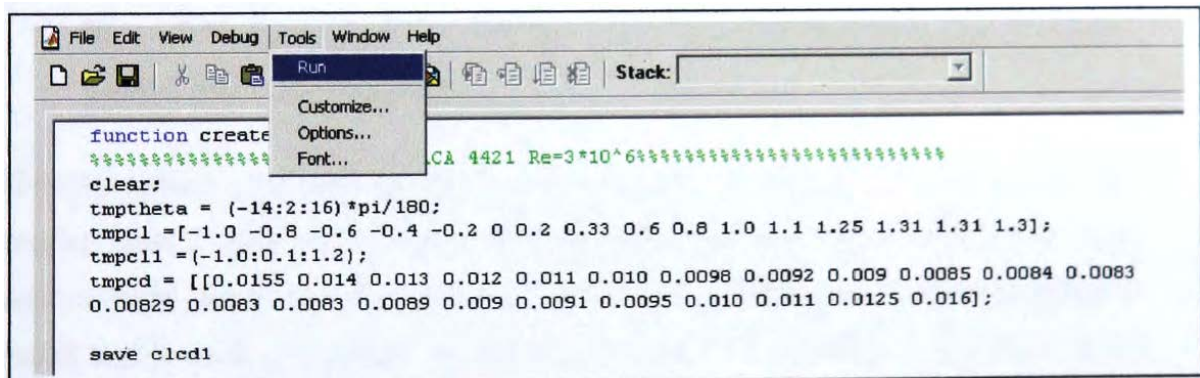


Fig. 3.6 The run command in Matlab tool

After compiling this M file function, the entire database for the lift and drag coefficient of NACA 4421 will be saved in M file function named *clcd* I for the database of this aerofoil characteristic and ready to use. The performance of Darrieus straight blades VAWTs will be computed using M file function subprogram named *power_coef* (see Fig. 3.7).

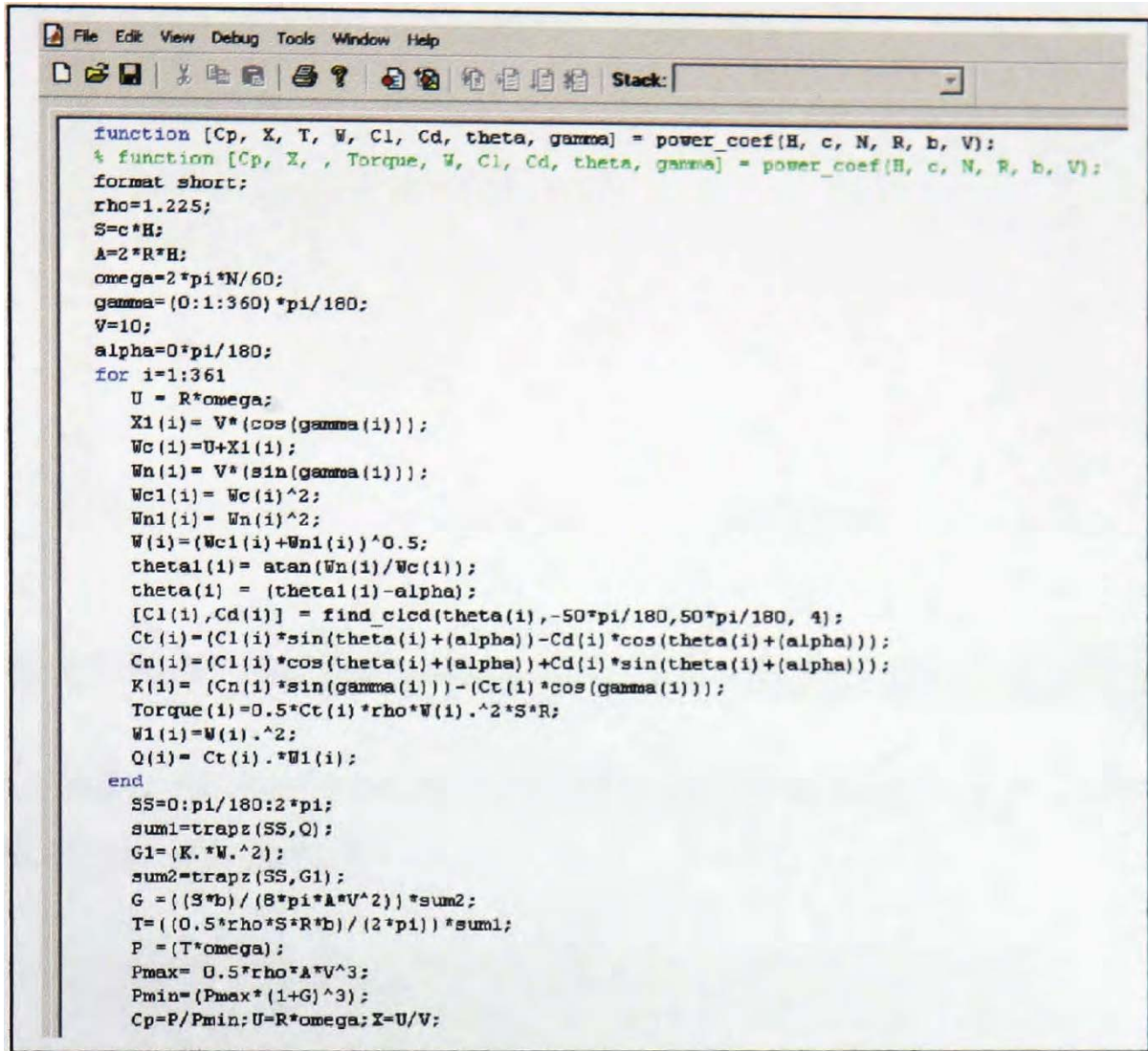


Fig. 3.7 The 'power_coef' M file function using to compute the performance of Darrieus wind machine

While the 'power_coef' M file function subprogram is running it will call the other subprogram named 'find_clcd' (Figure 3.8) to lookup lift and drag coefficient at every angle of wind attack (θ). The analytical models used polynomial fitting command in Matlab tool to lookup the table of these characteristics. The prediction results from the 'power_coef' M file (Fig. 3.7) will be recorded by the main program named 'Main'. After completing the step one, the user only clicks the run command in main program. The display when running the main program can be seen in Fig. 3.10.

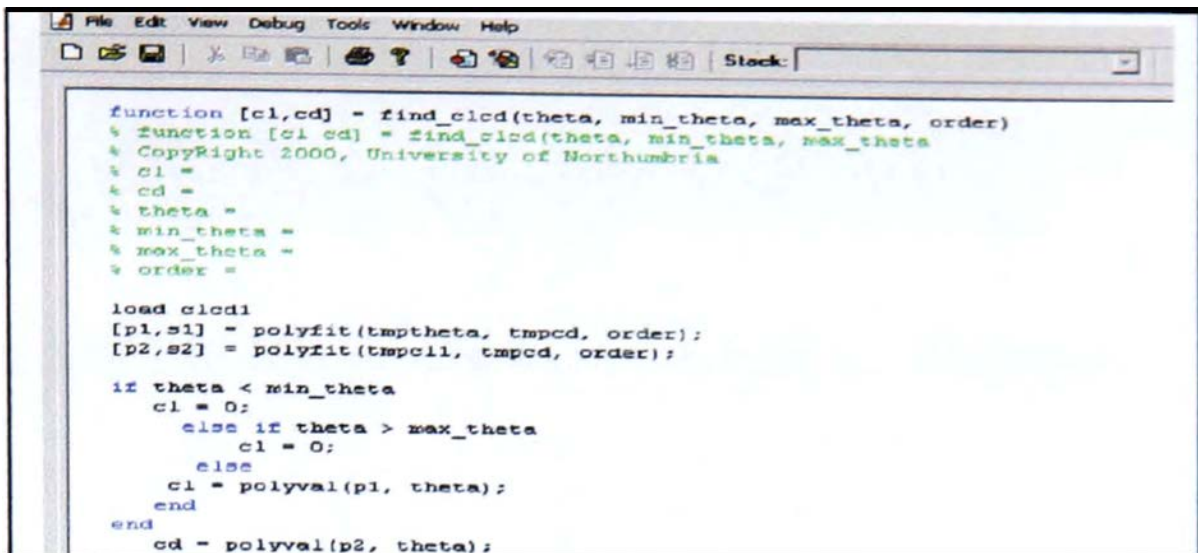


Fig. 3.8 Find_cld M file sub program for lift and drag coefficient database

- Fig. 3.9 shows the main programme used to predict the performance of the straight-bladed Darrieus wind machine.

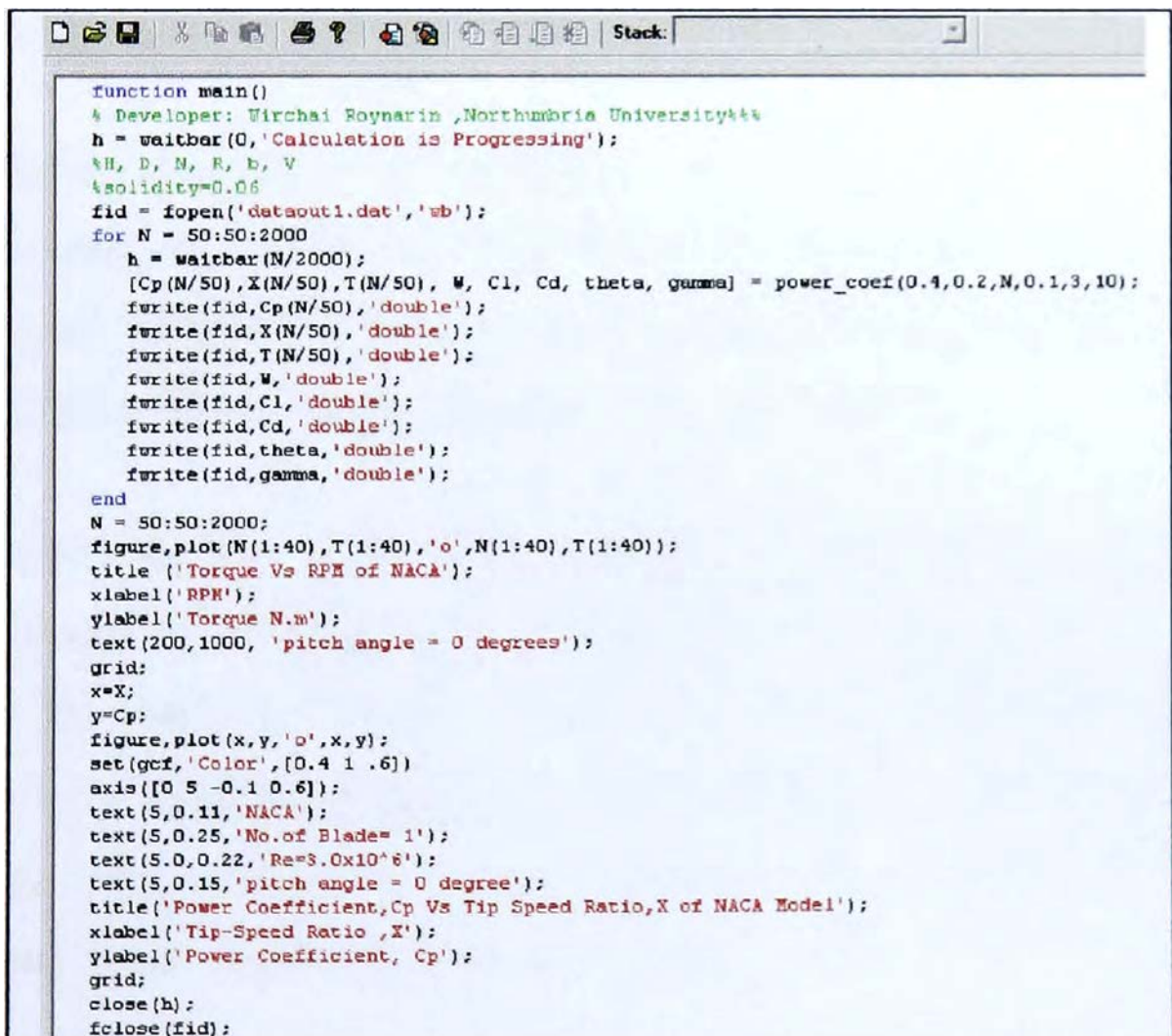


Fig. 3.9 The main program to predict the performance of D-rotor using C_l and C_d data of a selected aerofoil

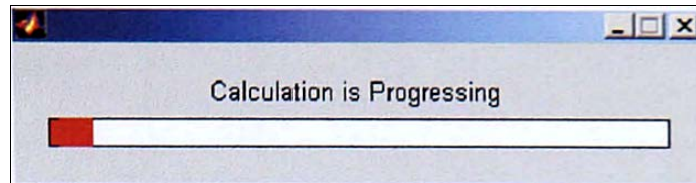


Fig. 3.10 The wait bar showing progress of the prediction

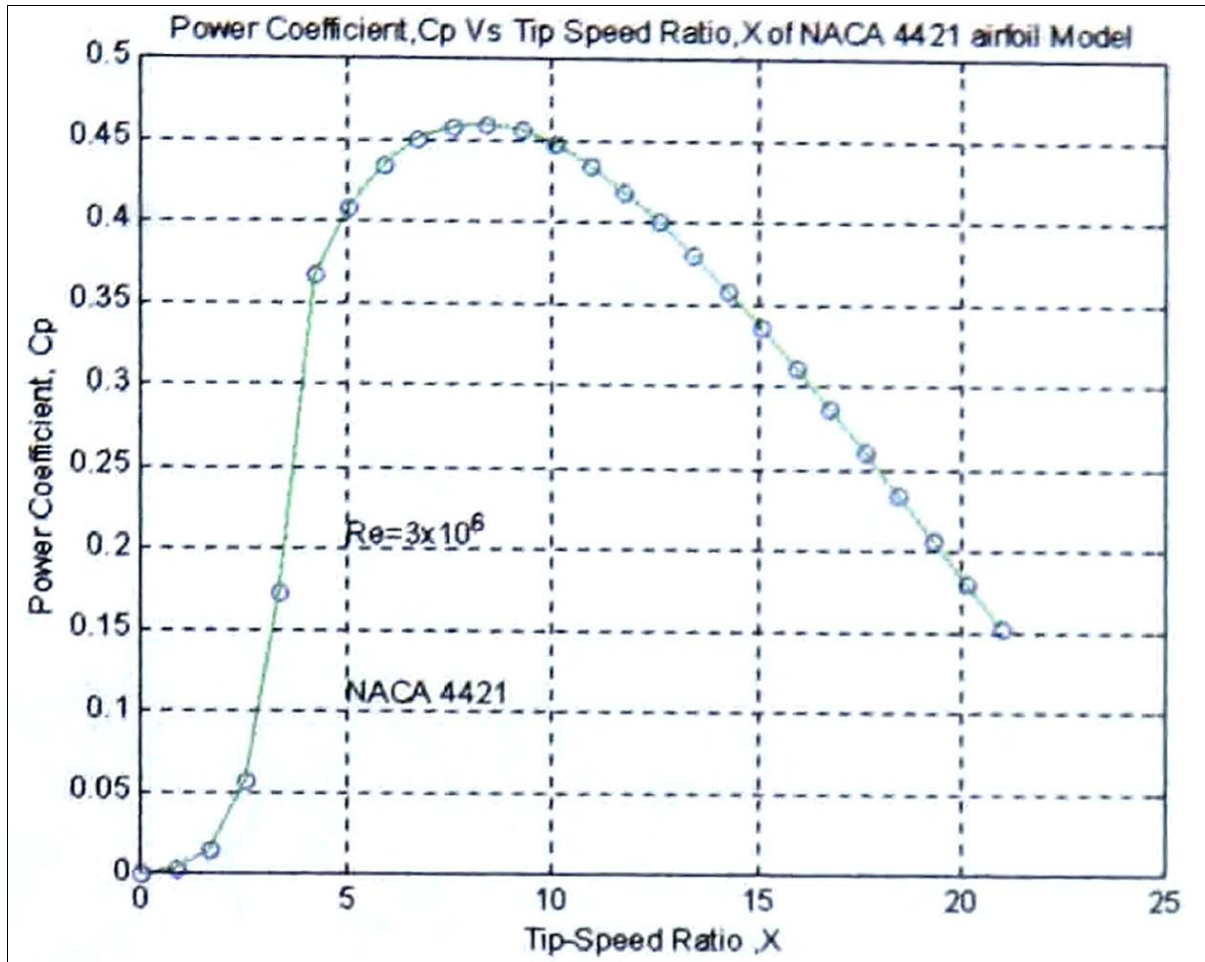


Fig. 3.11 The power coefficient versus tip speed ratio of NACA 4421 for straight-bladed Darrieus wind machine

Fig. 3.10 shows the progress of calculation. The steps of using analytical models above have been used to predict various parameters influencing the performance of the Darrieus wind machine. This main and subprogram can be modified for various purposes of the predictions by changing some parameters. During the investigation of NACA661-212 aerofoil profile, the study also developed an analytical model to investigate the individual torque generated at a given rpm. The details of this model are shown in Appendix G. A typical example of the torque developed by a Darrieus machine is shown in Fig. 3.12. The details of the Darrieus machine are: speed = 500 rpm, number of blades = 2, rotor height = 2 m., rotor diameter = 2 m, chord length = 0.24 m, rotation = 1 cycle.

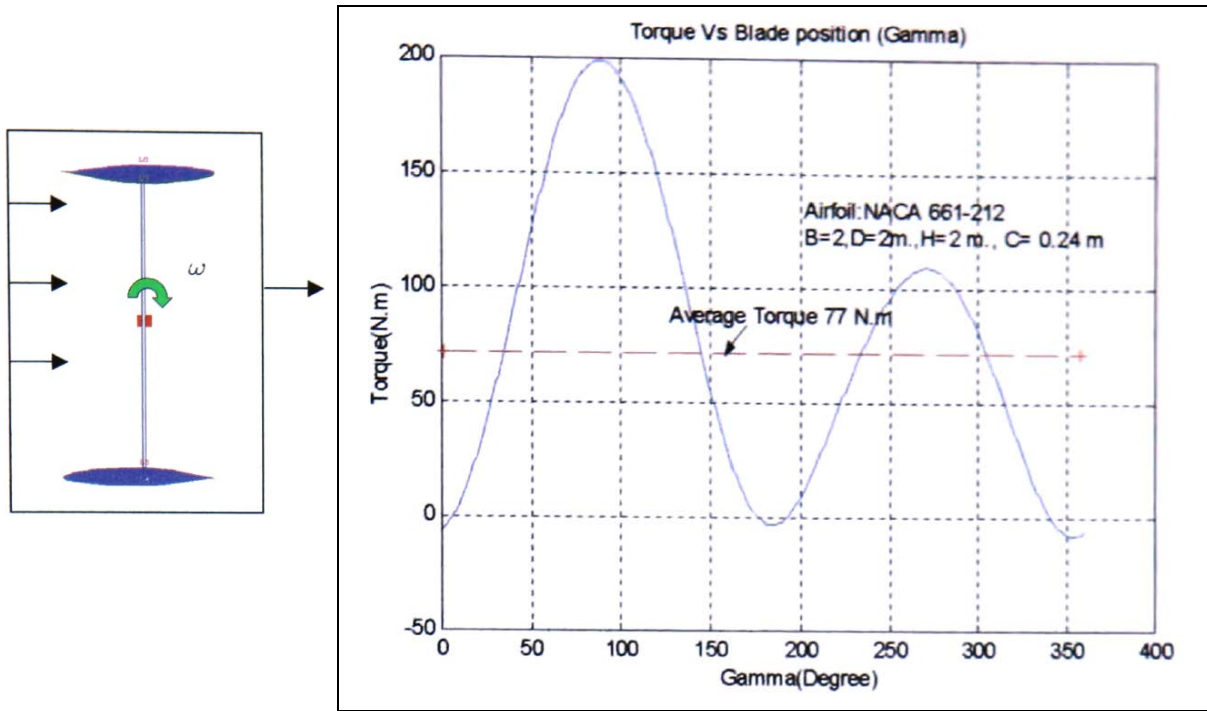


Fig. 3.12 Example of the generated torque using NACA661-212 aerofoil characteristics

3.5 Darrieus VAWTs Design Parameters and MATLAB results

As mentioned in Chapter 1, the main objective of this study is to optimise the performance of the vertical axis wind turbine, therefore this section shows a number of design parameters investigated in the light of their influence on the starting behaviour, overall performance on D-rotor using the analytical models prediction. The general design parameters of Darrieus VAWTs are studied in this section and the literature relating specifically to the performance of this type of wind machine has been reviewed in Chapter 2. The following are the main parameters, which have been concerned in this study in order to achieve the objectives of this study.

- ❖ The aerofoils section
- ❖ The Revnolds number Re
- ❖ Number of blades (b)
- ❖ The effect of chord ratio ($\frac{c}{r}$)
- ❖ Blade pitch angle α

3.5.1 The aerofoils section

Since the aerofoil section of the rotor in the wind machine is the critical element, it deserves especially careful thought. The aerofoil characteristics affect the rotor performance. This present study examined various shapes of aerofoils to optimise their rotor performance. The rotor of the wind machine must, as a minimum have satisfactory performance. From previous investigation and present study, many of the operational problems of wind machine could be solved by careful rotor design. Choice of a suitable aerofoil section can significantly improve both the peak performance and the starting characteristics of a wind turbine. In 1999, Mark Hampsey [52] presented the design of Wind turbine blades for optimal starting and power extraction and indicted that the aerofoil selection task has to be given the most consideration in the design of the wind machine. Most VAWT researchers have used one of the original US National Advisory Committee on Aeronautics (NACA) four digit series aerofoil sections, usually either a NACA 00 12 or NACA 00 15 section, although these were first developed in the 1930s [27] and are not necessarily the best sections available for the purpose. More information of aerofoils test can be seen in [8,18,53-55].

Generally, there are two types of aerofoil considered for wind turbine, symmetrical or cambered profile. Normally most researchers have assumed that symmetrical aerofoils should be used for wind machine. Since cambered sections are not designed to operate at negative incidence, (relative wind approaching the convex side of the aerofoil) any gain made by a cambered blade with a favourable angle of wind attack (θ) on the upstream pass would be lost on its downstream pass because of the unfavourable θ .

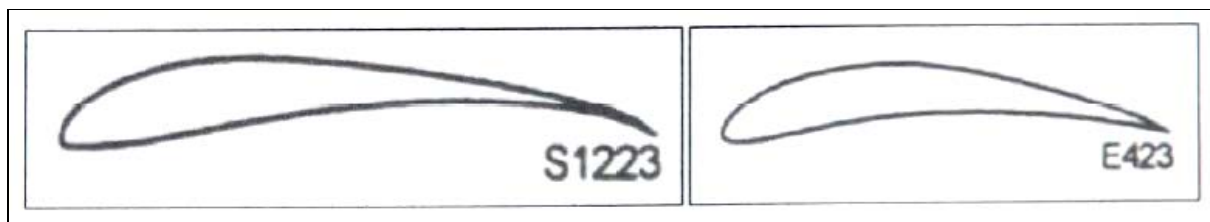


Fig. 3.13 Example of cambered aerofoils for VAWTs rotor blades 1561

However, it will be shown that the performance of some cambered aerofoils at low Re is vastly superior to that of symmetrical aerofoils and as a result, they can generate significant starting torque at low Re , unlike symmetrical blades. Examples for camber blade aerofoils are S1223 and E423 (Fig. 3.13). The symmetrical aerofoils are normally, as mentioned, preferred for use in either vertical or horizontal wind machines, because the symmetrical

profile generates high lift force at higher Reynolds number and low angle of wind attack in comparison to the cambered aerofoils. NACA 0006, NACA 661-212 (Fig. 3.14) are examples of the symmetrical profiles, which are normally used for the rotor of either VAWTs or HAWTs.

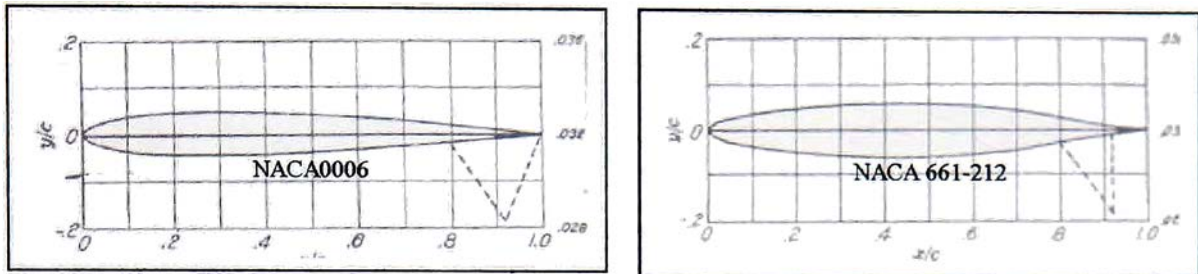


Fig. 3.14 Example of symmetrical aerofoils from [51]

The NACA 0006 and other symmetrical sections have presumably been used because their lift, drag and pitching moment characteristics are most well documented (see for example Abbott, 1958), making validation of theoretical predictions easier. But having validated the theory, the next step is to choose the section that gives the best performance. The following section shows some results for different aerofoils sections. In this study, 40 aerofoil sections have been analysed to predict and study the performance of D-rotor. The aerofoils, which were used in this study, can be divided into 2 categories as the following:

- ❖ 10 High Reynolds number NACA aerofoils section
- ❖ 30 Low Reynolds number modern aerofoils section

3.5.1.1 High Reynolds number aerofoils

10 aerofoils have been tested at high Re number; aerofoil characteristics are fully published and can be obtained from the reference [51]. The high Reynolds number (3×10^6) aerofoil characteristics C_l and C_d of these 10 aerofoils have been investigated and originally published in 1949. These 10 NACA aerofoils section include NACA0006, NACA661-212, NACA66 (215-016), NACA4421, NACA23024, NACA23021, NACA1421, NACA2412, NACA4418, and NACA23012. These aerofoils sections are most commonly used for airplanes and also in applications such as helicopter rotor blades, propeller blades and high performance fans. More details of these aerofoil sections can be seen in reference [51].

These 10 aerofoils given above were studied when employed to straight-bladed Darrieus wind machine.

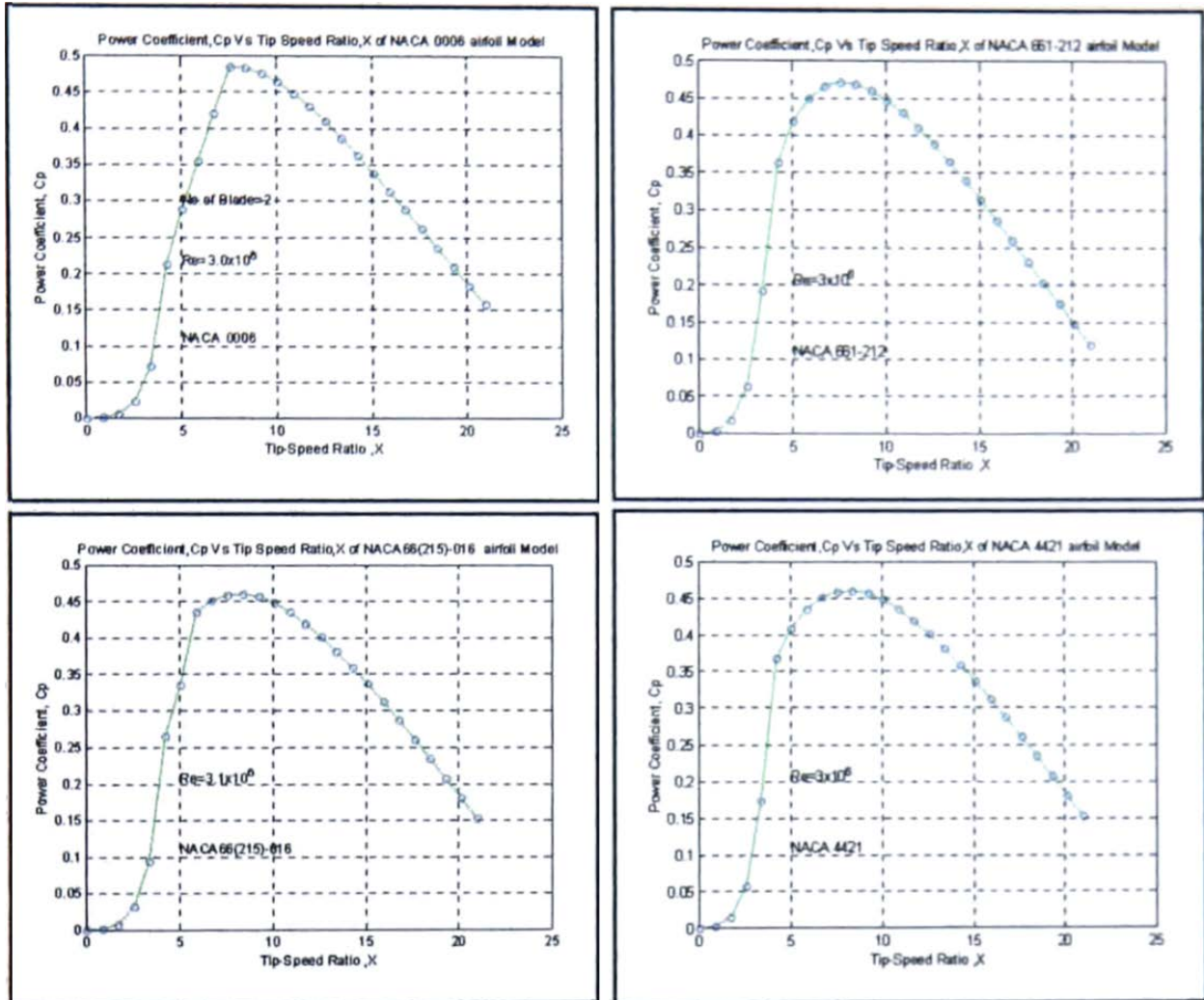


Fig. 3.15 Performance prediction results of 4 aerofoil sections on D-rotor

These 10 aerofoils characteristics (lift and drag coefficients) were treated by the analytical models to predict the performance of the D-rotor VAWTs. Fig. 3.15 displays some results obtained for four high Reynolds number aerofoil sections. Full report of these 10 aerofoils In graph forms of power coefficients C_p versus tip speed ratio X is given in Appendix H.

3.5.1.2 Low Reynolds number aerofoils

The details of the low Reynolds number aerofoils are given in Appendix I and [56, 57]. The aerofoils include A 18, Clark-Y, E 387, S 6062, SD 7037, NACA 2414, S 822, SD 6060, RG 15, S823, SG6042, Goe417a, SG6040, LRN1007 (B), CR-001, SA7035, Trainer 60, S6063, RG14, E231, SD 7032, SD 7062, SG6041, USNPS-4, S1223, E423, M06-13-128, Davis 3R, LD-79 and MH32. The characteristics of these 30 aerofoil sections have been treated by analytical models in order to investigate the power coefficients when employed in a D-rotor. Fig. 3.16 and Fig. 3.17 shows the comparison of the results of CP versus X of 20 candidate aerofoils section. The conclusion and observations are shown in section 4 of this chapter. The full results of this investigation are shown in Appendix 1.

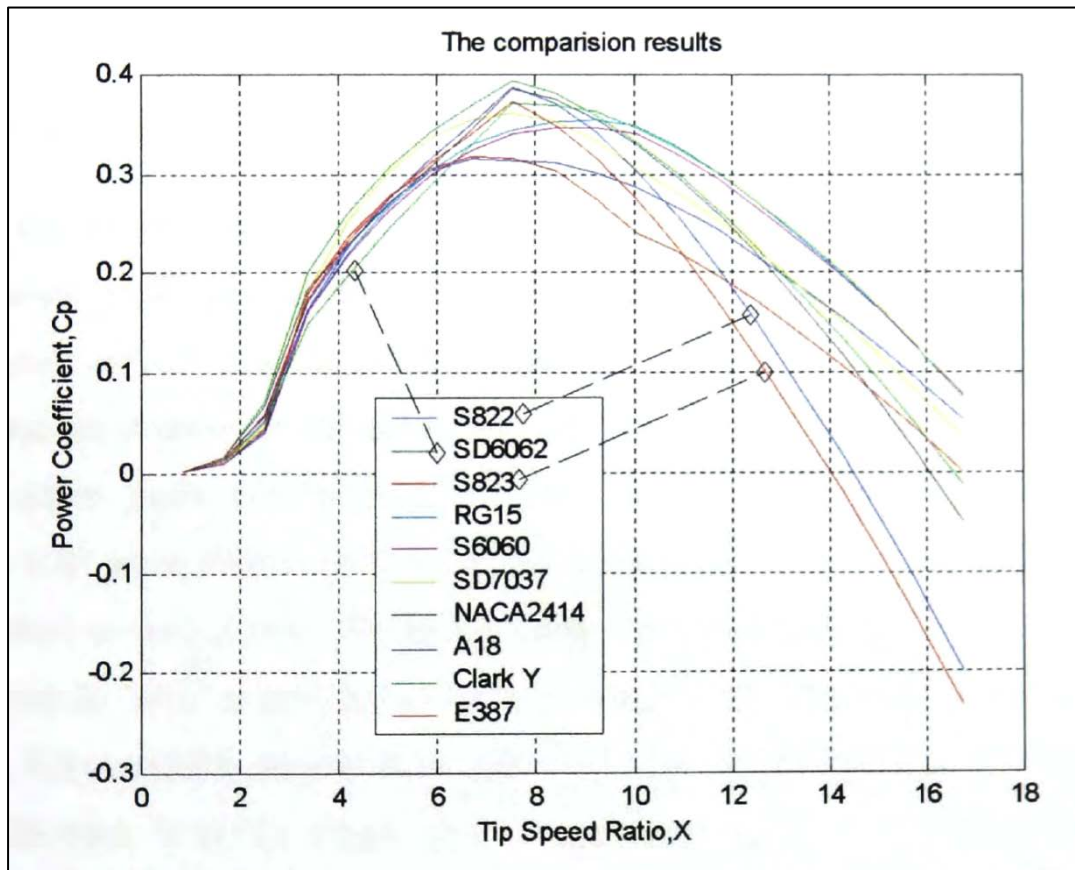


Fig. 3.16 Performance results of first set 10 low *Re* aerofoils on D-rotor

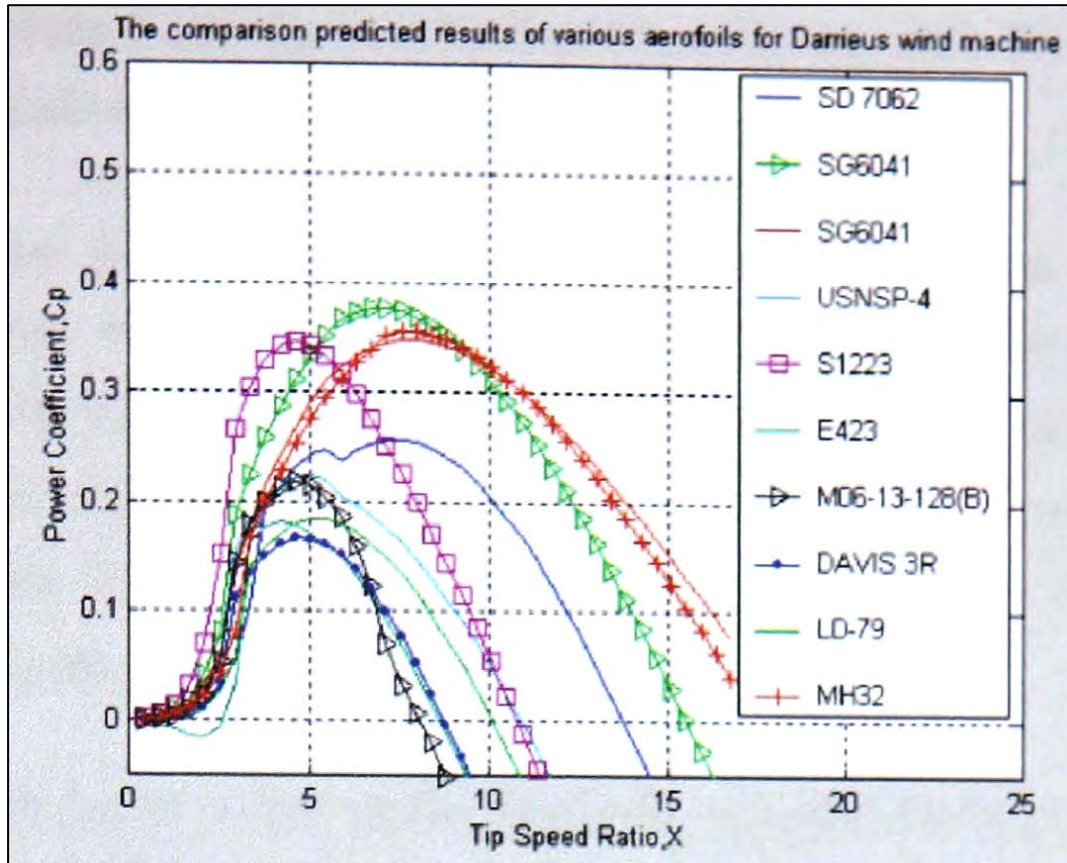


Fig. 3.17 Comparison of performance results of other 10 low Re aerofoils employed to D-rotor

3.5.2 Number of blades

This is the second parameter, which needs consideration in order to optimise the performance of D-rotor in this study. Generally for the wind machine the amount of power produced by a wind turbine depends primarily on the wind velocity and the swept area (as mention in the theory section), not on the blade area- The wind turbines with a single blade are technically feasible and potentially just as efficient as the turbines with more blades,, in terms of the percentage of kinetic energy intercepted that is converted to shaft power. Therefore, some wind machines have only one rotor blade in association with a well-balanced component. At least one company (MBB of Munich, Germany) has produced commercial single blade 14AWTs. In principle a single bladed D-rotor VAWTs could also be built. However, a counterweight would be required to balance the mass of the single blade and this counterweight would generate parasitic drag. Because forward torque is not produced at all blade positions, such a single blade turbine would not self-start and so is of no interest to the present study. A rotor with an even number of blades will give stability problems for a machine with a stiff structure. The reason is that at the very moment when the front blade

bends backwards, because it gets the maximum power from the wind, the rear blade passes into the wind shade in front of the tower.

The ideal number of blades may appear to be two and most Darrieus rotors have two blades. However, three blades offer some advantages for VAWTs in that cyclic variations in both the torque and the magnitude and direction of the net force on the rotor due to the combined effects of lift and drag on all blades are very much reduced with three blades. This is the case because the aerodynamic forces on the blades of a VAWT reach a peak twice per revolution.

The aerodynamic forces on two blades, 180° apart, will peak approximately in phase and will act in approximately the same direction on both blades, leading to potential problems with resonant vibrations in the tower, while those from three blades 120° apart will tend to produce an almost steady force. More details of these issues are presented in Chapter 5. It will be seen that there is a large cyclical variation in both the magnitude and the direction of the net force on a two blade rotor, but that the force is much steadier on the three blade rotor. The same is true of torque and vibration. The cyclical variations in torque and net force are apparently not major problems with the larger turbines since the 300 kW VAWTs manufactured by Heidelberg Motor and the 100 kW plus turbines produced by VAWT Ltd in the UK all have two blades.

However, from the author's experience of small-scale test of two blade machines in wind tunnel shows vibration of the whole structure at certain speeds. This study included the analysis using NACA 661-212 aerofoil characteristics to investigate the number of blades affecting the power coefficient of the wind machine. The summary of the prediction results shown in Fig 3.18 indicates that two blade generates high C_p of 0.48 at tip speed ratio of 7. At the higher number of blades for D-rotor, the C_p remains unchanged. The investigation showed a high rotor performance at number of blades 2 or 3. Full report of the influence of the number of blades to the performance of wind machine can be seen in Appendix J.

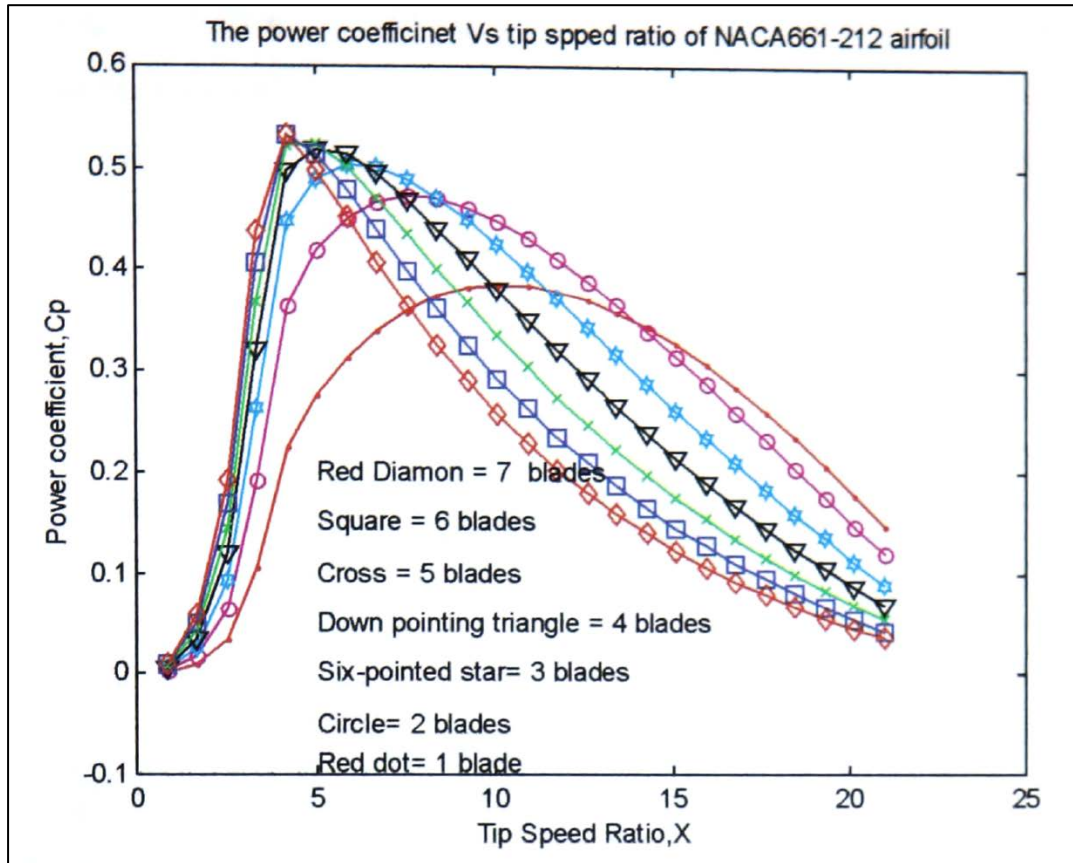


Fig. 3.18 Effects of number of blades on the performance of D-rotor

3.5.3 The Reynolds number Re effects

The wind machine design concept, either VAWTs or HAWTs, needs consideration of the Re effects on the power coefficient of the machine. The problem encountered in wind energy system analysis has been the presence of a significant Reynolds number dependence in the range of operation. Amos and Bragg [58] indicated in their study that the availability of aerofoil data at Reynolds numbers, appropriate for the range encountered by VAWTs blade, provides the ability to include Re variability in efficient design procedures. As the performance of the D-rotor wind turbine is dependent upon the aerofoil characteristics (drag and lift force coefficients) and these coefficients are affected by Reynolds number [3,52]. Moreover the Re effect is important as during a whole rotation of an aerofoil it can change considerably for a Darrieus wind machine. Hence this research has studied the Re effect on the C_p of D-rotor using available E374 aerofoil characteristics (C_l and C_d).

The results of the investigation showing the influence of Re on performance is shown in Fig. 3.19. Fig. 3.19 shows significant difference in power coefficient versus tip speed ratio at different Reynolds number. Full results of this investigation are displayed in Appendix K. The results indicate the higher the Re the higher the performance of a D-rotor machine but

not in all the range of tip speed ratio. The Re number is calculated by $Re = 69000Vc$ (at the sea level), as such at low Re the performance of most if not all aerofoils is very poor. The suitable aerofoil data could be concerned in order to investigate the behaviour of the wind machine.

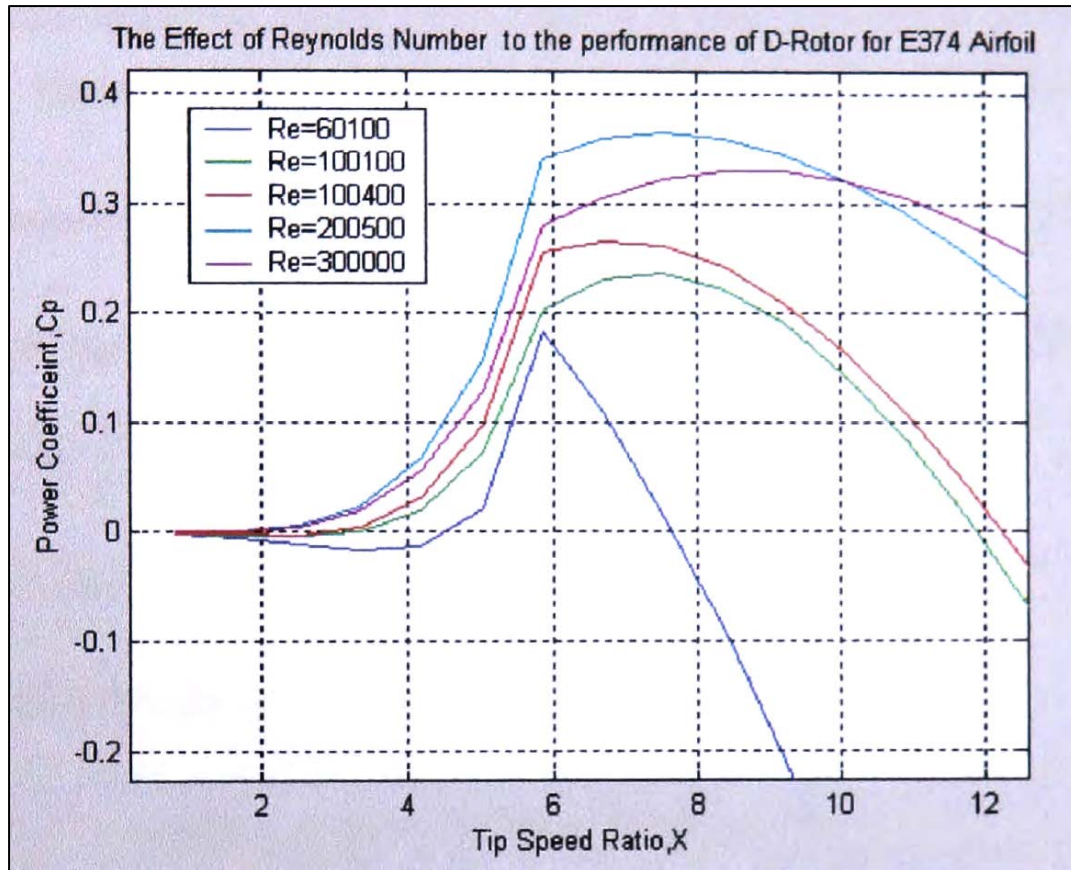


Fig. 3.19 Summary results of Re effects to the performance of D-rotor

The investigated results show that at low Re ($Re = 60100$) the performances of the machines is lower than that of the others and show negative power coefficient for tip speed ratio 0 to 4.5. Therefore, Re is one of the major variables that affect the rotor performance and might be the reason why D-rotor cannot be self-starting. Additionally, it could be explained that the large turbine might be starting in a strong wind. And it is not applicable for a small turbine in a light wind. Re could be increased in two ways, firstly by increasing the source of incoming wind velocity and secondly by making a larger chord length. Nevertheless, the effects of the high chord ratio ($\frac{c}{r}$) should be considered.

3.5.4 The effects of chord ratio ($\frac{c}{r}$) and the Results

This parameter affects the performance of vertical axis wind turbine, which is well mentioned in reference [37, 59, 60]. In this section, NACA 661-212 aerofoil data was used to analyse the effect of this parameter to the performance of D-rotor wind turbine. In the analyse procedure, 2 configurations were set up. Firstly, the value of the chord length (c) was kept constant with various values of the rotor radius (r), the second the value of the rotor radius (r) was kept constant with different aerofoil chord length (c) values. Matlab analytical model was used to predict the power coefficient versus tip speed ratio. The results shown in next section were plotted by Matlab tool.

❖ *Constant chord length of selected aerofoil at various radius of rotor*

The results in Fig. 3.20 displayed under the following chord ratio configurations:

$$\frac{c}{r} = \frac{0.24}{0.24} = 1, \frac{c}{r} = \frac{0.24}{0.5} = 0.48, \frac{c}{r} = \frac{0.24}{1} = 0.24, \frac{c}{r} = \frac{0.24}{2} = 0.12, \frac{c}{r} = \frac{0.24}{4} = 0.06,$$

$$\frac{c}{r} = \frac{0.24}{6} = 0.04$$

Where c = chord length in meter (m), r = radius of the rotor (m).

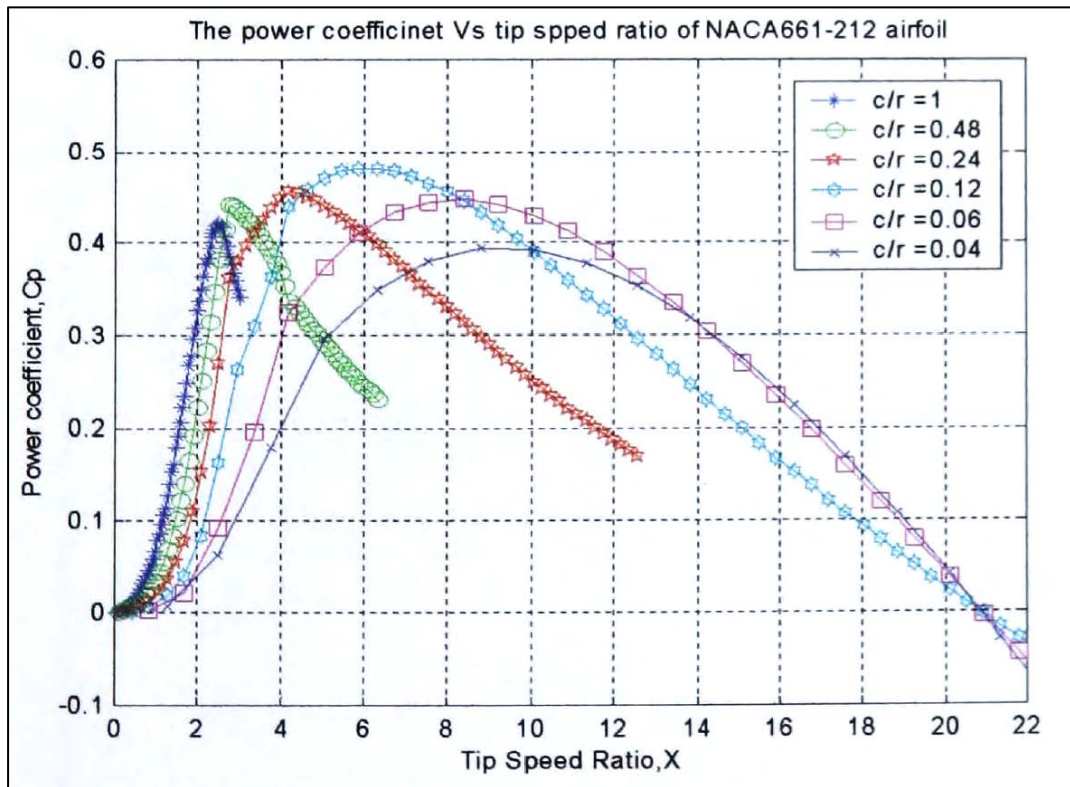


Fig. 3.20 Chord ratio effects on the performance of D-rotor (c constant)

❖ *Constant radius of rotor at various chord length of selected aerofoil.*

Fig. 3.21 displays the results of the prediction of NACA 661-212 aerofoil applied to D-rotor at different $\frac{c}{r}$. The results are shown at the condition that keeps the rotor radius, r , constant at various the aerofoil chord lengths, c of the selected aerofoil. This study investigates the performance of D-rotor at the same value of chord ratio $\frac{c}{r}$. The $\frac{c}{r}$ numbers in this study are:

$$\frac{c}{r} = \frac{4}{4} = 1, \frac{c}{r} = \frac{0.192}{4} = 0.48, \frac{c}{r} = \frac{0.96}{4} = 0.24, \frac{c}{r} = \frac{0.48}{4} = 0.12, \frac{c}{r} = \frac{0.24}{4} = 0.06,$$

$$\frac{c}{r} = \frac{0.16}{4} = 0.04$$

From the results of these two situations investigated, it appears that the chord ratio ($\frac{c}{r}$) was one of the major effects to the performance of Darrieus wind machine.

A comparison of the results obtained from the two method of investigation of the influence of chord ratios to the performance of the wind machine used in this study is shown in Fig. 3.22.

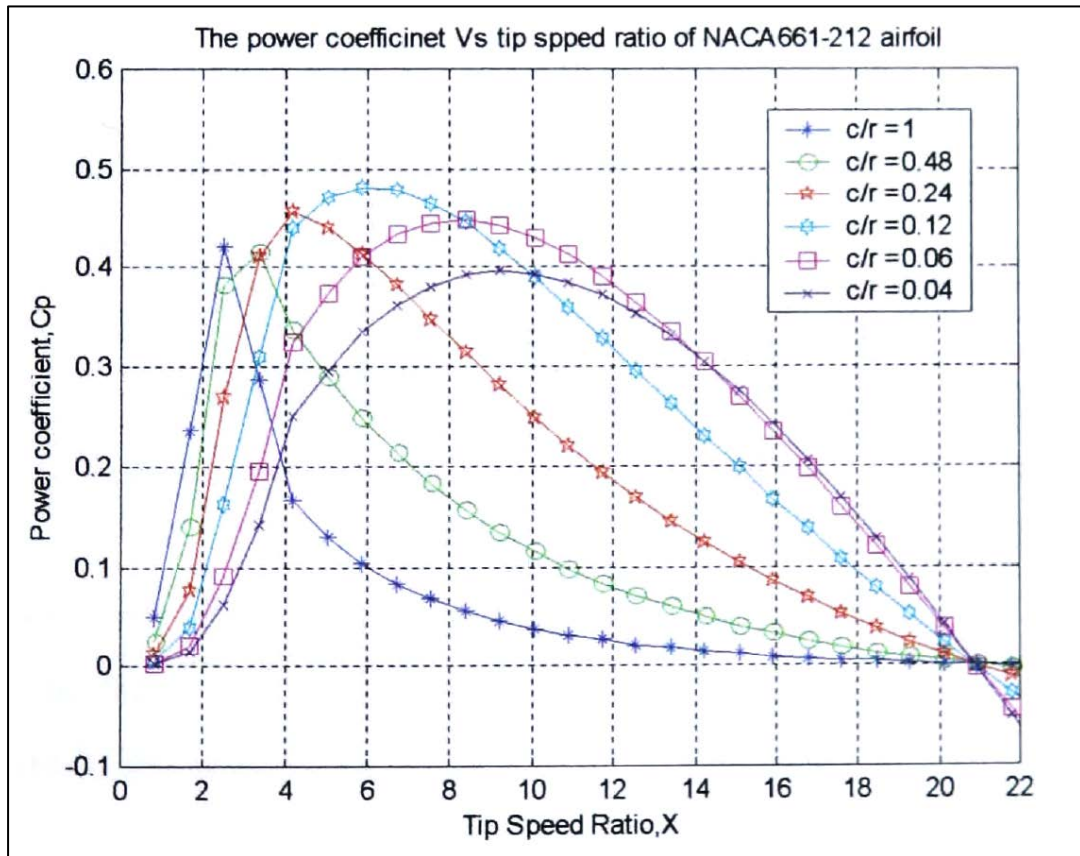


Fig. 3.21 Chord ratio effects on the performance of D-rotor (r constant)

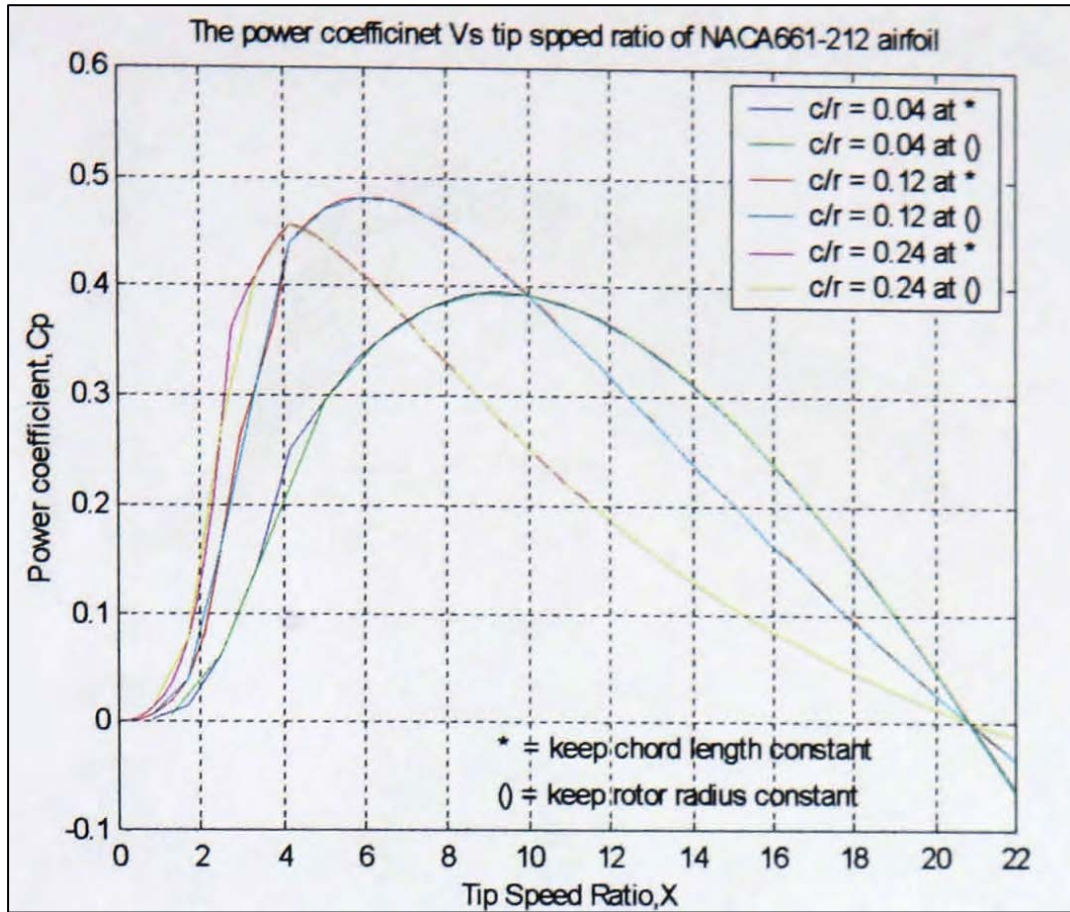


Fig. 3.22 Comparison graph between two methods

3.5.5 The Blade pitch angle α

The influence of the blade pitch angle α (positive and negative angle) on the performance of straight blades D-rotor was also studied. The aerofoil characteristics of NACA661-212 have been used as a case study. In this study a two blade with NACA 661-212 profile, with chord length of 0.24 and rotor radius of 4 meters, has been assumed. The analytical model used in this study is the same as the investigation of the effects of aerofoils shape in section 3.5.1 but various blade pitch angles. Fig. 3.23 shows the results of this investigation at various blade pitch angle (see the individual results in Appendix L). The results show that at zero blade pitch angle, the rotor developed the best result of power coefficient compared with the others.

In general the case with pitch angle = 0 shows the best results in the whole range of the tip speed ratio. The study indicates that the straight-blade D-rotor could generate higher performance at pitch angle of zero.

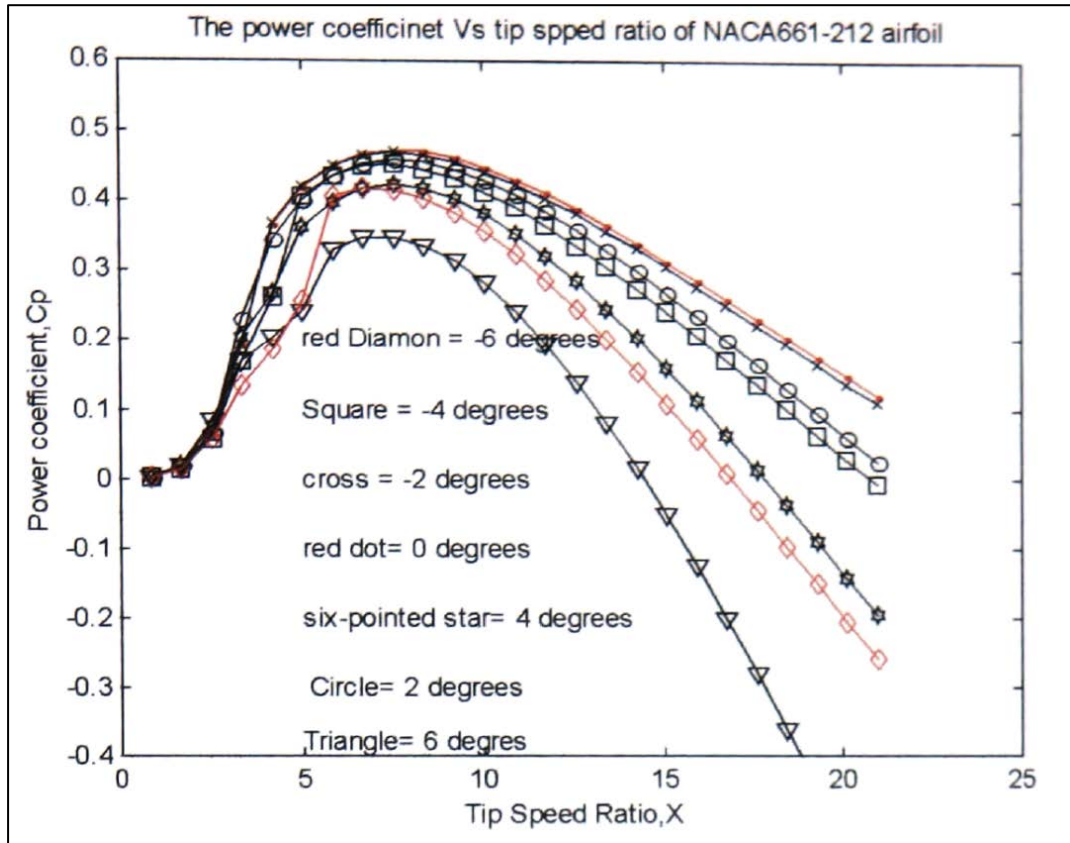


Fig. 3.23 Effect of blade pitch angle to the power coefficients on D-rotor

3.6 Observations and Conclusions of analytical method

This section describes the observed results obtained from the analytical models. The total 40-aerofoil shapes have been analysed in this Chapter. The power coefficient C_p results of all aerofoil configurations of the investigated wind machines have not exceed the Betz' number ($C_p = 0.59$).

In the aerofoil test section 3.5.1, the results can be classified into two aspects. Firstly, 10 blades with high Re number (accordingly to the results In Fig. 3.15 and Appendix H) indicated the most positive results for NACA 661-212 aerofoil section. This aerofoil section gave higher power coefficient along the range of tip speed ratio compared to other configurations. Secondly, the study of 30 aerofoils for low Re aerofoil characteristics showed that the aerofoil (Clark-Y) and high lift aerofoil (S 1223) showed good performance when employed to D-rotor VAWTs. These three mentioned aerofoils further investigated using CFD and experimental testing in the wind tunnel as described in Chapter 4 and 5 respectively. It will be shown later in this study that the performance of some cambered

aerofoils at low Re is vastly superior to that of symmetrical aerofoils (which have been used for long time) for the rotor of VAWTs. The results of the investigation showed that the feasible aerofoils section can generate significant starting torque at low Re , unlike the symmetrical blades (see more in [61-63]). In order to prove these suggestions, which are of crucial importance to the present study, they will be investigated further in Chapters 4, 5 and 6.

The investigation of the number of blades (b) affecting the behaviour of the Darrieus wind machine has been presented in section 3.5.2. From the results of this study, it can be concluded that the number of blades (b) has a major influence on the performance of the D-rotor. This study suggests that a machine with three blades is preferred. Therefore, straight bladed Darrieus wind machines with three blades are recommended to be concerned in the design process. Three blade wind machines generate steady forces and produce higher starting torque compared with two blade 'Wind machines. Further studies are shown in the CFD, experimental section and wind turbine field tests in Chapters 4, 5 and 6 respectively.

The point has already been made about the Reynolds number effect on the performance of the wind machine. Small wind turbines typically operate at Re about 100,000. And generally it is acknowledged that stall angle and C_{lmax} are very sensitive to changes in Re number. The aerofoil characteristics changes because of the behaviour of the laminar separation bubble which forms on the upper or low pressure surface of the aerofoil, as described by many researches[1,58]. Eppler E374 aerofoil characteristics were used to investigate the influenced of the Re . The results showed that the characteristic of aerofoil sections, C_l and C_d were sensitive to the range of Re 60100 - 100400. At these Re numbers, the aerofoil generated low performance at low angles of wind attack. However, this was not the case at higher number of Re . The study found that the Re numbers could be treated well to solve the disadvantages of Darrieus-rotor VAWTs.

The effect of chord ratio ($\frac{c}{r}$) on the D-rotor showed that the wind turbine gave higher performance at low number of chord ratio. In this study, the results indicated that a VAWT with chord ratio of 0.12 produced significant torque throughout the range of tip speed ratio. However, the model with higher number of chord ratio ($\frac{c}{r} > 0.5$) generated better self-starting ability, but it generated lower turbine performances at higher tip speed ratios. The results showed that the performance of the Darrieus wind turbine generated the same power output whether the radius or chord length is maintained constant (Fig. 3.22). Further studies are shown in the experimental test Chapter 5.

In the study of the blade pitch angles (α), the turbine with blade pitch angles from -6 to +6 were used to predict the machine performances. The results showed that the wind machine performed well at zero degree of blade pitch angle. Additionally, the study also found that the straight-bladed Darrieus wind machine generated better starting torque at this turbine configuration

Five parameters of the Darrieus wind machine have been studied using analytical model predictions, the following conclusions are recommended for further studies.

- NACA 661-212 aerofoil gave the best wind machine performance compared to the others 10 high Reynolds numbers aerofoils.
- S 1223 and Clark-Y aerofoil characteristics generated promising results compared to the other low Reynolds number aerofoils.
- S 1223 developed a lower power coefficient compared With NACA 661-212 and Clark-Y but generated higher starting torque
- The study recommended two or three blades for the Darrieus wind machine for the design process.
- The straight-bladed Darrieus wind machine worked well at the zero degree blade pitch angle.

The above conclusions will be carried out for further investigations including Computational Fluid Dynamics (CFD), experimental tests in the wind tunnel and also the wind machine prototype field-tests to validate the analytical model results.

Chapter 4

Computational Fluid Dynamics (CFD)

4.1 Introduction

This chapter focuses on the investigation of the aerofoil characteristics and the turbine performance using a commercial CFD package - ANSYS CFD version 6.1. In terms of the wind machine engineering, CFD can be widely used to investigate the fluid dynamics aspects of horizontal axis wind machine. Additionally, the study of using CFD on vertical axis Wind machines can be seen in references [64-67]. This study was carried out using two co-ordinate systems:

1. Cartesian co-ordinate system
2. Polar co-ordinate system

The purpose of this study was to examine the feasibility of using CFD to investigate the performance of wind machines.

4.2 The Cartesian coordination of CFD to investigate lift and drag coefficient

4.2.1 Problem descriptions

The problem involves investigation of the lift and drag generated when the air passes through the selected aerofoil profile. Consideration is given to the airflow in a two dimensional wind tunnel. To study this problem an arbitrary inlet wind velocity is selected. The resulting flow could be turbulent or laminar. Laminar and turbulent flow can be classified by Reynolds number R_e . The following equation is used to calculate the R_e . $R_e = \frac{\rho V D}{\mu}$, for air at standard, sea level condition, R_e can be found by $R_e = 69000 VC$. Where ρ and μ are the density and dynamic viscosity of fluid respectively. V represents the average fluid velocity. D represents the diameter of pipe and C is the chord length of the aerofoil. Normally the flow is said to be in a transition region (laminar) when R_e is typically between 2100 and 4000, the conservation of mass for a steady flow requires that the mass flow rate at any section of the wind tunnel remains constant [68].

In this analysis and as mentioned in Chapter 3, NACA 661-212 was used as a recommended aerofoil for further investigation of D-rotor. This aerofoil profile was used to verify the procedure of using ANSYS CFD package for the aerofoil analysis. Table 4.1 and Fig 4.1 describe the specification for this model.

Table 4.1 Model specifications for NACA661-212 aerofoil

Dimensions and properties	
Aerofoil chord length	2 m
Inlet wind velocity	21.74 m/sec
Wind tunnel size	100 x 10 m
Air density	12.225 kg/m ³
Reynolds number	3×10^6

From Table 4.1 the Reynolds number, Re is higher than the range of 2100-4000, which is the investigation of the turbulence mode in CFD.

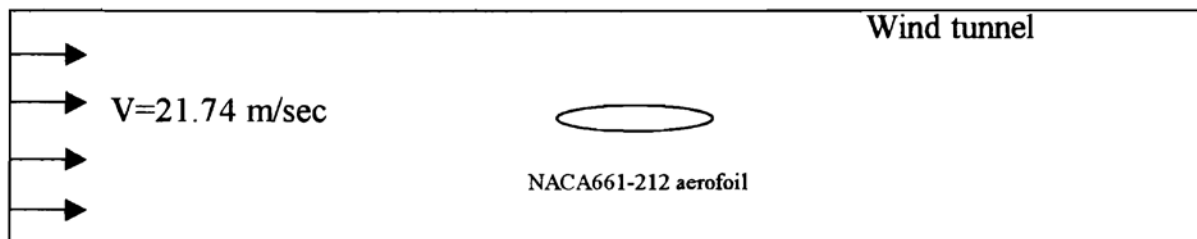


Fig. 4.1 Model description of the CFD analysis

4.2.2 The procedures to use the ANSYS CFD

The ANSYS Motran is suitable for analysing two-dimensional fluid flow fields. Using the information in the problem description and following the steps below the problem can be solved. The three essential steps are:

- Pre-processing
- Solution
- Post-processing

4.2.2.1 Pre-processing (Turbulent models)

1. Set preferences by going step by step

1.1 Go to **main menu**, preferences (Fig. 4.2)

1.2 Turn on **Flotran CFD**

1.3 Click **OK**

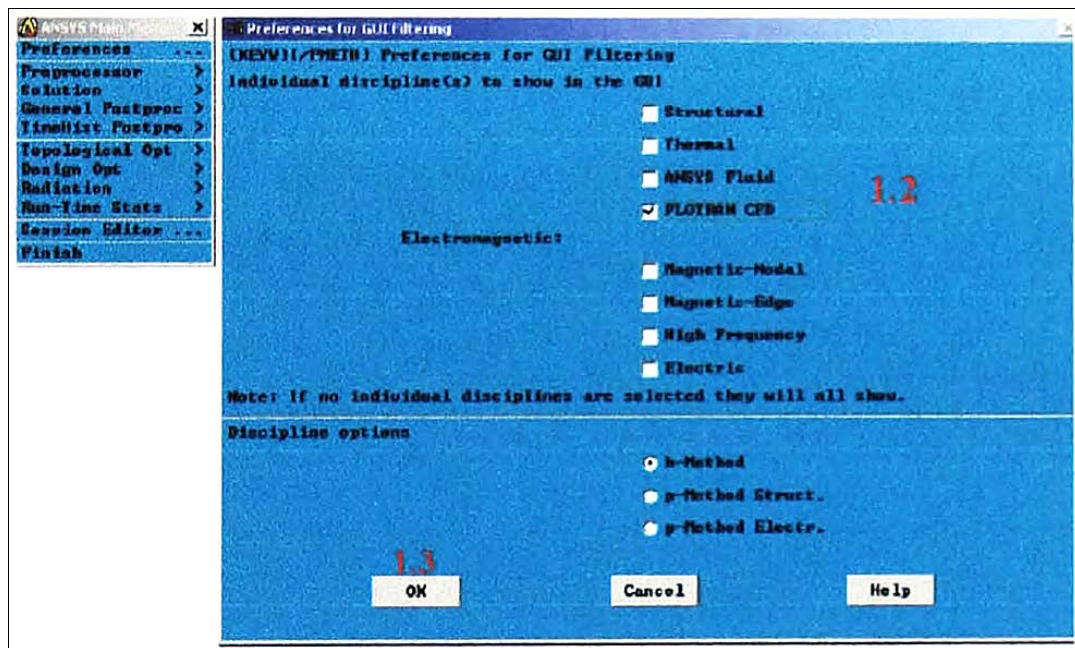


Fig. 4.2 The preference selection in Pre-processing of CFD

2. Define element type in main menu (Fig. 4.3)

2.1 Preprocessor- Element type

2.2 Add element

2.3 Choose Flotran CFD- Choose fluid 141 (for 2D analysis)

2.4 Click OK and close

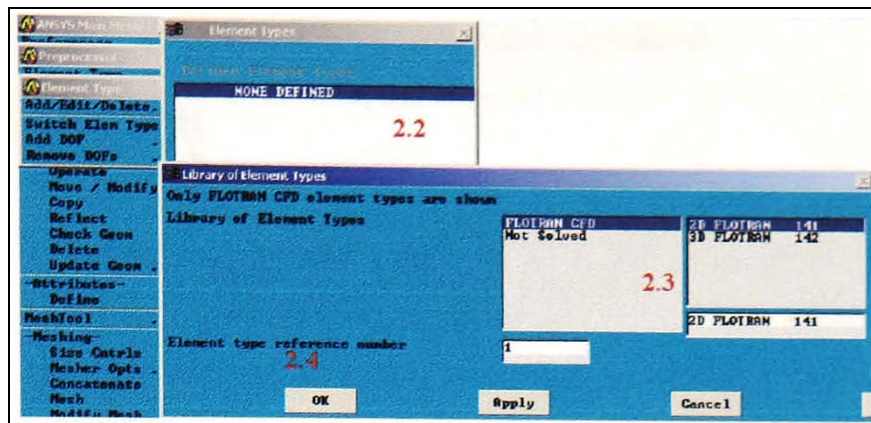


Fig. 4.3 Define element type in CFD

3. Create rectangular wind tunnel of 100 x 10 m. (Fig. 4.4)
 - 3.1 Pre-process, Model, Create
 - 3.2 Area; Rectangle; By dimensions
 - 3.3 Put the co-ordination; X1= -50 X2 =50, Y1= -5 Y2 =5
 - 3.4 Click Ok and the Rectangular area of wind tunnel will be displayed.

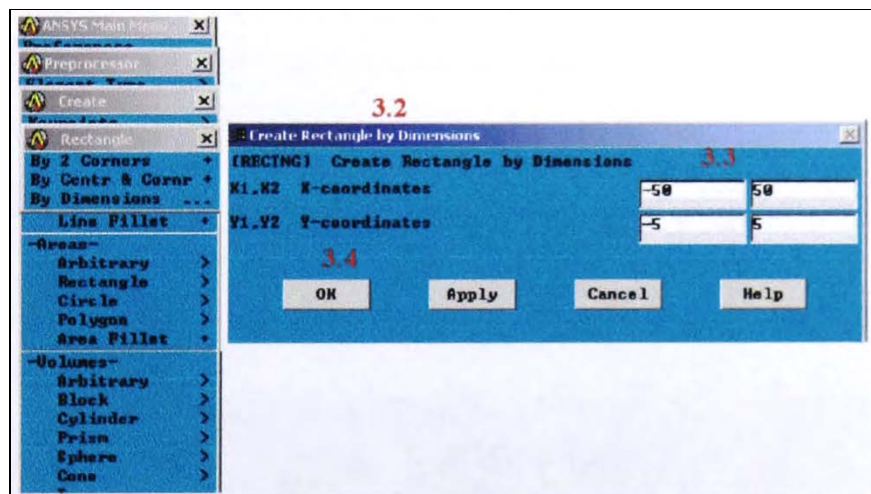


Fig. 4.4 Create the Rectangle wind tunnel

4. Create the selected aerofoils, for the NACA 661-212 profiles
 - 4.1 Preprocessing; Modelling; Create
 - Keypoints; In active CS
 - Put key point number and the co-ordinations of NACA661-212 aerofoills
 - 4.2 Corcct every keypomt with the Ime (Fig. 4-5)
 - Preprocessor, Create, Line, In active Coordinate
 - Pick every keypoint to form aerofoils shape
 - Click OK to complete command



Fig. 4.5 Line connect to the created keypoints to form the profiles

5. Subtract the area between aerofoil and wind tunnel
 - 5.1 Preprocessor
 - 5.2 Modelling; Operate; Booleans; Subtract; Area
 - 5.3 Pick the wind tunnel area, Click apply, Pick the aerofoil area
 - 5.4 Click OK to complete the operation
 - 5.5 The area between wind tunnel and aerofoil is subtracted (see Fig. 4.6)

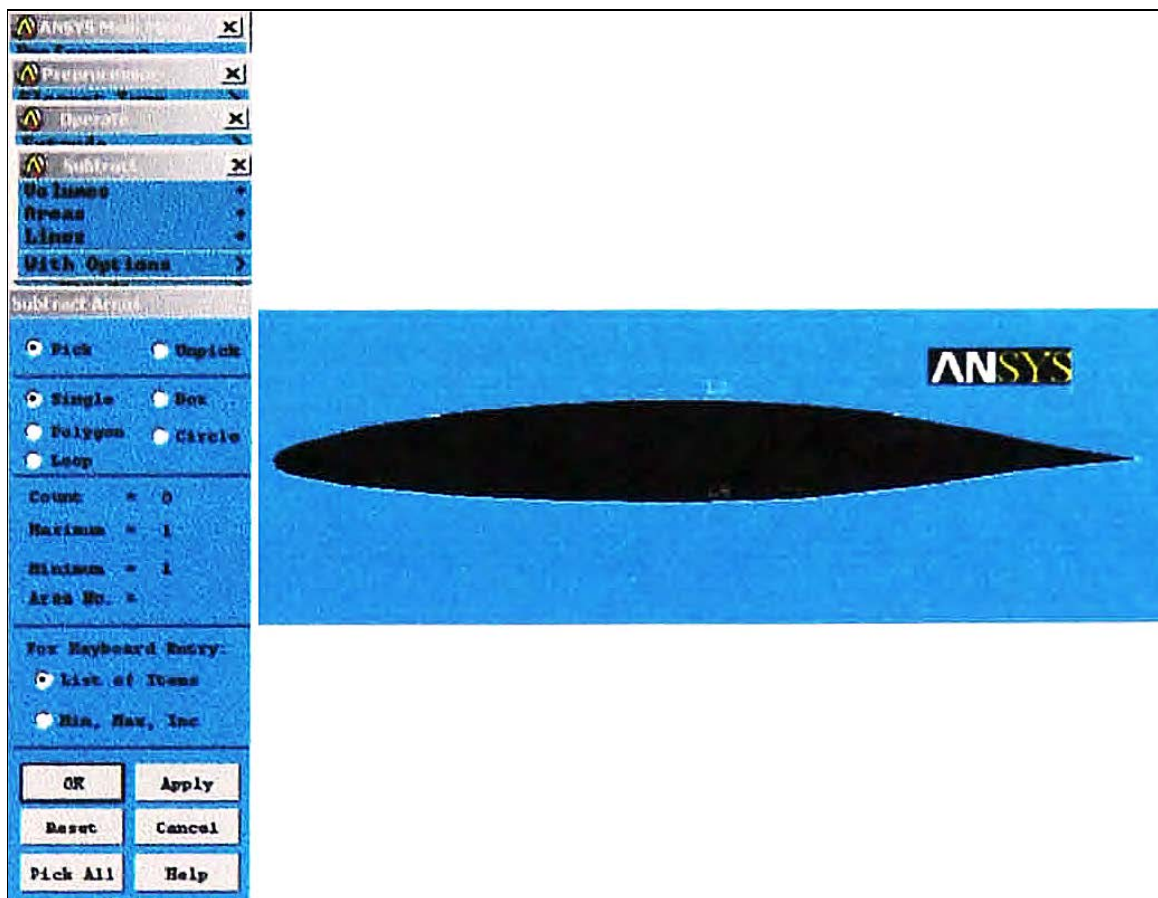


Fig. 4.6 Aerofoil and the wind tunnel is subtracted ready to create the mesh and element

6. Establish mesh patterns

The general finite element philosophy is to put more elements in regions with higher solution gradients e. g. to the edge of wind tunnel and around the aerofoils. The mesh density should be sufficient to enable the program to capture the nature of the phenomena. Create the mesh pattern using the following steps:

- 6.1 Preprocessor; pick a smart size to off, set global element size to 0.1.
- 6.2 Set line and pick to create more density of preferred area mesh for example at the edge of the aerofoils.
- 6.3 Select mesh shape to quadratic and free
- 6.4 Click mesh and pick all
- 6.5 Wait until the meshing area is completed and the mesh pattern will be displayed (Fig. 4.7)
- 6.6 If considered unsatisfactory then the refine mesh option can be used to recreate the mesh again. The package "I repeat this process of picking the lines and entering the number of divisions and the ratios, using the mesh division strategy.

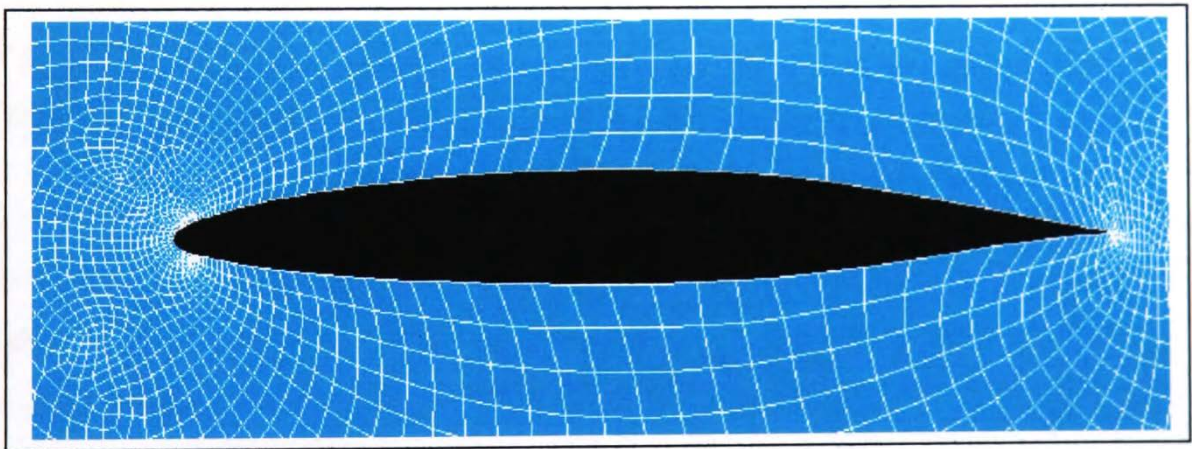


Fig. 4.7 Mesh generated around aerofoil by ANSYS CFD package

7. When the mesh generation is completed, go to tool bar and click Save DB. In order to prevent some mistakes this tool could be applied at every completed step described above.

8. Apply boundary conditions

A velocity of 21.41 meters/second is applied to the X direction (V_x) at the inlet of wind tunnel, and a zero velocity is applied in the transverse direction at the inlet (V_y in the Y direction). Zero velocities in both directions are applied all along the walls of the wind tunnel, and a zero pressure is applied at the outlet (see Fig. 4.8 for more details). These boundary conditions are being applied to the lines now so that they do not have to be applied again if re-meshing is required. The following steps show the procedure to apply the boundary conditions to the model.

8.1 Go to utility menu; Pick plot line, now the working area will be displayed only the line which will be more easy to apply the boundary conditions

8.2 In Preprocessor menu pick **Loads, apply, velocity, on line**, pick and apply the velocity as descnbed in Fig. 4.7. To apply the pressure to the model repeat the steps above and change the command to pressure instead of velocity.

After applying the boundary condition, go to tool bar and Save DB again. At this point, the finite element model is complete and the Flotran menus are accessed to specify the fluid properties along with any other Flotran controls that may be required.

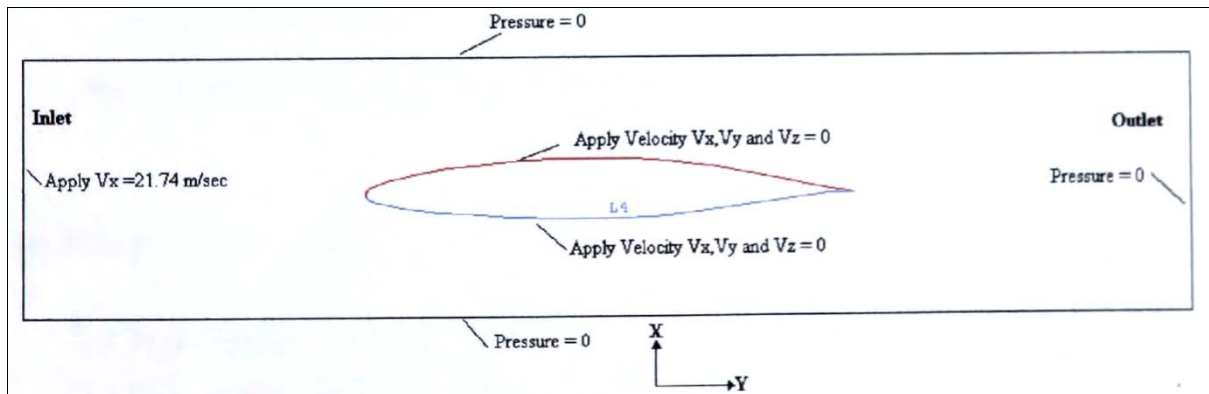


Fig. 4.8 Boundary conditions applied to the CFD model (Cartesian mode)

4.2.2.2 Solution (Turbulent model)

This process is used for setting the Flotran configurations to the model as described in the following steps:

1. Establishes the fluid properties. The fluid property for the air of this model is in m N-sec (SI unit).
 - 1.1 Go to **Main Menu**, **Solution**, **Flotran Set up**, **Fluid properties**, Pick all to AIR-SI (Fig. 4.9)
 - 1.2 Click **Apply** and **OK**

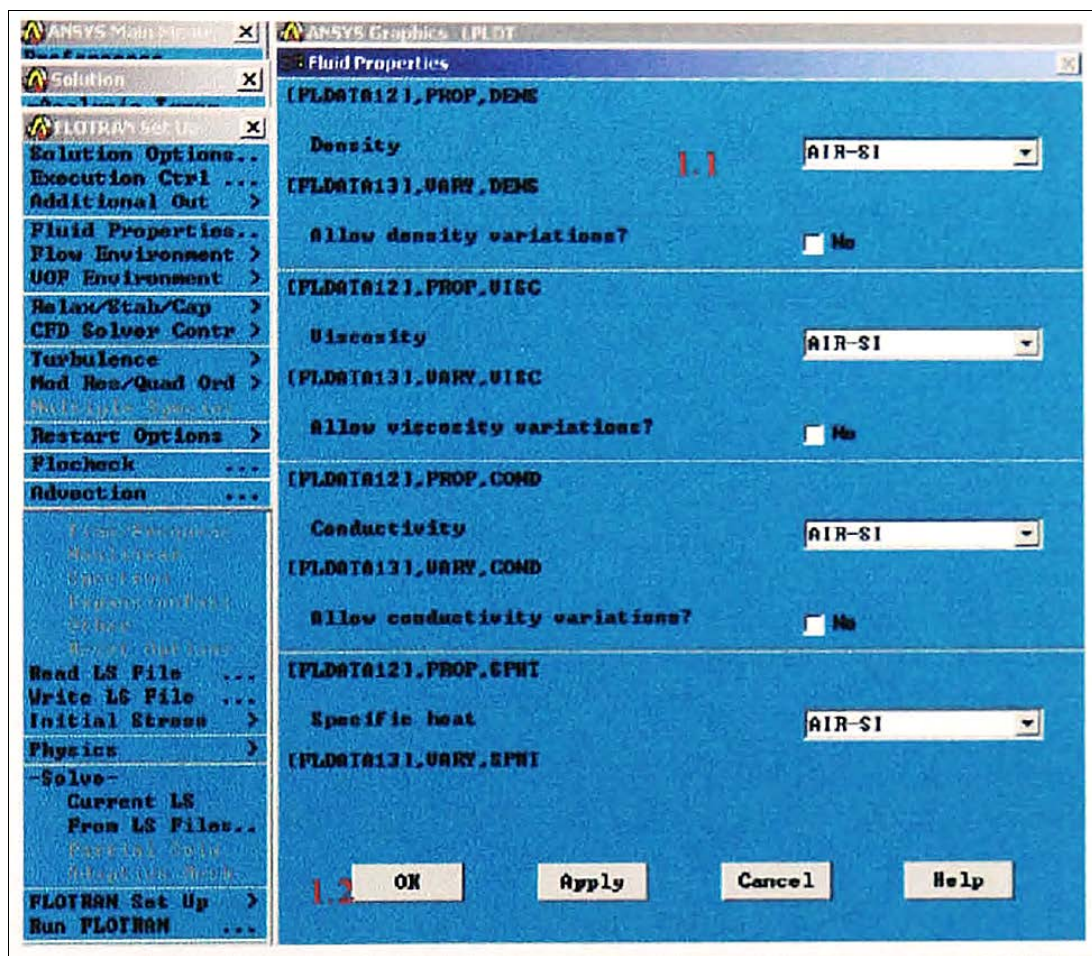


Fig. 4.9 Air properties apply to the CFD model

2. Set Flotran solution option
 - 2.1 **Main Menu**; **Solution**; Flotran set up; **Solution option**
 - 2.2 Pick **Solve Flow Equation**; Steady state; Adiabatic; Turbulent; and Incompressible to On (Fig. 4.10)
 - 2.3 Click **OK**

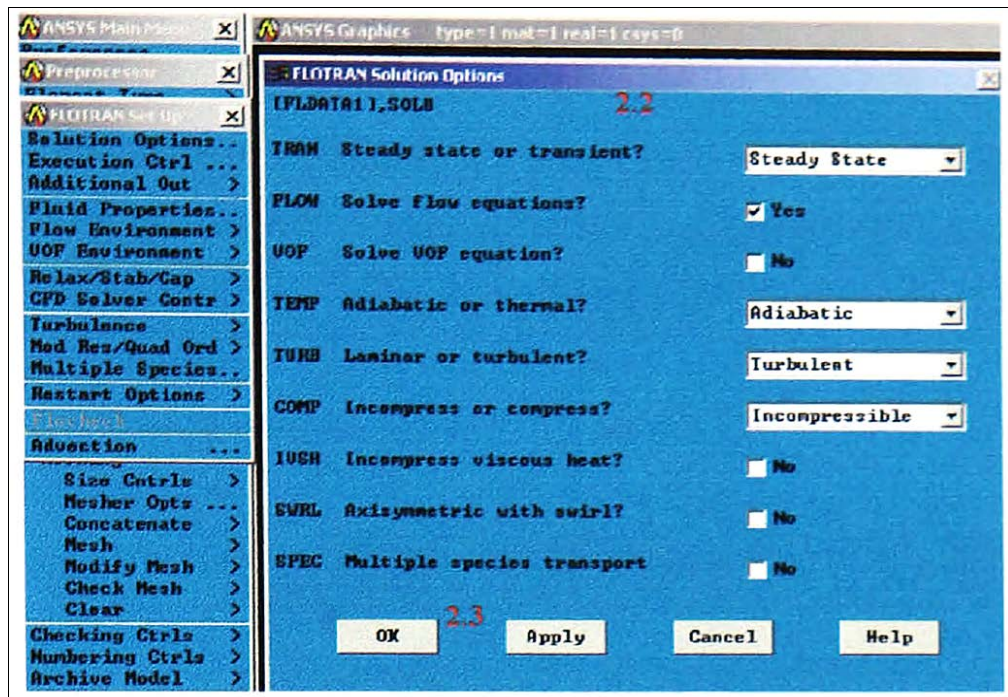


Fig. 4.10 The Flotran solution option apply to the model

3. Set execution controls. Choose the execution control from the Flotran Set-up Menu.
 - 3.1 Main menu; Solution, Execution control
 - 3.2 Set global iteration to 1000
 - 3.3 Set output summary frequency to 10 (Fig. 4.11)
 - 3.4 Click OK to confirm set up and save DB file.

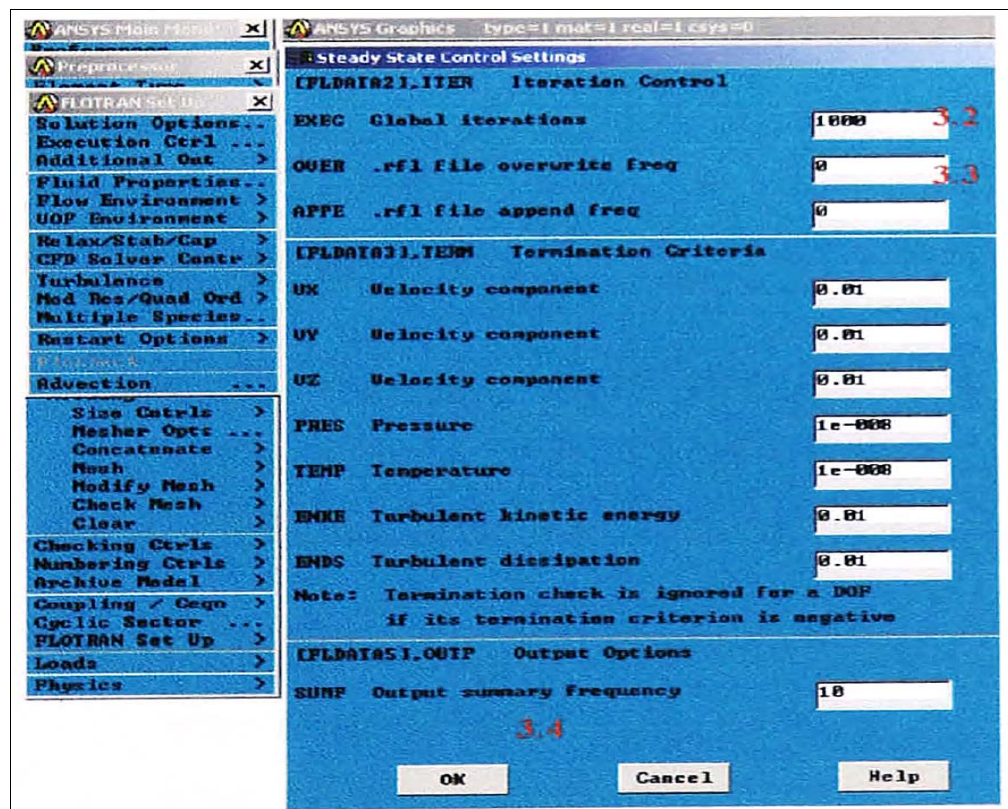


Fig. 4.11 Execution control set up for the model

4. Execute Flotran solution

4.1 Main Menu; Solution; Run Flotran. While running the Flotran solution, ANSYS will plot the "Normalized Rate of Change" as a function of the "Cumulative Iteration Number." This is the Graphical Solution Tracker, which allows visual monitoring of the convergence of the solution (Fig. 4.12).

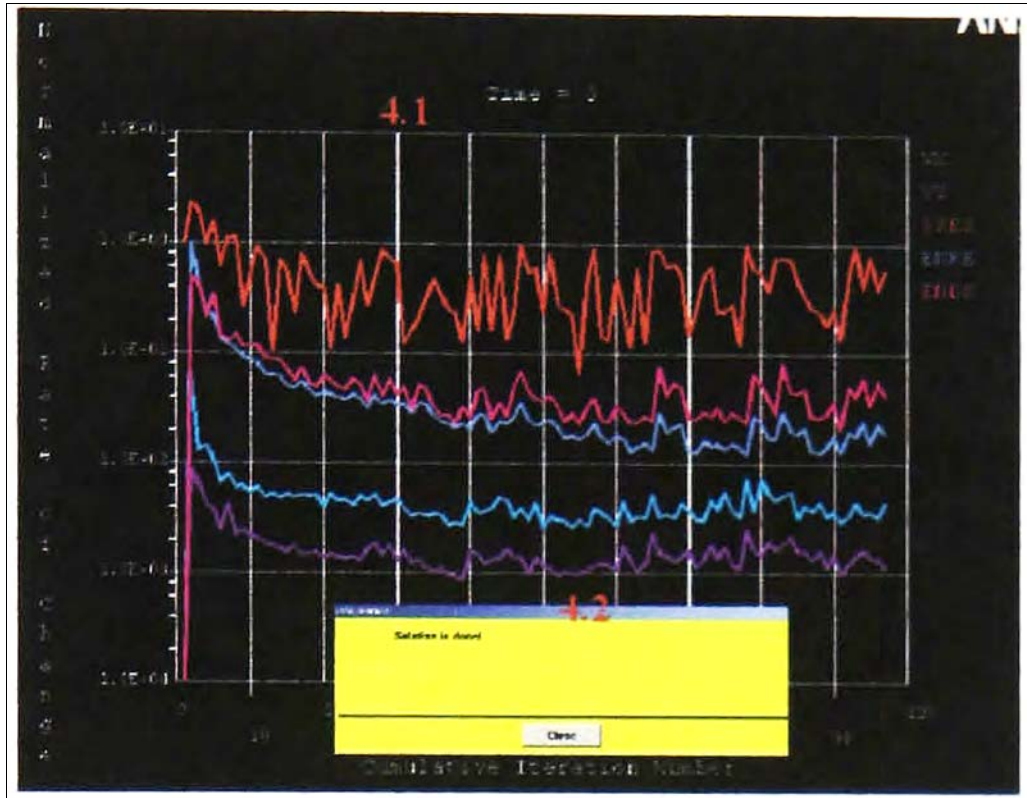


Fig. 4.12 The vision monitoring while running the execution

4.2 Close the information window when the solution is done

4.2.2.3 Post processing

This process is used for reading the computed results. To read the result enter the general Postprocessor and request the computer to read the latest set of the solution results, then we can study and plot all the results including:

- Plot the velocity
- Plot the pressure
- Plot the vector of flow

For example, Fig. 4.13 shows the velocity and pressure plot of NACA 661-212 at zero angle of the wind attack.

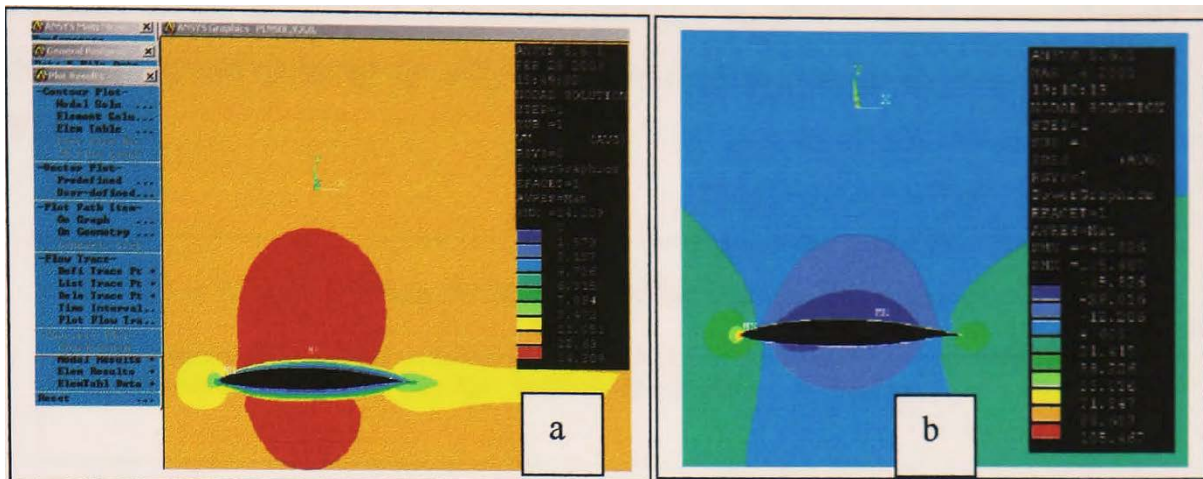


Fig. 4.13 The velocity (a) and Pressure (b) plot results by Post Processing command in ANSYS CFD

Fig. 4.13 shows the pressure contour around the aerofoil. The different colour contour indicates various wind velocities. The calculation of the lift and drag forces generated on the aerofoil section have been done using integration of pressure in nodal calculation section. The following steps show how to get the results of the aerofoil characteristics (lift and drag) using CFD technique.

1. Go to **Main menu, General Post-processor, Click Last Set, Nodal Calculation**
2. Surface integration, pick pressure (Fig. 4.14)
3. Click **OK**

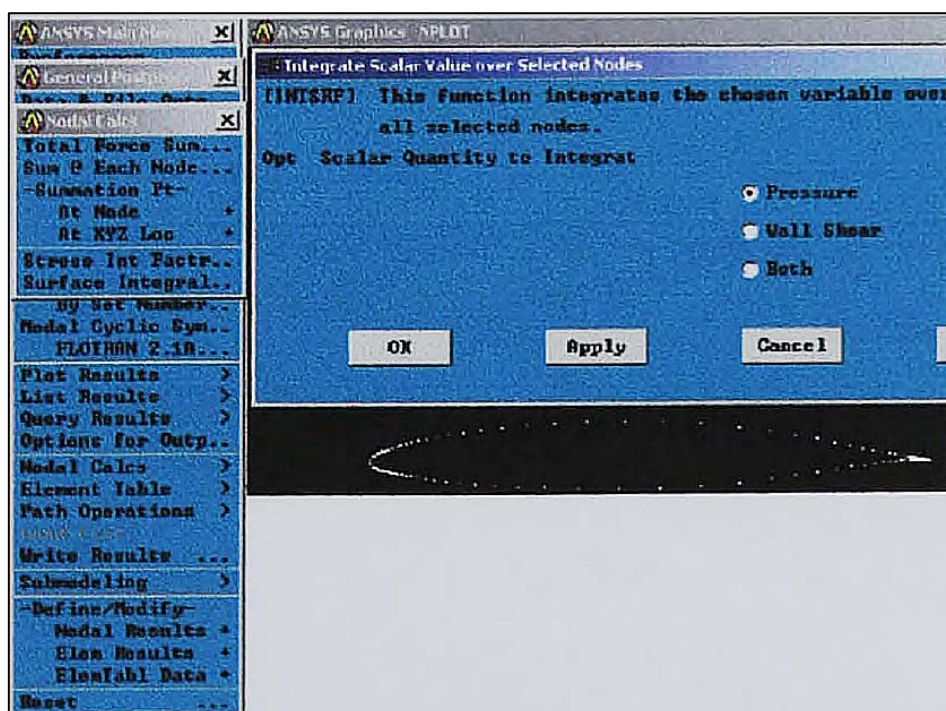


Fig. 4.14 Integration of pressure around aerofoil from CFD

The results of the integration of pressure overall the selected node (around aerofoil) show lift, drag and moment developed on this aerofoil section (NACA661-212) (Fig. 4.15).

SUM THE VALUES OF PRES OVER THE SURFACE DEFINED BY THE SELECTED NODES

X, Y, Z REACTION LOAD COMPONENTS = 0.564327523 2.62442874 0.00000000
MOMENTS ABOUT RSYS ORIGIN = 0.00000000 0.00000000 0.127228921

Fig. 4.15 The lift, drag and moment developed at zero degree wind attack on NACA661-212 by CFD

The following section 4.2.3 shows the results of the investigation of two aerofoil profiles using the CFD modelling as described in the previous section.

4.2.3 Lift and Drag Coefficient Results

Two aerofoil profiles studied included NACA661-212 and NACA 4424. The procedures of using CFD ANSYS 6.1 in Cartesian coordination system to compute lift and drag are shown in section 4.2.2. The lift and drag force generated when the wind passes through the upper and lower surface of an aerofoils were computed and studied. The resulting lift (L) and drag forces (D) were used to obtain the lift and drag coefficients.

For the lift coefficient
$$C_l = \frac{L}{\frac{1}{2}\rho AV^2} \quad (33)$$

and the drag coefficient
$$C_d = \frac{D}{\frac{1}{2}\rho AV^2} \quad (34)$$

if
$$K = \frac{1}{2} \rho AV^2 \quad (35)$$

In order to calculate the lift and drag coefficients, the K value is determined. In equation (35) above, A in 2 dimensional analysis represents the chord length of the aerofoil c and the air density ρ is 1.225 kg/m^3 at the sea level. Therefore, the K value becomes

$$K = 0.5 \times 1.225 \times 2 \times 21.74^2 = 578.96 \text{ N}$$

The drag coefficients C_d becomes

$$C_d = \frac{D}{K} \quad (36)$$

and the lift coefficients C_l becomes

$$C_l = \frac{L}{K} \quad (37)$$

4.2.3.1 NACA 661-212

A symmetrical aerofoil is suggested and recommended for the analytical model prediction (Chapter 3). In the analytical prediction section, this aerofoil generated promising results when employed to straight-bladed Darrieus Wind machine. Further investigation using CFD method has been computed using specific criteria, which are shown in the Table 1. This aerofoil was computed by CFD method using ST units and incompressible flow of fluid properties.

The dimensions of the computer model of the aerofoil were based on the experimental data in [51]. The results of the lift and drag force and also their coefficients are presented in Table. 4.2.

Table 4.2 Comparison results of CFD and NACA data

Angle of attack	Drag F_x (N)	Lift F_y (N)	C_d (CFD)	C_d (NACA)	C_l (NACA)	C_l (CFD)
0	17.16	115.371	0.0296	0.0041	0.15	0.1993
2	12.99	185.74	0.0224	0.0042	0.32	0.3208
4	29.66	289.03	0.0512	0.0082	0.51	0.3526
6	25.68	307.02	0.0433	0.010	0.7	0.5303
8	33.36	382.16	0.0575	0.012	0.95	0.6601
10	73.41	736.64	0.1268	0.016	1.15	1.2724
12	94.24	850.63	0.1628	0.021	1.35	1.4692
16	155.04	922.70	0.267	0.011	0.8	1.593
-2	18.34	-15.83	0.0317	0.0065	-0.05	-0.0274
-4	21.42	-107.24	0.0370	0.008	-0.25	-0.1849
-8	38.586	-406.51	0.0721	0.011	-0.65	-0.7018
-12	63.131	-518.73	0.1176	0.016	-0.92	-0.8960
-16	100.70	-564.55	0.172	0.0	-0.52	-0.97

The results of lift and drag forces (Table 4.2) were computed using CFD ANSYS 6.1 package in the 2-D mode. These data in graphic form were plotted to compare between the published NACA aerofoil characteristics and the results obtained from using CFD technique. The results of aerofoil characteristics are compared in Fig. 4.15 and Fig 4.16. As can be seen from the results in Fig. 4.16, the lift coefficients were similar to the NACA published results in the range of angle of attack θ of -12 to +14 degree, but some different results also occurred beyond these ranges. However, Fig. 4.16 shows that the drag coefficients from CFD technique were dramatically different from the published NACA results at all range of angles of wind attack θ . This problem requires further investigations.

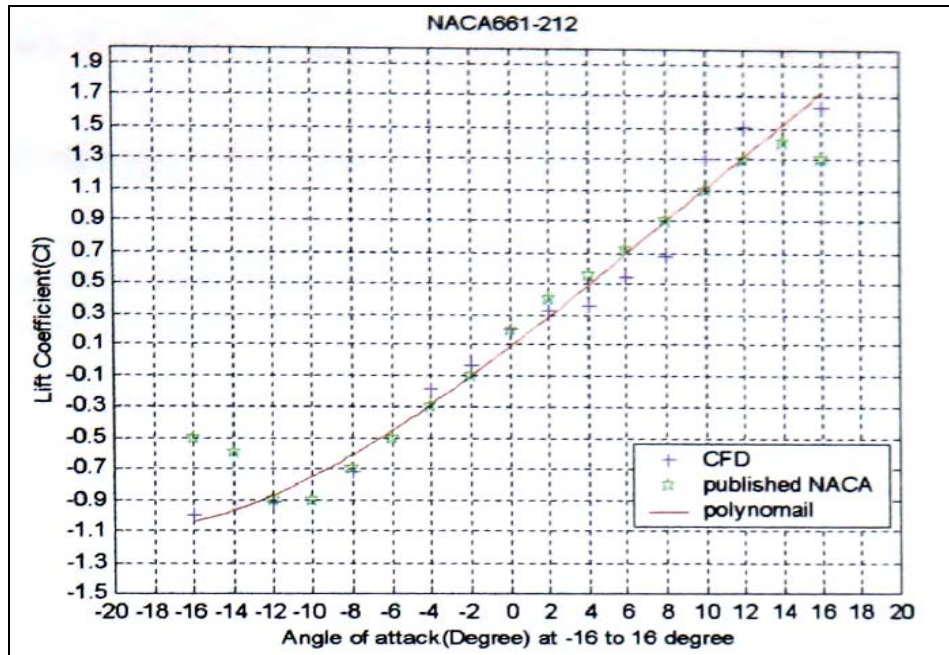


Fig. 4.16 Lift coefficients between CFD and NACA results

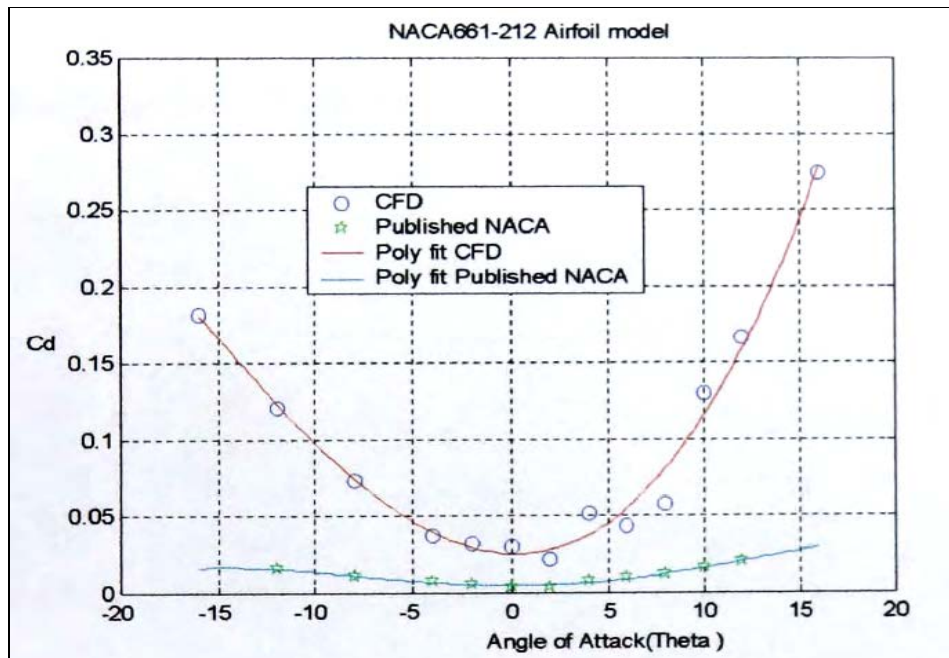


Fig. 4.17 Comparison of drag coefficient between CFD and NACA results

4.2.3.2 NACA 4424

The aerofoil characteristics (C_l and C_d) of NACA 4424 are available in reference [69]. The main objective of this section is to compare the results from three different published aerofoil data. As mentioned in section 4.3.1 the results of CFD method on NACA 661-212 aerofoil were significantly different from the NACA published source of drag coefficients. The model

was computed under the following specifications (Table 4.3), which are the same as used in other studies [51] and [69].

Table 4.3 Model specifications for NACA 4424 aerofoil

Dimensions and Properties	
Aerofoil chord length	0.2 m
Inlet wind velocity	34 m/sec
Wind tunnel size	10 x 1 m.
Air density	12.225 kg/m ³
Reynolds number	4692000
Air properties	Air SI, Incompressible Flow
CFD model	Turbulence

The CFD investigation was carried out by varying the range of wind attack from -5 degree to +20 in 5-degree intervals. The results of this study are shown in Table 4.4

Table 4.4 Comparison of results of NACA 4424 lift and drag coefficients

Angle of attack	Drag F_x (N)	Lift F_y (N)	C_d (CFD)	C_d (NACA)	C_l (NACA)	C_l (CFD)
0	13.07	81.74	0.09 / 0.85	0.009	0.35	0.57 / 0.45
5	16.49	143.72	0.11 / 0.09	0.015	0.85	1.01 / 1.0
10	25.06	223.41	0.17 / 0.1	0.017	1.2	1.5 / 1.3
15	35.14	290.41	0.24 / 0.15	0.020	1.250	2.0 / 1.75
20	42.28	340.21	0.29 / 0.2	0.017	1.2	2.4 / 1.9
-5	12.31	-18.34	0.086 / 0.09	0.0095	-0.2	-0.13 / -0.2

Fig 4.18 shows a comparison of the results obtained using the CFD method with the published data from [69].

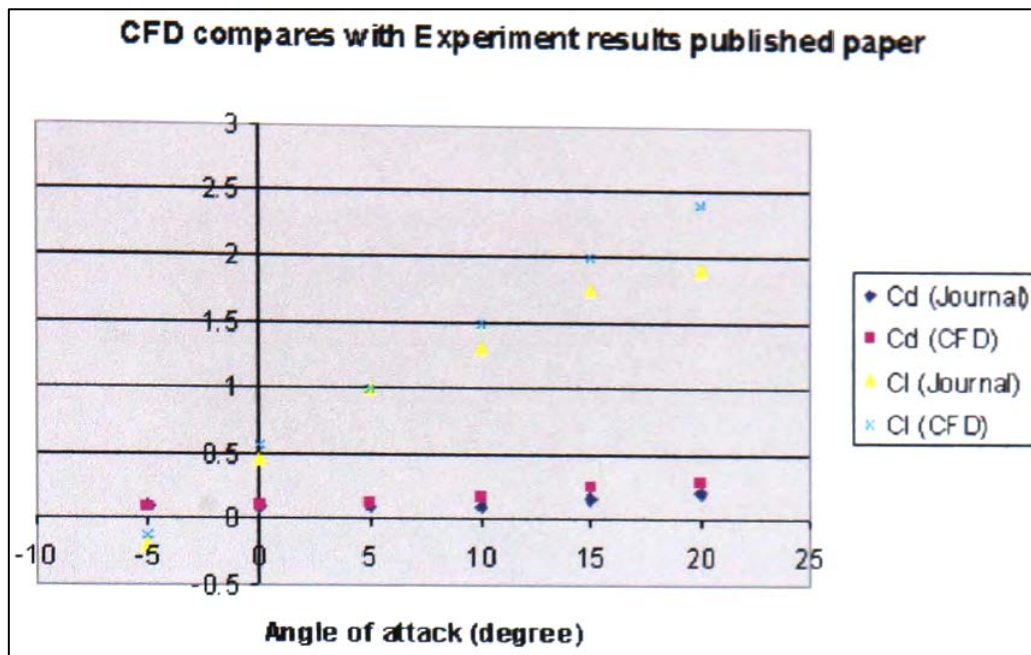


Fig. 4.18 Displays the comparison of NACA4421 aerofoils characteristics (C_l , C_d) results between CFD method and the published data

The investigation of using CFD to compute NACA 4421 aerofoil characteristics showed that the results agree fairly well with the data from reference [69] in terms of either lift or drag coefficients. However, the study found that the aerofoil characteristics data obtained from NACA experimental work [51] were different from those in the published paper in reference [69]. The experiment results on drag coefficients did not agree but only lift coefficients values were similar (see Fig. 4.19 and 4.20).

The study also found that aerofoils characteristics from [51] and [69] have been investigated using different aerofoil chord ratios. The results from NACA were experimented using longer size of chord length (2 meters) but the aerofoil model in the published journal [57] was only 0.2 meters. The further investigations and studies of the NACA 4421 from these references [57 and 69] are recommended.

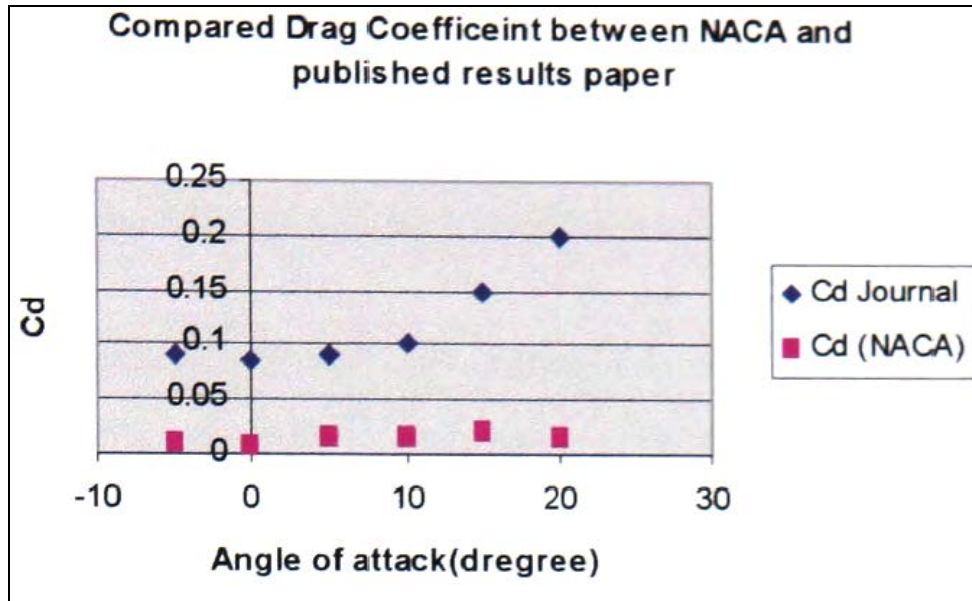


Fig. 4.19 Comparison of results: Drag Coefficients

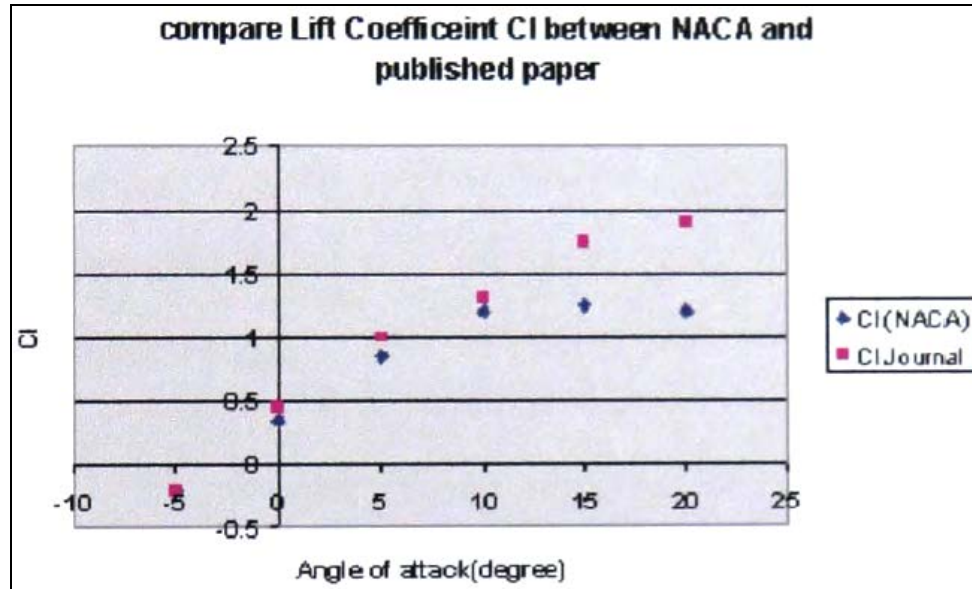


Fig. 4.20 Comparison of results: Lift Coefficients

4.3 The Polar co-ordinate CFD to investigate the torque on the rotor of wind machine

Computational Fluid Dynamics (CFD) was used as the tool to compute the torque T developed when the airflow passes over the surface of an aerofoil. The torque will be calculated and recorded by the CFD tool. And this torque becomes the useful power P by the following equation

$$P = T \times \omega \quad (38)$$

When ω is the angular velocity in rad/s and can be found by

$$\omega = \frac{2\pi N}{60} \quad (39)$$

N represents the rotor revolution in rpm (round per minute).

In this section, the desired aerofoil was applied to the ANSYS Flotran 6.1 using the polar coordinate system to compute the torque generated on the rotor of wind machine. The polar coordinate system enables the user to compute the behaviour of rotating objects.

4.3.1 Problem descriptions

Polar co-ordinates were used to the performance of a rotating turbine. The model comprises two parts; stationary and rotating. The stationary part was the wind tunnel and the rotating part was the aerofoil section. Figure 4.21 describes the details of the investigating model. In this study, the NACA661-212 section was selected as a desired profile for the vertical axis wind machine rotor.

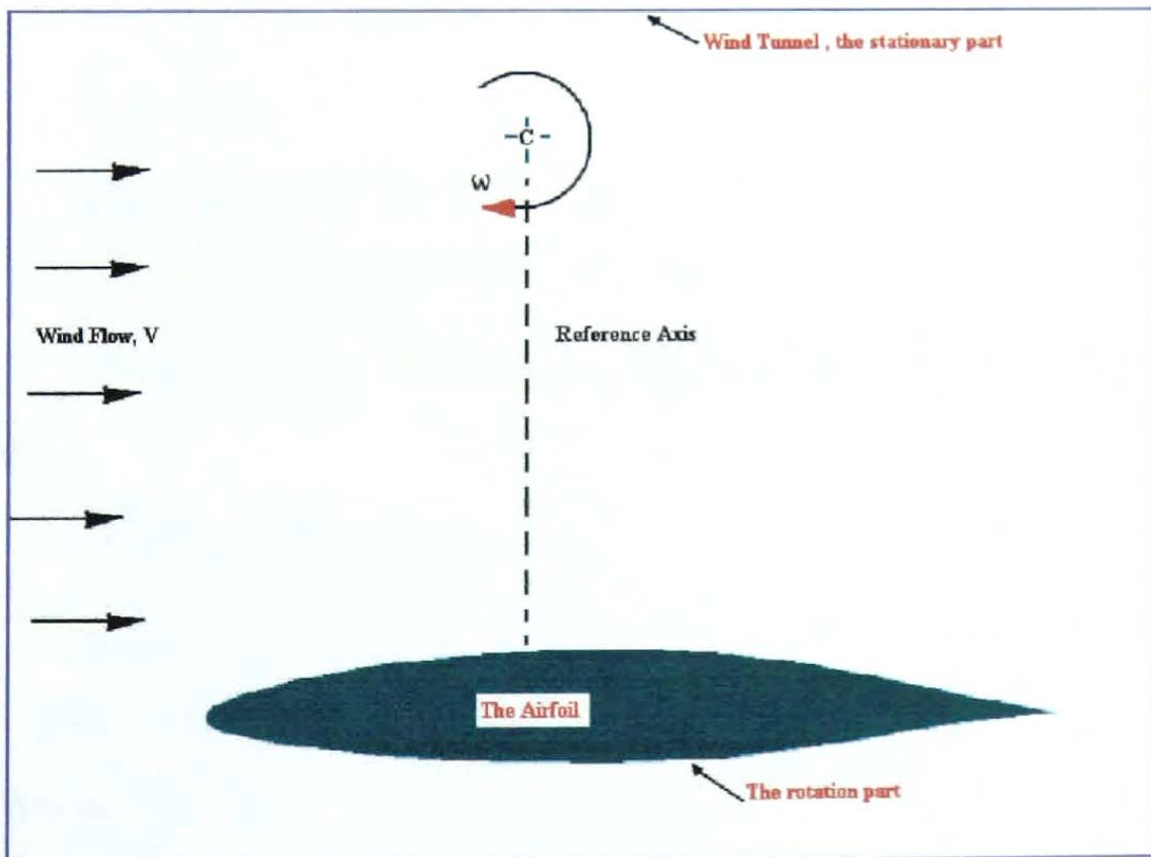


Fig. 4.21 Schematic drawing showing the rotating and non-rotating part of the present model study (Polar mode)

4.3.2 The procedures

Procedures are the same in both polar and Cartesian co-ordinate svstems as described in Section 4.2.2.

Table 4.5 The model specification

Dimensions and Properties	
Aerofoil chord length	0.2 m
Inlet wind velocity	10 m/sec
Wind tunnel size	20 x 2m.
Air density	12.225 kg/m ³
Rotor radius	0.2 in
Air properties	Air SI, Incompressible Flow

The steps below were used to investigate the performance of vertical axis wind machine using polar coordination in CFD.

❖ *Preprocessing (Turbulent Analysis)*

- Create the desired aerofoil section (NACA 661-212)
- Create the wind tunnel model (20 x2m.)
- Establish mesh patterns
- Create the finite element mesh (see Fig. 4.22)
- Apply the boundary conditions for the rotation speed of 50 rad/sec at incoming Wind velocity of 10 m/sec (see Fig. 4.23)
- Change the coordination to the polar system (see Fig. 4.24)

❖ *Solution*

- Establish fluid properties
- Set execution control
- Execute Flotran solution

❖ *Post processing*

- Read in the results for post processing
- Plot velocity vectors (see Fig. 4.25)
- Plot the pressure and velocity on the aerofoil (Fig 4.26)
- Integrate the torque generated in the aerofoil at every rotor position

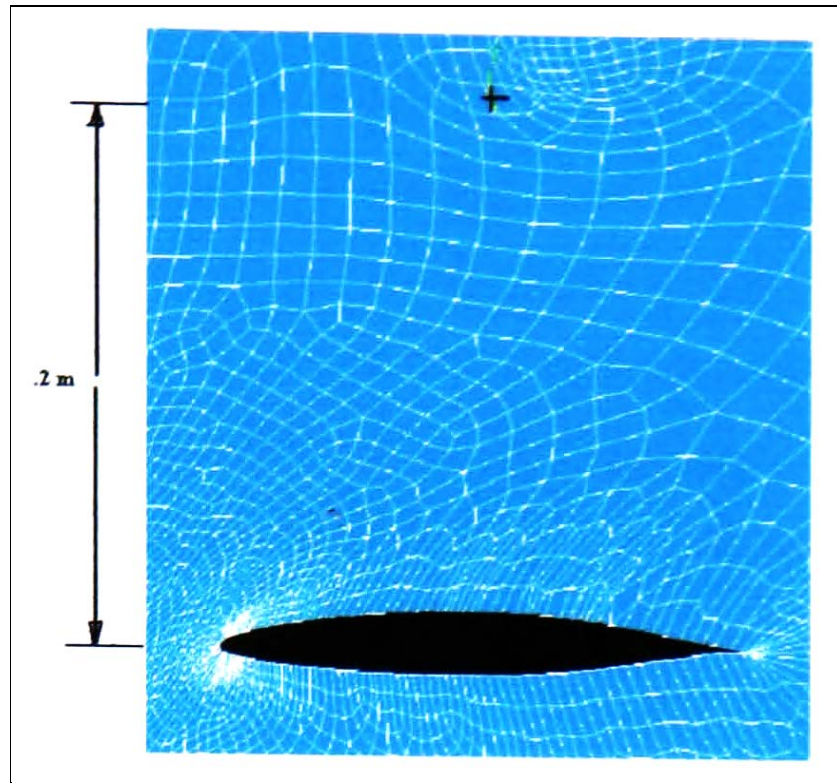


Fig. 4.22 Mesh generated using ANSYS mesh creator to the model

This study used the NACA661-212 section as the rotor of the Darrieus wind machine. This Wind turbine operates at rotational speed (ω) of 50, which is about 500 rpm (calculate from equation 39).

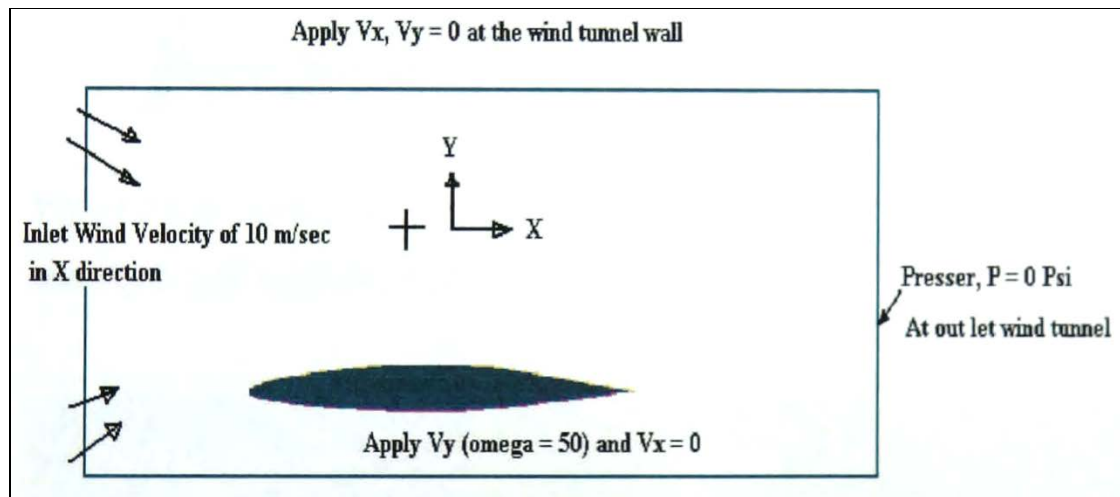


Fig. 4.23 Boundary conditions on the investigation model in CFD (Polar Mode)

In this study, the interval 10 degree of the blade position (γ) to 360 degree of revolution will be applied to analyse the torque on the 1 blade Darrieus wind machine. The torques were computed by the nodal integration tool in Flotran CFD in order to determine the power coefficients C_p using equation (38).

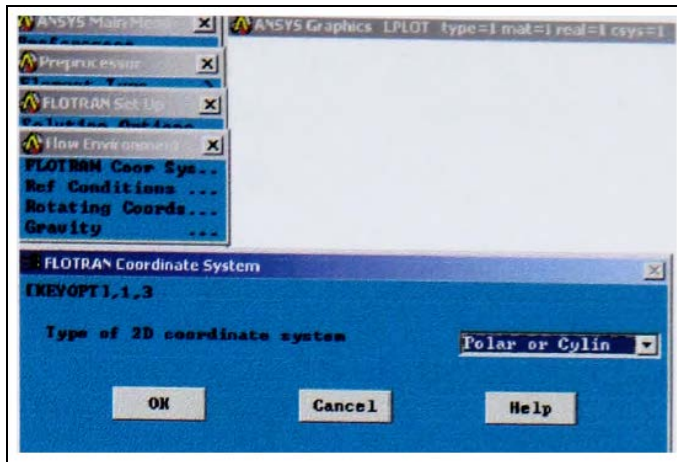


Fig. 4.24 Changing of Flotran coordinate system

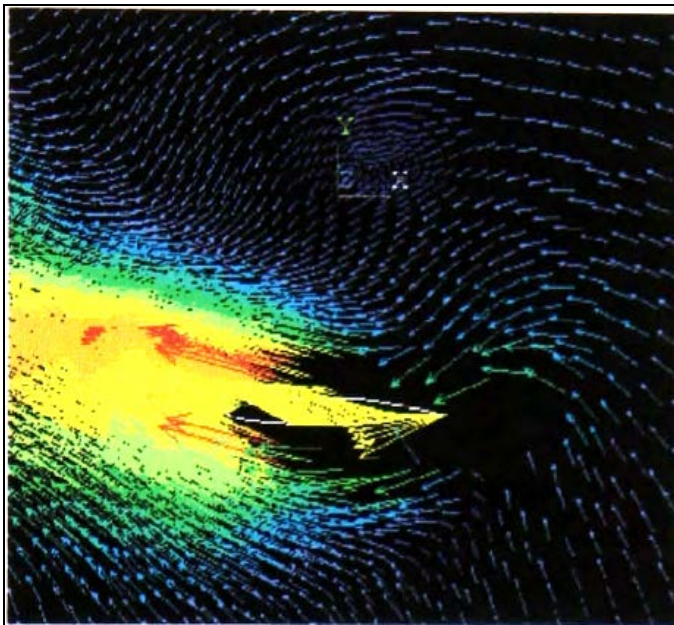


Fig. 4.25 Example of vector contour plot on the model at 1000 Iteration number and angular velocity of 50

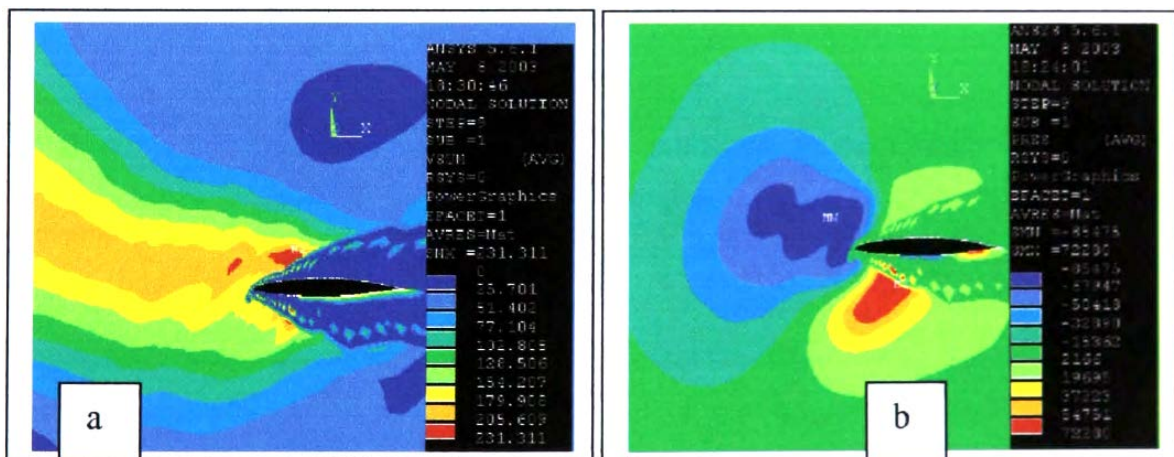


Fig. 4.26 (a) Contour plot of the wind velocity on aerofoil and (b) the pressure computed by CFD on the rotor blade of Darrieus wind machine

23-blade positions of single rotor Darrieus wind machine have been computed and the torque developed on the rotor investigated. The models were computed at the iteration number of 1000 and under the incompressible flow of fluid properties. The results of this study are shown in Table 4.6.

Table 4.6 Results of the investigation using CFD to compute the torque

Blade position	FX (N)	FY (N)	Moment (N.m)
0	13.842	-69.867	5.508
10	14.19	5.002	7.939
20	8.707	-27.031	7.057
30	19.94	6.18	6.09
40	40.782	25.198	5.708
50	35.02	13.7108	4.27
60	56.99	10.35	6.87
70	3.541	-20.042	9.33
80	16.537	-13.277	5.9885
90	34.149	-19.654	9.544
100	34.123	-24.62	8.942
110	52.94	-47.11	14.00
130	18.58	45.606	13.5045
140	-8.7882	-12.445	9.86
150	-21.79	15.4	8.289
160	-24.208	40.82	7.283
170	-20.725	75.591	5.531
180	-8.535	108.31	4.749
190	11.97	141.42	4.08
200	38.57	159.41	4.09
210	100.773	240.002	11.312
220	66.043	115.386	4.329
270	-144.92	13.93	2.375
$\sum_{0}^{270} m$	337.7308	691.0578	166.649
$Mean = \frac{\sum m}{n, (number)}$	337.73 / 23=14.83	691.05 / 23=30.04	166.649 / 23=7.24

From the results of investigation Table 4.5, the power coefficients can be found by

$$C_p = \frac{P}{P_{max}}. \quad \text{The area of the turbine for this model was } 0.16 \text{ m}^2.$$

From equation (24), power coefficient for the CFD investigation becomes

$$C_p = \frac{P}{P_{max}} = \frac{T \times \omega}{\frac{1}{2} \rho A V^3} = \frac{(7.24)(50)}{0.5 \times 1.225 \times 0.16 \times 10^3} = \frac{326}{98} = 3.326 \text{ (Over Betz limit, 0.593)}$$

The C_p results showed that it was not appropriate to investigate the performance of D-rotor using this particular Computational Fluid Dynamics (CFD) technique. High torque was developed at the rotor and it was impossible to achieve the correct answer.

4.4 The solution using ANSYS Flotran CFD

The results of this study suggest that the polar co-ordinate system in Flotran CFD is not suitable for wind turbine studies.

4.4.1 ICEM CFD

Because of the complexity of the vertical axis wind machine, the application of CFD requires good geometry integrated mesh generation and post-processing tools. ICEM CFD is available that maintains a close relationship with geometry during mesh generation and post-processing. ICEM CFD (Fig. 4.27) might provide the sophisticated mesh to the model as the mesh optimisation tool.

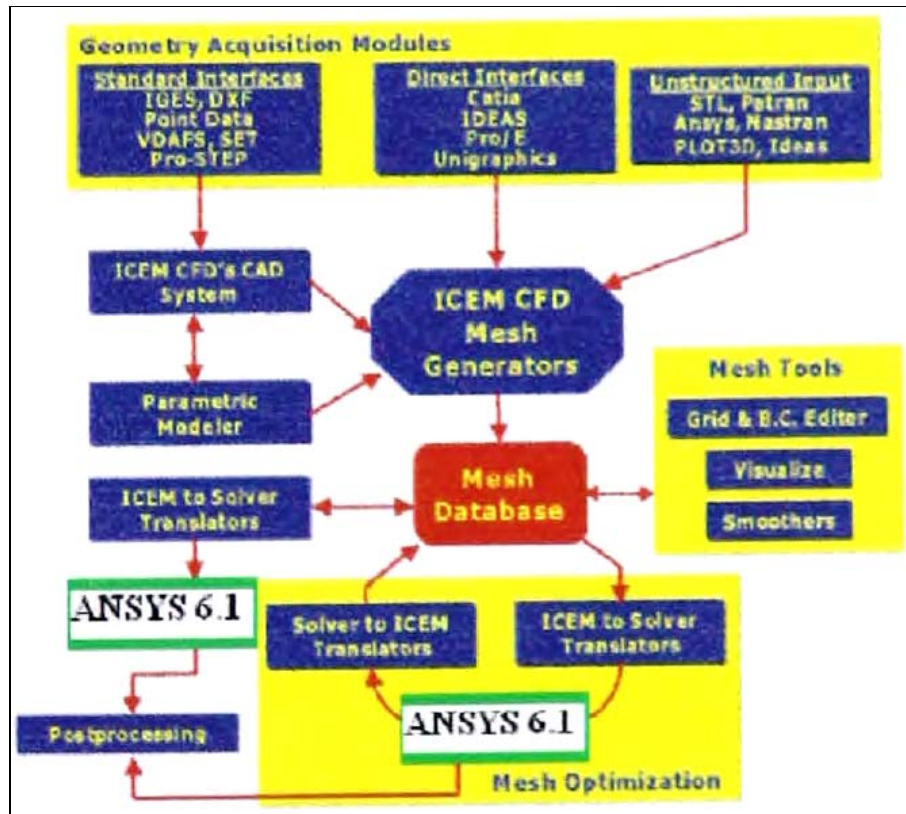


Fig. 4.27 The schematic diagram of ICEM CFD interface with ANSYS 6.1(modified from [70])

The main objective of this study is to find the solutions of the problems occurring in the previous investigation. New interface mesh creation software package was introduced to solve the previous problems. ICEM CFD is well interfaced with the solver. It was developed for pre- and post-processing of engineering applications including the investigation of the aerofoil characteristic by CFD technique. The parametric geometry creation tools are available in most CAD packages for the grid generation post-processing. ICEM CFD can be interfaced with the following file formats (see Fig 4.28).

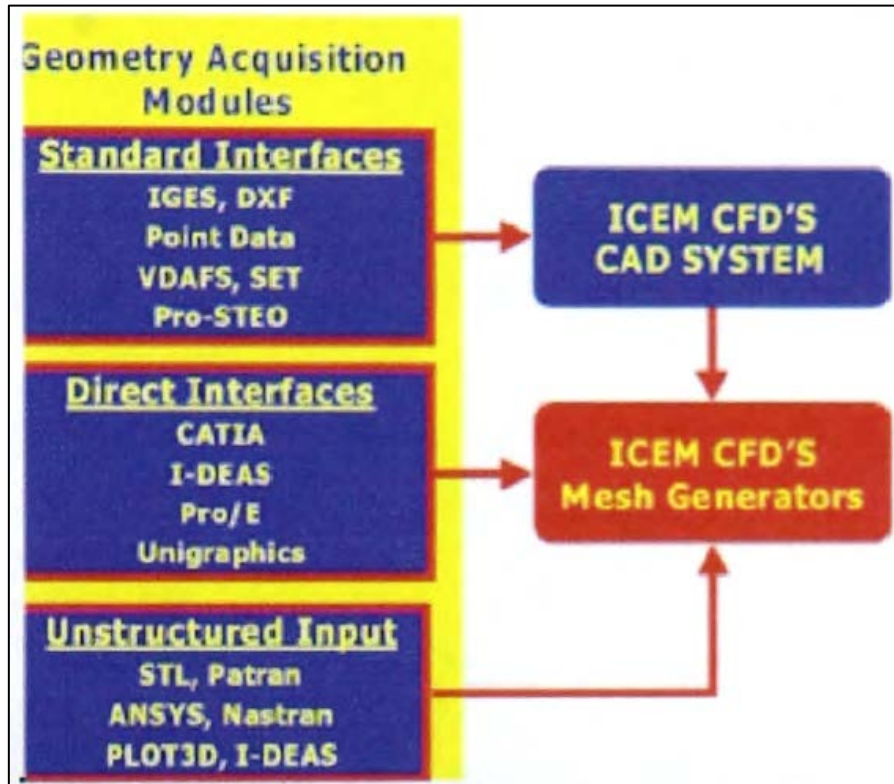


Fig. 4.28 Available formats using in ICEM CFD package [70]

Standard interfaces are available for IGES, DXF, VDAFS.SET, Pro-STEP and point data. Standard interfaces require ICEM CFD's geometry tool ICEM DDN, a professional 3D CAD/CAM system covering all applications, from 2D design and drafting to complex surface and solid modelling, in open systems architecture. ICEM DDN embodies the tools to prepare and if necessary to repair surfaces for mesh generation. Driving curves and points can also be generated with ease. The Direct CAD interface allows the users to operate in their own CAD systems. The selected geometry can be transferred directly into ICEM CFD's geometry database where the user can launch meshing modules of ICEM CFD. These interfaces are also available for CATIA, ICEM Surf, Pro/Engineer, and Solid Works [70].

4.4.2 Apply ICEM CFD to the model

For the 2 dimension analyses of the investigation of lift and drag coefficients of the aerofoils, the hexahedral element has been preferred and used in this study. The completed mesh creation model was transferred to the CFD solver in a pre-processor state. Then ANSYS 6.1 was used as a solver to compute the solution in post-processing and display the results. In this investigation, NACA 661-212 was used as the typical aerofoil section to investigate its characteristics. The difference between the mesh creation pattern of the ANSYS 6.1 mesh creator and that of ICEM CFD will be compared, and the results are also presented in this section. The following steps show the procedures to generate the mesh using the ICEM CFD mesh creator.

Procedures to generate the mesh using ICEM CFD

- Create aerofoil section and wind tunnel using CAD packages (Fig. 4.29).

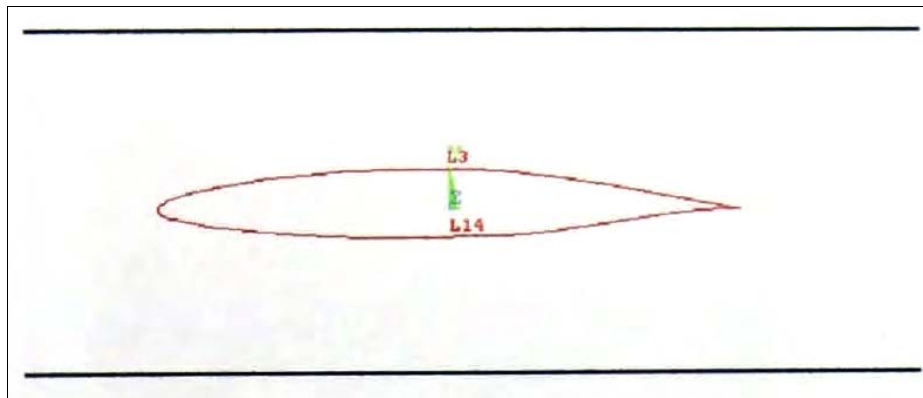


Fig. 4.29 NACA 661-211 and wind tunnel was create by CAD program

- Export CAD model to the format of IGES files (Fig. 4.30).

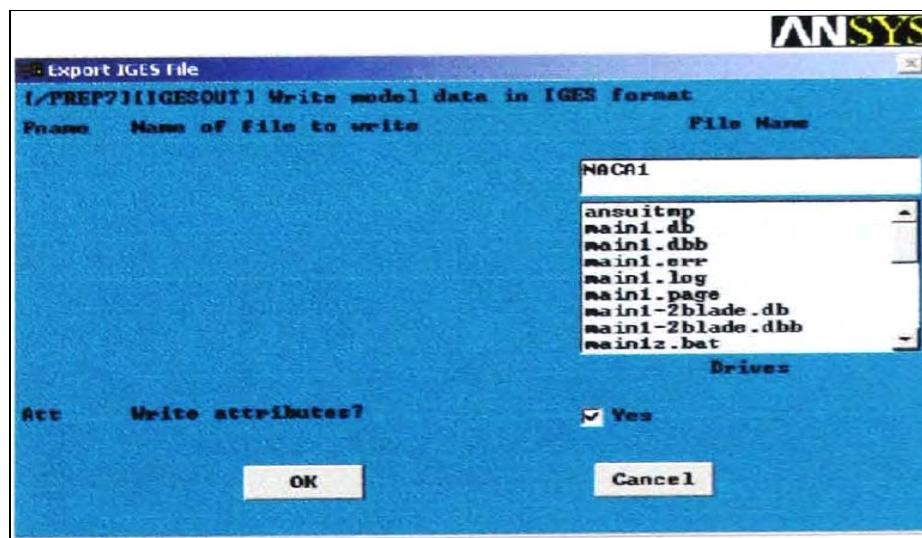


Fig. 4.30 Export CAD model to IGES format

- Open ICEM CFD program, go to File, import geometry from File menu and select the file, which was exported from CAD package (Fig. 4.3 1).

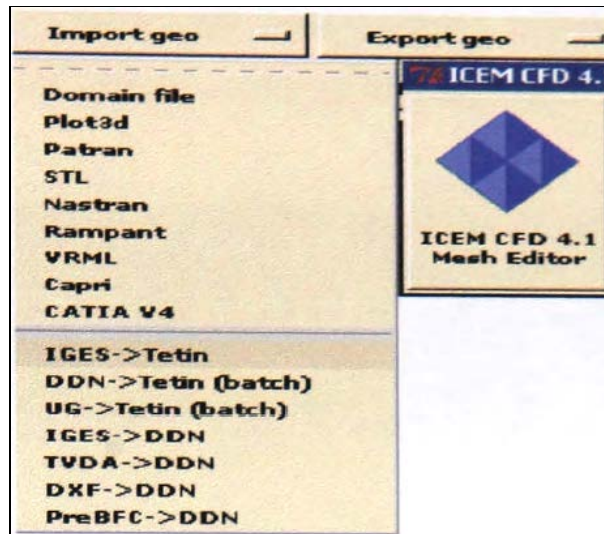


Fig. 4.31 ICEM CFD package at import geometry state transfer to tetin format

- Import IGES files and transfer to format of **tetin** files using ICEM CFD tools.
- In ICMCFD go to meshing, Hexa, interactive and select **No blocking** (Fig. 4.32).

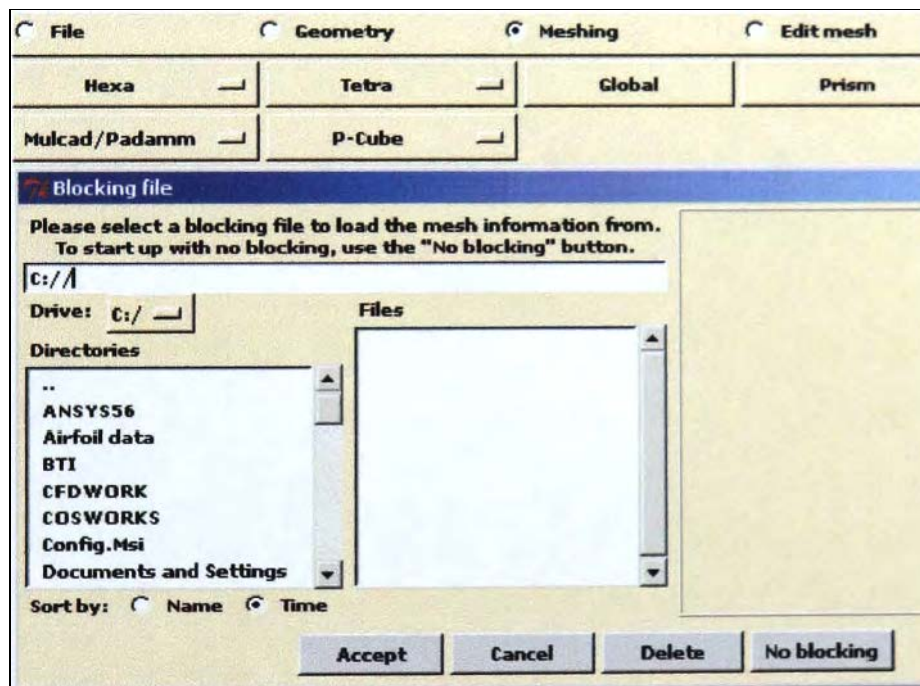


Fig. 4.32 State of hexagonal mesh creation in ICEM CFD

- Generate the mesh using Hexahedral tools option.
 - **Blocking** > int blocking > 2 D > select volume family > Live > Okay.
 - **Blocking** > Split > split line around an aerofoil.
 - **Blocking** > Material > select block > select the blocks inside an aerofoil.

- **Projection** > vertex to curve, >select aerofoil curve> select vertex (using the middle mouse button to accept the command. left mouse button to select object, right mouse button will cancel the previous command (see Fig. 4.33 when complete this command).

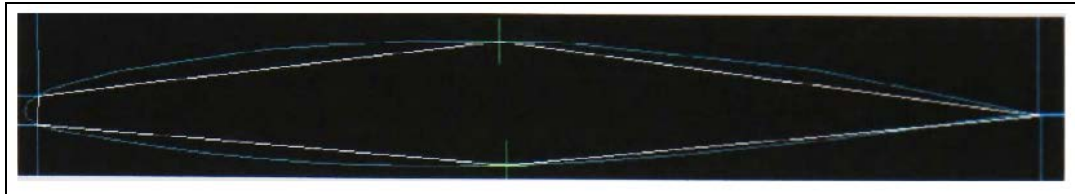


Fig. 4.33 Model after finishing the Projection command

- **Meshing** > Edge parameter> specify the number of mesh around the aerofoil and wind tunnel as desired.
- Use **split line** again to create more element around aerofoil.
- At **Edge parameter** (see Fig. 4.34), use linear option to generate edge distance around an aerofoil to control number of mesh in the model.

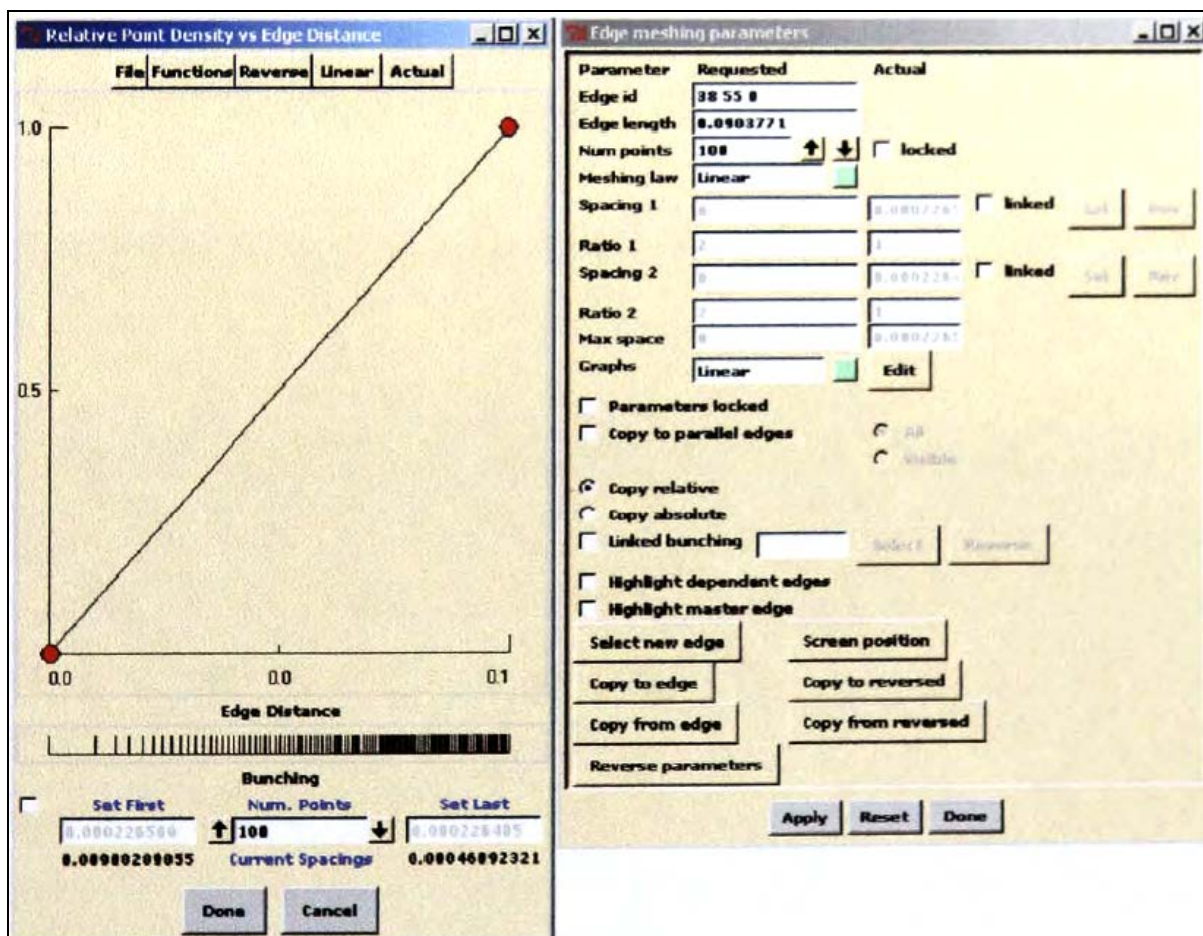


Fig 4.34 Edge meshing parameters window to create the Relative Point Density of the mesh

- Generate the mesh in the model by selecting the project edge options (Fig. 4.35)

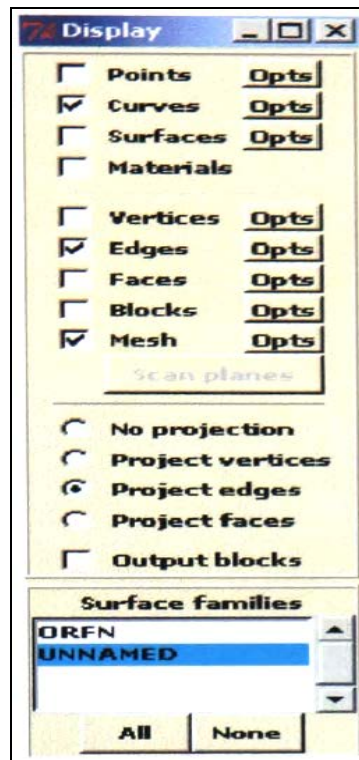


Fig. 4.35 Display windows in CEM CFD mesh editor

- File > save blocking to desired name > save
- File > Unstructured, enter domain file to save the unstructured mesh (Fig. 4.36)

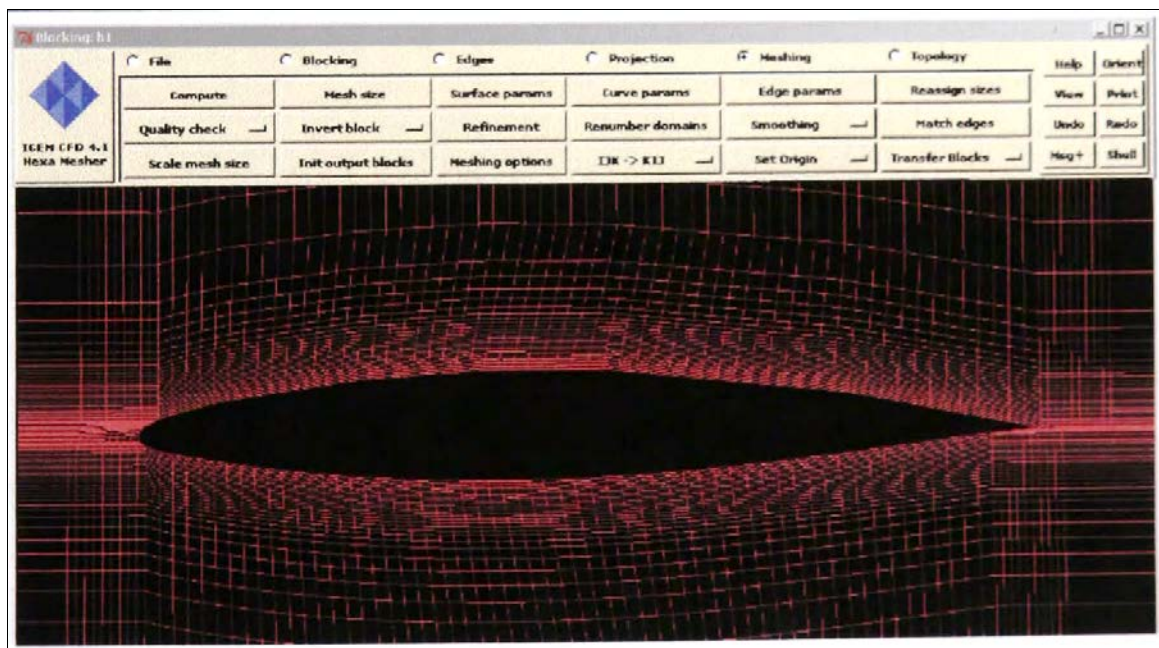


Fig. 4.36 Final unstructured mesh generated by the ICEM CFD

- Quit the mesh generating window and return to the ICEM main menu
- Select output>select solver >ANSYS > Transfer the created mesh to desired directory
- Finish work in ICEM CFD and close the program
- Open ANSYS 6.1 Flotran CFD >Press File, read input file from the mesh created directory
- Load the mesh into ANSYS Flotran, Operate the works in ANSYS CFD in pre-processing and post-processing to analyse the aerofoil characteristics (Fig. 4.37)

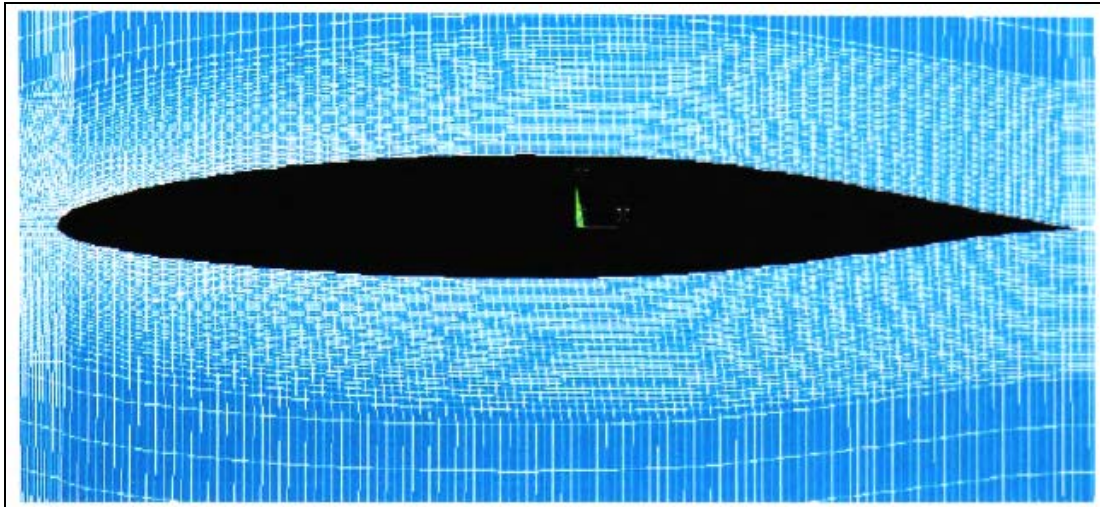


Fig. 4.37 The final mesh generated around aerofoil loaded from the ICEM CFD to ANSYS.

4.4.3 Mesh creations and results investigation

This section shows the details of using different packages to generate the mesh in the investigation of aerofoil characteristics using CFD method. In this study, two commercial packages were studied. There are ANSYS Flotran CFD and ICEM CFD mesh creator.

4.4.3.1 ANSYS Flotran CFD

ANSYS Flotran allows the user to refine the mesh at specified areas or some local locations by using a refinement tool. Fig. 4.38 shows the mesh generated by ANSYS Flotran V. 6.1.

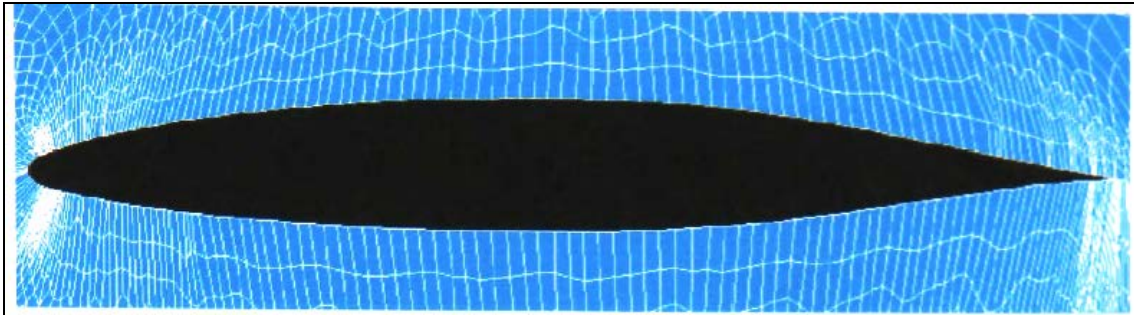


Fig. 4.38 Elements around the aerofoil generated using ANSYS Flotran

4.4.3.2 ICEM CFD

Fig. 4.39 shows the mesh generated by ICEM CFD mesh creator packages. This model was transferred to pre-processing step In ANSYS solver in order to investigate the aerofoil characteristics

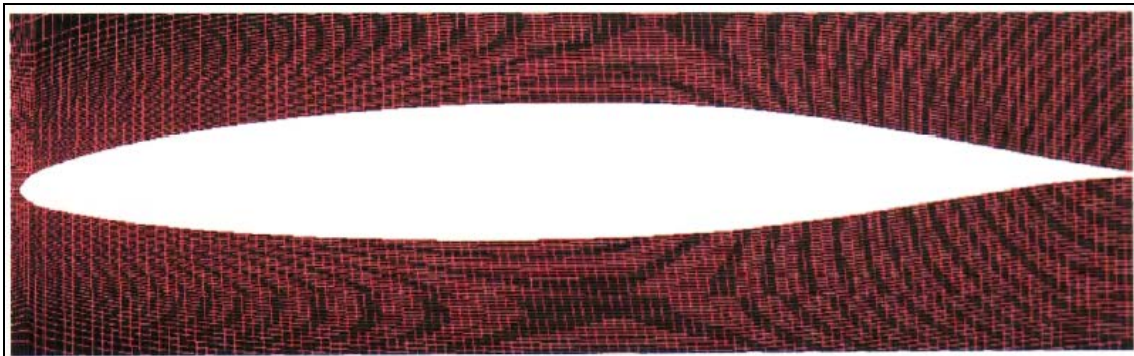


Fig. 4.39 Mesh and elements created using ICEM CFD package

As can be seen, the mesh created using ICEM CFD is of better quality compared to that obtained by using ANSYS Flotran. The following section describes the investigation of NACA 661-212 aerofoil characteristics using the mesh model generated from ICEM CFD with Reynolds number = 3×10^5 , aerofoil chord length $C=2$ m.

4.4.4 Results and Observations

Fig. 4.40 shows typical example results of the average pressure flow field around an aerofoil at zero degree angle of the wind attack. The wind flows faster at the upper section than at the lower part resulting in the pressure difference. Lower pressure at the upper part of an aerofoil generates lift force and drag force will be always perpendicular to the lift force. Drag forces are the result of the friction around an aerofoil.

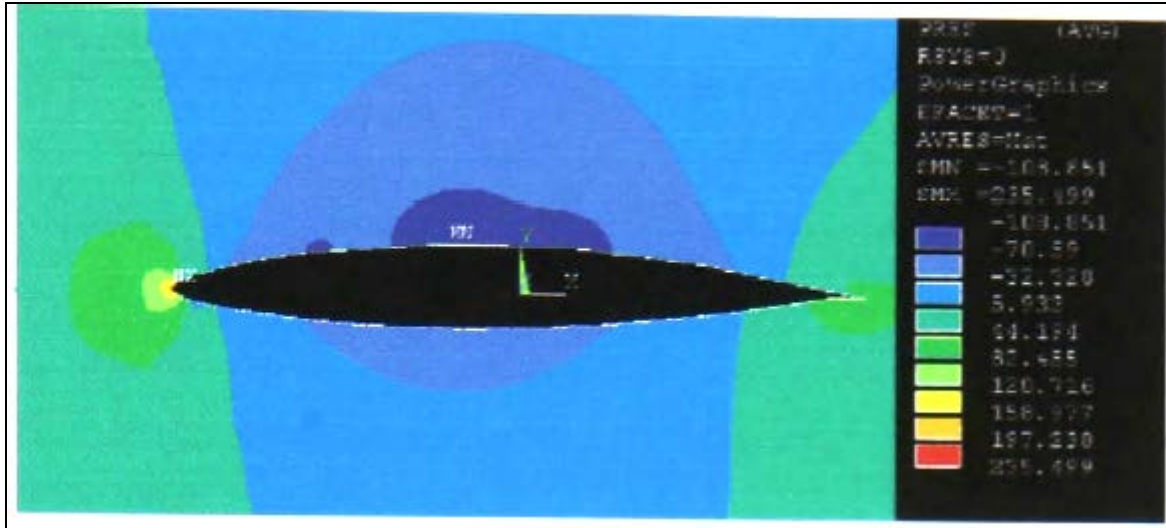


Fig. 4.40 Example of new result of the CFD investigation using mesh created by ICEM CFD

Table 4.7 shows the results of this study obtained from the investigation of aerofoil characteristics at angle wind attack from + 12 to - 12 at intervals of 2 degree.

Table 4.7 The results of the investigation

Angle of attack	Drag1 / Cd1	Drag2 / Cd2 ICEM	Lift1 / Cl1	Lift2 / Cl2 ICEM	Cd (NACA)	Cl (NACA)
0	17.16 / 0.029	3.85 / 0.0066	115.371 / 0.1993	107.12 / 0.185	0.0041	0.15
2	12.99 / 0.022	4.21 / 0.0072	185.74 / 0.3208	202.54 / 0.349	0.0042	0.32
4	29.66 / 0.051	8.58 / 0.0143	289.03 / 0.352	275.65 / 0.476	0.0082	0.51
6	25.68 / 0.043	13.2 / 0.022	307.02 / 0.503	315.25 / 0.544	0.010	0.71
8	33.36 / 0.057	15.21 / 0.026	382.16 / 0.660	395.78 / 0.683	0.012	0.95
10	73.41 / 0.126	24.42 / 0.042	736.64 / 1.272	613.01/1.058	0.016	1.15
12	94.24 / 0.162	28.21 / 0.048	850.63 / 1.469	790.54/1.36	0.021	1.35
-2	18.34 / 0.0317	3.63 / 0.0062	-15.83 / -0.0274	-34.93/-0.06	0.0065	-0.05
-4	21.42 / 0.037	4.63 / 0.0079	-107.24 / -0.185	-102.43 / -0.176	0.008	-0.25
-8	38.586 / 0.072	12.43 / 0.021	-406.51 / -0.702	385.64 / -0.66	0.011	-0.65
-12	63.131 / 0.117	21.69 / 0.037	-518.73 / -0.896	481.52 /-0.831	0.016	-0.92

Table 4.7 shows the new results of the investigation of the aerofoil characteristics using ICEM CFD mesh creation package and compare the results from the previous study and NACA published data. The quality of mesh significantly affects the results on the characteristics of the aerofoils. The results are compared and shown m Fig. 4.41 and 4.42.

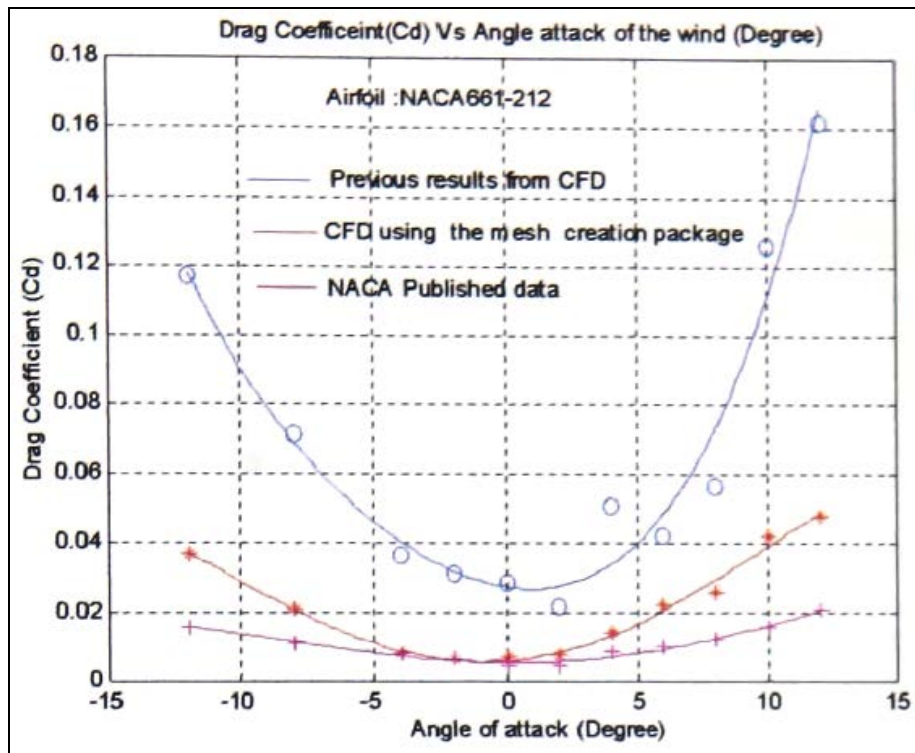


Fig. 4.41 Comparison of results of drag coefficient between previous investigation and new results using mesh creation package

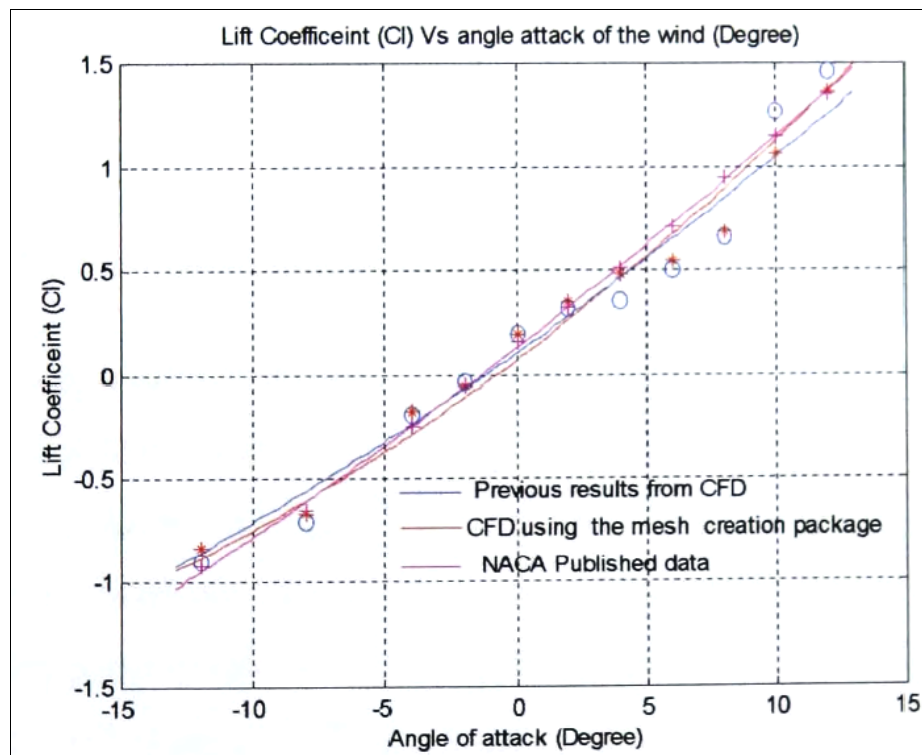


Fig. 4.42 Comparison of results of lift coefficient between previous investigation and new results using mesh creation package

There were no solutions using the polar co-ordinate method. The investigation model failed to give the solution (see Fig. 4.43), the solution was obtained using ICEM CFD method.

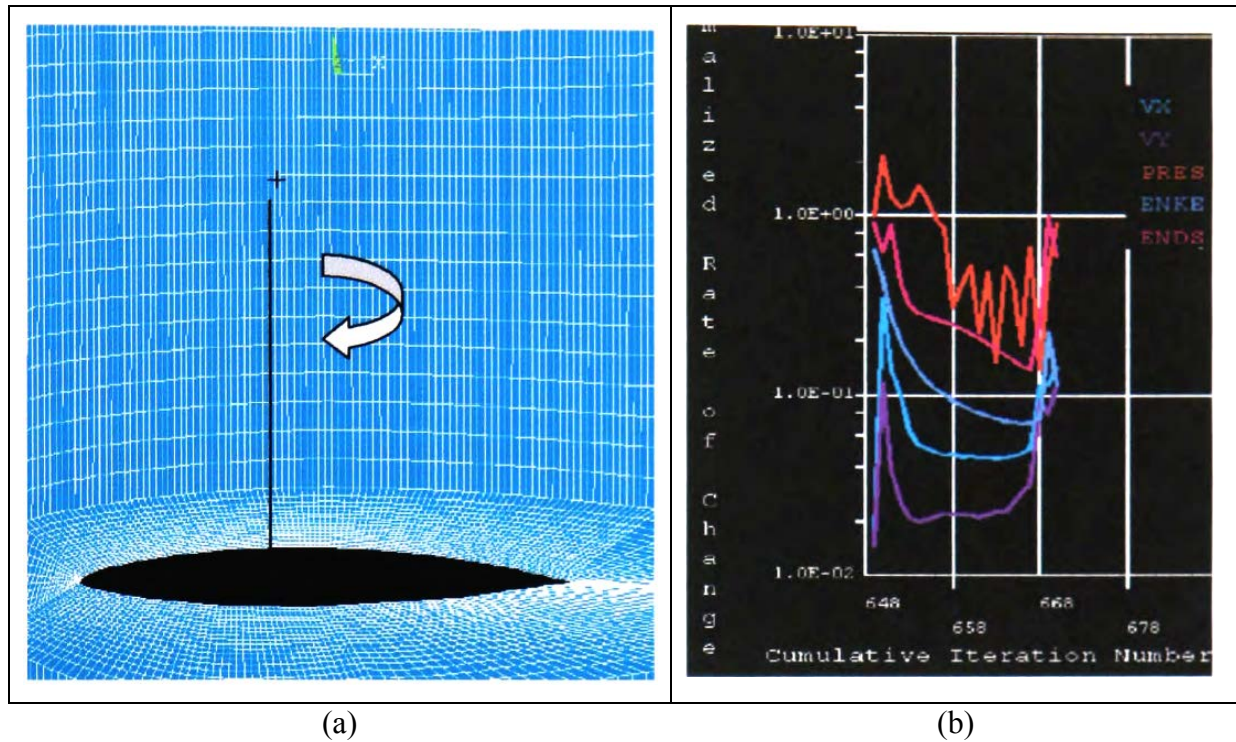


Fig. 4.43 (a) the model in polar coordination (b) the failure of the solution

The lift and drag coefficients were used to investigate the rotor performance of D-rotor using MATLAB analytical models. These results were then compared with those from previous investigations and the data from NACA. The lift and drag coefficients were applied to the analytical model to predict the performance of the Darrieus rotor at various blade tip speed ratios. Fig. 4.44 demonstrates that the results obtained by ICEM CFD method were better than those obtained using ANSYS method.

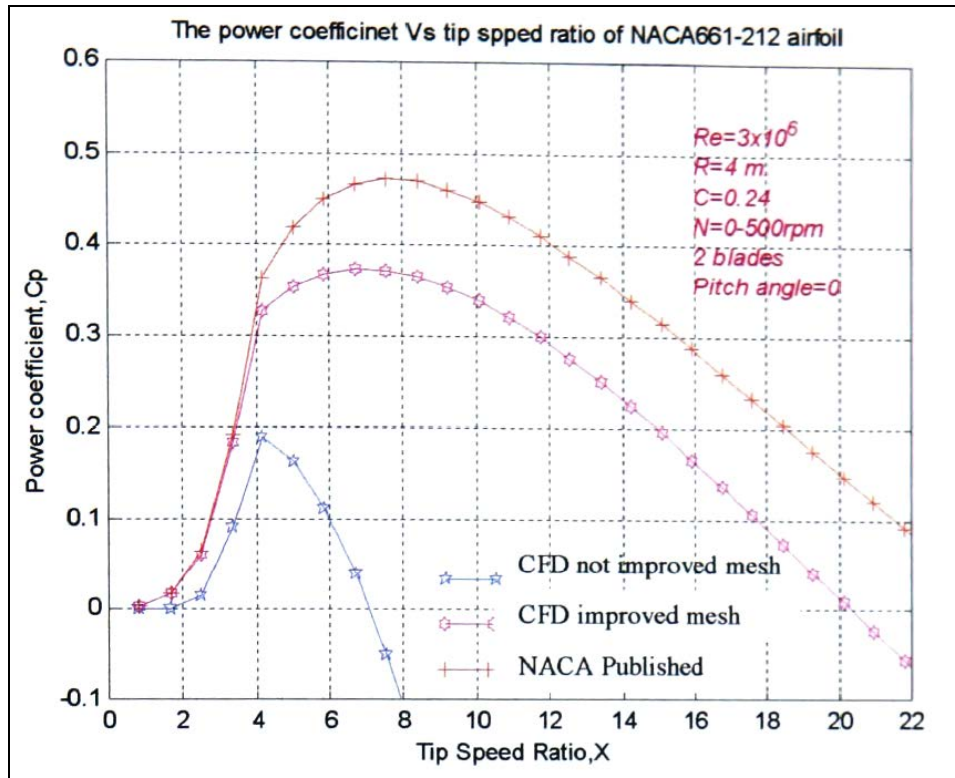


Fig. 4.44 Performance comparison using the analytical models

4.5 Conclusion of CFD technique

The study shows that good results are obtained when using mesh improvement editor package (ICEM CFD). Mesh editor package improves the quality of the element in CFD models. Using this package, the dense mesh needed at the local areas was easier to generate compared with ANSYS tool. This study shows that the quality of mesh would improve accuracy at the expense of the computational effort.

Chapter 5

Experimental Testing

5.1 Introduction

The performances of 40 aerofoil shapes employed in Darrieus wind turbines that have been studied by analytical models (Chapter3) to predict the relationship between Power Coefficients and Tip Speed Ratios. Based on the results from the analytical models, three aerofoils with greater performance were selected for experimental testing. Prototypes of the Darrieus rotor were built by using the three aerofoils NACA661-212, Clark-Y, S1223 and subjected to wind tunnel testing.

The small working section area of the wind tunnel used imposed a limitation on the size of the model that was built (Fig. 5.1). This in turn limited the tip speed ratio that can be achieved. The relationship $X = \frac{R\omega}{V}$ shows that for the same wind speed (V) and the same rotational speed (ω), the model requires greater radius (R) to obtain higher tip speed ratio (X).

5.1.1 Aims of the experimental testing

- To study and investigate the performance of Darrieus wind turbine using different shapes of aerofoils
- To compare the performance results between the analytical and experimental models
- To observe the starting behaviour of the Darrieus rotor using various type of blade shapes
- To search for an optimised aerofoil that would be suitable for the Darrieus wind turbine.

For each configuration the following relationships were investigated:

- ✓ The blade effect on the power coefficients of D-rotor
- ✓ The number of blades affecting the performance of the wind machines
- ✓ The investigation of the influence of the chord ratio (c/r) on the performance of vertical axis wind machine

5.2 Wind Turbine Design

Small models of the wind machine were designed and constructed for the purpose of the experimental study. Fig. 5.1 shows a 3-dimensional model used.

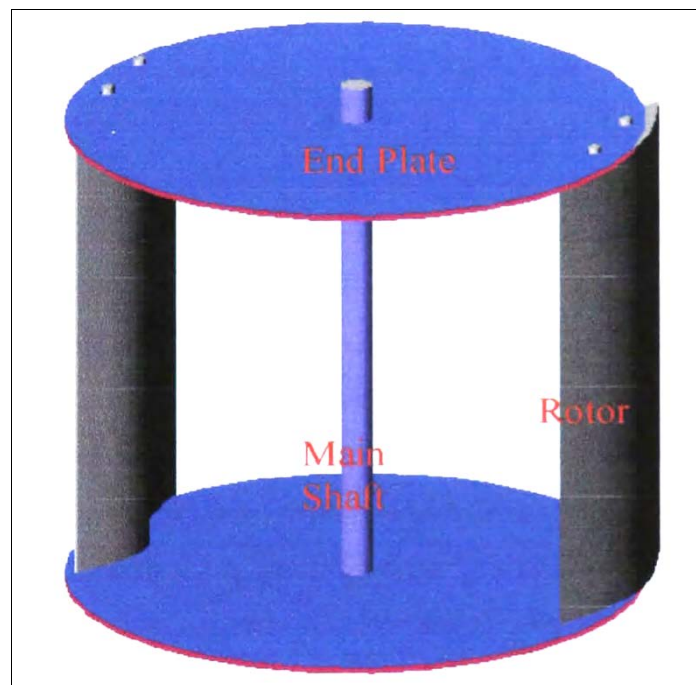


Fig. 5.1 3-D model of two-bladed D-Rotor for wind tunnel testing

The two end plates (aluminium 3 mm thickness) were used as the support to fix the blades and the main shaft to form the wind turbine model. The main shaft (steel 25 mm diameter) was joined with removable couplings at the top and the bottom part of the end plate. The pitch angle of the blades was adjustable.

The wind turbine specifications used for experimental testing are as follows:

- Aerofoil Chord Length = 0.2 m
- Rotor Diameter = 0.4 m
- Shaft Diameter = 0.025 m
- Turbine Height = 0.4 m

5.2.1 The rotor construction

An aerofoil rotor blade profile was made from a material called MDF. The coordinates of the aerofoil profile were drawn on the material and a piece of cross section was cut using Band Saw cutting machine (see Fig. 5.2).



Fig. 5.2 Band Saw, the power tool used for cutting the aerofoil cross-sections

These cross sections were constructed and fitted with a special adhesive and M6 thread and nuts as shown in Fig. 5.6 (a). The aerofoil section was covered with a tempered aluminium sheet of 0.3 mm thickness. These were joined together by using glue and some nails. The completed aerofoil shape is presented in Fig. 5.6 (b).

The co-ordinates of 3 aerofoils (Table 5.1-5.3) and the AutoCAD model are illustrated in Fig. 5.3-5.5.

Table 5.1 NACA 6691-212 Co-ordinations

Source: Ref. [51]

Upper Surface		Lower Surface	
Station	Coordinate	Station	Coordinate
0	0	0	0
0.424	0.947	0.576	-0.847
0.666	1.150	0.834	-1.010
1.157	1.447	1.343	-1.233
2.995	1.986	2.605	-1.614
4.884	2.797	5.116	-2.165
7.379	3.441	7.621	-2.593
9.878	3.997	10.112	-2.963
14.884	4.885	15.116	-3.539
19.895	5.574	20.105	-3.982
24.909	6.112	25.091	-4.322
29.925	6.522	30.075	-4.578
34.945	6.816	35.057	-4.756
39.962	7.005	40.038	-4.863
44.981	7.093	45.019	-4.903
50.00	7.075	50.00	-4.869
55.019	6.939	54.981	-4.749
60.036	6.665	59.964	-4.523
65.051	6.195	64.949	-4.135
70.062	5.507	69.939	-3.563
75.066	4.683	74.943	-2.893
80.065	3.759	79.939	-2.167
85.058	2.770	84.942	-1.424
90.043	1.760	89.957	-0.726
95.022	0.792	94.978	-0.160
100.00	0	100.00	0

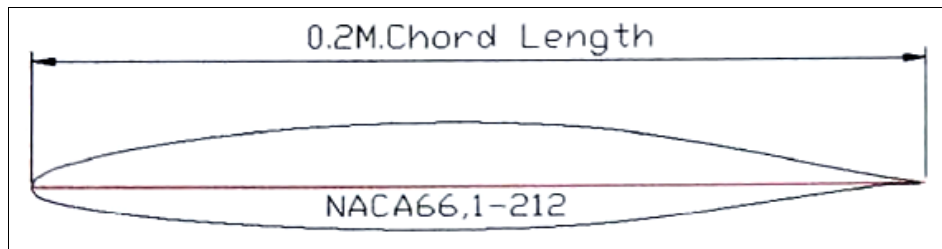
**Fig. 5.3 NACA 66,1-212 model which was created by AutoCAD software**

Table 5.2 S1223 Co-ordinations

Source: Ref [57]

Upper Surface		Lower Surface	
Station	Coordinate	Station	Coordinate
1	0	0.001370	0.009654
0.987364	0.11152	-0.00003	0.00069
0.979923	0.017051	0.000030	-0.00208
0.962492	0.026857	0.001801	-0.00995
0.939838	0.036314	0.008320	-0.01439
0.911121	0.046204	0.018272	-0.01554
0.876651	0.056327	0.031921	-0.01583
0.817677	0.070994	0.052123	-0.01498
0.754092	0.084333	0.085234	-0.01228
0.688352	0.096166	0.135255	-0.00634
0.621327	1.06563	0.17389	-0.00006
0.553369	0.115670	0.240456	0.012576
0.484972	0.123599	0.309105	0.025068
0.418119	0.130034	0.376071	0.035985
0.354865	0.134178	0.442182	0.045064
0.295990	0.135280	0.507662	0.052147
0.243797	0.132558	0.572570	0.057057
0.194845	0.125526	0.636774	0.059980
0.148226	0.113427	0.69996	0.05976
0.105797	0.098114	0.720752	0.059210
0.070598	0.080943	0.781822	0.055700
0.044285	0.064054	0.840177	0.049265
0.026174	0.048922	0.893753	0.039949
0.021648	0.044297	0.939232	0.028326
0.011456	0.031365	0.974467	0.014762
0.005025	0.019856	1.00	0.00

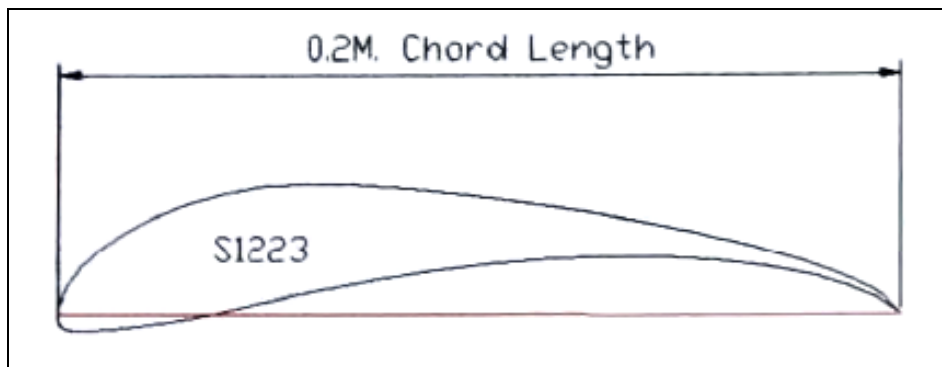
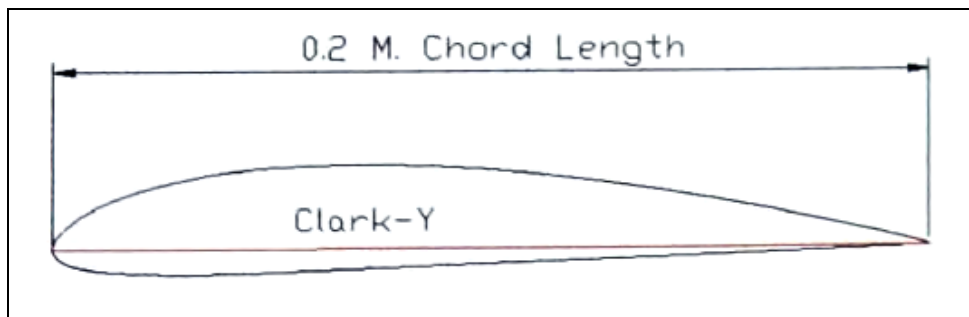
**Fig. 5.4 S1223 model which was created by AutoCAD Software**

Table 5.3 Clark-Y Co-ordinations

Source: Ref [57]

Upper Surface		Lower Surface	
Station	Coordinate	Station	Coordinate
1.00	0.00599	0.00008	-0.002318
0.946295	0.013187	0.001483	-0.00691
0.882540	0.027250	0.006483	-0.013019
0.817527	0.040508	0.013903	-0.017962
0.752114	0.052655	0.023678	-0.021256
0.686589	0.063560	0.035685	-0.0231726
0.621196	0.073047	0.050418	-0.026099
0.55598	0.080769	0.06913	-0.0278311
0.490882	0.086575	0.093702	-0.029122
0.42610	0.090332	0.126562	-0.030086
0.361756	0.091627	0.169930	-0.030177
0.298101	0.090624	0.22338	-0.029046
0.237351	0.087634	0.283376	-0.026941
0.182349	0.081437	0.346527	-0.024578
0.135467	0.072408	0.410804	-0.022240
0.098667	0.062594	0.475436	-0.019867
0.071217	0.053229	0.540183	-0.017485
0.050834	0.044672	0.583370	-0.01590
0.03559	0.036563	0.626562	-0.014314
0.023991	0.028652	0.691346	-0.011935
0.015168	0.020959	0.756098	-0.009557
0.012660	0.08514	0.820723	-0.007183
0.006117	0.011610	0.884907	-0.004826
0.001464	0.004765	0.92700	-0.003280
0.000207	0.001214	0.947633	-0.001781
0.000	0.000	1.00	0.00

**Fig. 5.5 Clark-Y model which was created by AutoCAD**

Three aerofoils were constructed using the co-ordinate shown in Table 5.1-5.3. The number shown in Table 5.1- 5.3 is given in relative value of 100%.

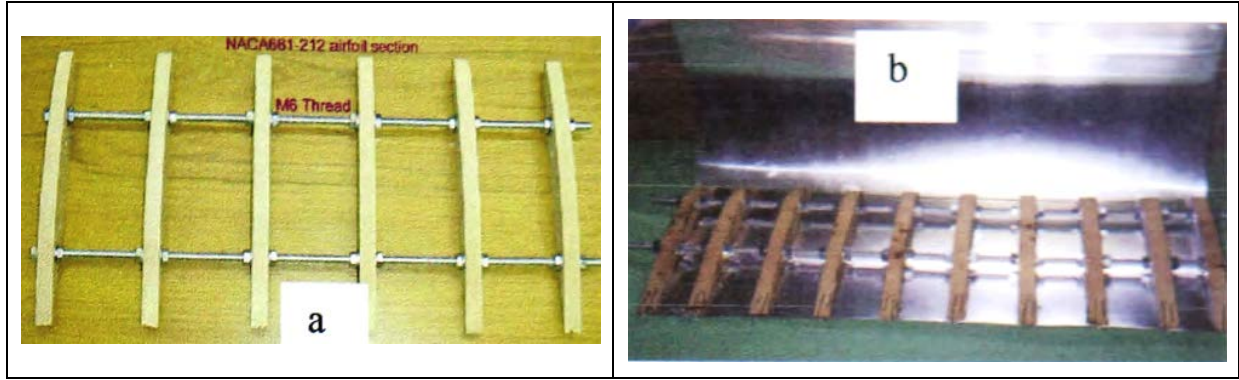


Fig. 5.6 (a) Photograph of an example aerofoil structure made by MDF material (b) The aluminium sheet covered the aerofoil section making the aerofoil prototype

Fig 5.7 shows the completed construction of the rotor blades used in the wind tunnel experimental testing.

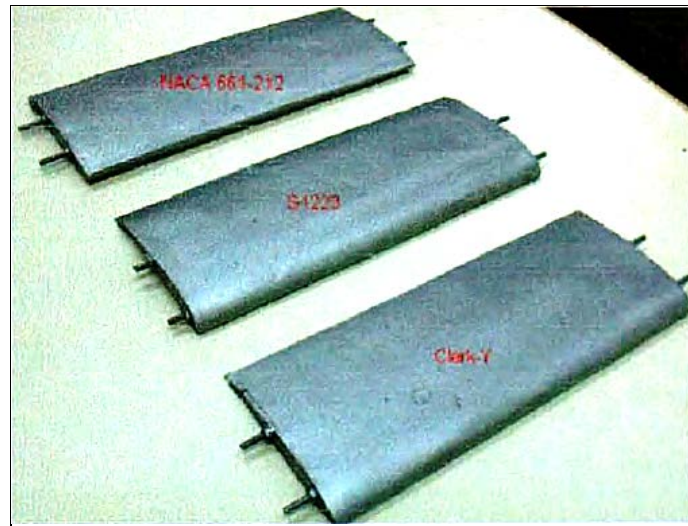


Fig. 5.7 Three completed rotor blades for wind tunnel testing of D-Rotor

5.3 Experimental Methodology

This section describes the testing procedure. The size of the model was chosen according to the size of the wind tunnel. The experiment was conducted in an open circuit type wind tunnel with a twelve-blade fan (*Mech. No. ME761*). Fig 5.8 illustrates the experimental set up of the wind tunnel for wind machine experimental testing. The 12-bladed centrifugal fan in the wind tunnel is driven by a DC motor (*McFarlane Eng. No. 33005*). The rectangular test section of this wind tunnel is 0.6 m. high, by 0.84m wide (which is sufficient space for the wind turbine model to place in the tunnel).

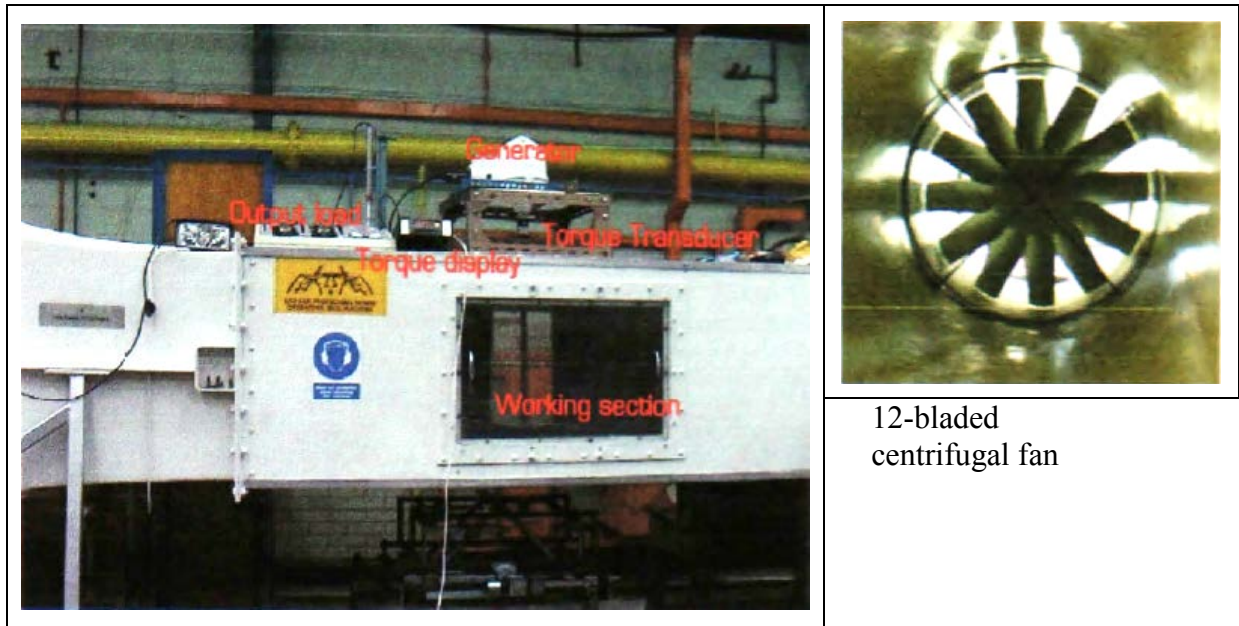


Fig. 5.8 Photograph of wind tunnel experimental set up

The wind velocity was adjusted using the fan speed (Fig. 5.9). Wind velocity at the test section of the tunnel was measured by a digital display anemometer placed at the centre of the tunnel, 0.5m upstream of the rotor axis. The operating wind section and the anemometer probe position are shown in Fig. 5.10.



Fig. 5.9 Display and Control panel of the wind tunnel

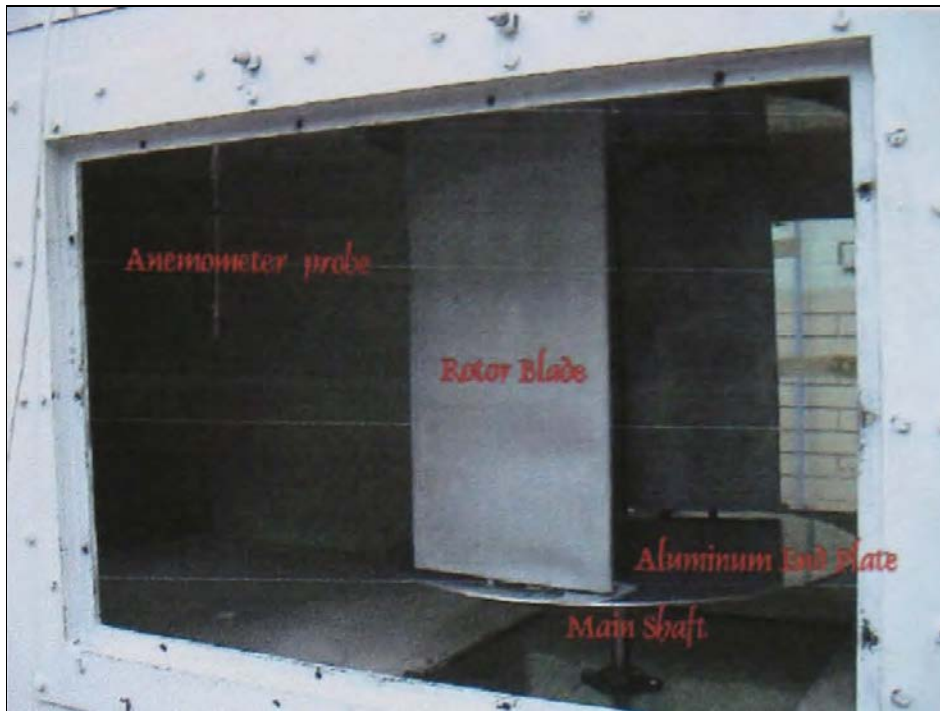


Fig. 5.10 Working section area of the wind tunnel experimental set up

The aerofoil blades were attached to the aluminium endplates that were coupled to a main drive shaft (see Fig. 5.10). The top and the bottom part of the main shaft were supported by steel bearings. The top of this main shaft was connected with a torque transducer and coupled to a single-phase DC generator (Model Ampair 100 12/24 Volts). The loading system for measuring the performance of Darrieus rotor was made of electric light bulbs. The circuit contained of a rheostat, which allowed a specific resistance to be applied as a load to the system. A strain gauge type torque transducer was used to measure the average torque, which was generated from the model wind machine. This 10 N. m torque transducer (Fig 5.11) was connected between main shaft of Wind turbine and the generator. The specifications for this torque transducer are shown in Table 5.4.

Table 5.4 Torque transducer specifications

Technical Specification	
Max. Speed	8000 rpm
Max. Torque	10 N. m
Nominal Sensitivity	1.5 mv/v
Bridge supply	10 V
Full scale output	0 ⁺ 5 v
Operating Temperature	0 to +70°C
Supply Voltage	16-30 VDC
Reparability	<+ 0.05 %fs
Maximum Frequency	1 kHz



Fig. 5.11 Strain gauge torque transducer

The torque transducer was fitted with a digital readout panel with an averaging facility. The transducer and the panel were factory calibrated to 0.1% accuracy. The rotational speed of the Wind turbine model was obtained from the handheld non – contact tachometer (Veeder Root Model 661100-003). This device operates by a small reflective mark attached at the top of the main shaft. The testing included a voltmeter and ammeter from which measurement were taken in order to determine the performance of the model Wind machine.

To start the rotor (due to the reluctance of Darrieus rotors to self-start) a length of string was wound at the bottom end of the rotor drive shaft. The test was started at sufficient wind speed by pulling the chord. The schedules of a typical test are as follows:

- Install rotor blades of the wind machine to the correct position
- Check the whole system.
- Switch on the power of the wind tunnel.
- Reset anemometer and reset torque meter.
- Turn off all out put loads (bulbs and rheostat).
- Adjust and rotate wind turbine rotor to the zero angle of rotor position.
- Increase Wind speed to 10 m/s.
- Pull start cord or spin the shat by hand to help the rotor start.
- Allow turbine to settle down to constant speed (about 10 seconds).
- Apply load by switching on the bulbs.

- Monitor the speed while it becomes steady.
- Read the voltage and current of the output load.
- Read the torque from the display and record value.
- Increase wind speed by 2 m/s intervals.
- Repeat the procedure until the experimental test is complete.

5.4 The Experimental Results

This section presents the experimental results as mentioned in Section 5.1.

5.4.1 The experimental study of the three aerofoils sections employed in the D-rotor

This section describes the experimental results of three aerofoils employed in the Darrieus wind turbines. The sequence of the experimental testing of an aerofoil shape on Darrieus rotor was Clark-Y, NACA661-212 and S1223 respectively. The number of blades in this section was 2 and the chord ratio of this wind turbine model was equal to 1. The results are also shown in graphical form using Matlab package (comparison between the experimental and the analytical models prediction (Chapter 3)). However, it could be noted that only the high-lift aerofoil S1223 can achieve good performance at the wind speed of 10 m/sec. NACA661-212 and Clark -Y generated low starting torque and performed not very well at this wind speed even at the no load condition. Therefore, these aerofoils have shown the results at the range of wind speed from 12-18 m/sec instead. Table 5.5-5.8 shows the experimental results of Clark-Y aerofoils. Table 5.9-5.12 presents the results of NACA661-212 and the results of aerofoil S 1223 are shown in table 5.13-5.14. The experimental results of these three aerofoils applied to Darrieus wind turbines were obtained from the same turbine configurations as described in Section 5.2 using set-up procedures described in Section 5.3.

5.4.1.1 Aerofoil: Clark-Y**Table 5.5 Clark-Y at wind velocity, V= 12 m/sec**

Volts, V	Current, I (Amp)	RPM, N (rev./min)	Torque, T (Nm)	Omega (Ω)	Power $P = T \times \Omega$	Power $P = V \times I$	C_p	TSR, X
15	1.35	750	0.61	78.53	47.90	20.25	0.28	1.31
20	0.75	600	0.50	62.83	31.41	15	0.37	1.047
18	0.87	500	0.96	52.35	50.26	15.66	0.29	0.872
21.6	0.7	400	0.67	41.88	28.06	15.2	0.16	0.698
10	1.7	350	0.64	36.65	23.45	17	0.13	0.610
6.14	1.4	300	0.38	31.41	11.93	8.59	0.07	0.523
6.4	1.53	260	0.47	27.22	12.79	9.79	0.075	0.45
4.2	0.5	230	0.45	24.08	10.83	2.1	0.06	0.40

Table 5.6 Clark-Y at wind velocity, V= 14 m/sec

Volts, V	Current, I (Amp)	RPM, N (rev./min)	Torque, T (Nm)	Omega (Ω)	Power $P = T \times \Omega$	Power $P = V \times I$	C_p	TSR, X
17.53	1.76	660	0.87	69.11	60.13	30.85	0.22	0.98
18.0	1.38	600	0.89	62.83	55.96	24.84	0.20	0.89
15.02	1.46	560	0.90	58.64	52.77	21.92	0.19	0.83
18.42	2.17	550	1.24	57.59	71.41	39.97	0.26	0.82
14.23	2.01	530	1.04	55.50	57.72	28.62	0.21	0.79
12.5	1.8	500	0.8	52.35	41.88	22.5	0.15	0.74
11.02	1.2	400	0.76	41.88	31.83	13.22	0.11	0.59
8.9	1.4	300	0.55	31.41	17.27	12.46	0.06	0.44
6.5	0.35	200	0.42	20.94	8.79	2.275	0.032	0.29

Table 5.7 Clark-Y at wind velocity, V= 16 m/sec

Volts, V	Current, I (Amp)	RPM, N (rev./min)	Torque, T (Nm)	Omega (Ω)	Power $P = T \times \Omega$	Power $P = V \times I$	C_p	TSR, X
25.89	4.65	800	1.40	83.77	117.27	120.38	0.292	1.04
20.43	3.58	770	1.41	80.63	113.69	73.13	0.283	1.00
18.9	3.25	690	1.51	72.25	109.10	61.42	0.271	0.90
17.5	2.95	650	1.55	68.06	105.50	51.62	0.262	0.85
16.24	2.58	600	1.57	62.83	98.64	41.89	0.245	0.78
12.52	2.31	500	1.48	52.35	77.49	28.92	0.193	0.65
10.56	2.38	400	1.35	41.88	56.54	25.13	0.140	0.52
8.59	0.9	200	1.11	20.94	23.24	7.731	0.057	0.26

Table 5.8 Clark-Y at wind velocity, $V = 18$ m/sec

Volts, V	Current, I (Amp)	RPM, N (rev./min)	Torque, T (Nm)	Omega (Ω)	Power $P = T \times \Omega$	Power $P = V \times I$	C_p	TSR, X
25.6	4.5	950	1.09	99.48	108.43	115.2	0.189	1.10
23.25	4.62	930	1.15	97.38	111.99	107.41	0.195	1.08
20.56	4.81	880	1.35	92.15	124.40	98.89	0.22	1.02
19.85	3.987	820	1.23	85.97	105.62	75.15	0.18	0.95
18.52	3.25	720	1.25	75.39	94.24	60.19	0.16	0.83
17.89	3.55	660	1.36	69.11	93.99	63.50	0.16	0.76
13.58	2.98	600	1.30	62.83	81.68	40.46	0.14	0.69
12.15	2.10	500	1.30	52.35	68.06	25.51	0.11	0.58
10.89	2.58	450	1.20	47.12	56.54	28.09	0.099	0.52
9.75	1.58	280	0.96	29.32	28.14	15.40	0.044	0.32

Observation results of Clark -Y

The experimental results from Tables 5.5-5.8 are presented in graph format in Fig. 5.12. Fig. 5.12 describes the average line and the raw data from the experimental testing of Power Coefficient, C_p versus tip speed ratio, X

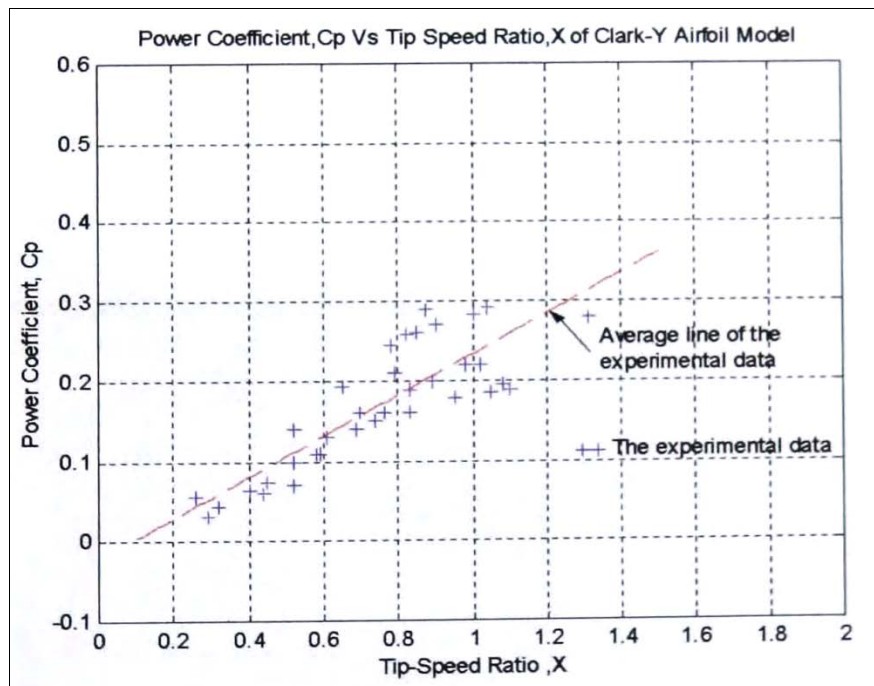


Fig. 5.12 Summary of the experimental data and average line at wind velocity from 12-18 m/sec of Clark-Y aerofoil section

As can be seen in Fig. 5.12 the experimental results at these various wind velocities fall close to the average line, before agreement was achieved at tip speed ratio of 0.6-0.8. At tip speed ratios of 0.8-1.0 the experimental results showed deviations. Figure 5.13 presents the prediction results using analytical prediction on the performance characteristic of Clark-Y

aerofoil applied to the D-rotor on 0.4-meter height and 0.21 meter of radius wind turbine model from tip speed ratio. X of 0.2-2. The experimental results of Clark-Y blades were compared to analytical results (Fig. 5.14). From Fig. 5.14 it can be observed that experimental results indicate the development of higher power coefficient at low tip speed ratio than the analytical prediction. The average line of the experimental results on Clark-Y aerofoil and the analytical model is intersected at the tip speed ratio about 1.1 and the power coefficient of 0.25. Full range of the theoretical power coefficient against tip speed ratio from zero to about 6 can be seen in Section 5.4.1.4.

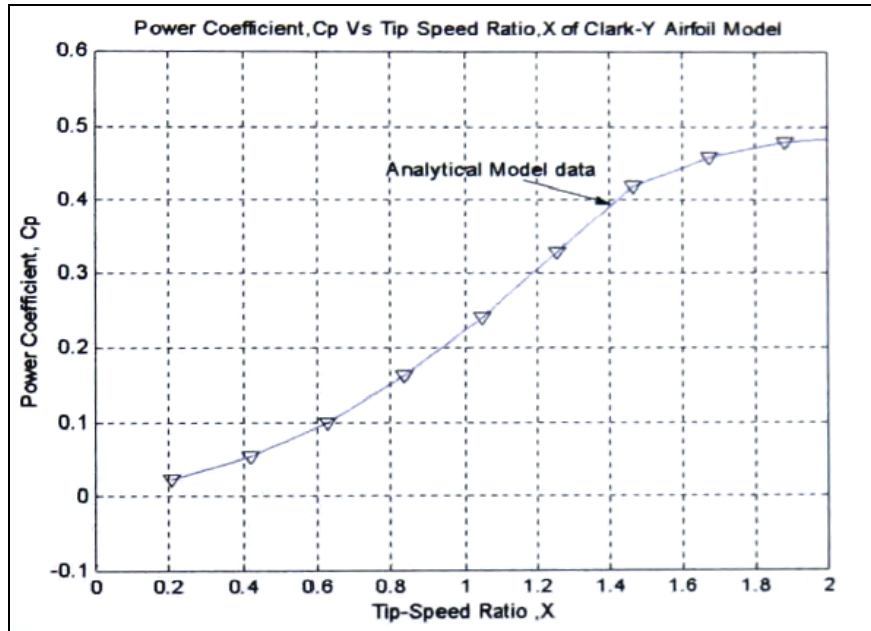


Fig. 5.13 The analytical prediction of Clark-Y on the D-Rotor

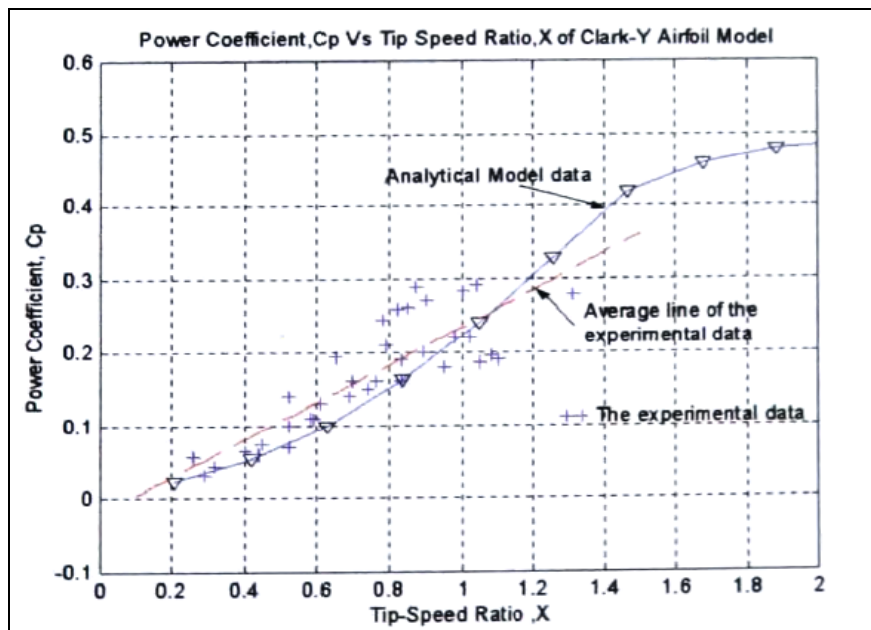


Fig. 5.14 Comparison of results of Clark-Y between analytical prediction and experimental results

5.4.1.2 Aerofoil: NACA 661-212

Table 5.9 NACA 661-212 at wind velocity, $V = 12$ m/sec

Volts, V	Current, I (Amp)	RPM, N (rev./min)	Torque, T (Nm)	Omega (Ω)	Power $P = T \times \Omega$	Power $P = V \times I$	C_p	TSR, X
16	1.5	500	0.80	52.3	41.84	21	0.24	0.871
18.9	0.82	600	0.61	62.8	38.30	15.49	0.22	1.046
20.5	0.86	660	0.72	69.08	49.73	17.63	0.29	1.16
21.6	0.87	670	0.60	70.12	42.07	18.8	0.24	1.168
10	1.7	300	0.55	31.4	31.08	17	0.18	0.52

Table 5.10 NACA 661-212 at wind velocity, $V = 14$ m/sec

Volts, V	Current, I (Amp)	RPM, N (rev./min)	Torque, T (Nm)	Omega (Ω)	Power $P = T \times \Omega$	Power $P = V \times I$	C_p	TSR, X
13.4	1.2	550	0.90	57.56	51.80	16.08	0.192	0.822
11.23	1.82	474	0.85	49.61	42.16	20.43	0.156	0.708
11.16	1.78	467	0.83	48.8	40.50	19.86	0.150	0.69
8.0	1.70	300	0.70	31.4	21.98	13.6	0.081	0.44

Table 5.11 NACA 661-212 at wind velocity, $V = 16$ m/sec

Volts, V	Current, I (Amp)	RPM, N (rev./min)	Torque, T (Nm)	Omega (Ω)	Power $P = T \times \Omega$	Power $P = V \times I$	C_p	TSR, X
18.6	3.0	900	1.36	94.2	128.11	55.8	0.31	1.17
16.5	2.1	840	1.22	87.92	107.26	34.65	0.267	1.099
15.74	2.05	800	1.35	83.7	112.99	32.26	0.28	1.046
12.4	1.9	570	1.30	59.66	77.55	23.56	0.193	0.745
10.20	1.71	550	1.32	57.5	75.9	17.44	0.189	0.718
8.90	1.83	500	1.26	52.33	65.93	16.28	0.164	0.654
7.0	1.8	380	1.25	39.77	49.71	12.6	0.123	0.497
4.2	1.28	200	0.47	20.9	9.82	5.37	0.024	0.26

Table 5.12 NACA 661-212 at wind velocity, $V = 18$ m/sec

Volts, V	Current, I (Amp)	RPM, N (rev./min)	Torque, T (Nm)	Omega (Ω)	Power $P = T \times \Omega$	Power $P = V \times I$	C_p	TSR, X
13.66	4.11	900	1.6	94.2	150.72	56.14	0.26	1.04
9.22	5.6	800	1.55	82.66	128.123	51.63	0.22	0.918
11.9	3.82	750	1.46	78.5	114.61	45.45	0.20	0.87
8.0	5.3	700	1.47	73.26	107.69	42.4	0.188	0.81
6.5	4.7	570	1.59	59.66	94.85	30.55	0.165	0.66
6.52	4.7	560	1.45	58.61	84.98	30.64	0.148	0.65
6.0	4.84	560	1.52	58.61	89.08	29.04	0.155	0.65

Observation results of NACA 661-212

The plot between power coefficients C_p of the experimental result and tip speed ratio X of NACA 61-212 aerofoil is shown in Fig. 5.15. This aerofoil section when employed to the small-scale wind machine generates the highest power coefficient of 0.3 at tip speed ratio of 1.2. Fig. 5.16 presents the analytical model prediction computed and Fig. 5.17 compares the experimental results with the analytical results. The intersection between the two curves occurs at tip speed ratio about 0.9 with power coefficient C_p 0.23, after this point the power coefficient results of the experimental are lower than that of the analytical prediction (Fig. 5.17).

However, because of the limitation of the rotor size, higher tip speed ratio could not be achieved in our experimental studies. A comparison of the results covering the full range of tip speed ratio is given in 5.4.1.4.

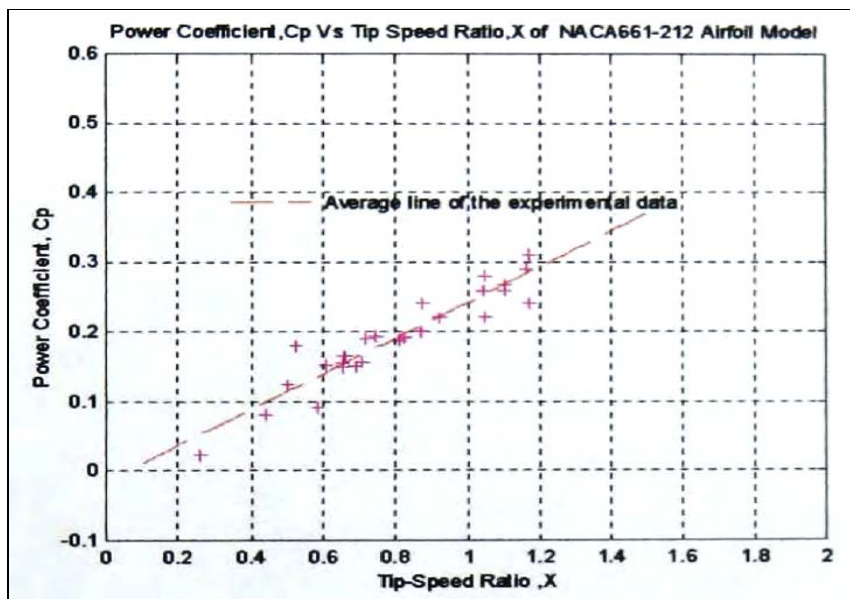


Fig. 5.15 Experimental data and the average line on wind velocity from 12-18 m/sec of NACA 661-212 aerofoil

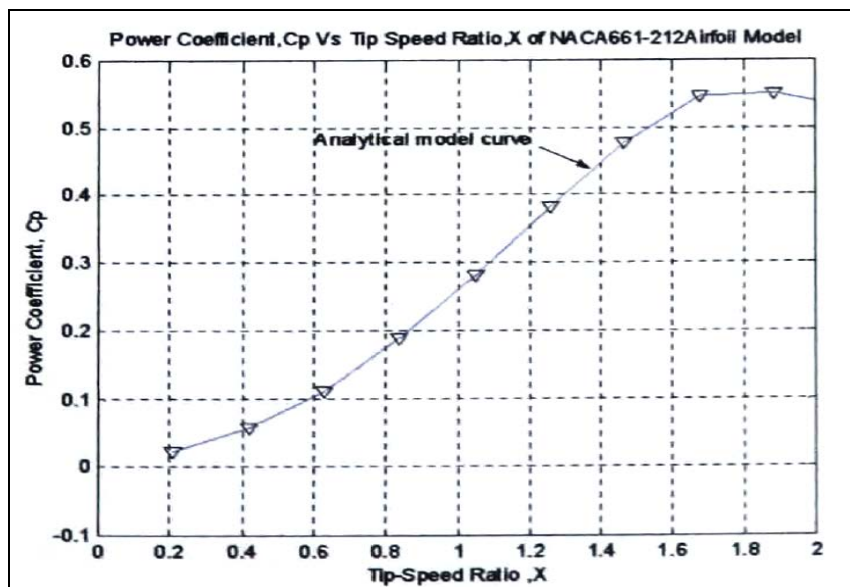


Fig 5.16 Analytical model prediction results of NACA 661-212 aerofoil

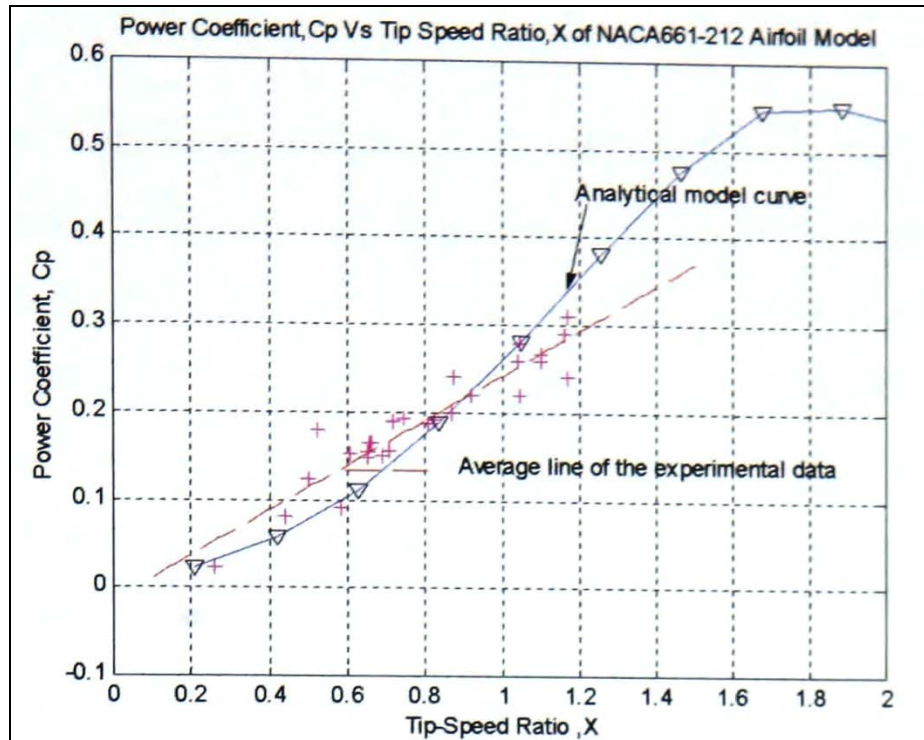


Fig. 5.17 Comparison of results of NACA661-212 between analytical and experimental studies

5.4.1.3 Aerofoil: S1223

Table 5.13 S1223 at wind velocity, $V=10$ m/sec

Volts, V	Current, I (Amp)	RPM, N (rev./min)	Torque, T (Nm)	Omega (Ω)	Power $P = T \times \Omega$	Power $P = V \times I$	C_p	TSR, X
19.1	0.83	608	0.76	63.6	48.33	15.83	0.492	1.272
15.0	1.42	558	0.83	58.40	48.472	21.3	0.494	1.168
11	1.78	448	0.93	46.89	43.607	19.58	0.44	0.937
11.7	1.13	480	0.95	50.24	47.72	13.22	0.48	1.00
8.5	1.15	382	1.00	39.98	39.98	9.775	0.40	0.799

Table 5.14 S1223 at wind velocity, $V=12$ m/sec

Volts, V	Current, I (Amp)	RPM, N (rev./min)	Torque, T (Nm)	Omega (Ω)	Power $P = T \times \Omega$	Power $P = V \times I$	C_p	TSR, X
15.2	2.39	663	0.90	69.39	62.45	36.32	0.369	1.15
12.8	2.75	635	1.03	66.46	68.45	35.2	0.405	1.107
11.4	3.06	597	1.12	62.48	69.97	34.88	0.41	1.041
10.0	3.23	525	1.10	54.95	60.44	32.3	0.357	0.915
7.83	3.19	465	1.0	48.67	48.67	24.97	0.287	0.811
6.15	2.95	340	0.95	35.58	33.80	18.14	0.20	0.593
8.90	3.09	500	1.05	52.33	54.33	27.501	0.32	0.872
5.9	3.04	250	0.95	26.16	24.85	17.93	0.15	0.436

Observation results of S1223

S1223 is a high lift aerofoil or 'Camber blade aerofoil'. The results of this aerofoil between the experimental and the analytical are shown in Fig. 5.18. The analytical results are shown in Fig. 5.19. The comparison between the experimental and analytical models is illustrated in Fig. 5.20. It is to be noted that this aerofoil test had less experimental data than the two previous aerofoils, because of uncontrollable rotational speed of the turbine model at high incoming wind speed (higher than about 14 m/sec). And, as mentioned in the previous section, this aerofoil can achieve good experimental results only at low wind speed (10 m/sec). This rotor showed good performance compared to Clark-Y and NACA661-212 in all range of testing of tip speed ratio. It developed high torque and good performance at low range of tip speed ratio. However, more careful tests should be considered in order to gain more precise results.

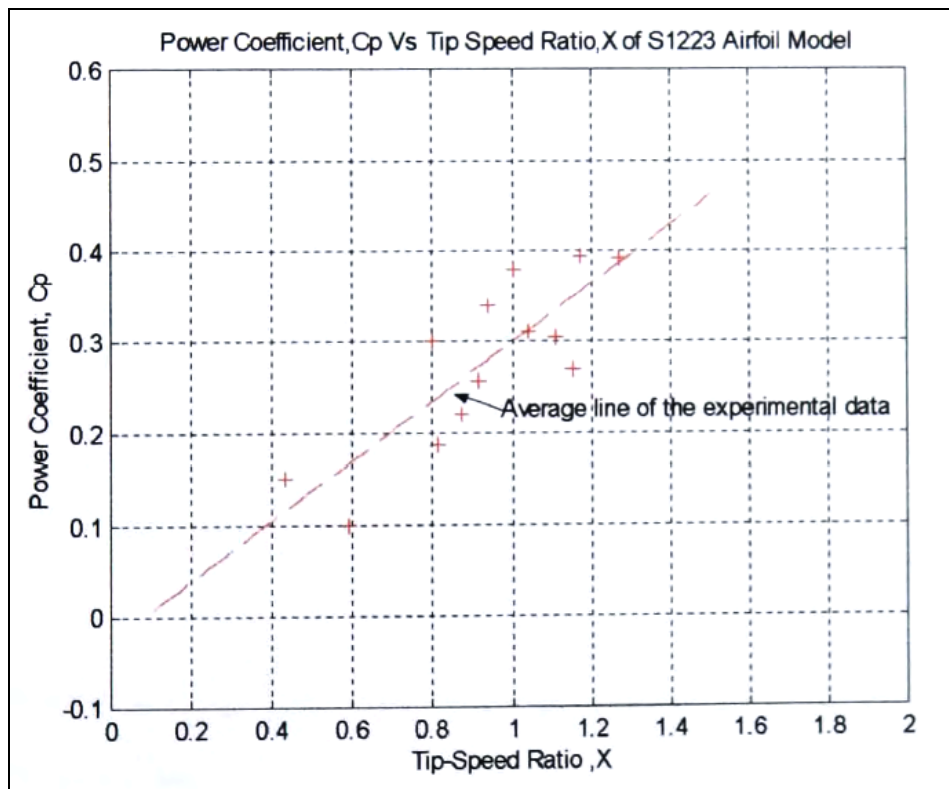


Fig. 5.18 Average line of the experimental results of wind velocity 10-14 m/sec of S1223 aerofoil

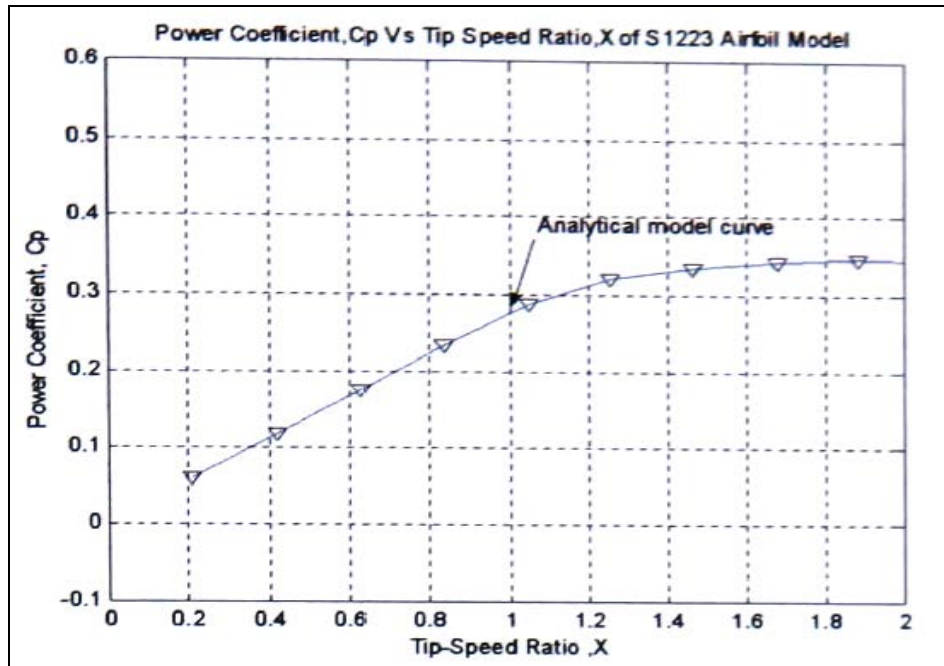


Fig. 5.19 Analytical model prediction of S1223 aerofoil on D-Rotor

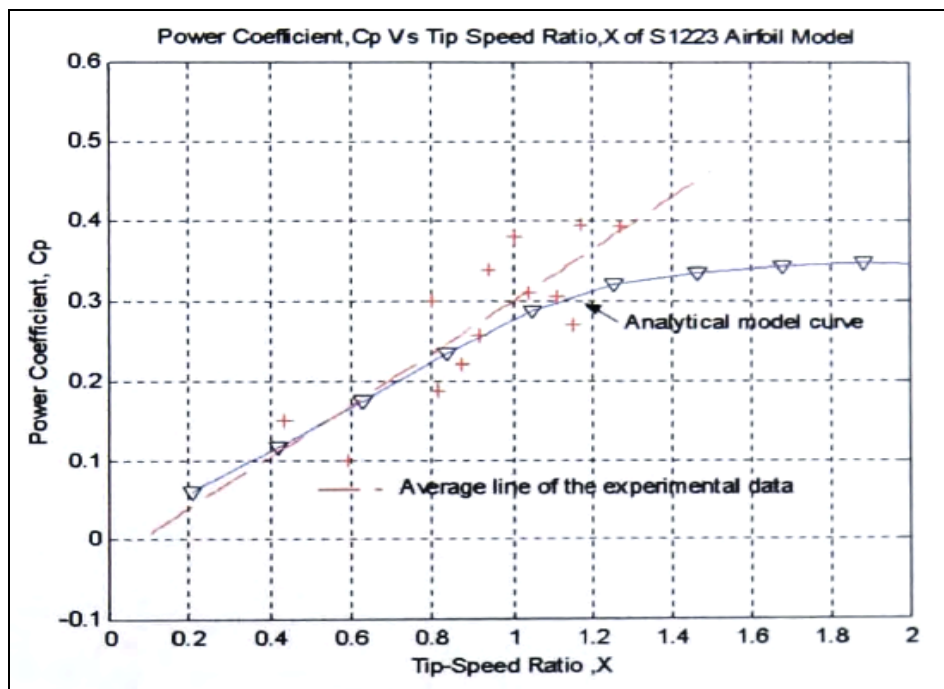


Fig. 5.20 Comparison results of the power coefficient Vs tip speed ratio of S1223 aerofoil

5.4.1.4 The discussion on the aerofoils shape effects

This section investigates and observes the experimental results of the power coefficients versus the tip speed ratio of three aerofoil sections when employed to D-Rotor. The comparisons of the experimental data on these three aerofoils are presented in Fig. 5.21.

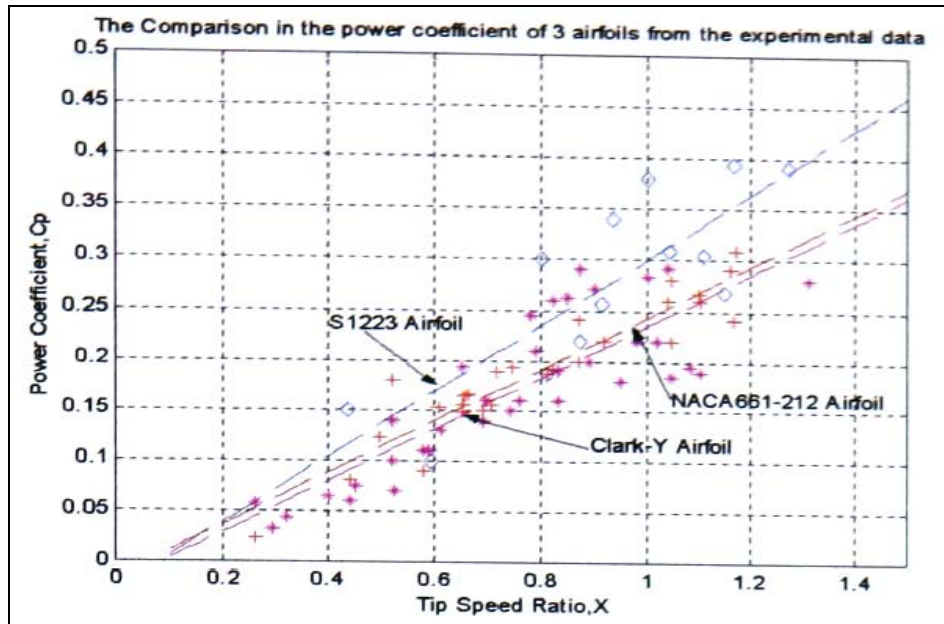


Fig. 5.21 Result from the experimental models

Using the analytical models prediction in Chapter 3 to predict these three aerofoil sections on D-Rotor can be seen in Fig. 5.22.

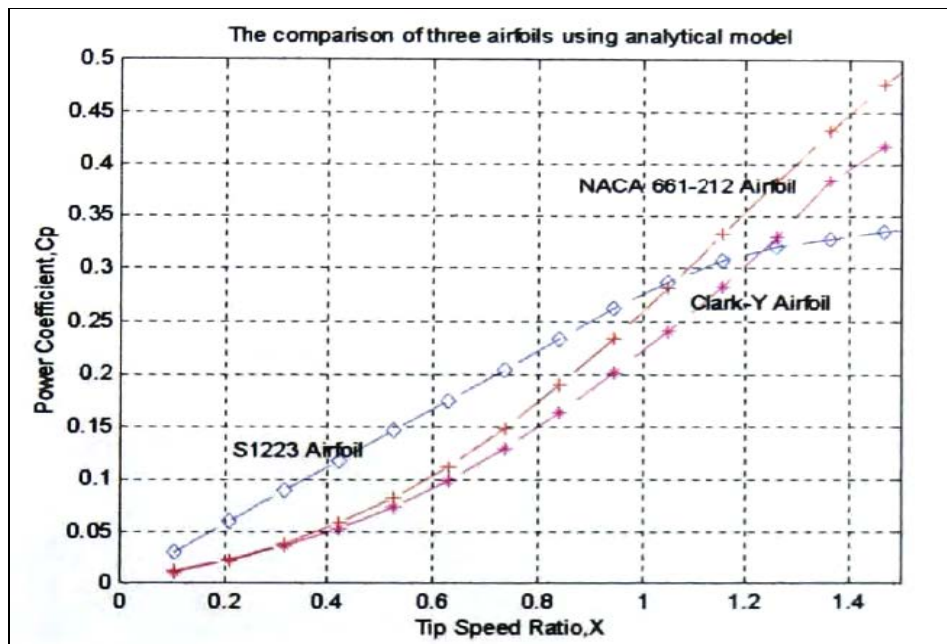


Fig. 5.22 Result from the analytical models prediction

From the comparison of the results of these three aerofoils In Fig. 5.21 and Fig. 5.22, it can be seen that the S1223 aerofoil developed higher power coefficient than the others. However, the result of the analytical models predictions (Fig. 5.22) shows that at the tip speed ratio of 1.05, the performance of this aerofoil will decline and this contrasts the experimental results (see Fig. 5.20). The power coefficient curves for full range of tip speed ratios at 3 aerofoil models are presented in Fig. 5.23. The analytical prediction results

showed that the NACA 661-121 has good performance at high tip speed ratios but poor in the region of tip speed ratio lower than 1, compared to the results for the high lift aerofoil section (S1223). A comparison of the characteristics of three aerofoils between analytical models and experimental results of Clark-Y, NACA661-212. And S1223 is shown in Fig. 5.24 - 5.26 respectively.

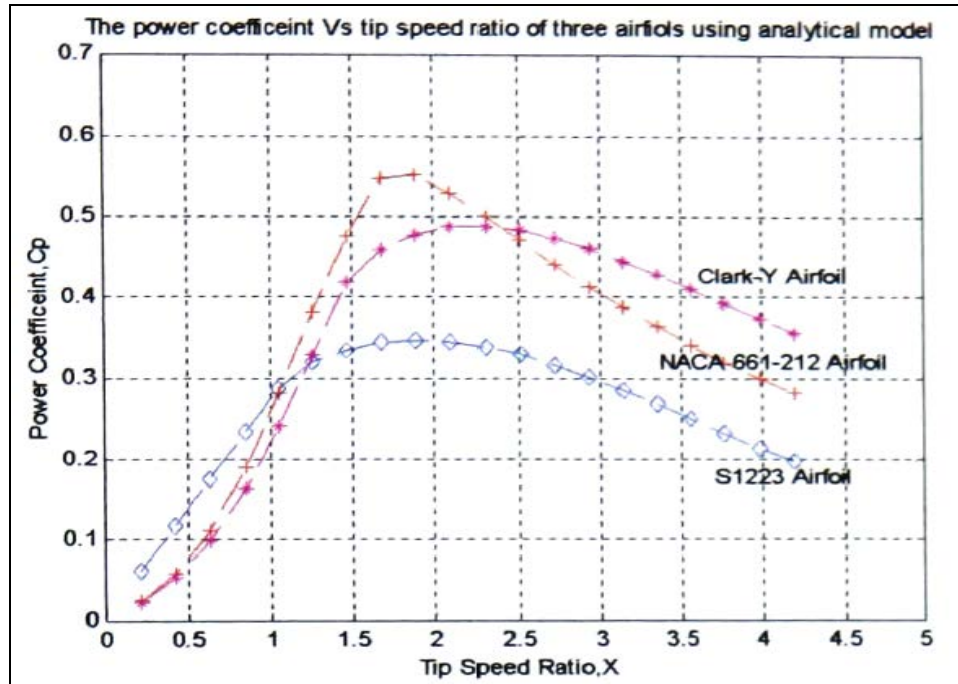


Fig. 5.23 Full range of prediction results from analytical models

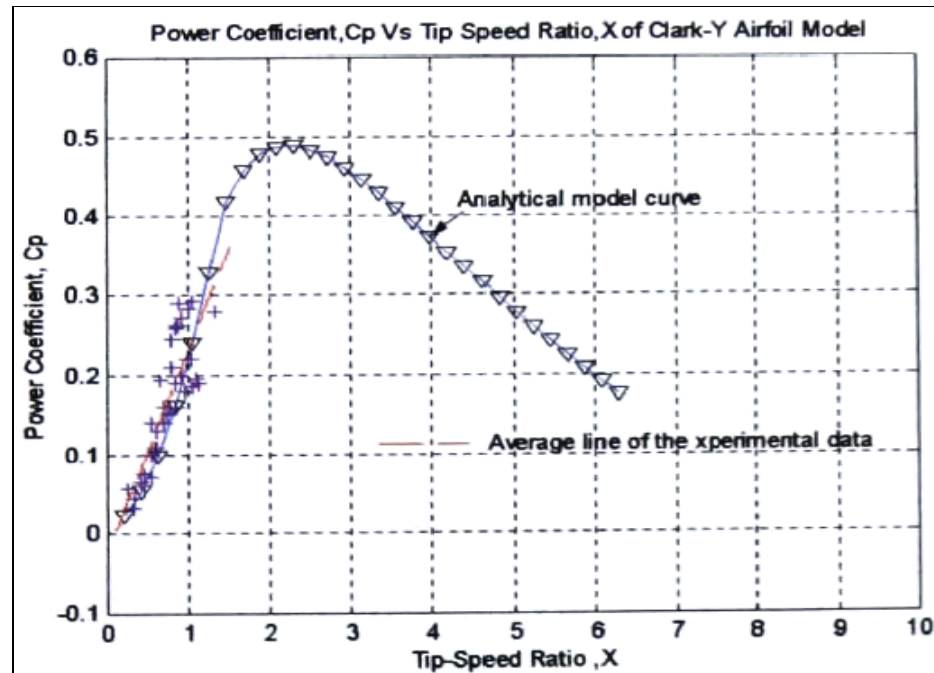


Fig. 5.24 Comparison results between analytical and experimental models of Clark-Y aerofoil

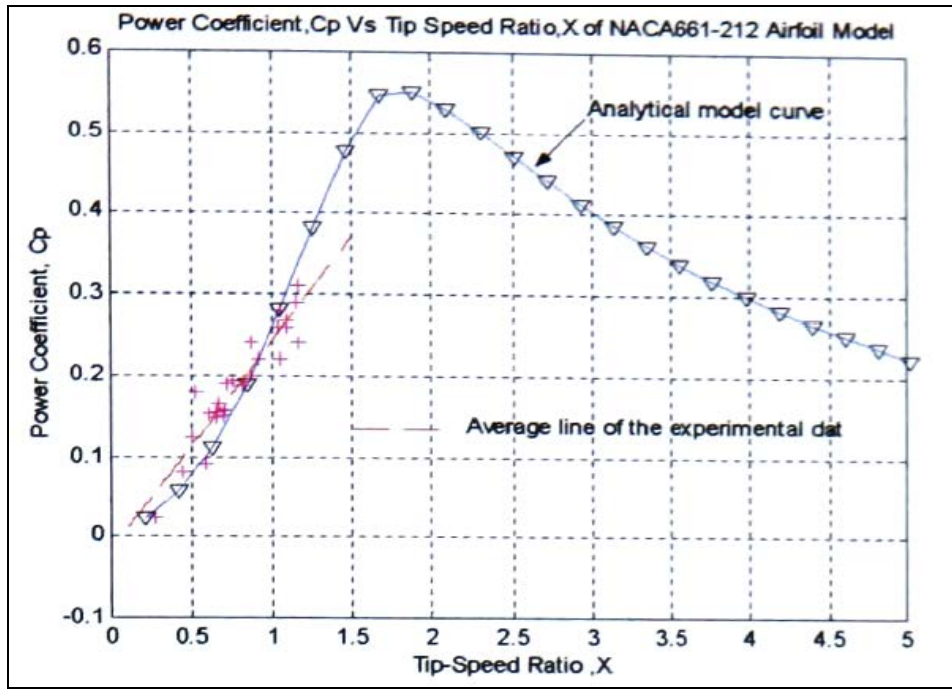


Fig. 5.25 Comparison results between analytical and experimental model of NACA661-212 aerofoil

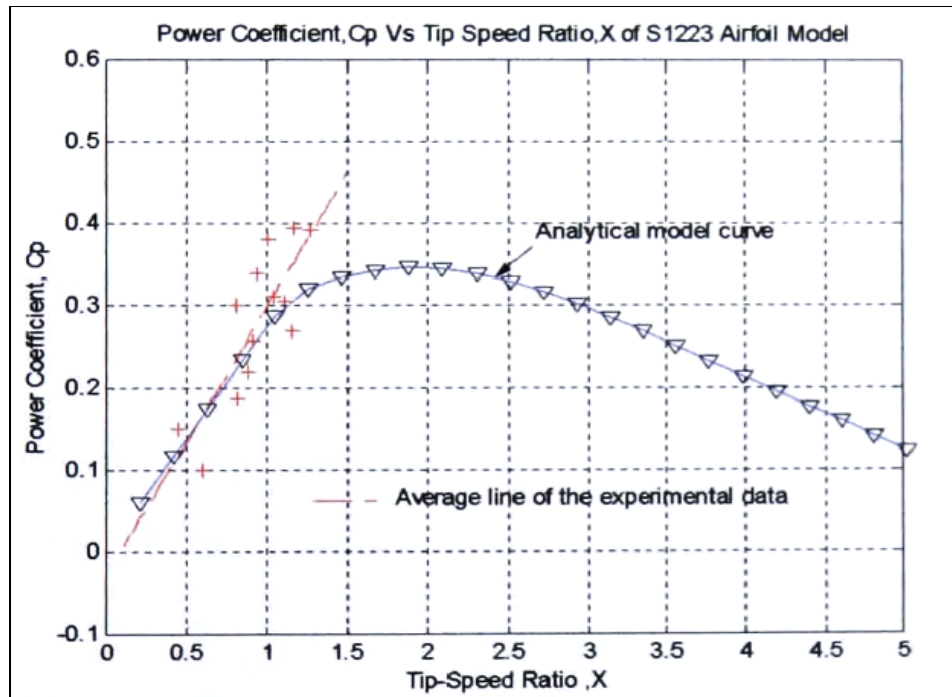


Fig. 5.26 Comparison results between analytical and experimental model of S1223 aerofoil

Errors involved in experimental and analytical work have been evaluated. Table 5.15 - 5.17 show the evaluation errors results of Clark-Y, NACA661-212, and S1223 respectively.

Table 5.15 Evaluation of the errors on Clark-Y experimental results

TSR	Clark-Y		Differences	Percent errors (%)
	Experimental	Analytical		
0.2	0.025	0.02	0.005	20
0.4	0.08	0.05	0.03	37.5
0.6	0.13	0.1	0.03	23.07
0.8	0.18	0.15	0.03	16.6
1.0	0.23	0.22	0.03	13
1.2	0.28	0.3	0.05	17.8
			Average	21.37

Table 5.16 Evaluation of the errors on NACA 661-212 experimental results

TSR	Clark-Y		Differences	Percent errors (%)
	Experimental	Analytical		
0.2	0.03	0.02	0.01	33.3
0.4	0.09	0.05	0.04	44.4
0.6	0.14	0.1	0.04	28.5
0.8	0.19	0.18	0.01	5.26
1.0	0.25	0.26	0.01	3.8
1.2	0.3	0.35	0.05	14.28
			Average	21.59

Table 5.17 Evaluation of the errors on S1223 experimental results

TSR	Clark-Y		Differences	Percent errors (%)
	Experimental	Analytical		
0.2	0.05	0.06	0.01	16.6
0.4	0.1	0.11	0.01	9.09
0.6	0.17	0.17	0	0
0.8	0.23	0.22	0.01	4.34
1.0	0.03	0.28	0.02	6.66
1.2	0.37	0.31	0.06	16.2
			Average	8.88

These positive results (Figs. 5.21-5.22) support that the S1223 aerofoil could overcome the problem of rotor self-starting of the Darrieus wind turbine. The analytical models show that at the full range of the tip speed ratio NACA 66,1-212 has performance better than shown by others. The results of this test showed that the curves for the experimental and the computational data are comparable. The experimental results indicate good agreement with the prediction results. The curves all follow approximately the same shape; the average of the

differences shown was about 21 percent for both Clark-Y and NACA 661-212 aerofoil and at about 9 percent of S1223 model (see Table 5.15-5.17). Nevertheless, the results in this section support the hypothesis that the analytical model prediction in Chapter 3 provides reliable information. Additionally the analytical models could be used to predict the rotor performance over a greater range of tip speed ratios.

S1223 aerofoil developed high power coefficient at low tip speed ratio. And also from the author's experience, the rotor with this aerofoil (S1223) was very easy to start. Clark-Y and NACA 661-212 showed similar results at low tip speed ratio, and poor starting torque.

5.4.2 The study of chord ratio effect ($\frac{c}{r}$)

This section presents the experimental results from investigations of the chord ratio effects on the performance of Darrieus wind machine. New wind turbine rotor blades of three-selected aerofoil sections of vertical axis wind turbine models were constructed and their performances tested in the wind tunnel. The blade of chord length c on these new wind turbine models was 0.15 m (0.20 m in the previous study). This modification leads to decrease in the $\frac{c}{r}$ from the previous value of 1 to 0.75 m this present study (maintaining the same rotor radius 0.2 m).

The study also investigated the results from the analytical models analysis and compared with the experimental results. The following results have shown the performance of the 2 blades machine with the following specifications: blade chord length of 0.15 m, rotor diameter of 0.4 m and rotor height of 0.4. Table 5.18-5.19 shows the experimental results of NACA 661-212, Table 5.20-5.21 presents the result of Clark-Y and the last aerofoil experiment results S1223 are shown in Table 5.22-5.23.

5.4.2.1 Aerofoil: NACA 661-212

Table 5.18 NACA661-212 at wind velocity, $V=12$ m/sec

RPM	Torque, T (Nm)	Omega (Ω)	Power $P = T \times \Omega$	C_p	TSR, X
900	0.72	94.2	67.2	0.39	1.57
860	0.68	90.0	61.2	0.362	1.50
700	0.54	73.26	39.56	0.23	1.22
550	0.42	57.56	24.17	0.14	0.96
480	0.38	50.24	19.91	0.12	0.83
300	0.32	31.4	10.04	0.06	0.52

Table 5.19 NACA661-212 at wind velocity, $V=16$ m/sec

RPM	Torque, T (Nm)	Omega (Ω)	Power $P = T \times \Omega$	C_p	TSR, X
1020	1.25	106.76	133.45	0.33	1.33
900	1.14	94.2	107.38	0.27	1.17
820	0.98	85.82	84.10	0.21	1.07
690	0.82	72.22	59.22	0.15	0.90
550	0.78	57.56	44.89	0.11	0.719
320	0.68	33.49	19.42	0.056	0.41

Observation results of NACA 661-212

From the experimental result from Table 5.18-5.19 can be plotted to show C_p / tip speed ratio relationship (Fig. 5.27). The experimental results compared with the analytical model prediction are shown in Fig. 5.28.

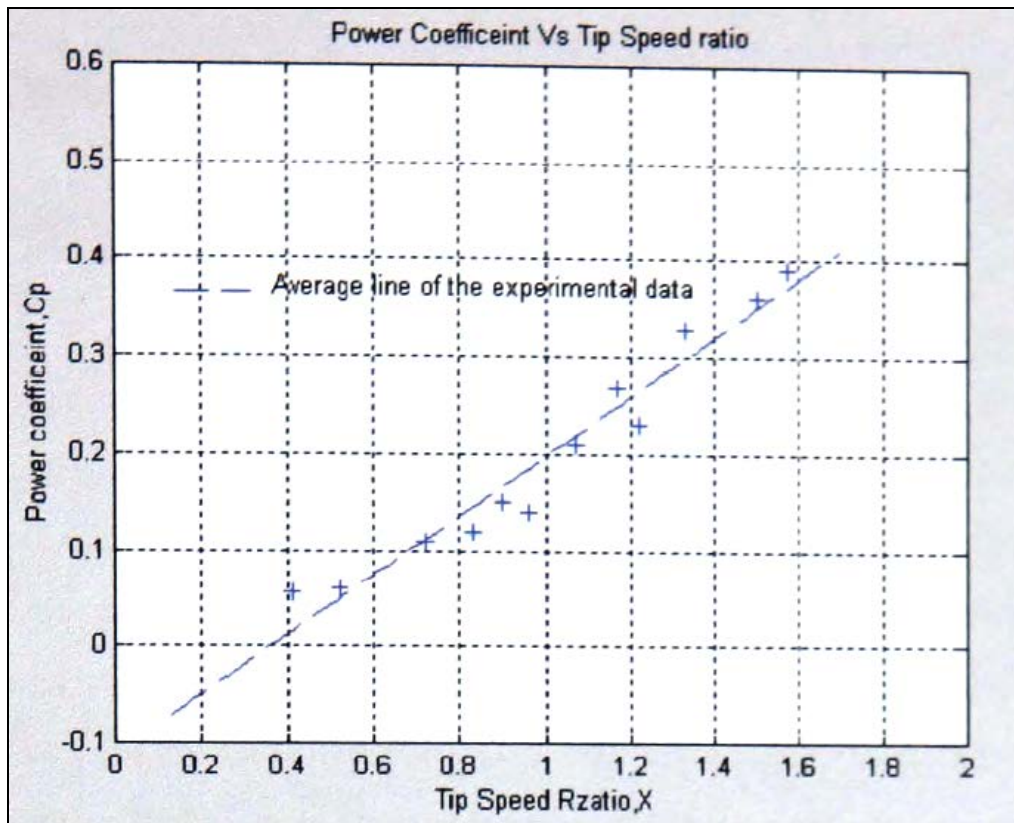


Fig. 5.27 Experimental results for NACA 661-212

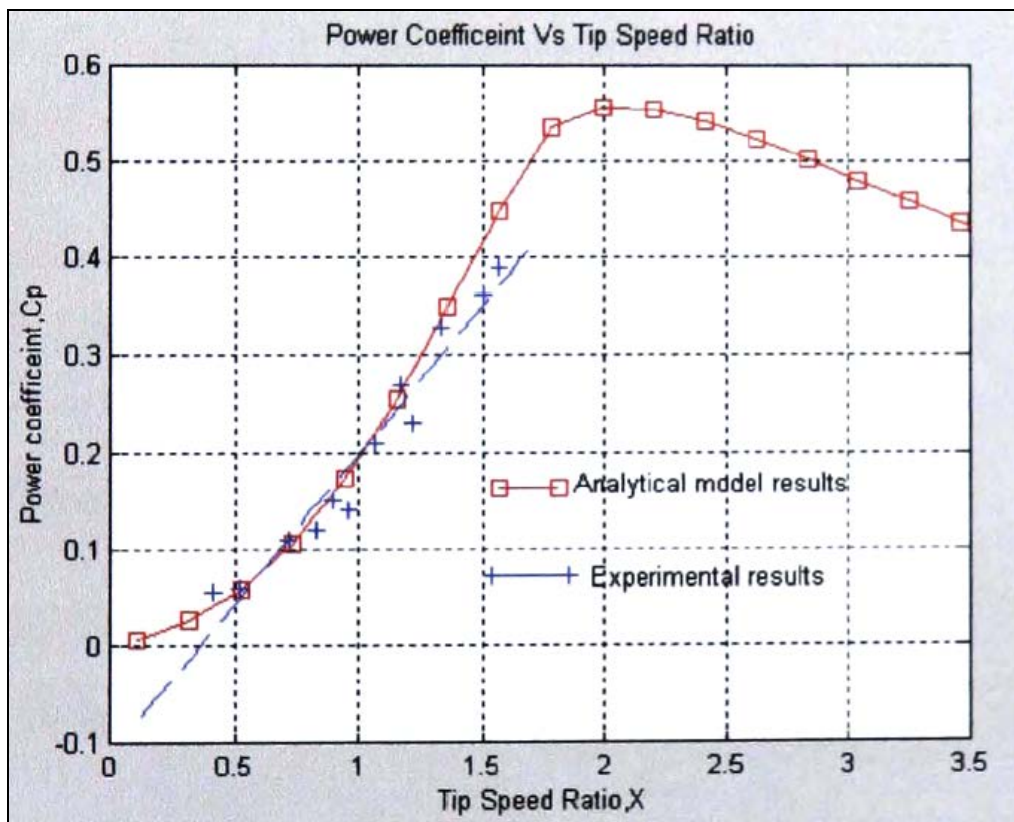


Fig. 5.28 Comparison between analytical and experimental results

5.4.2.2 Aerofoil: Clark-Y

Table 5.20 Clark-Y at wind velocity, V=12 m/sec

RPM	Torque, T (Nm)	Omega (Ω)	Power $P = T \times \Omega$	C_p	TSR, X
870	0.69	91.06	62.83	0.37	1.51
750	0.62	78.5	48.67	0.28	1.30
630	0.53	65.94	34.94	0.20	1.09
560	0.40	58.61	23.44	0.138	0.976
450	0.31	47.1	12.92	0.07	0.78
300	0.28	31.4	8.79	0.05	0.52

Table 5.21 Clark-Y at wind velocity, V=16 m/sec

RPM	Torque, T (Nm)	Omega (Ω)	Power $P = T \times \Omega$	C_p	TSR, X
1015	1.32	106.2	140.18	0.35	1.32
920	1.21	96.29	116.5	0.29	1.20
850	0.94	88.4	83.09	0.20	1.105
740	0.92	76.96	70.80	0.18	0.962
690	0.69	71.76	49.51	0.12	0.897
430	0.61	44.72	27.27	0.068	0.55

Observation results of Clark-Y

The experimental results In Table 5.120-5.21 are presented in graphical form by Matlab tool in Fig. 5.29 and are also compared with analytical model predictions in Fig. 5.30.

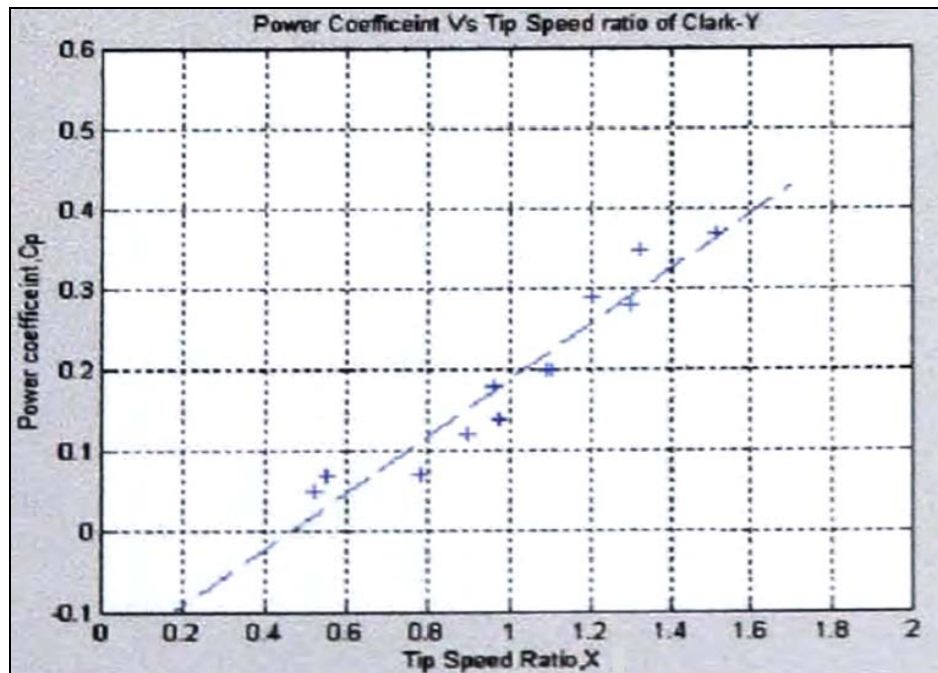


Fig. 5.29 Experimental and the average line for Clark-Y aerofoil

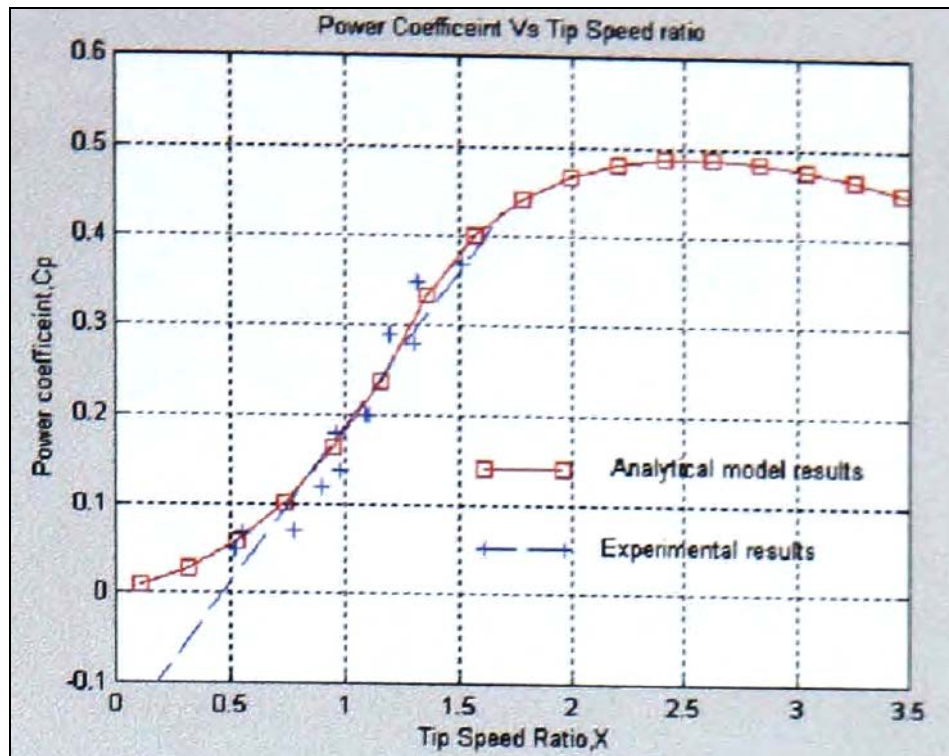


Fig. 5.30 Comparison between analytical and experimental results on Clark-Y aerofoil

5.4.2.3 Aerofoil: S1223

Table 5.22 S1223 at wind velocity, $V=12$ m/sec

RPM	Torque, T (Nm)	Omega (Ω)	Power $P = T \times \Omega$	C_p	TSR, X
860	0.82	90.0	73.8	0.43	1.5
720	0.69	74.88	52.39	0.31	1.25
500	0.65	52	33.8	0.20	0.86
400	0.73	41.6	30.42	0.18	0.69
320	0.76	33.28	25.35	0.15	0.55
300	0.70	31.2	21.97	0.13	0.52

Table 5.23 S1223 at wind velocity, $V=16$ m/sec

RPM	Torque, T (Nm)	Omega (Ω)	Power $P = T \times \Omega$	C_p	TSR, X
1090	1.53	114.0	174.42	0.43	1.43
936	1.42	97.96	139.10	0.34	1.25
910	1.34	95.24	127.62	0.31	1.20
835	1.25	86.84	108.55	0.27	1.085
750	1.02	78.5	80.07	0.199	0.98
640	0.95	66.98	63.63	0.158	0.83
500	0.85	52	44.2	0.11	0.65

Observation results of S1223

The results of experimental study of S 1223 at chord ratio of 0.15 were plotted using Matlab tool in Fig 5.31 with the averaging data line. Fig. 5.32 illustrates the comparison with the analytical model prediction.

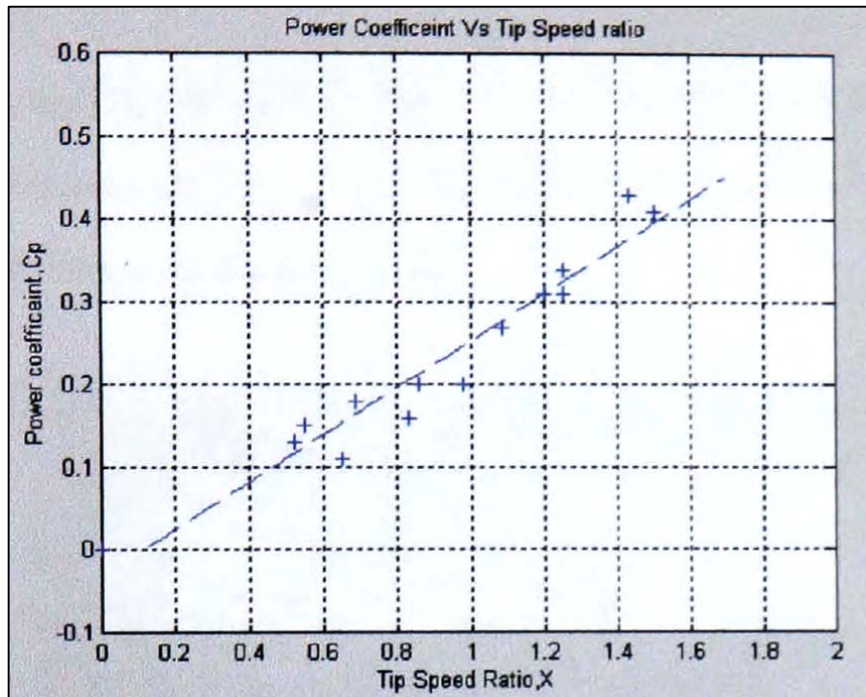


Fig. 5.31 Experimental results and average line of S 1223 on Darrieus turbine

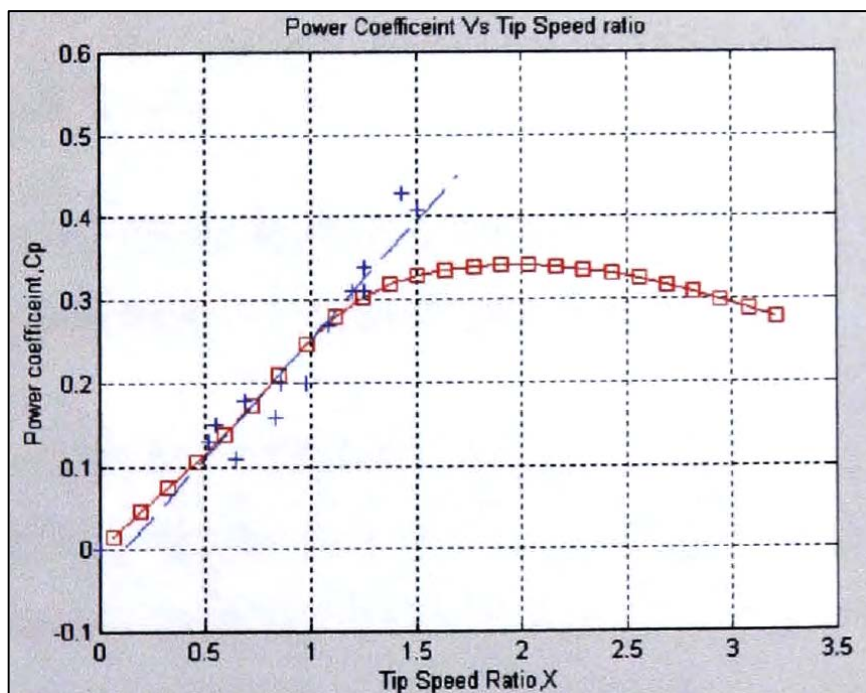


Fig. 5.32 Comparison between the analytical and the experimental results of S1223

5.4.2.4 The discussion of chord length ratio effect

This section focuses on the study of the influence of chord ratio on the performance of the Darrieus wind machine. The detail of the effects of this parameter is well investigated in literature survey Chapter 2 and Chapter 3, the analytical model analysis. Previous studies indicate that wind turbines with high chord ratio would produce high starting torque but low power coefficient at higher range of tip speed ratios. The result of the experimental analysis seems to agree with the results from the previous study. And as can be seen in Fig. 5.33, compared to Fig. 5.21 wind turbines with lower chord ratio produce lower starting torque.

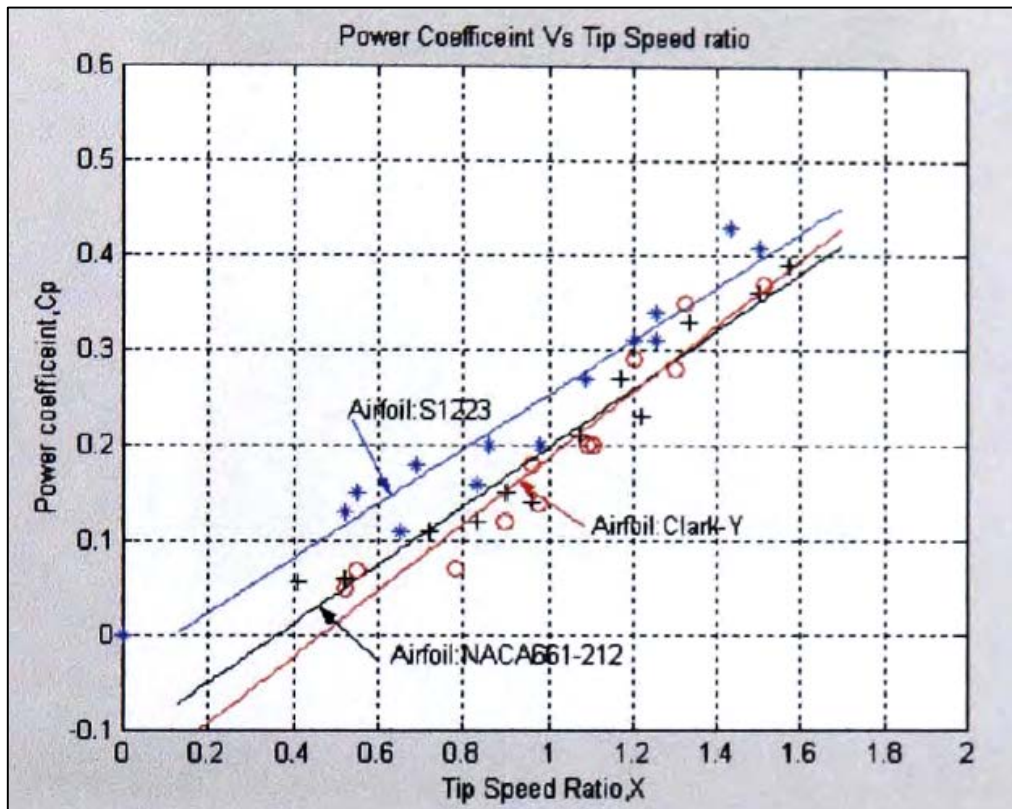


Fig. 5.33 Performance comparison results of three experiments for 2 blade Darrieus rotor at chord length of 0.15 m

The experimental and analytical analyses support and confirm that this type of wind machine generates higher starting torque at higher chord ratio. However, the same wind machine with low number of chord ratio generated higher performance at higher tip speed ratio. This is also true and agreed well with the analytical predictions Chapter 3. Therefore, this wind machine could start the rotor by itself with a high chord ratio aerofoil and could generate the desired performances. The self-starting capacity and the performance of this machine therefore need to be compensated against each other to optimise the performance.

5.4.3 The study of number of blade (b) effect

This section shows the results of the study of the investigation of the effect of number of blade on the performance of wind machine. The models were tested in the wind tunnel with the same specifications In previous section (section 5.4.2) by changing the number of blades from two to three. The following tables describe the detail of the experimental results of the three aerofoils sections chosen.

5.4.3.1 Aerofoil: NACA661-212

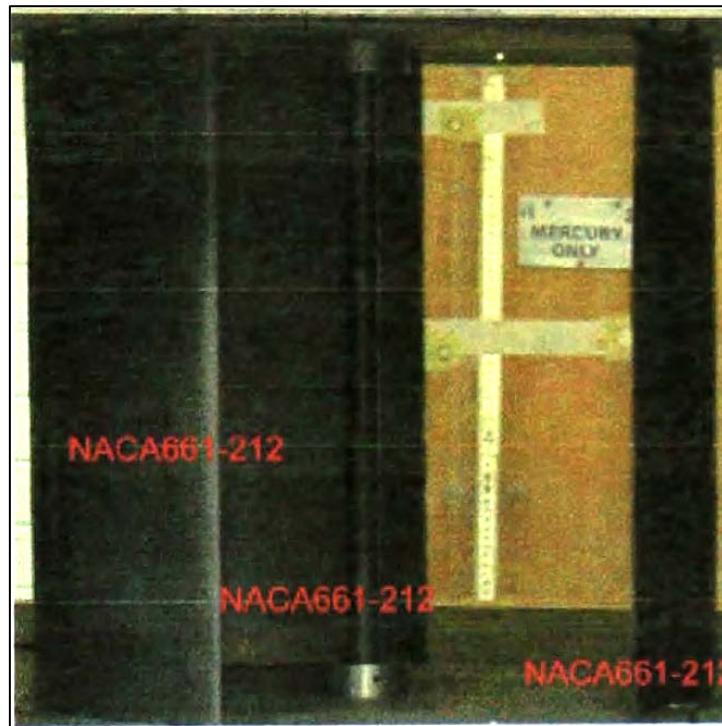


Fig. 5.34 Experimental set up of three blades NACA 661-212

Table 5.24 NACA 661-212 at wind velocity, $V = 14$ m/sec

RPM	Torque, T (Nm)	Omega (Ω)	Power $P = T \times \Omega$	C_p	TSR, X
1060	0.36	110.24	39.68	0.147	1.57
800	1.46	83.20	121.47	0.45	1.19
600	1.08	62.4	67.39	0.25	0.89
400	0.75	41.6	31.2	0.12	0.59
300	0.51	31.2	15.91	0.05	0.45
200	0.40	20.8	8.32	0.03	0.29

Table 5.25 NACA 661-212 at wind velocity, $V = 16$ m/sec

RPM	Torque, T (Nm)	Omega (Ω)	Power $P = T \times \Omega$	C_p	TSR, X
930	1.46	95.68	140.49	0.35	1.196
845	1.327	87.88	116.64	0.29	1.09
780	1.28	81.12	104.36	0.26	1.01
600	1.22	62.4	76.26	0.19	0.78
500	1.15	52	60.21	0.15	0.65
410	0.94	42.64	40.14	0.1	0.53

Observation results of NACA 661-212

Fig. 5.35 presents the experimental results of three rotor blades with the average line. These results were compared with the analytical model prediction in Fig. 5.36.

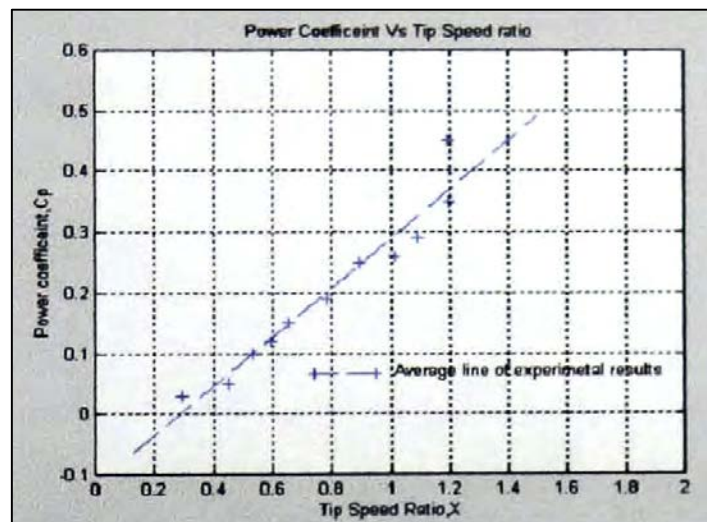


Fig. 5.35 Experimental results and average line of three bladed NACA 661-212 on Darrieus wind machine

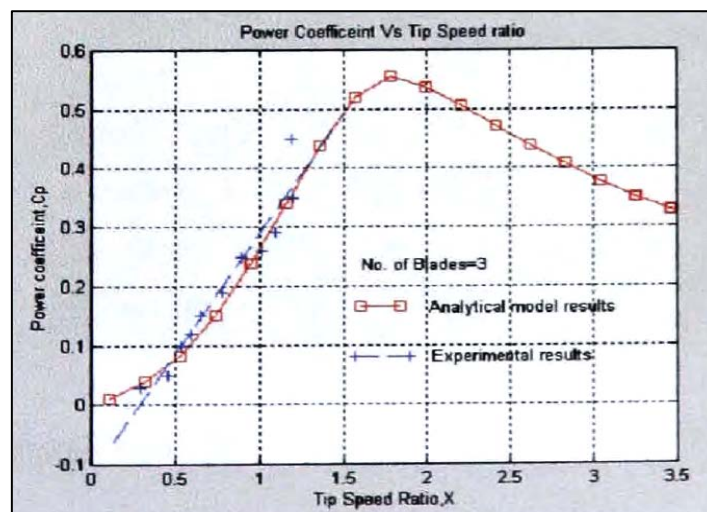


Fig. 5.36 Comparison of experimental and analytical prediction of NACA 661-212 on Darrieus wind machine

The experimental comparison of NACA 661-212 aerofoils between two and three blades can be seen in Fig. 5.37. From these results showed that the machine with three blades generates higher starting torque and also higher power coefficients at low range of tip speed ratio.

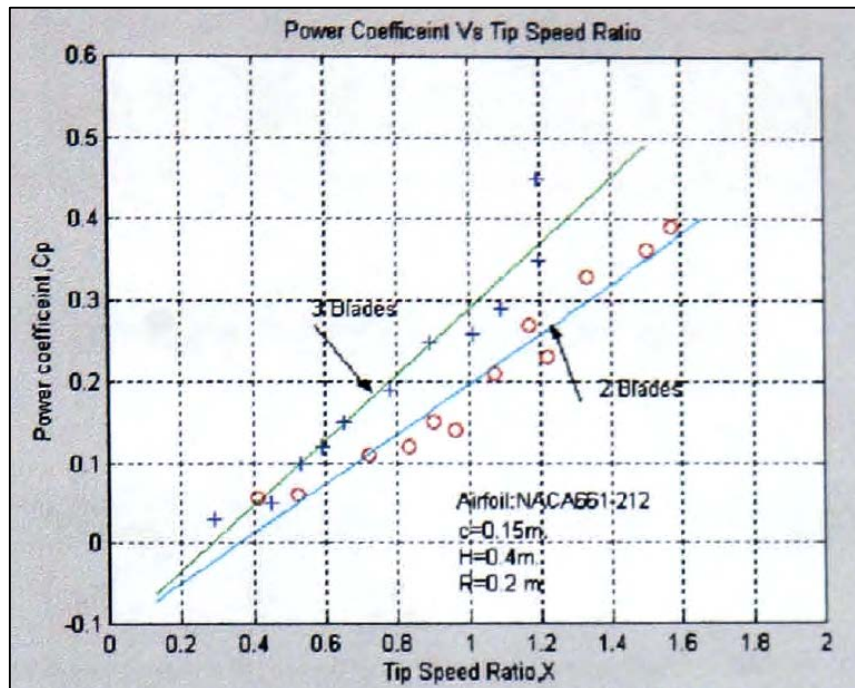


Fig. 5.37 Comparison results of the experimental testing between two and three blades of NACA 661-212

5.4.3.2 Aerofoil: Clark-Y

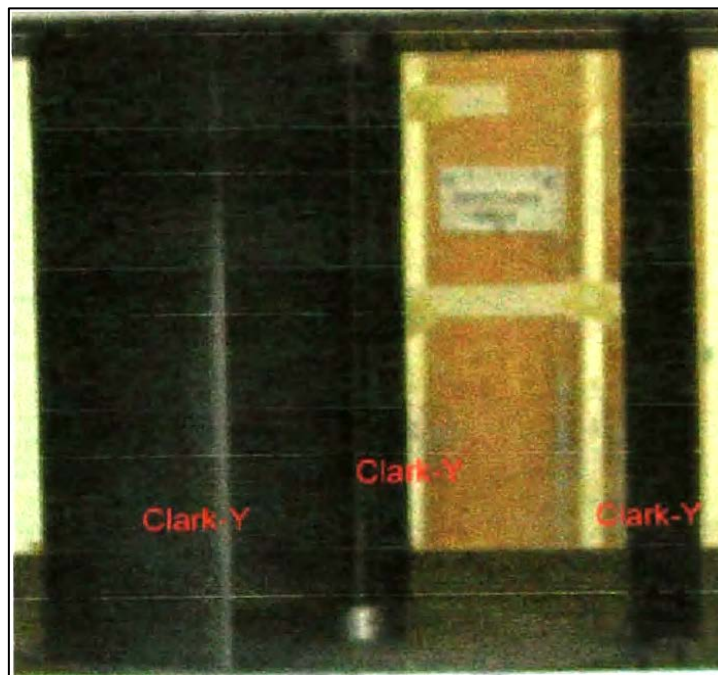


Fig. 5.38 The experimental set up of three blades Clark-Y

Table 5.26 Clark -Y at wind velocity, V= 14 m/sec

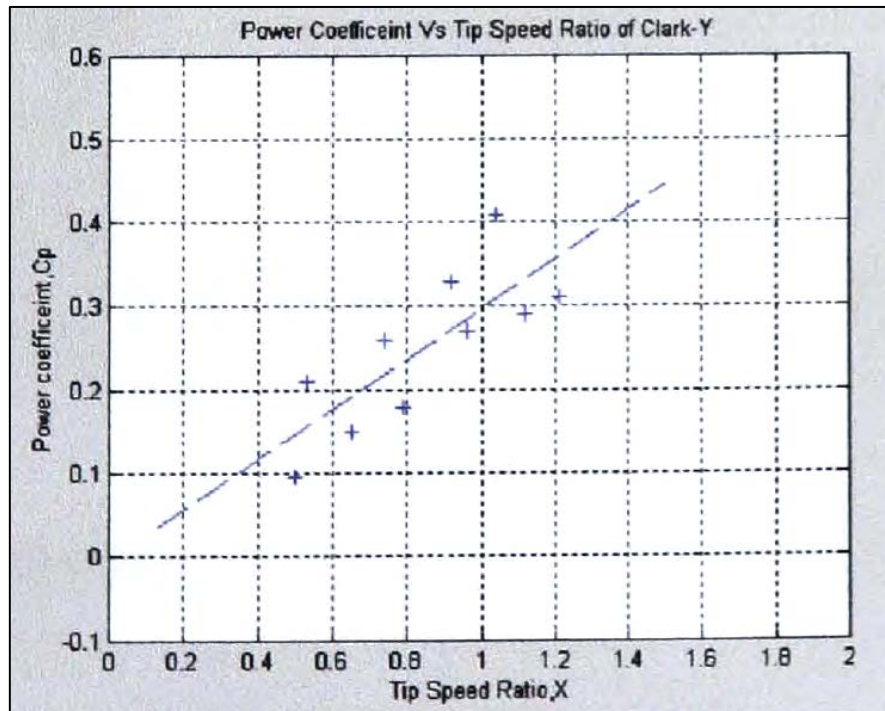
RPM	Torque, T (Nm)	Omega (Ω)	Power $P = T \times \Omega$	C_p	TSR, X
700	1.52	72.8	110.65	0.41	1.04
620	1.41	64.48	90.91	0.33	0.92
500	1.39	52	72.28	0.26	0.74
360	1.53	37.4	57.28	0.21	0.53

Table 5.27 Clark -Y at wind velocity, V= 16 m/sec

RPM	Torque, T (Nm)	Omega (Ω)	Power $P = T \times \Omega$	C_p	TSR, X
930	1.286	96.72	124.43	0.31	1.209
860	1.30	89.44	116.4	0.29	1.12
740	1.408	76.96	108.37	0.27	0.96
610	1.13	63.44	72.25	0.18	0.79
505	1.14	52.52	60.21	0.15	0.65
380	0.99	39.52	38.13	0.095	0.5

Observation results of Clark-Y

The experimental results from Table 5.26-5.27 were plotted using Matlab tool and presented in graph form shown in Fig. 5.39.

**Fig. 5.39 Experimental results and average line of three blades Clark-Y**

The comparison between the experimental and the analytical analysis is presented in Fig. 5.40, and indicates the higher power coefficient generated from experimental result. The comparison between two and three blades of the experimental can be seen in Fig 5.41. This result showed that Wind turbine with three blades generates higher starting torque.

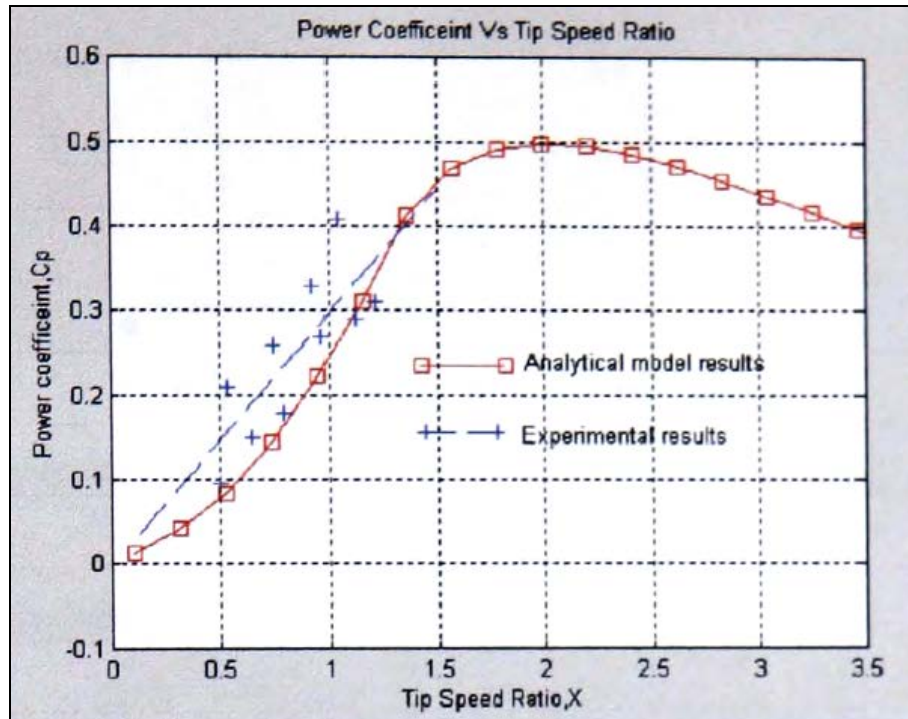


Fig. 5.40 Comparison of 3 blades machine's analytical and experimental results

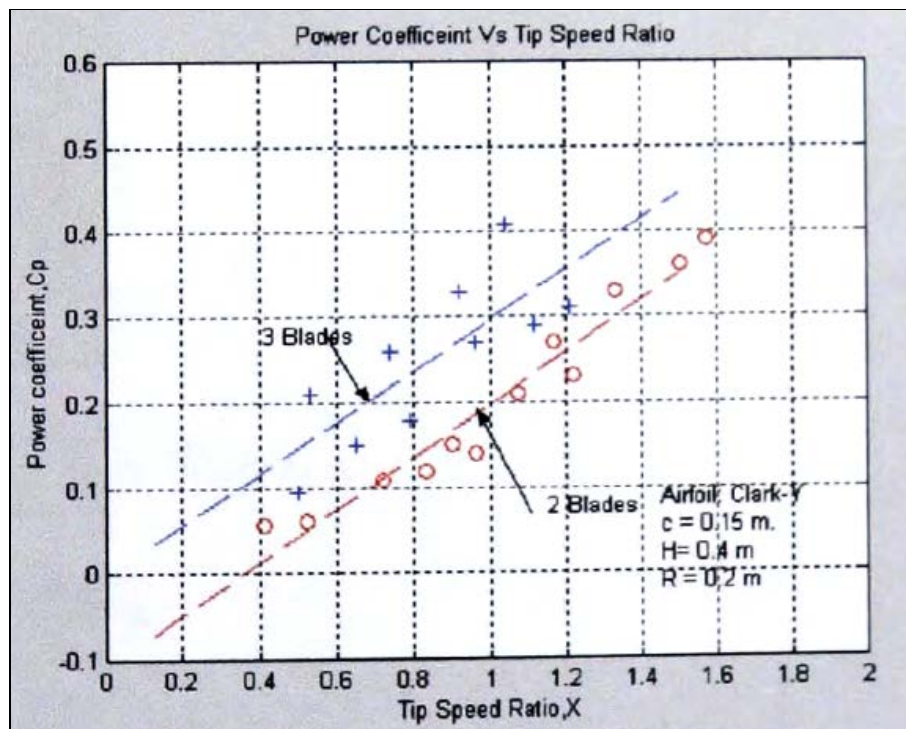


Fig. 5.41 Experimental results of two and three blade Clark-Y

5.4.3.4 Aerofoil: S1223



Fig. 5.42 Experimental set up of three blades S1223 machine

Table 5.28 S1223 at wind velocity, $V = 10$ m/sec

RPM	Torque, T (Nm)	Omega (Ω)	Power $P = T \times \Omega$	C_p	TSR, X
200	1.01	20.9	21.14	0.21	0.418
220	0.88	23.02	20.26	0.206	0.46
179	1.02	18.73	19.11	0.19	0.3746
193	1.05	19.1	20.06	0.204	0.38
267	1.132	27.94	31.63	0.32	0.55
260	1.04	27.21	28.30	0.28	0.544
100	0.48	10	4.8	0.04	0.2

Table 5.29 S1223 at wind velocity, $V = 12$ m/sec

RPM	Torque, T (Nm)	Omega (Ω)	Power $P = T \times \Omega$	C_p	TSR, X
750	0.54	78	42.12	0.25	1.3
600	1.52	62.4	94.84	0.55	1.04
450	1.24	46.8	58.03	0.34	0.78
350	1.13	36.4	41.13	0.24	0.60
339	1.027	35.25	35.95	0.21	0.58

Table 5.30 S1223 at wind velocity, $V=12$ m/sec

RPM	Torque, T (Nm)	Omega (Ω)	Power $P = T \times \Omega$	C_p	TSR, X
880	1.62	91.52	148.26	0.37	1.14
850	1.76	88.4	155.59	0.38	1.105
820	1.88	85.28	160.32	0.39	1.06
800	1.95	83.2	162.24	0.404	1.04
780	2.00	81.12	162.24	0.404	1.01

Observation results of S1223

The experimental results from Table 5.28-5.30 were taken to be investigated in graphical form in Fig. 5.43. The experimental results are different compared to the analytical predictions, which can be seen in Fig. 5.44.

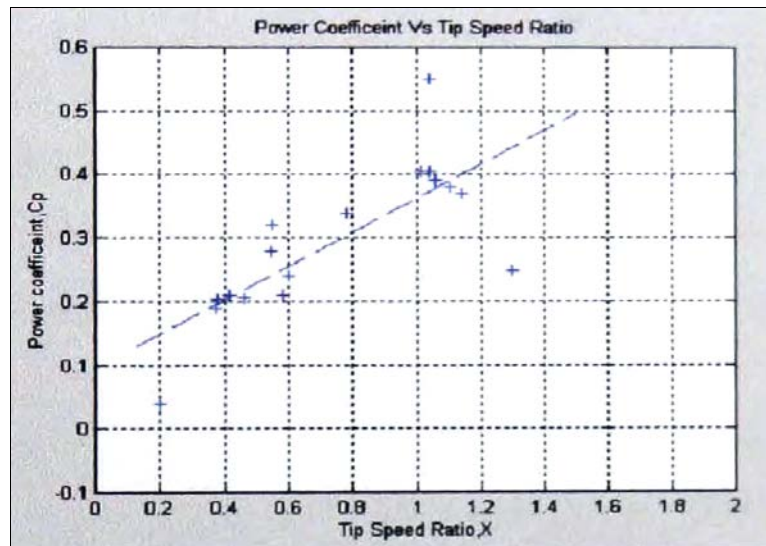


Fig. 5.43 Experimental results and average line of three bladed S1223

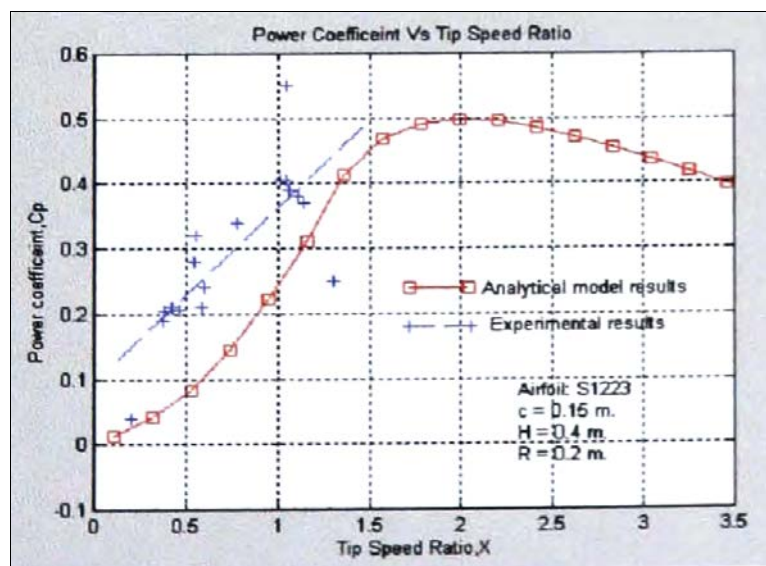


Fig. 5.44 Experimental results and average line of three bladed S1223

However, this study showed that S 1223 with three blades generated higher performance at these range of experimental results (Fig. 5.45)

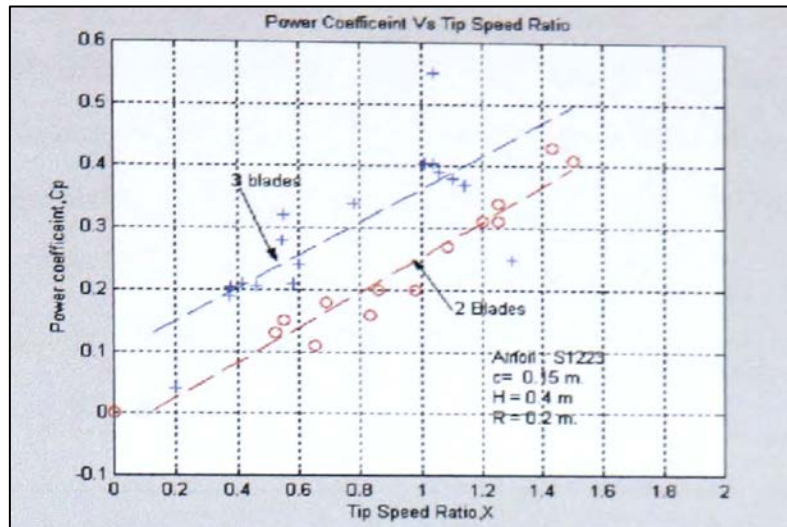


Fig. 5.45 The experimental results of two and three blade of S 1223

5.4.3.5 The Discussion of number of blade (b) effect

The results confirmed that the number of blades affects the performance of the wind turbines. The experimental experience also shows that the three bladed wind turbine model was easier to start. S1223 aerofoil profiles showed better power coefficients compared to NACA 661-212 and Clark-Y (See Fig. 5.46). At low tip speed ratio the higher number of blades can generate higher performance. Nevertheless, if the wind machines have been designed to operate at low tip speed ratio, then a greater number of blades would be preferred. This is confirmed by the results of this study.



Fig. 5.46 Summarised experimental results of 3 blades D-Rotor

Typical example results supporting this matter can also be seen at the tip speed ratio of 0.6 of two blade models in Fig. 5.33. The results showed the power coefficient of 0.15, 0.08, 0.5 for S1223, NACA661-212 and Clark-Y respectively. For the same tip speed ratio, the three-bladed machine (Fig. 5.46) showed higher power coefficient to all 3 models (S1223 = 0.25, NACA661-212 = 0.12 and Clark-Y = 0.17). This supports the conclusion that those wind turbines with higher number of blades at low tip speed ratio generate higher performance. However, as mentioned and studied in Chapter 3, it has been suggested that the higher number of blades can reduce the performance and increase production cost.

5.4.4 The study of combination of aerofoils for Darrieus rotor

This section describes the new idea of hybrid approach to optimise vertical axis wind machine. The experimental results, and author's experience and the analytical prediction in Chapter 3 show that S1223 generates higher starting torque but does not perform well at high tip speed ratio compared with NACA 661-212 and Clark-Y. Therefore, the study combined these three aerofoils constructed to the same shaft of wind machine and tested their performance in the wind tunnel (Fig 5.47). The advantages of each aerofoil section could produce better performance.



Fig. 5.47 The wind turbine model set up for rotor blade combination

Table 5.31 Three aerofoil sections at wind velocity, V= 10 m/sec

RPM	Torque, T (Nm)	Omega (Ω)	Power $P = T \times \Omega$	C_p	TSR, X
500	0.62	52	32.24	0.33	1.04
330	0.54	34.32	18.5	0.189	0.68
230	0.37	23.92	8.85	0.090	0.47

Table 5.32 Three aerofoil sections at wind velocity, V= 12 m/sec

RPM	Torque, T (Nm)	Omega (Ω)	Power $P = T \times \Omega$	C_p	TSR, X
670	0.73	69.68	50.86	0.30	1.16
660	0.67	68.64	45.98	0.27	1.14
500	0.96	52	49.92	0.295	0.866
200	0.59	20.8	12.27	0.072	0.34

Table 5.33 Three aerofoil sections at wind velocity, V= 14 m/sec

RPM	Torque, T (Nm)	Omega (Ω)	Power $P = T \times \Omega$	C_p	TSR, X
780	1.30	81.12	105.45	0.392	1.15
620	1.15	64.48	74.15	0.275	0.92
300	1.28	31.2	39.93	0.148	0.445

Table 5.34 Three aerofoil sections at wind velocity, V= 16 m/sec

RPM	Torque, T (Nm)	Omega (Ω)	Power $P = T \times \Omega$	C_p	TSR, X
900	1.51	93.6	141.33	0.35	1.17
850	1.63	88.4	144.09	0.36	1.105
750	1.67	78	130.26	0.32	0.975
690	1.72	71.76	123.42	0.30	0.90
100	1.70	10.4	17.68	0.05	0.13

5.4.4.1 Observation results of combination of aerofoils on D-Rotor

The experimental results from Table 5.31-5.34 are presented in graphical form in Fig. 5.48. The results show that this hybrid wind model produced better performance than that of NACA 661-212 and Clark-Y aerofoils section. Additionally this model generated higher starting torque than those two aerofoils. The model was easier to start the rotor compared with NACA 661-212 or Clark-Y. However, this wind turbine model generated low performance and low starting torque compared with three blades S1223 aerofoil. It also encountered vibration problems at rotor revolutions of 500-900 rpm. This model was not a satisfactory way to optimise the D-Rotor performance.

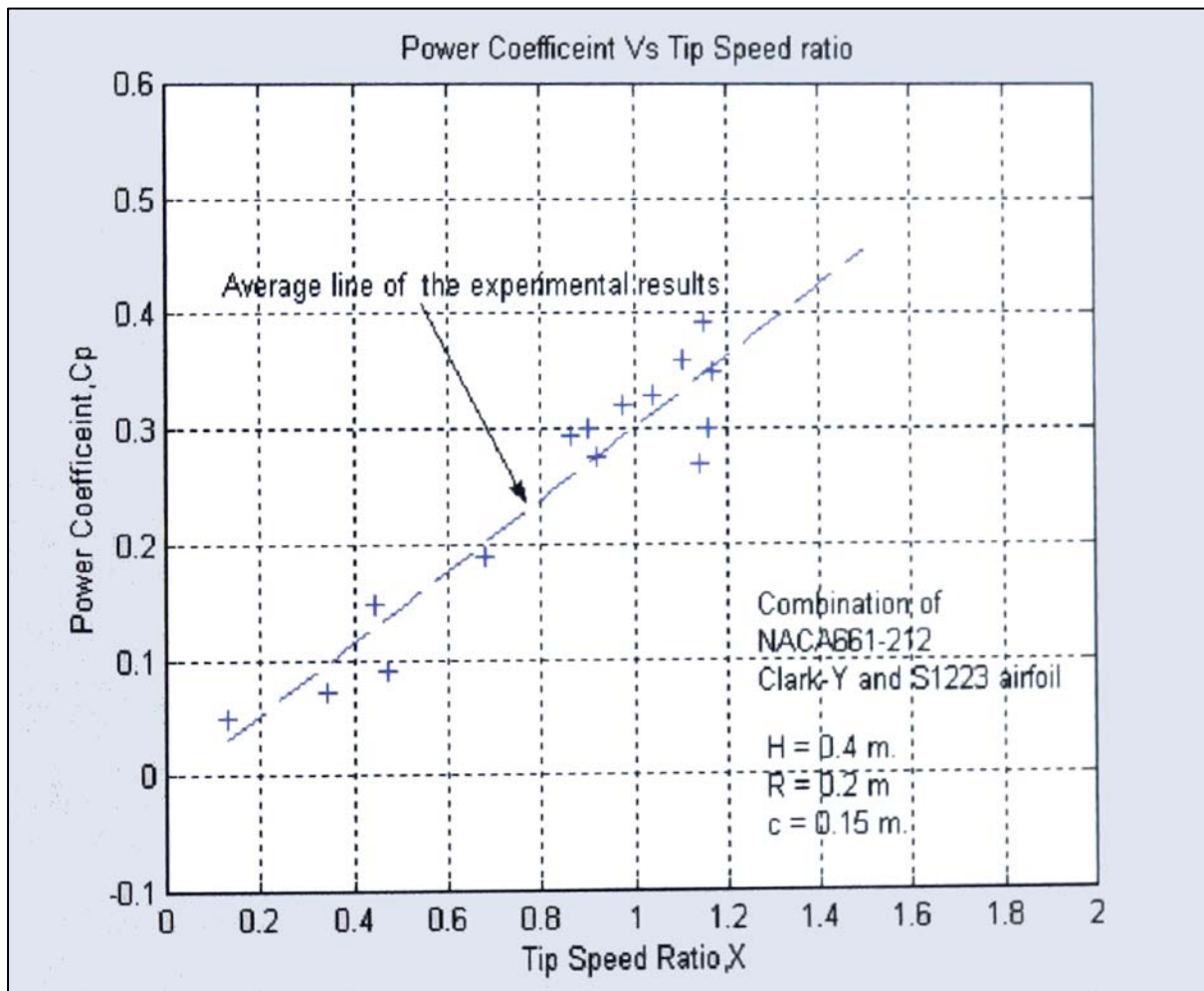


Fig. 5.48 Power coefficients of three aerofoils combined on D-Rotor

5.5 The conclusion from experimental testing

This chapter describes the performance of three aerofoil sections, which were built and tested to investigate the performance of straight-bladed Darrieus rotor. The wind turbine models were tested for their performance in the wind tunnel. The results from the experimental tests are concluded as follows:

- S1223 aerofoil generated higher performances compared with NACA661-212 and Clark-Y profiles
- In order to generate higher starting torque, D-rotor could have three rotor blades
- High values of chord ratio help the wind turbine to start rotor itself, in a stand-alone application
- The combination of different blade geometries on the same shaft of wind machine was not recommended due to unbalanced coupling
- The wind machine with zero blade pitch angle performs better than positive and negative pitch angles.

The experimental results showed promising performance of vertical axis wind machine.

Vertical Axis Wind Turbines (VAWTs) with suitable rotor aerofoil section could overcome the self-starting problem and generate the promising power output. S1223 cambered blade aerofoil is recommended to build the small prototype straight-bladed Darrieus VAWTs for the turbine field test in Chapter 6.

Chapter 6

Wind Turbine Field Test

6.1 Introduction

This chapter deals with the field test of the prototype of Vertical Axis Wind Turbines. Based on previous studies, vertical axis wind machines were constructed. Firstly, the stand-alone, 3 straight-bladed Darrieus wind machine of 0.7 kW using the aerofoil S1223 was constructed. The prototype was designed and its performance was tested in three different locations in Northeast.

The second wind machine combining the S and D rotor was used for the shrimp farm aeration process. This wind machine was designed to generate high start torque and was tested in a selected shrimp farm in southern Thailand for the wind speed from 2.6 m/sec.

6.2 The stand-alone '3 bladed' Vertical Axis Wind Turbines

The prototype was used to verify and compare with the results from the analytical models and from the wind tunnel tests. The results from these previous studies on the optimisation of VAWTs confirmed that this type of wind machine with S1223 aerofoil rotor would generate sufficient torque to start rotor itself. The test locations included:

- St Mary's Island, Whitley Bay
- Amble Caravan Park, Northumberland
- NaRec, Blyth, Northumberland

6.2.1 Design and construction of the wind machine

Based on the results from previous studies the following specifications were used.

- The turbine rotor profile: S1223 aerofoil section
- The number of rotor blades: 3
- Blade chord length: 0.2 m

- Blade pitch angle: 0°
- Rotor height: 1 m
- Rotor diameter: 2 m

In the design state for this wind turbine, the power output was calculated using

$$P_{out} = \frac{1}{2} \rho A C_p \eta_d \eta_g V^3 \quad (36)$$

However, for this type of wind machine previous study showed that the maximum power coefficient C_p was about of 0.3. The drive tram efficiency η_d , was assumed to be 0.8 and the generator efficiency η_g , was assumed to be 0.7. The turbine rotor area was 2 m² and the air density ρ was 1.225 kg/m³ at room temperature. Assuming the wind velocity is 15 m/sec, then the power output of this prototype wind machine was

$$P_{out} = \frac{1}{2} \times 1.225 \times 2 \times 0.3 \times 0.8 \times 0.7 \times 15^3$$

$$P_{out} = \sim 0.7 \text{ kW}$$

This maximum power output was used to select the generator and to design the control output unit for the wind machine prototype. However, as can be seen in equation (36) the power of the wind machine is dependent on 6 main parameters. The most important parameter is the wind resource. In high wind speed areas, a small wind rotor can develop a large amount of power while in the low wind speed area a large wind rotor will be required.

Fig. 6.1 shows the 3-D prototype modelling used for this study. The following section describes the details of each parts of this prototype.

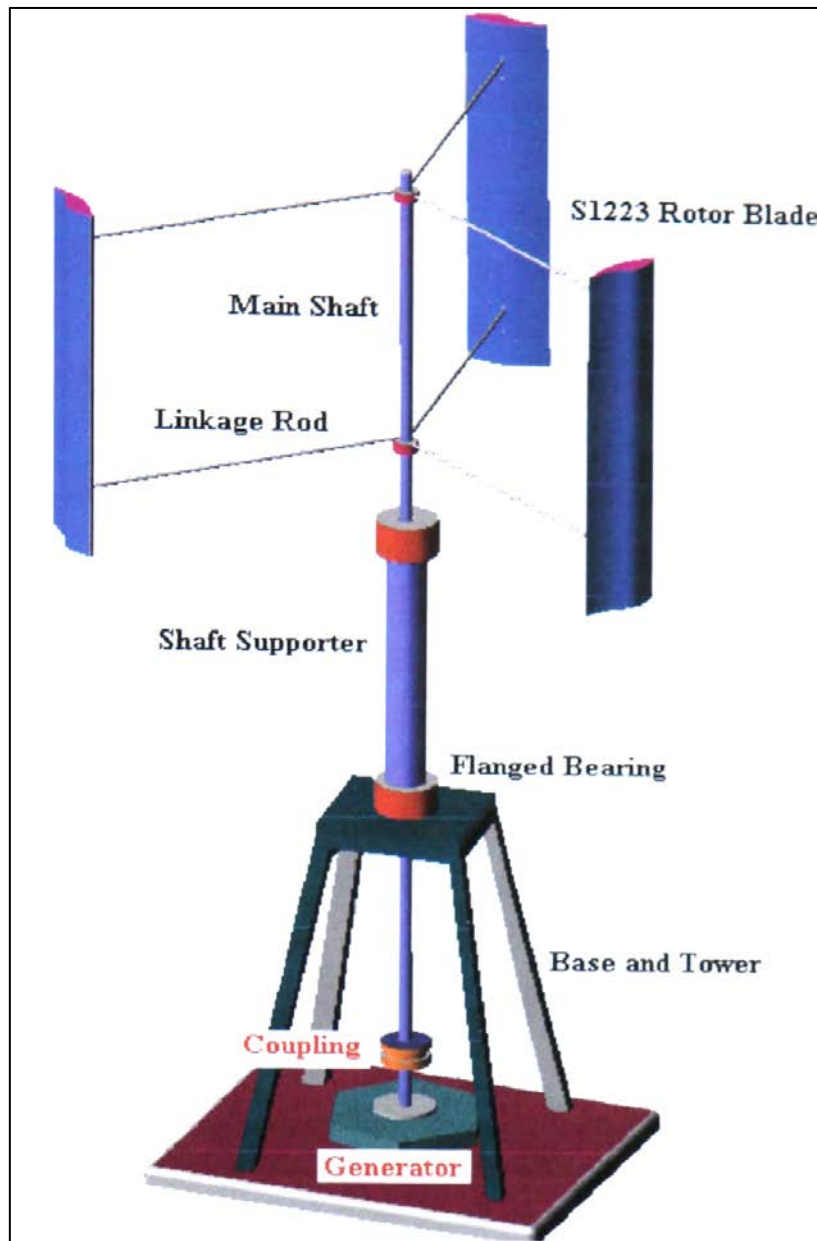


Fig. 6.1 3-D modelling prototype of the straight-bladed Darrieus Vertical Axis Wind Turbine

6 2.1.1 The rotor blades

The turbine rotors were made from a special wood available in Thailand (Fig. 6.2). Generally, wood has good strength to weight ratio, and has also good fatigue properties [71]. The rotor blades were coated with a water resistant solvent. Additionally, these rotor blades were painted for cosmetic reason and also to protect them from the ram and sunshine. Fig. 6.3 shows the rotor blade after the coating and painting process. The painting was used to reduce friction and drag.



Fig. 6.2 The process of fine finish surface of a rotor blade



Fig. 6.3 The painting of the rotor blades

Fig. 6.4 illustrates the first three blades. This set of rotor blades were used in the field test at St. Mary's Island, Whitley Bay.

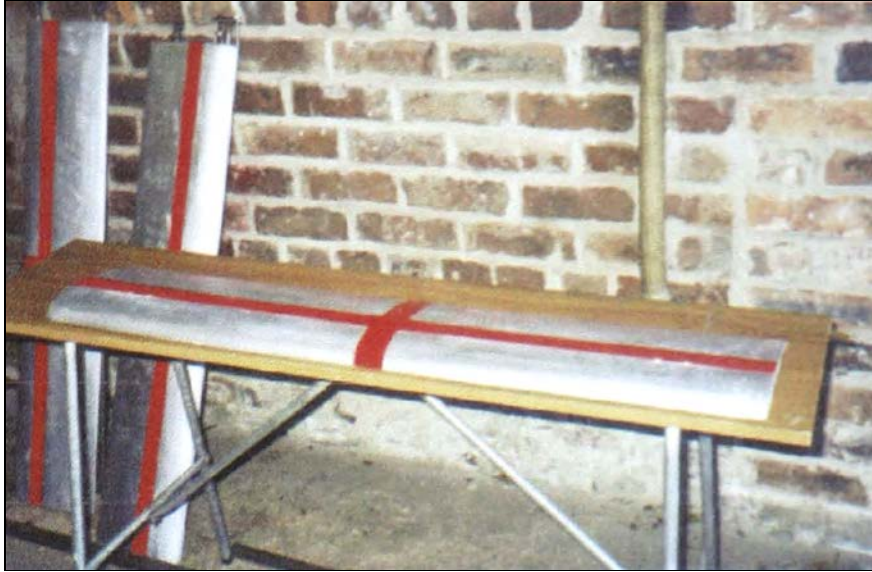


Fig. 6.4 Completed set of S1223 rotor blades ready to use for VAWTs

6.2.1.2 The main shaft and the supporting frame

The main shaft used in this prototype was a round steel shaft. This component is used to transmit the torque from the rotor blades to the generator. They are attached to gears, pulley or coupling. The main shaft used in this Wind machine prototype was of 30 mm diameter and 3 meters length. Details of the supporting framework are shown in the diagram 6.5.



Fig. 6.5 Shaft and Shaft supporter on pre-assembling the wind machine

6.2.1.3 The wind turbine base

The wind turbine base and the tower in this prototype were constructed using angled steel bar of dimension 38 x 38 x 2.5 mm. The dimension of the turbine base was of 1200 x 1200 mm. Fig. 6.6 shows the welding process to form the tower and the base for this prototype wind machine.



Fig. 6.6 Welding process to construct the tower and the base of the prototype

The components were test-assembled to ensure proper functioning of the turbine in the field test (see Fig. 6.7).



Fig. 6.7 Test-assembly of the prototype

6.2.2 The instruments used for the field test

The following devices and instruments were used in wind turbine prototype field tests:

- The generator and the control loads
- The torque transducer and visual interface software with PC
- The anemometer and the interface software support

6.2.3 Generator and control loads

The generator used in this wind machine was Rutland FM 1803 3-phase brushless permanent magnet generator (Fig. 6.8). It produces AC current of a maximum output 0.75 M. However the project was designed to control the wind turbine using direct circuit (DC). The output of this generator was changed from AC to DC using a rectifier unit which was placed inside the control box of the output loads as can be seen in Fig. 6.9. The output loads were designed and constructed to control the maximum power of 700 watts of this wind machine prototype.



Fig. 6.8 The permanent magnet induction generator Rutland FM1803

This control box combined various types of 12 volts light bulbs controlled by on/off switches on parallel circuits. The voltage (V) and current (I) were measured using an ammeter and a voltmeter.

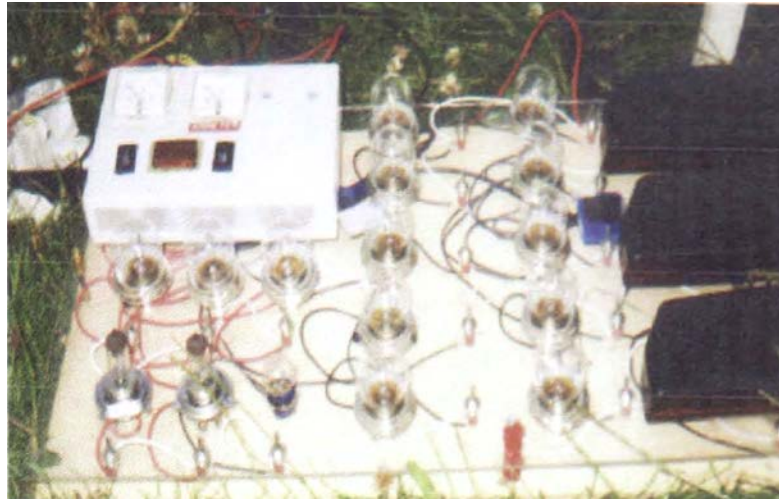


Fig. 6.9 The control loads box used to control output of the prototype

6.2.4 Torque Transducer and Visual Interface Software

Torque transducer was used to measure the torque generated from the wind machine. This device was installed between the bottom end of main shaft of the prototype and the generator shaft. In this wind turbine prototype, E300/RWTI-2 torque transducer was used to measure the torque and the results were displayed using E302 advanced torque transducer display interface. This torque transducer was also used to measure the main shaft revolution using the optional RPM pickoff.

Fig. 6.10 shows the torque transducer model E300/RWTI-2 and the indication panel.

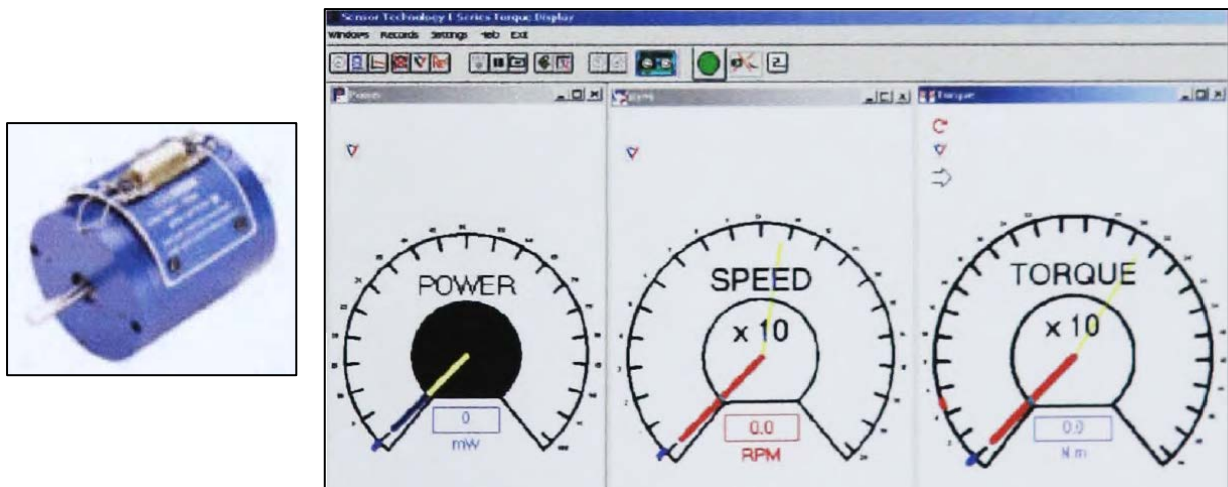


Fig. 6.10 E300/RWTI-2 Torque Transducer and Torque view software

Table 6.1 describes the model specification of the torque transducer used to measure the performance of the wind machine prototype at three different field locations in the Northeast of England.

Table 6.1 E300/RWTI-2 specifications

Max. Operation Speed	0 - 20,000 rpm
Temperature range	-10 to +50°C
Temperature coefficient	Less than 0.01% per °C
Max. Torque	50 N. m
Safety Mechanical overload	200% of rating
Shaft diameter	20 mm.
Length	125 mm
Accuracy	0.25%

6.2.5 The anemometer and its interface software

An anemometer was used to measure the wind speed. In this research, the Kestrel Tracker 4000 was used to measure the weather conditions at the fields test. The chart mode from this device allows users to recall and graph up to 250 measurements along with the date and time of storage. Fig. 6.11 shows the anemometer used in this study. The physical specifications for this device are shown in Table 6.2.



Fig. 6.11 The Kestrel 4000 digital anemometer

Table 6.2 Physical speciation of the Kestrel 4000

Battery	Two AAA alkaline batteries. Typical life, 400 hours.
Impeller	25 mm [1 in.] diameter, sapphire bearings, lightweight. User-replaceable impeller/housing assembly.
Temperature Sensor	Hermetically sealed precision thermistor.
Humidity Sensor	Solid state silicon capacitive sensor.
Pressure Sensor	Monolithic silicon piezoresistive sensor.
Dimensions	12.7 x 4.5 x 2.8 cm. [5 x 1.8 x 1.1 in.]
Weight	102 g. [3.6 oz.]

This portable anemometer uploads the data of the weather at turbine field tests to a PC using the Kestrel interface software, version 1.6.

6.2.6 Field Test set up and observation results

This section deals with the information of the test set up at three locations of project site as mentioned in section 6.2. The section also describes certain problems, which are observed in the test set up after trial run. These data were analysed in detail and the test set up was fine-tuned based on early experiences.

6.2.6.1 The first test at St. Mary's Island, Whitley Bay

Introduction

This site is located near the coast of the Northeast of England (Fig. 6.12). As can be seen the site terrain is nearly flat but the field surrounding the turbine was covered with short grass, which was not expected to provide considerable shear and turbulent effects on the wind near the ground. However, the wind machine prototype was levelled at a height not to be affected by this. The machine was on the field for 2 days to study and investigate the first trial of this prototype. In the first test, the machine was not connected to the instruments. It was only attached to the generator and the output load of 700 watts was used to measure the performance of the turbine. The results and the encountered difficulties of this first trial can be seen in the observation results section. Fig 6.13 displays the wind machine installed at St Mary's Island.



Fig. 6.12 The site before wind machine instillation at St Mary's Island

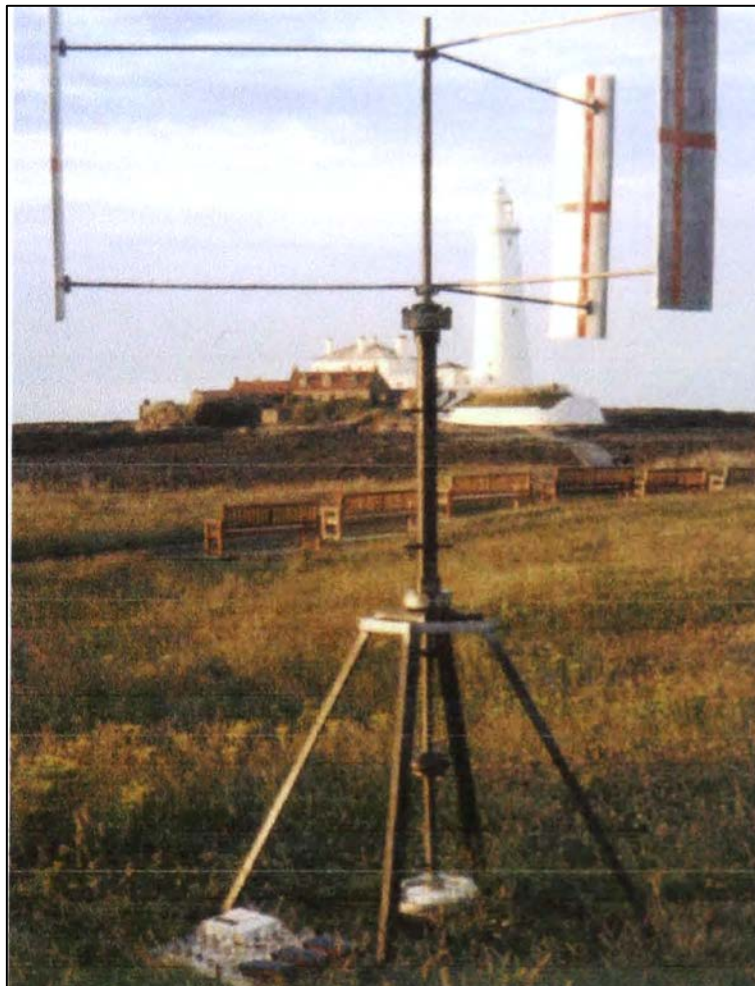


Fig. 6.13 The wind machine at St Mary's Island, Whitley Bay

Results and Observations

The results and observations obtained from the first field test of wind turbine prototype are presented in this section. Using the portable anemometer and visual observations it was found that this Wind machine initially rotated at the wind speed of 5-6 m/sec. The wind turbine was rotated about only 10 rpm constantly even at different wind speeds for a long period of testing. Fine adjustments of the starting pitch angle (α) close to zero degree were made to improve the starting behaviour. And also the rotor blades were covered with a special tape to reduce the skin friction.

Unfortunately, after fine adjustments were improved, the wind speed dropped to about 1-2 m/sec, which was not enough for the test. The prediction (Chapter 3) showed that a wind machine requires the wind speed of about 4-5 m/sec to start the rotor. Additionally this study also investigated the effects of pitch angle using optimised technique on the Cartesian coordination in CFD.

Table 6.3 shows the results of using this technique to investigate the pitch angle effects to the starting behaviours of this wind machine with S1223 aerofoil-blade. CFD results indicated that the rotor would generate the best aerofoil characteristics at zero degree pitch angle (highest number of L/D). Fig. 6.14 (a-d) displays the CFD post-processor results of the velocity contours plot around S 1223 aerofoil rotor.

Table 6.3 The investigation results of pitch angle on S1223 using CFD

Pitch Angle (Degree)	Drag Force (Fx) N	Lift Force (Fy) N	L/D
0	0.59	13.54	22.94
-5	0.665	8.68	13.05
+5	0.97	20.2	20.82
+10	1.53	23.1	15.09

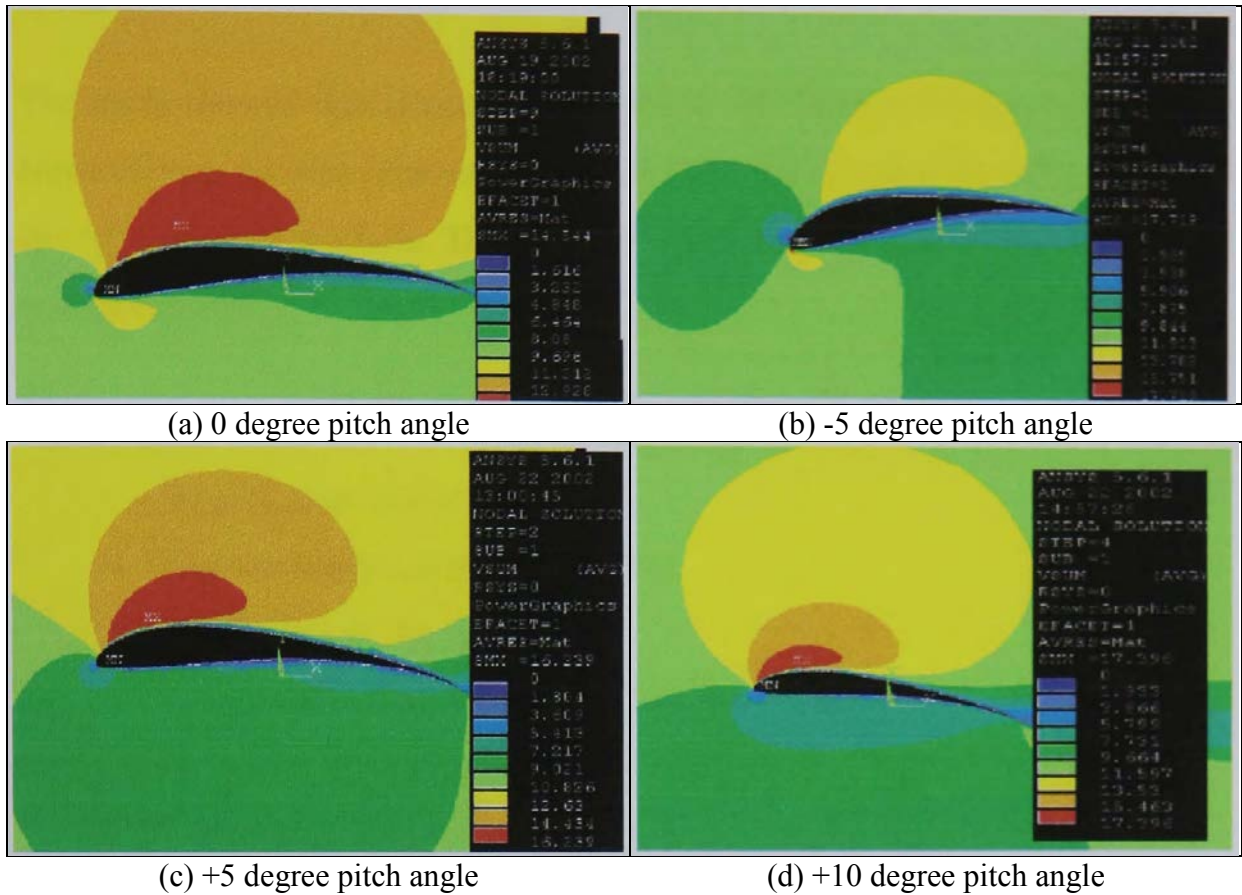


Fig. 6.14 (a-c) Velocity contours plot of S1223 aerofoil rotor blade at various pitch angles

From the observations on this first field-test it was found that the friction drag force from the linkage arms might be another factor to reduce the performance of this wind turbine and makes the prototype unable to accelerate to the operating speed. The friction drag may cause the rotor to slow down. The friction drag force can be found by using the equation $D = C_d \frac{1}{2} \rho V^2 d \Delta L$. Assuming that the investigation length ΔL is 0.1 m, d is linkage rod diameter = 0.02 m, C_d for the rod was assumed to be 1, air density $\rho = 1.225 \text{ kg/m}^3$.

Therefore, at typical wind speed V of 6 m/sec, a linkage arm will generate drag force of 0.06 N. Thus, the torque generated by the linkage arm can be found using equation of $T = D \times R$. Assuming the radius of the arm = 0.1 m, the torque developed on one linkage arm was 0.06 N.m and 0.36 N.m for 6 linkage arms.

The study showed that friction torque generated by the linkage arms was not very high. Nevertheless, the size (diameters) of the linkage arm was found to be a drawback part of this

type of wind machine. The size of this part could also be a concern. Test in this site was abandoned.

The suggestions and the solutions for the next turbine field test

These results suggested that considerations need to be given to the following parameters

- Skin friction of a rotor blade
- The starting pitch angle of rotor blade
- The effect of the linkage arms
- The attachment of the starting aids devices

Using these factors, the prototype was improved for the next test

- The rotor blades were painted carefully to reduce the friction drag
- The rotor blades can be adjusted to zero pitch angle using the flexible joints between the rotor blades and the linkage arms
- Semi Cylinder Starting set-up was installed
- The instrumentations (Torque transducer, the monitoring and display, the data storage) were installed to this prototype for the measurements

6.2.6.2 Wind turbine site testing at Amble Caravan Park, Northumberland

Introduction

This section provides information on the second field test of the wind machine. The modified machine was tested for the second time at Amble caravan park, Northumberland, UK. In this test the wind machine was fully instrumented. The main shaft of the wind turbine was coupled to the Torque Transducer. The portable anemometer was located firmly far from the rotor blade to avoid effect of the wind turbulence when the turbine rotates. The anemometer was fixed at a diameter twice the diameter of the rotor blades (BS 61400-12 part 12). Fig. 6.15 shows the recommended distance of meteorological mast from reference [72].

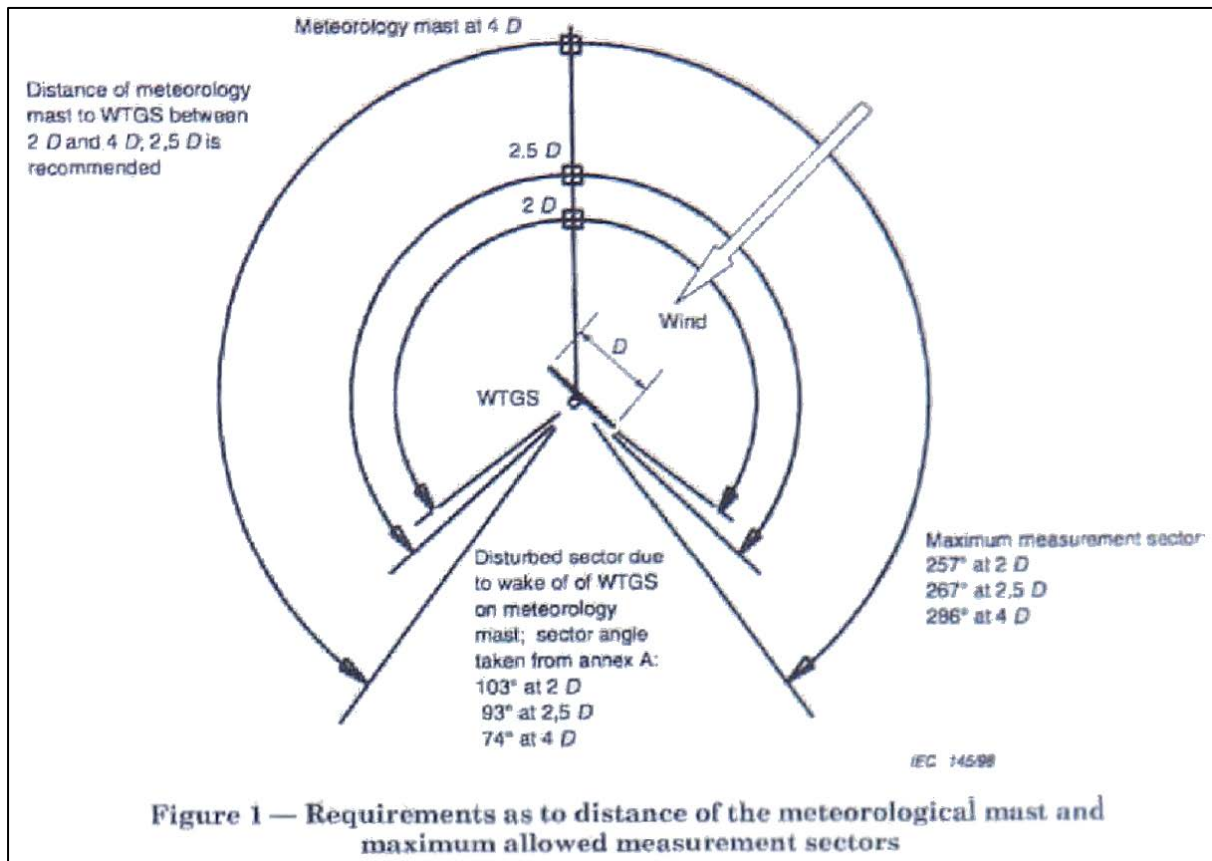


Fig. 6.15 The anemometer distance recommended from [72]

The improvements of the wind machine prototype had significant effects on the second test. The differences between the first and second trial are described below and can be seen in Fig 6.16.

The turbine blades were painted in such a way to make the rotor skin smoother and reduce the rotor skin friction. The linkage arms were modified to enable the operator to adjust the rotor blade to zero degree starting pitch angle. The combined rotor with Semi-Cylinders Turbine (SCT) was constructed to the prototype to investigate operation of the wind machine at low wind speed (Fig. 6.17). The SCT were attached to the linkage arms at different radius positions with same prototype.



Fig. 6.16 Full set-up wind machine at Amble Caravan Park

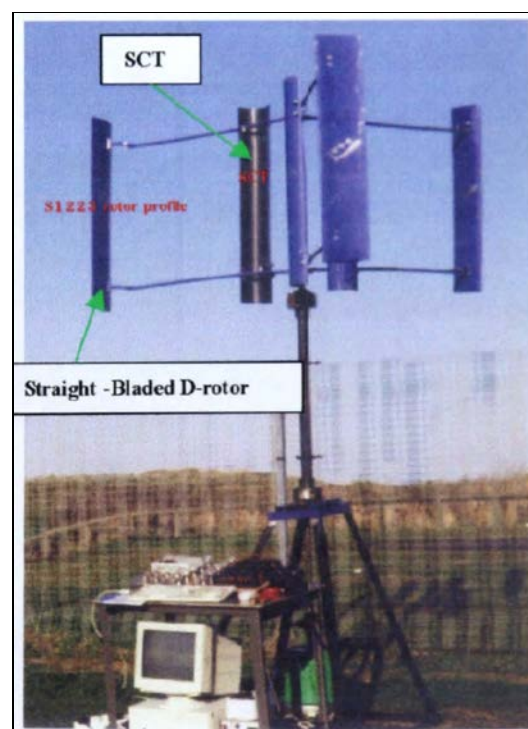


Fig. 6.17 The Semi Cylinder Turbine (SCT) as the starting aids device

Results and Observation

This section presents the results obtained from the second wind turbine field test at Amble Caravan Park. After completing the installation process, the test could not be started as it was raining. The instrumentation devices including PC were kept inside the car. The RPM pick off device used to measure the speed of the wind machine prototype was working well. The anemometer worked well to record the wind speed and the weather conditions. Due to the torque transducer failure, it was not possible to measure the generated torque from the wind machine, therefore only the rpm and the wind speeds were studied and observed. The study found that the turbulence flow of the wind may affect the starting behaviour of the machine. Steady wind speed is preferred to make VAWTs self-start. Fig. 6.18 shows the fluctuation of the wind speed in this site (see Appendix M for full details). This three-bladed prototype wind machine started itself at a wind speed about 4m/sec. This model showed the highest revolution of about 50 rpm at wind speed of 7 m/sec which was recorded by the RPM pick up on E300/RWTI-2 torque transducer (Fig. 6.19).

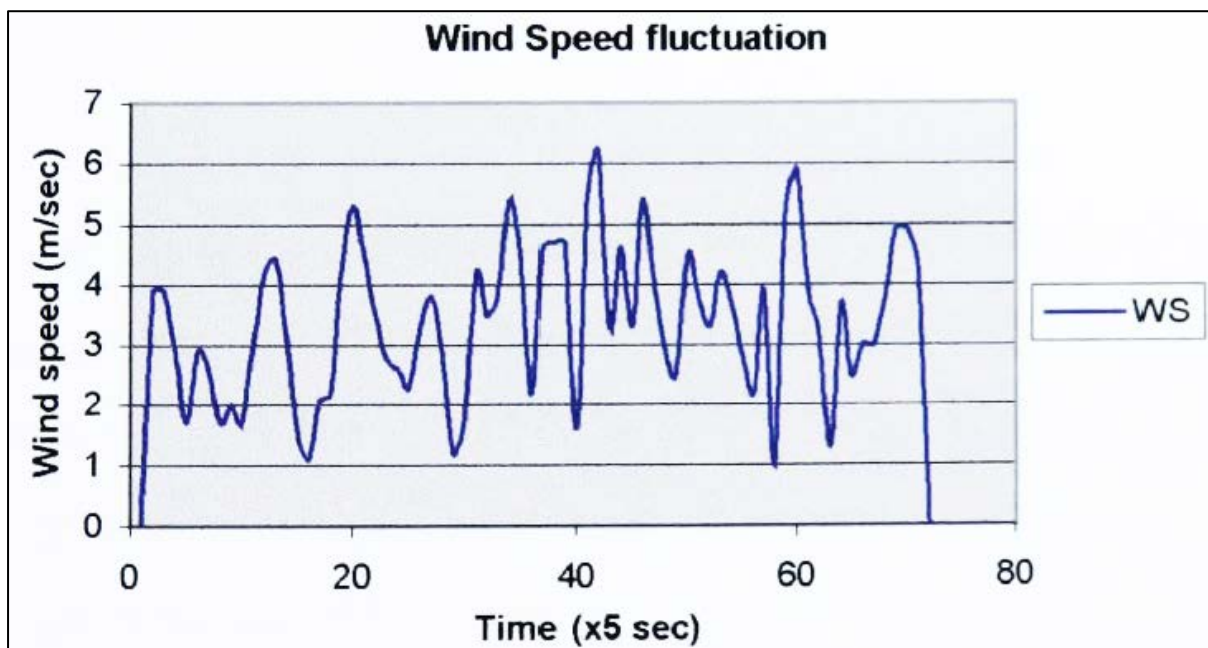


Fig. 6.18 The wind flow fluctuation on Amble Caravan Park

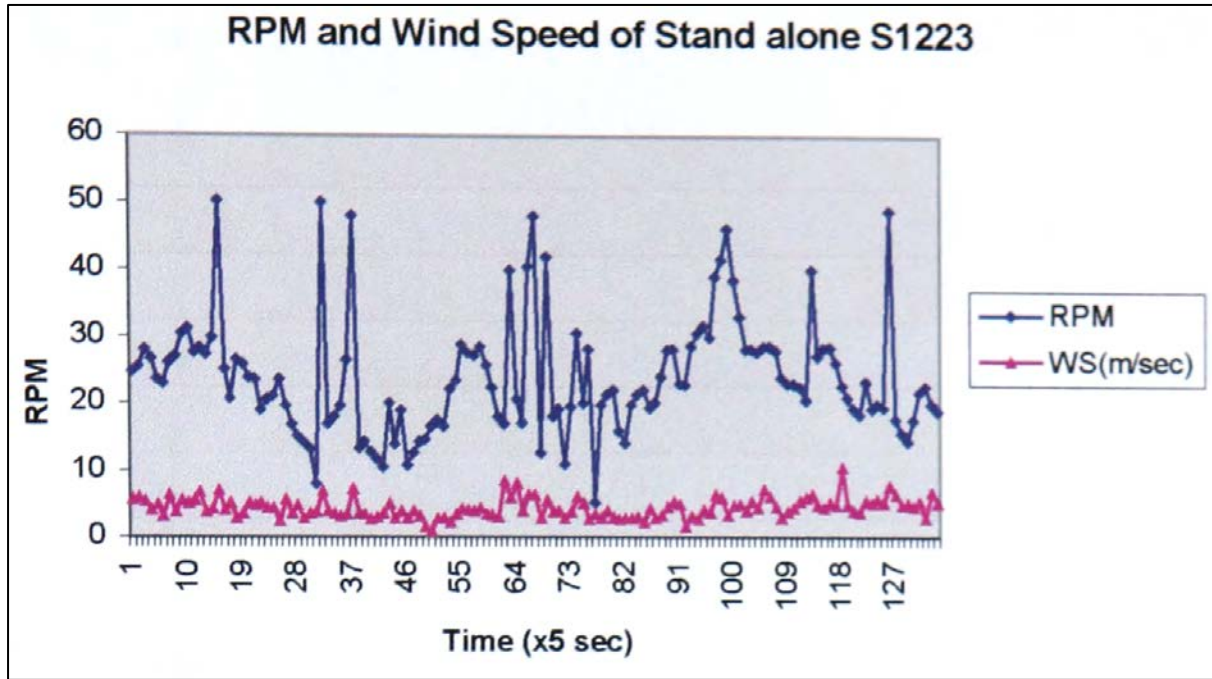


Fig. 6.19 The RPM of stand-alone of three S1223 rotors versus wind speed at Amble Caravan Park site testing

As mentioned in previous section, the combination of Semi Cylinder Turbine (SCT, Fig. 6.17) was also investigated at this site. SCT was made from water piping of thickness of 5 mm and 0.16 m diameter and was attached to the linkage arms using U bolts and nuts. The SCT was located at various radius positions to find the optimum location to use as the starting aid device for low wind speed. The results of RPM versus wind speed were also recorded.

Fig. 6.20 shows the results of the first test of SCT attached at radius of 0.2 m from the centre of the main shaft. At this position and at average wind speed about 5 m/sec the wind machine rotates at about 30 rpm. This was slower than the standalone S1223 rotor blades prototype. At this site, other 4 positions of SCT were tested. They were attached at locations of radius of 0.4, 0.6, and 0.8 m from the shaft centre and the results of the test are shown in Fig, 6.21, 6.22 and 6.23 respectively.

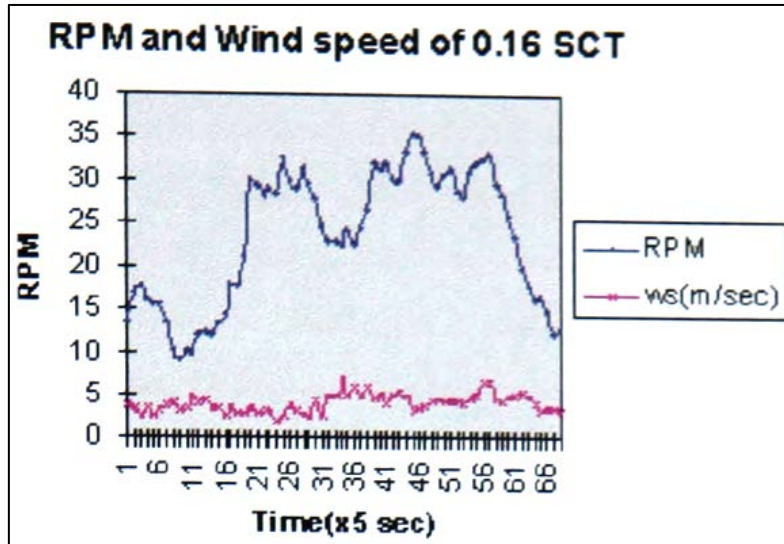


Fig. 6.20 VAWTs combined with 0.16m SCT at 0.2 m

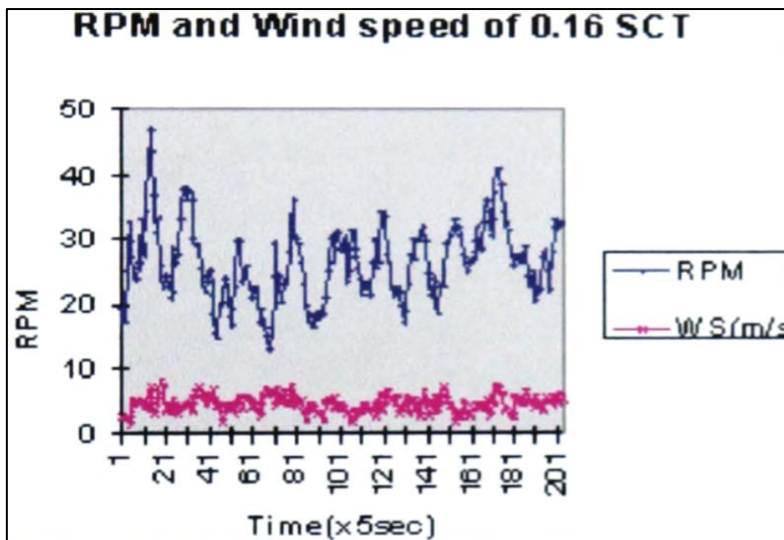


Fig. 6.21 VAWTs combined with 0.16m SCT at 0.4 m

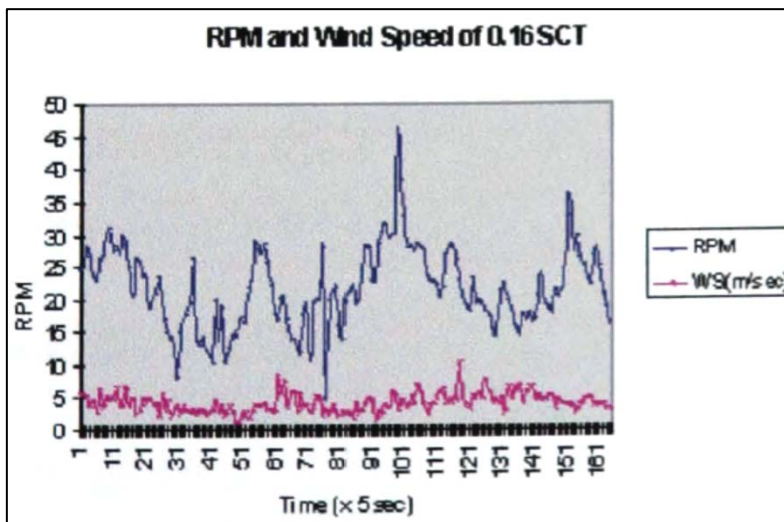


Fig. 6.22 VAWTs combined with 0.16m SCT at 0.6 m

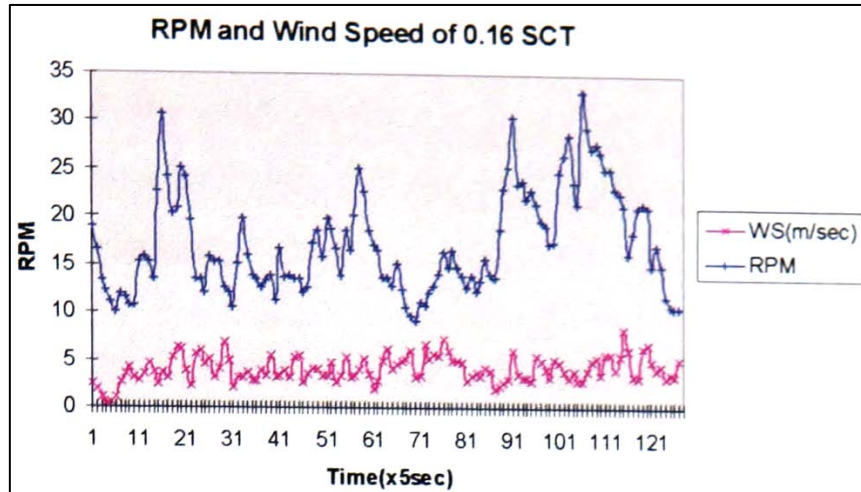


Fig. 6.23 VAWTs combined with 0.16m SCT at 0.8 m

The result of RPM versus speed of the wind in Fig. 6.20-6.23 showed that the SCT at attached location of 0.4 in radius generated the most power and rotated at about 35 rpm at an average wind speed of 5 m/sec. This configuration could be further studied in order to optimise the performances of VAWTs for low wind speed application. The following observations were made from this test

Steady Wind flow is required to make the wind turbine prototype self-starting. The fluctuation and turbulence of the wind in direction and speed reduces the starting ability of stand-alone VAWTs

- The different sizes of rotor diameters of VAWTs require different cut in wind speed for the self-starting
- The experimental results obtained from the wMid tunnel test (Chapter 5) might not be comparable and agree well with the wind turbine field tests.
- In order to maintain the rpm of this prototype at the low wind speed the SCT could be attached to the system
- Skin friction of the rotors and linkage arms affects the performance of this type of the wind turbine prototype

The suggestions and the solutions for the next turbine field test

The second test of the wind machine prototype showed the improvements of the performance for this type of wind machine. The optimised aerofoil profiles or high lift aerofoils (S1223) performed well to overcome the self-starting drawback for this type of wind machine for

stand-alone application VAWTs. However, because of the failure of the torque transducer and lack of strong wind the power coefficients and the performances of this wind machine could not be measured and analysed. Another field test was still required with the following suggestions to improve the testing and turbine's performances.

- The instruments (especially the transducer) have to be covered to protect from wet conditions. The torque transducer normal bearing to be replaced with the special seal for outdoor use
- The speed of generator was not sufficient to generate the electricity. The gearbox was installed to the wind turbine prototype in order to increase the performance of the generator.
- The SCT attached to the wind machine prototype at 0.4 m radius was recommended for further studies.

6.2.6.3 The final test at NaRec, Blyth, Northumberland

Introduction

This is the final test of wind turbine prototype field test. This site provided a better place for the wind machine field test. The wind machine prototype and the anemometer were installed on the top of the container to get the better wind resource and avoid the turbulence of the wind speed near to the ground level. The control Units, the instruments display unit and PC data storage were located inside the container. The most difficult of the installation process of this site testing was to fix the rotor to the Wind turbine tower and structure, as the height of the wind turbine structure was more than those in two previous tests. Fig. 6.24 shows this wind machine that was installed. In this test, the rotor blades of this wind machine prototype were painted and were coated with the lacquer to reduce the rotor skin friction. The normal bearing in torque transducer device was replaced to the outdoor used bearing seal. The main shaft of this wind machine was connected to the stepping up gear system with ratio of 1-3. Fig. 6.25 illustrates the control unit and PC data storage with the torque view interface software, which was located inside the container. The schematic diagram of the turbine field test is displayed in Fig. 6.26. The completed set-up for this wind machine prototype with 1:3 stepping up gear for the turbine field test is shown in Fig. 6.27.



Fig. 6.24 Folk lift used for assembling the rotor to the structure



Fig. 6.25 The control and instrumentations unit

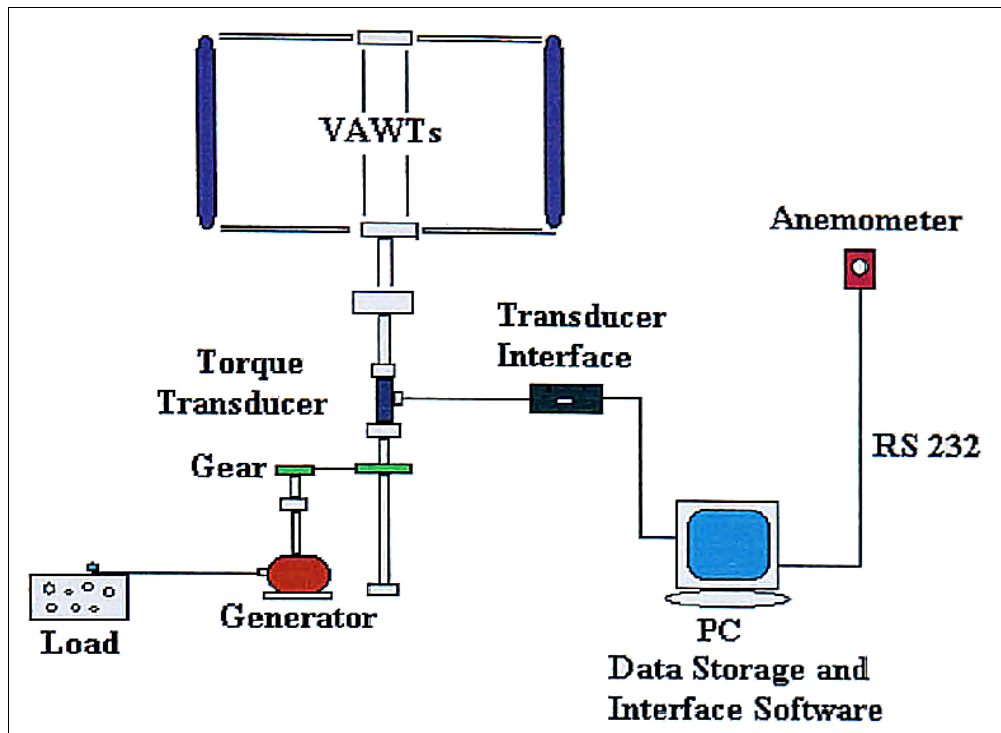


Fig. 6.26 Schematic diagram of the wind turbine field test

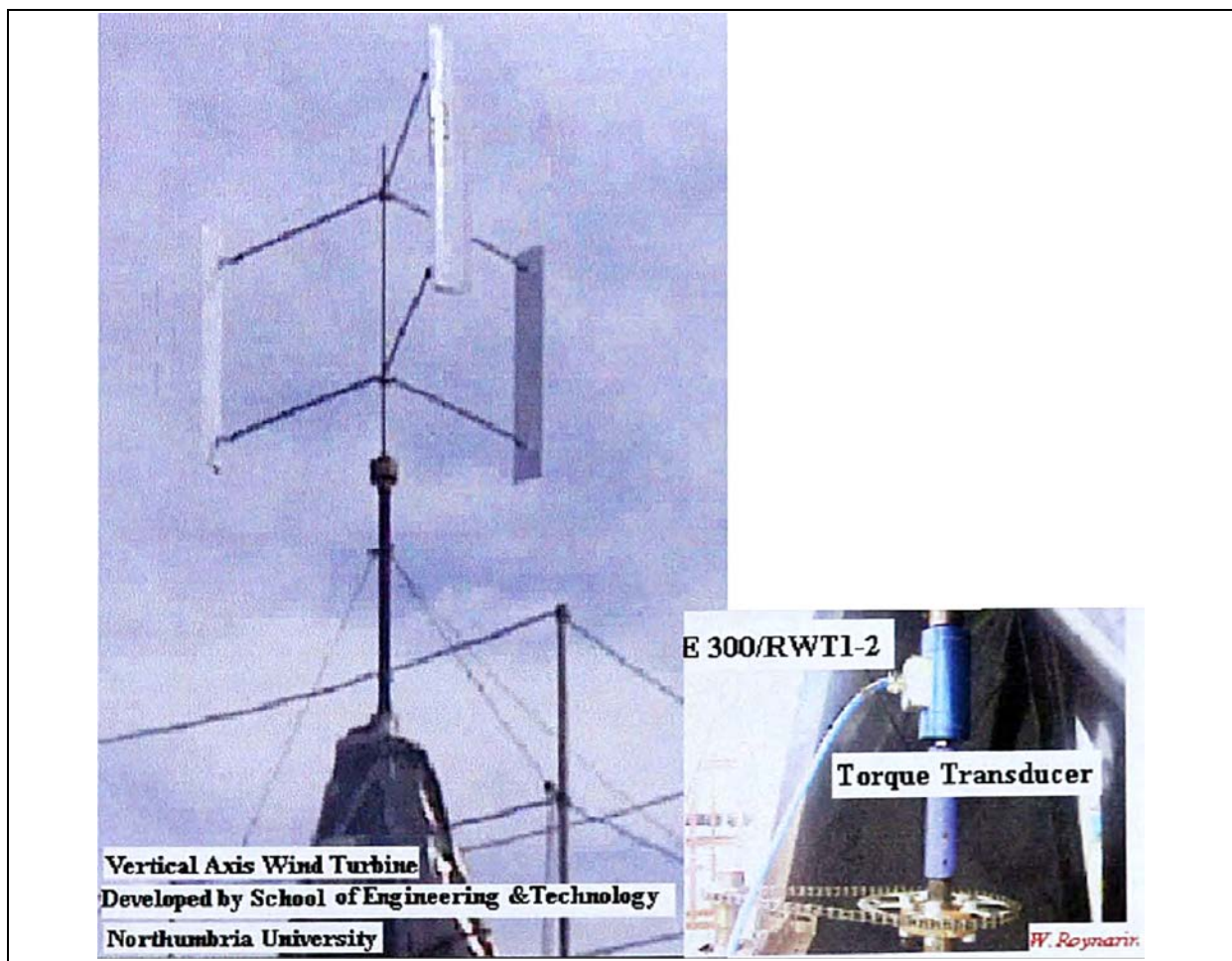


Fig. 6.27 The completed set up with 1:3 stepping up gear unit of D-Rotor VAWTs at NaRec, Blyth, Northumberland

After finishing the installation, the wind machine was tested at various wind speeds. The results were analysed and presented in graph form of power coefficient C_p versus the tip speed ratio X .

Results and Observation

After about 4 days of the installation time, the wind machine was ready for investigation. The results of three-bladed stand-alone of S1223 aerofoil can be seen in Appendix N. And the results of the SCT attached on 0.4 m radius as the starting aids device are shown in Appendix O. This site testing provided promising data for the analysis of the performance characterises. The wind machine worked in case of three bladed S1223 VAWTs, the wind machine prototype was self-starting at wind speed of 4 m/sec. At this wind speed the output load of this wind machine prototype developed to 4.5 N.m, provided the power coefficient of 0.15 at tip speed ratio about 0.8 (see Appendix N for more details). This is the typical result, which was recorded from this site testing. The power coefficient versus tip speed ratio for this wind machine prototype can be seen in graph form In Fig. 6.28.

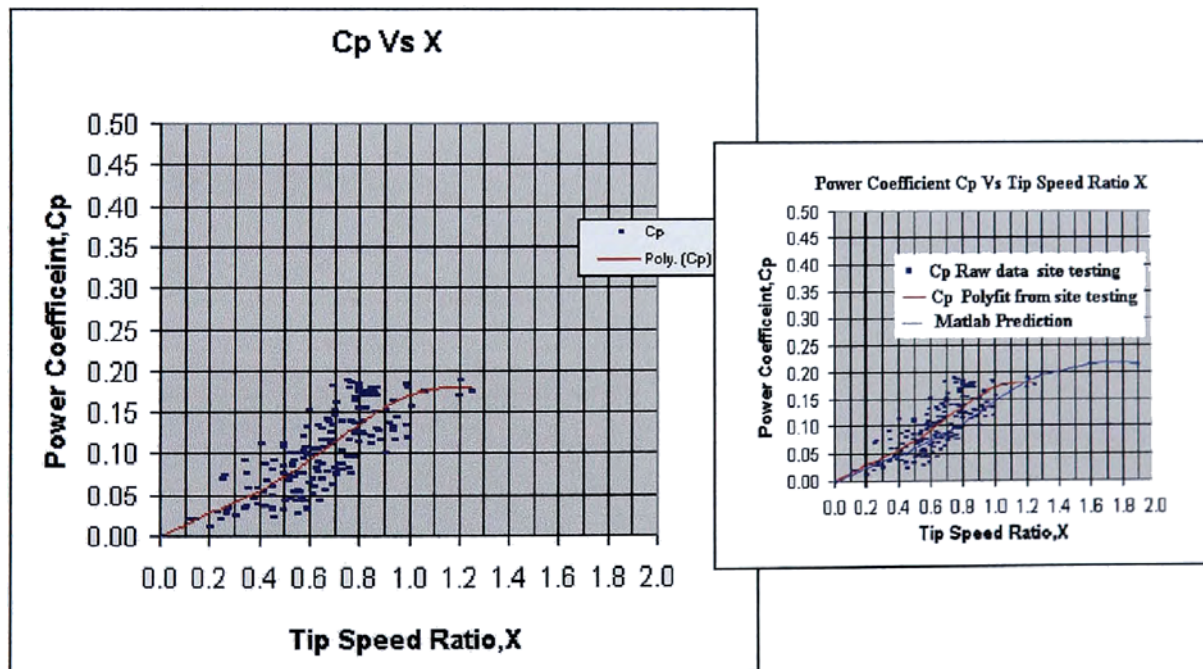


Fig. 6.28 Power coefficient versus tip speed ratio of Straight-Bladed VAWTs from site test and compared with Matlab prediction (inset)

According to the results, the maximum power coefficient C_p was 0.17 at the tip speed ratio X of about 1.2 and the wind speed V of about 7 m/sec. At this point the turbine generated torque of 9.5 N. m (see appendix N). This wind machine was found to be self-starting at the optimum rotor configurations. In case of the wind machine prototype with the aid of SCT, the power coefficient drops dramatically at the tip speed ratio higher than 1 (Fig. 6.29). This model developed the maximum power coefficient C_p of about 0.1 at tip speed ratio of 1.1 (see Figure 6.30).



Fig. 6.29 The SCT attached to D-rotor at 0.4 m radius of VAWTs

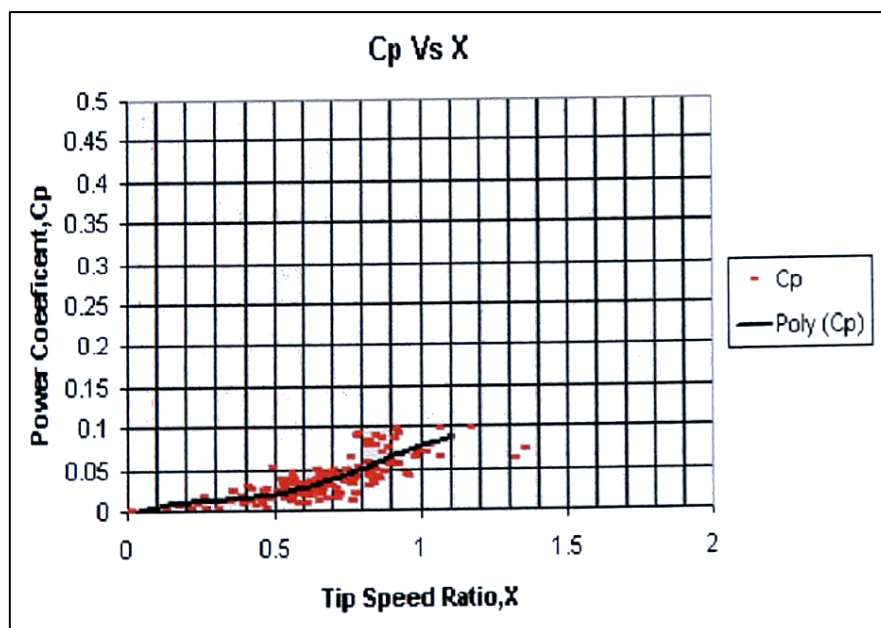


Fig. 6.30 Power Coefficient versus Tip Speed ratio of SCT with D-Rotor

6.3 The novel wind machine for shrimp farm aeration process

This section focuses on the study of Vertical Axis Wind Turbines (VAWTs) for new applications in a farm area; the vertical axis wind turbine for a shrimp farm aeration process. The combined VAWT was designed, manufactured, constructed and tested for performance at a selected shrimp farm within Southern Thailand. The objectives of this project were:

- To invent a new application for the VAWT Wind machine
- To study the beneficial effects of using renewable energy for the agriculture industry
- To reduce the noise and CO₂ pollution in shrimp farms diesel engines
- To study the characteristics of combined wind machine VAWTs

6.3.1 General information about the shrimp farm

The global shrimp fanning industry saw rapid growth in 1980s mainly due to the high consumer demand for shrimp, resulting In a high price and a high profit to the shrimp farmer [73]. Shrimp fanning arrived in Thailand during the 1980s and developed virtually unregulated until 1987. It became an important export industry for Thailand which has been the world's largest producer of tiger shrimp since 1991 [74,75]. However, shrimp farms have generated many environmental problems such as decrease in the amount of mangrove forest, air pollution from the black-smoke of diesel engines and water pollution etc. The problems of water pollution and deteriorated environment have become so serious that some shrimp farms can no longer be used. However, as the demand for shrimp is still high and as this is an important source of income these problems with shrimp farming have to be addressed.

As mentioned in Chapter 2 the use of wind turbines has been growing around the world for many years. Nevertheless, mostly it converts the kinetic energy from the wind to electrical energy. The development and application of the wind power to new applications has to be continued and studied. In some areas, the resource of wind is not suitable for bigger wind turbines and not cost effective to generate electricity. But in these locations the wind energy could be applied for other uses. The present study investigated and designed the wind machine to connect to the mechanical device for the aeration process at the selected shrimp farm. The study indicates that VAWTs has some advantages for shrimp farm applications over HAWTs. VAWTs can generate high starting torque, which is an important

characteristic for the aeration process (see Chapter 2 for more information). The project was established in southern Thailand at Surathani province. Fig. 6.31 shows an example area that is used for shrimp farm industry.



Fig. 6.31 The typical tiger shrimp farm in southern Thailand

The average wind speed within the selected farm was about 2-6 m/sec [76], suitable for a small wind machine.

The conservation of wind energy into mechanical power seems to have several advantages. This study also indicates that the direct use of mechanical shaft power from wind machines may be simpler and more economical. In this study, a VAWT has been applied as a power source for shrimp farm aeration process and replaces two-stroke diesel engines or electric motors, resulting in low cost production, which is environmentally friendly. Vertical axis wind turbines are well suited to drive aerators for a shrimp farm where there are sufficient wind resources. Normally, shrimp farm is located close to the coast for the purpose of seawater irrigation. The source of power is a 2 Horse Power (HP) diesel engine for 1 unit of 6-aerator propeller. Shrimp farm crop cycle is of 4 months duration. The cost of the diesel engine is about 500 pounds and diesel fuels costs over 4 months for 1 unit in aeration process is about 200 pounds. Additionally, the maintenance cost for a diesel engine is approximately 50 pounds during a crop cycle. This leads to an overall cost of £750 per crop cycle. This

study also indicated that about 10 percent of variable cost used during the farm aeration process is due to the diesel fuel costs (see Table 6.4 and pie chart, Fig 6.32). The pie chart in Fig. 6.32 shows the present cost structure of a selected farm per crop cycle.

Table 6.4 The variable cost in selected shrimp farm (Unit baht/rai)

Cost Item	Cash Cost	% of total
Seed	10,000	17
Feed	35,000	61
Teased cake and lime	1,500	3
Drugs and other chemicals	3,000	5
Diesel fuel and lubricant	5,000	10
Labour	1,500	3
Others	300	1
Total	56,300	100%

Source: Present study in a shrimp farm business. Note: 65 baht = 1 Pound; 1 rai = 1600 sq.m; 1 ha = 6.25 rai (Date: January 2003).

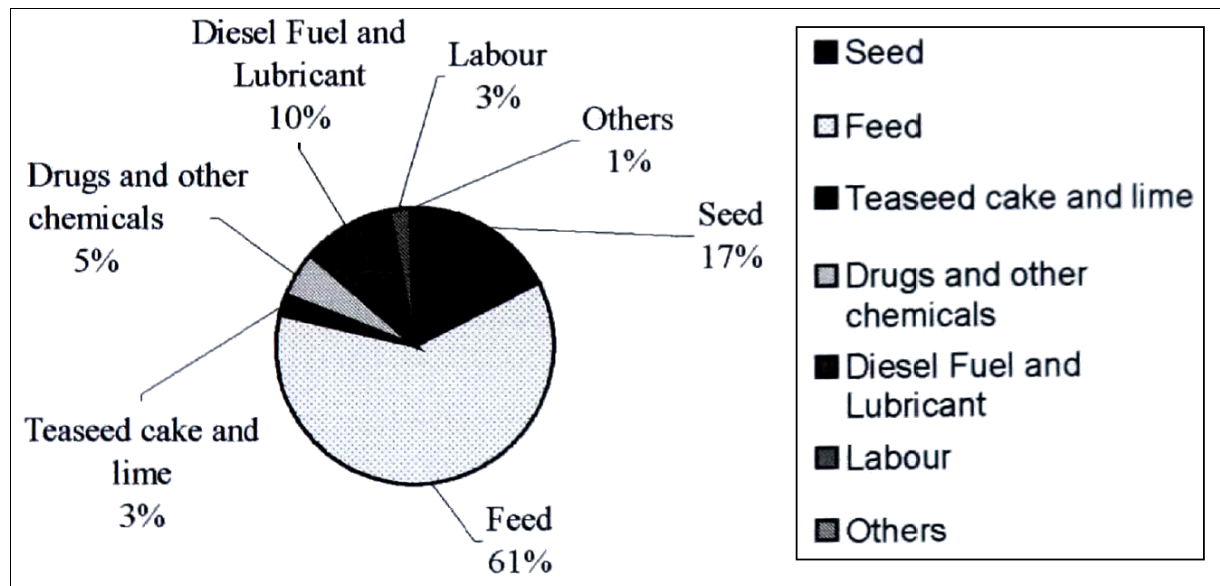


Fig. 6.32 Pie chart displaying the contribution of each value to a total cost in a selected farm

6.3.2 Aeration process

The aeration process is an extremely important one in shrimp farming used to increase the amount of oxygen in the shrimp pond. Aeration is the process of bringing water and air into close contact in order to remove the dissolved gases, such as carbon dioxide, and to oxidize the dissolved metals such as iron. In shrimp farming, the aeration process brings water and air into close contact by exposing drops or a thin sheet of water to the air by introducing small bubbles of air and letting them through the water. Generally, there are two major types in the system of water treatment - in the farm area or elsewhere. The efficiency of the aeration system depends almost entirely on the amount of surface contact between the air and water. This contact is controlled primarily by the size of the water droplet or the air bubble. Most of the shrimp farm aeration process uses the first system. The conventional shrimp farm uses a two-stroke diesel engine connected directly to the aerator shaft operating at about 100 rpm to produce the turbulence of water and air mix together (Fig. 6.33).



Fig. 6.33 Two-stroke diesel engine for conventional water treatment

At some farm areas, which are near the electrical grid, the shrimp farmers prefer to use motors (Fig. 6.34) as a power source to run the aeration system and their facilities. However, the electrical motor used for shrimp farming aeration process causes many problems including increased capital cost. And in some places the electrical wires must be taken to the motors out in the water. Insulation breakdowns and shorts circuits are major problems. The use of wind machines can solve these problems.



Fig. 6.34 Electrical motor used for water treatment in shrimp farm

6.3.3 The test site

The selected shrimp farm had to be sufficient in wind resource to use a wind machine for farm aeration. Southern Thailand has an average wind speed about 2-6 m/sec, which is confirmed in this study. Fig. 6.35 shows the author with the portable anemometer in the process of selecting the spot and location for the turbine field test.



Fig. 6.35 The author with portable anemometer at shrimp farm

The average wind speed for 12 hrs on June 2002 at the selected farm was about 5 m/sec while the maximum wind speed was about 7 m/sec. This wind resource is suitable for using a smaller wind machine. The big wind machines are not recommended. Figure 6.36 shows the wind energy resource atlas of Thailand and Fig. 6.37 shows the wind resource at southern Thailand where the combined wind machine was installed and its performance tested in a selected shrimp farm.

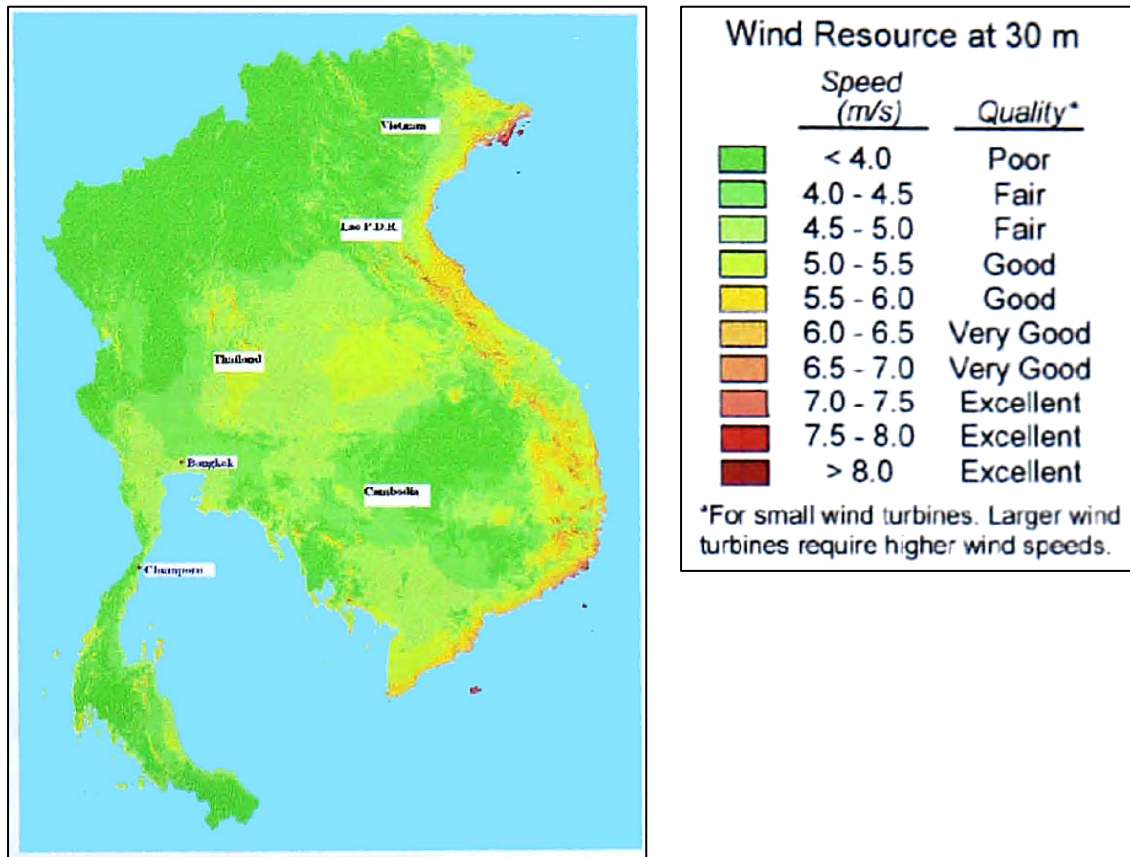


Fig. 6.36 The wind energy resource atlas in Thailand and some neighbour countries [76]

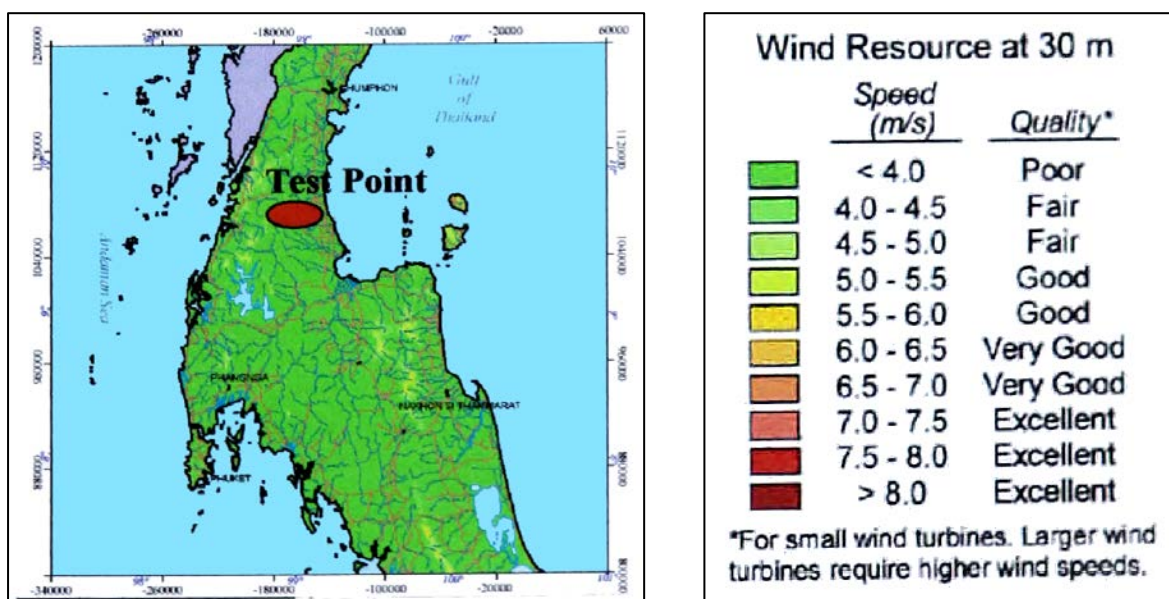


Fig 6.37 Wind resource at test point in southern Thailand [76]

6.3.4 The wind machine design

The wind machine used in this study was a combination of the Darrieus (D) and the Savounius (S) rotor. The main advantage of the Savorilus rotor is high starting torque and the D rotor has higher working performance at high tip speed ratio (>1). The combination of these two rotors shows high potential for this application. In this study, the combination of the S and D rotors has been established for the first time as a source of energy In shrimp farming. The power output for this wind turbine can be found by the power combination of the S and D rotors. The total torque can be defined as follows

$$\text{Total Torque } (T_t) = \text{Torque from S rotor } (T_s) + \text{Torque from D rotor } (T_d)$$

And therefore the total power from this machine can be calculated using the following simple equation.

$$\text{Total power } (P_t) = \text{Power from S rotor } (P_s) + \text{power from D rotor } (P_d)$$

One Unit of the aerator propeller (see Fig. 6.38) requires about 10 N. m to operate the system. The propeller operates at approximately 100 rpm. Therefore, the power requirement for this application is about 100 watts for this speed. The wind velocity used in the design condition was 5 m/sec.

Fig. 6.39 displays the specification of combined wind machine, which is designed for this application.



Fig. 6.38 Aerators used for the test in a shrimp farm aeration system

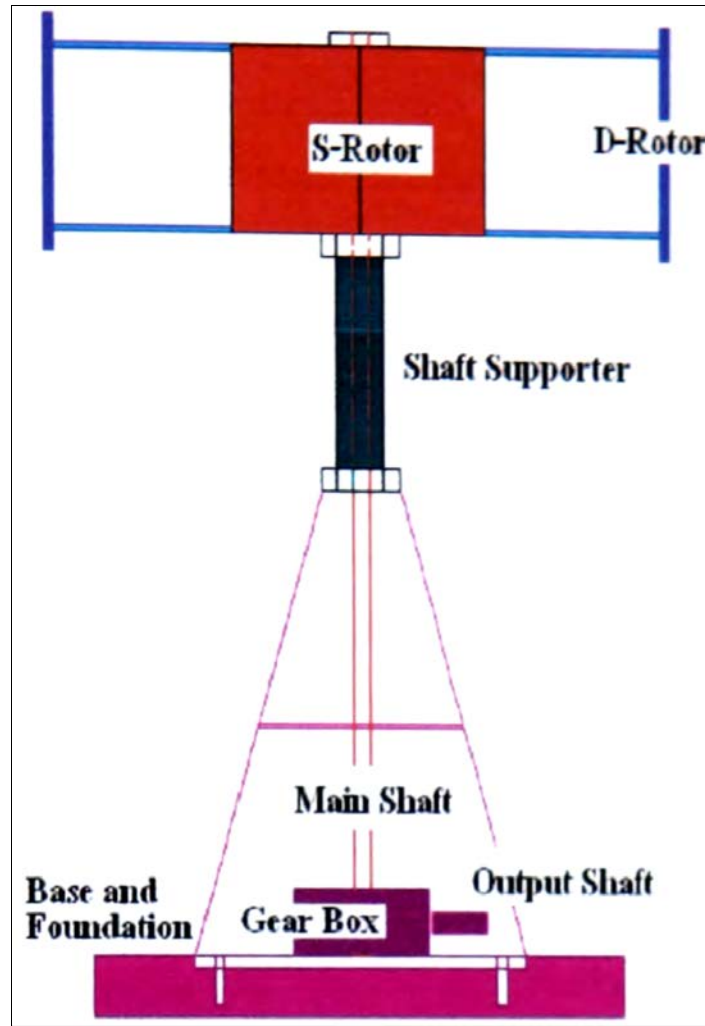


Fig. 6.39 The wind turbine specification for shrimp farm aeration process

The rotor blade of the D-rotor was made from special wood using S 1223 cambered profiles. The design of S-rotor is the optimum configurations [31] to achieve the maximum turbine coefficient. The calculation steps of the power output for this application are explained in the following:

S-rotor power output (P_s) can be found using equation of $P_s = \frac{1}{2} \rho A_s C_p V^3$. Assuming that this wind turbine operates at the power coefficient C_p of 0.3 and the area of the turbine is 0.96 m^2 at the wind speed (V) of 5 m/sec. Therefore the power generated from the S-rotor is equal to 22 watts. For D-rotor, the power output at power coefficient of this machine $C_p = 0.35$ the rotor can generate a power output of 82 watts.

Hence, the total power output from this machine is $P_s + P_d = 104$ watts, which is sufficient to run one set of the aerators in a shrimp farm. Table 6.5 describes the specification of this combined wind machine for farm uses.

Table 6.5 The specifications of designed VAWTs for shrimp farm process

Savonius Rotor with end plate support	Darrieus Rotor with S1223 profiles
Rotor Diameter, $D_s = 1.2$ m	Rotor Diameter, $D_d = 3$ m
Rotor Height, $H_s = 0.8$ m	Rotor Height, $H_d = 1$ m
Overlap Ratio (e/d) = $20/120 = 1/6$	Chord Length., $C = 0.2$ m.
Rotor weight with end plate = 50 kg	Chord ratio= $0.2/1.5 = 0.13$, The weight of a rotor blade =2 kg.

Note: Total weight of wind machine is about 55 kg without gearbox, tower and support.

6.3.5 The wind machine manufacturing

The wind machine was manufactured in Southern Thailand. The rotor blade for Darrieus machine was built from wood. The rotor was created using the coordination of S1223 aerofoil. A shaft support was made from a steel pipe (as in the previous prototype). In this wind machine, mild steel of 3 mm thicknesses was folded to form a shape of 2-semi circle. These semicircle parts were joined using arc-welding technique to form S rotor (Fig. 6.40).



Fig. 6.40 External side welding to the end plate for S-Rotor

The combination of S and D rotors was made using a steel link-age rod and welded together as can be seen in Fig. 6.41. The wind turbine was test-assembled before the test in the farm area.



Fig. 6.41 Final welding and pre-assembling combined VAWTs

The wind turbine was erected for the test. It was connected to a gearbox with a speed ratio of 2:1 in order to increase the revolution speed at low wind velocity. The output shaft from the gearbox was connected to the main shaft of propeller using universal joint for flexible and misaligned condition. The working of this machine has been observed and investigated for further studies and developments.

6.3.6 The results and the observation

The completed wind machine prototype for the test is shown in Fig. 6.42. Table 6.6 shows the results of this study. The results indicate that the wind machine worked satisfactorily. The combination of the S and D rotors worked fairly well at wind speed over 5 m/sec. The advantages of the high starting torque from S rotor have been confirmed. At higher tip speed ratio X , for example at wind speed of 5 m/sec (tip speed ratio of about 1.5) the advantages of the D-rotor become relevant. That is because normally the D-rotor works better than S -rotor at tip speed ratio higher than 1.



Fig. 6.42 Illustrates the completed set of the combined wind turbine at the selected shrimp farm

During the installation process, the shaft alignment can be a problem. The vertical axis wind machine can easily encounter vibrations and noise if the set-up is not balanced. The main shaft of the VAWTs is longer compared to that of the HAWTs, which may cause shaft misalignment. The author has encountered this condition and it caused the turbine not to self-start in the early stages of the wind machine installation. The operating control system also caused minor concerns. This study used the manual control between the main shaft and the gearbox at the operating wind speed (about 5-6 m/s). Consequently, it was not convenient for longer periods of operation.

Table 6.6 Observation of site testing

(V) (m/s)	(RPM)	The observation of the rotor and propeller
2	20	Wind turbine was started but not enough torque to turn the aerators.
3	30	Same situation as at wind speed of 2 m/s
4	40	The turbine was rotating with a vibration occurred at the main shaft but still not enough torque for the aerators.
5	60	The aerators were manually started for the aeration process
6	70	The system was working fairly well

The study found that the designed wind turbine was capable of replacing a small two-stroke diesel engine, which produces 2400 kg carbon dioxide per crop cycle. The study suggests that the combined S+D rotor VAWTs could be well applied to the shrimp farm aeration process.

6.4 Discussion of the Results

The straight-bladed Darrieus wind machine is a major focus in this study. Three site tests confirmed that the S1223 aerofoil profile could improve the performance of the machines. This wind machine was found to be self-starting at the wind speed about 4 m/sec. The results showed that this machine can achieve the highest power coefficient of 0.17 at tip speed ratio of 1.2.

The combined vertical axis wind machine, which was installed to the selected shrimp farm in southern Thailand, was found to be satisfactory for this type of application. The combination of the S and D rotors worked well at wind speed over 5 m/sec. At low wind speed, the advantages of the high starting torque from S-rotor (drag force based) generated the useful torque for the aeration process. And at higher wind speed and also at higher tip speed ratio over 1 the advantage of D-rotor becomes relevant because D-rotor works based on lift force which works well at higher tip speed rotation. The beneficial effect of using this wind machine has been proved in this application. The study suggests that this combined S+D rotor V A WT could be used as energy source to the selected shrimp farm aeration process where there is sufficient wind resource of at least 5-6 m/sec.

Chapter 7

Discussions

Four different approaches have been used to optimise the performance of the vertical axis wind machine. This Chapter discusses these four major parts of the investigation presented in Chapter 3-6.

7.1 The analytical method of the aerofoils employed to Darrieus wind machine

Forty aerofoils were investigated by using analytical models giving different performances for the Darrieus vertical axis wind machine. The vertical axis wind machine was not self-starting unless a suitable aerofoil profile was used as the rotor blades. The symmetrical aerofoil sections such as NACA 661-212 generated higher power coefficients at higher tip speed ratios (for example, $C_p \sim 0.45$ for a tip speed ratio of 6).

However, this aerofoil was not able to generate a high starting torque and caused the vertical axis wind machine to be in a stall condition at the starting state. A vertical axis wind turbine (VAWT) with symmetrical aerofoil blades essentially requires combination with a starting-aid device - for example, a high starting torque Savonius rotor or an electrical motor to speed up the turbine rotor to the required operating condition. Studies using analytical models found that when the high lift aerofoil section S1223 was used, the self-starting ability of the vertical axis wind machine could be improved. This aerofoil section developed a high power coefficient of ~ 0.2 at a tip speed ratio of ~ 2.5 . The analytical models showed that there were other important factors, which needed correction in order to optimise the performance of the vertical axis wind machine; these included the influences of Reynolds number (Re), the starting blade pitch angle (θ), chord length ratio (c/r) and the number of blades (b).

The results of the analytical model showed that a wind turbine using low chord length ratio gives a better performance in terms of efficiency. Higher solidity increases the material cost, the blade mass and results in a peak power curve that causes extreme sensitivity to short-term changes in the wind speed. The research found that the chord ratio of 0.12 generated a higher performance ($C_p = 0.47$ at a tip speed ratio = 6) compared to other values ($C_p = 0.25$ at a

chord ratio = 0.48 and a tip speed ratio = 6). The vertical wind machine generated a better power coefficient (~ 0.42) at a starting blade pitch angle of zero degrees using three blades. A higher number of blades increased the material cost, but did not achieve higher performance.

7.2 CFD analysis

Computational techniques have been used to compute the performance of the straight-bladed vertical axis wind machine. The Cartesian and the Polar co-ordination system are presented in this thesis. The results showed that the ANSYS Flotran 6.1 package required some modifications to give more accurate results, especially with polar co-ordination, which was used to compute the performance of the vertical axis wind machine. The data obtained from the analytical model were significantly different from those obtained during wind turbine operation, with an over-prediction of performance of $\sim 500\%$.

However, the Cartesian co-ordination system that was used to investigate lift and drag forces on the aerofoils, gave more accurate results after improvement of the quality of the mesh by using the mesh creator interface software ICEM CFD (see Figure 4.41). This was accompanied by an increase in computational time, which can be offset by the use of a faster PC (a 700 MHz Pentium III based PC compatible microcomputer with 384 MBytes of RAM was used for modelling during this study).

7.3 The wind tunnel test for small models

This section describes experimental model testing in a wind tunnel. This study showed the benefits of using the wind tunnel to test the small but practical models of the wind machine. The results were compared with those obtained from the analytical models and used for further application developments (any application).

NACA 611-212, Clark-Y and S1223 aerofoil sections performed differently from predicted performance characteristics. Clark-Y and NACA 661-212 aerofoil rotors generated similar results for all configurations. These aerofoil sections lowered starting torque T (0.38 Nm for Clark-Y and NACA 661-212) and lower power coefficients (0.07 for Clark-Y and 0.18 for NACA 661-212) compared with the S1223 aerofoil rotor ($T=0.95$ Nm and $C_p = 0.20$). The three-bladed wind turbine models generated higher starting torque with low value chord length ratio ($C_p = 0.35$ at chord length ratio 0.15).

Additionally, no advantage was gained from using different aerofoil profiles combined in the same shaft for the vertical axis wind machine. The experiment results from the wind tunnel test showed that the starting torque and the whole performance of this wind machine configuration were lower than the S1223-only three bladed profiles. Also, the combination of aerofoil sections is difficult to manufacture and will increase the cost. The combined wind machine model generated a degree of vibration and noise after an extended period of testing.

The results of the wind tunnel testing showed that the optimum solution of VAWTs was to use the camber blade section profile such as the S1223 configuration with three blades.

7.4 The field test of '3-bladed' prototype in the UK

The three straight-bladed S1223 profile rotors were tested at three different locations in North East England. This showed that this vertical axis wind machine was able to self-start the rotor with the optimum configuration, but with some adjustments. The first test near St. Mary's Island did not generate much data from the field test and the wind machine was not able to self-start the rotor after a two day trial. After improvements were made to the instrumentation system, a second test was carried out at Amble Caravan Park in Northumberland. The torque and rotational speed (in r.p.m.) were measured using a torque transducer and the wind speed was measured using a portable anemometer.

The results of the second field trial can be summarised as follows:

- The S1223 profile VAWTs prototype was sensitive to the wind direction. The wind machine at Amble Caravan Park site was located at ground level and surrounded by stationary objects.
- This made the wind machine hard to start by itself because of the turbulence of the wind passing through the rotor (due to the stationary objects). A steady and consistent wind direction is preferred for this wind machine.
- It is essential to adjust the pitch angle to zero degrees. There is a degradation in the performance of the wind machine at pitch angles other than zero degrees and if the pitch is not corrected, the rotor may not be able to start.
- The optimum size of the wind machine is related to the wind speed. A larger rotor size requires higher wind speed for the wind machine to operate. However, turbine operation at higher wind speeds also becomes more efficient.
- The results from the wind tunnel testing can be used for primary study only. The performance of the wind machine in field-testing was not emulated by that of the wind machine in wind tunnel testing. In field testing conditions, the wind speed and direction cannot be controlled as in the wind tunnel and the performance of the wind machine is significantly influenced by this.
- At low wind speed the Semi Cylinder Turbine (SCT) may be required as a starting device for the straight-bladed Darrieus wind machine.

Additionally, the results from the wind turbine field test showed that the skin friction of the rotor blades decreases the performance of Darrieus rotor vertical axis wind turbines

The final test of the wind turbine prototype for this project was at NaRec, Blyth, also in Northumberland. The results from this testing confirmed that this wind turbine prototype can be self-starting at wind speeds of about 4 m.s^{-1} . The performance of a direct drive vertical axis wind turbine was higher than the wind machine attached with the starting-aid rotor SCT ($C_{p_{\max}} = 0.18$ for a direct drive and $C_{p_{\max}} = 0.1$ for SCT).

This wind turbine prototype rotates at a maximum speed for a tip speed ratio of 1.2, which is faster than the wind speed and generates maximum power coefficient of approximately 20%.

However, the study found that a major disadvantage of straight blade VAWTs is that radial arms (or linkage rods) are required to hold the rotor blades in position. Some designs use one linkage arm per blade but this results in high bending moments. Some designs, similar to the one used in this study, use two arms to prevent this. The observations from the final site testing, showed that these radial arms add to the weight and cost and they generate parasitic drag which reduces the net power output.

From the results of this study it has been found that when starting-aid devices are used, the high starting torque produced by high-chord length blades became unnecessary. The low-chord length ratio wind turbines may be used with the starting aids, giving more shaft power per unit cost. This coupled with the large increase in system efficiency resulting from optimum matching could result in very large improvements in the cost-effectiveness of non-electrical wind power systems. Additionally, the final test results at NaRec, Blyth, showed that the well-designed VAWTs produces sufficient starting torque to overcome friction for a straight-bladed vertical axis wind turbine. But very high starting torque is only important for small systems such as for the direct drive of the VAWTs for shrimp farm aeration processes (see Section 7.5).

7.5 Thailand test of combined wind machine

The results of the wind turbine field-test for combined V A WTs used in shrimp farm aeration processes are discussed in this section. For this particular application, the high starting torque of the designed wind machine was required and the system showed a significantly improved performance. The combined VAWT showed the advantages of their characteristics over the Horizontal Axis Wind Turbines (HAWTs). This particular designed V A WT generated a high starting torque so that direct coupling with the aerators for the water treatment in the shrimp farm business was achieved.

The horizontal axis wind machine in comparison would not be able to generate sufficient starting torque with the same rotor size for this application. The horizontal axis wind machine also needs a higher tower to avoid turbine rotor edge accidents (i.e. collision of blades with the ground or ground-based objects). However, the study found that the shrimp farm must have access to sufficient wind resources. The study also found that this wind turbine operated well at wind speeds of above 5 to 6 m.s⁻¹, the average wind speed in Southern Thailand.

Chapter 8

Conclusions

This study has investigated the methodologies used to optimise the vertical axis wind machine and the conclusions are presented below.

- 8.1 It has been shown by analytical models and confirmed by wind tunnel and prototype turbine field tests, that a small straight-bladed VAWT based on the Darrieus principle can be designed in such a way that it will reliably self-start.
- 8.2 A symmetrical aerofoil could not be set up to be self-starting. However, a non-symmetrical aerofoil would help.
- 8.3 The high lift aerofoil section S 1223 is recommended for straight-bladed Darrieus VAWTs - from a MATLAB assessment of 40 aerofoils, the best performance was observed over wind speeds of between 4 and 10 m.s⁻¹.
- 8.4 The optimum S 1223 aerofoil chord length ratio was found to be 0.2, pitch angle zero degrees.
- 8.5 Performance predictions and field tests indicated that a practical small turbine of 2 m in diameter with three S1223 blades would reliably self-start at a wind speed of 4 m.s⁻¹ (Cp ~0.2 at tip speed ratio X - 1.2)
- 8.6 A higher chord length ratio is recommended to improve the rotor starting torque, however, the chord length ratio is very sensitive to the wind speed and will generate lower performance at higher tip speed ratios (Figure 3.20).
- 8.7 A higher starting torque was achieved by adding a Savonius rotor to the basic Darrieus design, at wind speeds of 4 to 6 m.s⁻¹ in practical application.
- 8.8 In another design of VAWT, 0.16 m diameter semi-cylindrical blades were attached at 0.4 m radius from the main shaft – this machine self-started during testing and is recommended for wind speeds of 3 m.s⁻¹ producing a maximum power coefficient of 0.1 at a tip speed ratio of 1.2.

- 8.9 The alternative practical design shown in Figure 6.17 gave a lower power coefficient, for example, 50% less than the stand-alone three bladed S 1223 wind machine.
- 8.10 The performance of V AWTs is affected by the Reynolds number, the chord length ratio, the number of blades and the turbine rotor skin friction.
- 8.11 The CFD analysis using Cartesian co-ordinates for the prediction of static lift and drag coefficients, was found to be within 30% of published empirical data, provided a suitable interface mesh creator software package was used.
- 8.12 CFD predictions for the performance of vertical wind machines in rotational motion (using polar co-ordinates) were found to be inaccurate in the current work, giving an over-prediction of performance of ~500%.
- 8.13 The wind tunnel test results for all three aerofoil sections agreed within a range of 9 to 22% of the analytical prediction, but best results were produced for the S1223 aerofoil.
- 8.14 The author has developed a practical wind turbine suitable for slow wind speeds expected in Thailand. The two-bladed machine effectively replaced a two-horse power two-stroke diesel engine application in a shrimp farm water treatment plant. The machine was based on a Savonius rotor combined with a straight bladed Darrieus rotor, as shown in Figure 6.39.
- 8.15 The author has shown how V AWTs with their inherent low cost and pollution-free technology can be designed with good self-starting characteristics that make them ideal for a variety of remote area applications where there are sufficient wind resources.

Chapter 9

Suggestions for Further Work

Further research in several areas on VAWTs is necessary before the potential of small VAWTs served as significant prime movers in stand-alone situations can be assessed. Firstly, for a small straight-bladed Darrieus wind turbine the recommendations include:

- Investigate or develop special engineering design of high lift aerofoils for VAWTs.
- Carry out longer period of wind turbine prototype field tests, obtain more data to analyse the full range of power coefficients versus tip speed ratios.
- The CFD requires further improvement to model rotational motion accurately

And secondly for the wind machine for shrimp farm aeration process, the study recommended that the control system could be further investigated in order to improve the whole performance of the aeration process. The study suggested two alternative schemes for further development for the shrimp farm industry. These schemes (see Appendix P) could demonstrate the possibilities to improve the cost effectiveness and environmental aspects to the shrimp farm business.

References

- [1] B. S. Lissaman Robert E. Willson, *Applied Aerodynamics of Wind Power Machine*. Oregon State, 1974.
- [2] Fugsang and Helge Aa. Madsen, "Optimisation of Stall Regulated Rotor," *Wind Energy*, vol. 16, 1995.
- [3] Desire LE GOURIERES, *Wind Power Plants Theory and Design*. Headington Hill Hall: Pergamon Press Ltd, 1982.
- [4] <http://www.windpower.dk>. 9 Sep. 2000.
- [5] <http://www.fortunecity.com/greenfield/bp/16/savonius2.htm>.
- [6] <http://www.windpower.org/tour/design/horver.htm>, 2000.
- [7] <http://aerolab.virtualave.net/index.html>, 1999.
- [8] Brian Kirke, "Cambered blades: A New Way to Overcome V A WT self-starting problems," ADS Pacific Wind Energy Workshop July 2001.
- [9] J. G. McGoWan J. F. Manwell, A. L. Rogers, *Wind Energy Explained*. West Sussex: John Wiley & Sons Ltd, 2002.
- [10] <http://www.hornsrev.dk>. 2002.
- [11] Vestas, "Accident with Vestas V80-2 MW offshore test turbine," Ringkobing 5 November 2002.
- [12] The British Wind Energy Association, "End of an era at Burgar Hill," BWEA 13 November 2000.
- [13] Harrison, R., Hall, E. and Snel, H., *Large Wind Turbines Design and Economics*: John Wiley and Sons, Ltd, 2000.
- [14] David Sharpe, Tony Burton, Nick Jenkins, Ervin Bossanyi, *Wind Energy Handbook*. West Sussex, UK: John Wiley and Sons, Ltd, 2001.
- [15] <http://www.afm.dtu.dk/wind/turbines/gallery.htm>, 2000.
- [16] <http://www.orknet.co.uk/ose/> : Orkney Sustainable Energy Ltd, 1997.
- [17] Thomas G. Came and Ado R. Nord, "Model Testing of a Rotating Wind Turbine," Sandia National Laboratories, Albuquerque June 1983.

- [18] James L. Tangier Dan M. Somrnerns, "Wind - Tunnel Tests of Two airfoils for Wind Turbines operating at High Reynolds Numbers," *ASME Wind Energy Symposium, Nevada, 2000*.
- [19] Suitable Energy Technologies, "Chinook 2000 Reliable Energy, Anywhere," 2000.
- [20] H. Kalli, A. Frantsi, J. Larjola and J. Montonen, "Direct Heat Production Through The Use of a Straight-Blade V A WTs," presented at European Wind Energy Conference, Hamburg, 1984.
- [21] P. T. Smulders, F. J. Folling, "Wind Energy and Cooling," presented at European Wind Energy Conference, Hamburg, 1984.
- [22] D. J. Hilton, "A low cost Darrieus wind machine for farm use," presented at Agricultural Engineering, Bundaberg, 1984.
- [23] A. Guichard, C. Brown, and D. Lyons, "Analysis of the Potential for Wind and Solar energy system in Antarctica," presented at Wind Energy Conference, Exeter University, UK, 1996.
- [24] D. G. Infield, "*Wind power for desalination – a Potential market*," presented at Wind Energy Conference, Exeter University, UK, 1996.
- [25] Frank R.Eldridge, *Wind Machines*: National Science Foundation, October 1975.
- [26] R. A. W. Shock, "Comparison of Variable Geometry VAWTs with HAWTs," ETSU, Harwell Laboratory, Oxfordshire, UK, 16-AUG-1990.
- [27] Forrest S. Stoddard David M. Eggleston, *Wind Turbine Engineering Design*. New York: Van Nostrand Reinhold, 1985.
- [28] O.De Vries, "Fluid dynamic aspects of wind energy conversion," *AGARD-ag-243*, 1979.
- [29] J. H. Strickland, "The Darrieus turbine, a performance prediction method using multi stream tube," Sandia Laboratories, Albuquerque SAND 75-0431, Oct. 1975.
- [30] H. Glauert, *The Element of Airfoil and Airscrew Theory*. New York: MacMillan, 1943.
- [31] O. Holmes, "A contribution to the aerodynamic theory of the vertical-axis wind turbine," presented at Wind Systems, St. John's College, Cambridge, 1976.
- [32] M. T. Brahimi, I. Paraschivoiu, A. Allet, "On the Aerodynamic Modelling of a VAWTs," *Wind Engineering*, vol. 21, pp. 351-365, 1997.

- [33] Jose L. Cardona, "Flow Curvature and Dynamic Stall Simulated with an Aerodynamic Free-Vortex Model for V A WTs," *Wind Engineering*, vol. 8, pp. 135-143, 1984.
- [34] M. N. Nahas, "A Self-Starting Darrieus-Type Windmill," *Energy*, vol. 18, pp. 899-906, 1993.
- [35] B. N. Sreedhard Sumitabh Biswas, Y. P. Singh, "Dynamic Analysis of a VAWTs using a new wind load estimation technique," *Computers and Structures*, vol. 65, pp. 903-916, 1995.
- [36] A. Dadone, B. Fortunato, V. Trifoni, "A Two-Dimensional Methodology to Predict VAWTs Performance," *Solar Energy Engineering*, vol. 117, pp. 187-193, 1995.
- [37] E. William Beans, "Approximate Aerodynamic Analysis for multi-blade Darrieus wind machine," *Wind Engineering and Industrial Aerodynamics*, pp. 131-150, 1987.
- [38] L. Lazauskas, B. K. Kirke, "Enhancing the performance of Vertical Axis Wind Turbine Using a Simple Variable Pitch System," *Wind Energy*, vol. 1, pp. 157-194, 1991.
- [39] N. C. K. Pawsey and A. J. Barratt, "Evaluation of a Variable Pitch Vertical Axis Wind Turbine," *Wind Engineering*, vol. 23, pp. 23-30, 1999.
- [40] S. Rajaoferson and R. Comolet, "Self-Starting Process of the Darrieus Wind Turbine," *European Wind Conference*, pp. 523-527, 1984.
- [41] P. Vittecoq and A. Laneville, "The Aerodynamic forces for a Darrieus rotor with straight blades: Wind Tunnel Measurements," *Wind Engineering and Industrial Aerodynamics*, vol. 15, pp. 381-388, 1983.
- [42] D. A. Bayly and J. A. C. Kentfield, "A Vertical Axis Cyclogiro type Wind-Turbine with Freely-Hinged Blades," presented at Intersociety Energy Engineering Conference, Atlanta, Georgia, 1981.
- [43] Aristide Massado Martino Marini, Antino Satta, Giuseppe Zamparo, "Theoretical Aerodynamic Methods for VAWTs Analysis," *IEEE*, pp. 2021- 2027, 1989.
- [44] Izumi Ushiyama and Hiroshi Nagai, "Optimum Design Configurations and Performance of Savonius Rotors," *Wind Engineering*, vol. 12, pp. 59-75, 1988.
- [45] A. T. Sayers, "Blade configuration optimisation and performance characteristics of a simple Savonius rotor," *IMechE*, vol. 199, pp. 185 -191, 1985.

- [46] Helsingfors Finland S. J. Savonius, "The S-rotor and Its Applications," *Mechanical Engineering*, vol. 53, pp. 333-338, 1931.
- [47] Md. Quamrul Islam, A. C. Mandal, A. K. M. Sadrul Islam, "Aerodynamic Characteristics of a Stationary Savonius rotor," *International Energy*, vol. 15, 1993.
- [48] Nobuyuki Fujisawa, "Velocity measurements and numerical calculations of flow field in and around Savonius rotors," *Wind Engineering and Industrial Aerodynamics*, vol. 59, pp. 39-50, 1996.
- [49] J. Massons, J. N. A. Gavalda, F. Diaz, "Experimental Study on A Self-Adapting Darrieus-Savonius Wind Machine," *Solar & Wind Technology*, vol. 7, pp. 457-461, 1990.
- [50] Nobuhiro Okamoto and Izumi Ushiyama, "Experimental Studies for the Hybrid Wind Turbine," *International Energy*, vol. 3, pp. 465-471, 1993.
- [51] Ira H. Abbott and Albert E. Von, *Theory of Wing Sections*. New York: Dover Publications ,inc, 1949.
- [52] Mark Hampsey and David H. Wood, "Designing Small Wind Turbine Blades for optimum Starting and Power Extraction," *Wind Engineering*, vol. 23, pp. 31-39, 1999.
- [53] James I. Tangler, "Assessments of Blade-element analysis for HAWTs," *Wind Energy Conference and Workshop, Golden, Colorado, U.S.A.*, pp. 437-445, 1983.
- [54] Ir. W. E. de Bore, "Design, Construct and Performance of WPX Wind Turbine Rotor Blades," *European Wind Conference*, pp. 108-114, 1984.
- [55] Giovanni M. Giancarlo Chiatti, Raffaele Ruscitti, "Performance Analysis of New Wind Turbine Blade Profiles," *Wind Engineering*, vol. 21, pp. 295-307, 1997.
- [56] Christopher A. Lyon Micheal S. Selig, Philippe Giguere, *Summary of Low-Speed Airfoils Data*, vol. 2: SoarTech, 1996.
- [57] Andy P. Broeren Christopher A. Lyon, Philippe Giguere, *Summary of Low-Speed Airfoil Data*, vol. 3: SoarTech, 1998.
- [58] G. W. Amos and G. M. Bragg, "Reynolds number dependence of vertical axis low solidity wind turbine," *INTOSOL*, pp. 1999-2002, 1985.
- [59] Yoshio Shimizu Kazuichi Seki, "A study of straight blade VAWT and its application," presented at Wind conference, Hamburg, 1984.

- [60] E. W. Bean, "Approximate aerodynamic analysis for Darrieus rotor wind turbines," presented at British Wind Energy Association, Cambridge, UK, 1986.
- [61] V. H. Morcos and O. M. E. Abdel-Hafez, "Testing of an arrow-Head vertical axis wind turbine model," *Renewable Energy*, vol. 7, pp. 223-231, 1996.
- [62] W. P. Wolfe, P. G. Migliore, "Aerodynamic Tests of Darrieus Wind Turbine Blades," *Energy*, vol. 7, pp. 101-106, 1983.
- [63] J. V. Healy, "The Influence of Blade Thickness on the Output of Vertical Axis Wind Turbines," *Wind Engineering*, vol. 2, pp. 1-9, 1978.
- [64] M. O. L. and Soresen D. N. Hansen, "CFD model for Vertical Axis Wind Turbine," *Wind Engineering*, pp. 485-487, 2001.
- [65] E. G. Laddopoulos, "Non-linear Singular integral computational analysis for unsteady flow problems," *Renewable Energy*, vol. 6, pp. 901-906, 1995.
- [66] H. Sobieczky, "Parametric Airfoils and Wings," Numerical Fluid Mechanics 1998.
- [67] Stuart S. C. and Walter P. Wolfe, "CFD Calculations of S809 Aerodynamic Characteristics," Engineering Sciences Centre, Sandia National Laboratories, Albuquerque 1998.
- [68] William F. Hughes and John A. Brington, *Theory and Problems of Fluid Dynamics*. New York: Mc Graw-Hill, 1999.
- [69] I. Masters J. A. Corne, R. T. Griffiths, "Investigation of the effect of bio fouling on the efficiency of marine current turbines," presented at Marine Renewable Energy, Newcastle, 2001.
- [70] ICEMCFD, *ICEM CFD Engineering Tutorial Manual*: Bereley, CA 94705, 2000.
- [71] P. P. Benham & R. J. Crawford, *Mechanics of Engineering Materials*: Longman Scientific & Technical, 1987.
- [72] British Standard, "Wind Turbine Generator Systems, Wind Turbine power performance testing," *BS EN 61400-12*, 1998.
- [73] Pingsun Leung Yung C. Shang, Bit-Hong Ling, "Comparative economics of shrimp farming in Asia," *Elsevier Science B. V*, pp. 183-200, 1998.

- [74] Carl Folke Miriam Huitric, Nils Kautsky, "Development and government policies of the shrimp farming industry in Thailand in relation to mangrove ecosystems," *Elsevier Ecological Economics*, pp. 441-445, 2002.
- [75] Oopatham Pawaputanon, "Reduction of Water Pollution from Shrimp Aquaculture", Coastal Aquaculture Division, Department of Fisheries, Thailand, Bangkok 1999.
- [76] TrueWind Solution, "Wind Energy Atlas of Southeast Asia," The World Bank Asia Alternative Energy Program, New York September 2000.

Publications

1. Poster presentation, *Enhancing The Performance of Straight Blade Darrieus Rotor Wind Turbines*, 2-5 April 2002, CNIT La Défense, Paris, France, (Appendix A).
2. Paper publication, *The Performance of a Vertical Darrieus Machine with Modern High Lift Aerofoils*, 10-11 October 2002, Marine Conference, Newcastle University, Newcastle upon Tyne, UK (Appendix B).
3. Paper presentation, *Using Wind Turbine Machine to Reduce CO₂ Emission in Shrimp Farm Aeration Process* Postgraduate Conference in Environmental Thought Environmental Practice, 31st January 2003, Manchester, UK (Appendix C).
4. Paper publication, *Wind turbine for shrimp farm aeration process*, European Wind Energy Conference, 16-20 June 2003, Madrid, Spain (Appendix D).
5. Paper publication, *The Investigation of aerofoil characteristics using CFD technique*, IMECHE 'Up and Coming Fluid Machinery' 9 October 2003, One Birdcage Walk, London, UK, (Appendix E).

Appendix A

Enhancing the performance of straight blade Darrieus Rotor Wind Turbines



Enhancing the Performance of Straight Blade Darrieus Rotor Wind Turbines

W. Roynarin, Dr. P. S. Leung and Prof P. K. Datta.

University of Northumbria at Newcastle, NE1 8ST, England

Objectives of the project

- To review the airfoil geometry used in Darrieus wind machine.
- To select the proper geometry of airfoil shape for straight blade Darrieus rotor.
- To study the starting torques behaviour of Darrieus rotor.
- To optimise the performance of Darrieus rotor vertical axis wind turbine.

Introduction

Among the Vertical Axis Wind Turbines (VAWTs), the straight blade Darrieus rotor (D-rotor) has been the most studied and investigated. D-rotor have some advantages over the propeller blade Horizontal Axis Wind Turbines (HAWTs) such as their simple construction, no requirement of a yaw mechanism to turn the rotor toward the wind direction etc. However VAWTs are not usually considered suitable for stand-alone applications, mainly because of their poor starting behaviour resulting from blade stall at low wind speeds and high angles of attack. Several ways have been proposed to improve the starting behaviour of Darrieus turbines. These include Savonius auxiliary rotors, variable pitch angle, increased turbine solidity and inclined blades. However, none of these is likely to result in competitive designs to the propeller type of HAWTs. Furthermore, most previous researchers have adopted airfoil shape published from US National Advisory Committee on Aeronautics (NACA) a long time ago. More recently, new airfoils are available and preliminary investigating suggest that NACA airfoil section are not necessary the best airfoil for D-rotor. In this study, the feasibility of using modern airfoils for D-rotor have been carried out. Their performance had been compared with good NACA airfoils. A total of 30 airfoils have been studied in this paper. Analytical technique was used to pre-select high performance airfoils. These airfoil sections were then used for experimental testing. The VAWTs self-starting problems have been improved and a high power coefficient was achieved. A new approach for designing the D-rotor has been shown in this study.

The investigated airfoils include:

10 High Reynolds number NACA airfoil sections:

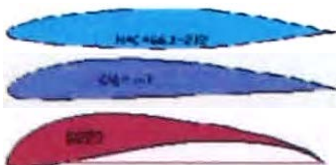
NACA 0006, NACA 66,1-212, NACA66 (215)-016, NACA 4421, NACA 23024, NACA 23021, NACA 1424, NACA 2412, NACA 4418, NACA 23012.

20 Low Reynolds number (3×10^5) modern airfoil sections:

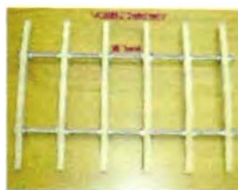
A18, Clark-Y, E 387, S 6062, SD 7037, NACA 2414, S 822, SD 6060, RG 15, S 1223, SG6042, Goe417a, SG6040, LRN 1007 (B), CR-001, SA7035, Trainer 60, S6063, RGI 4, E231.

3 feasible airfoil sections were selected:

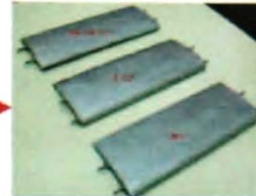
1. NACA661-212
2. Clark-Y
3. S1223



The Rotor Constructions



1. Airfoil structured made by MDF material



2. Al sheet covered the airfoil section

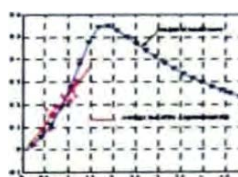
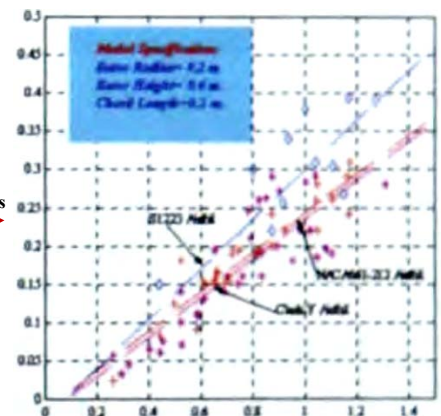


3. VAWTs constructed and test section

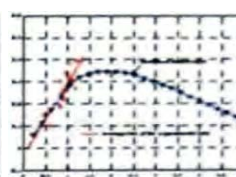
The experimental set-up



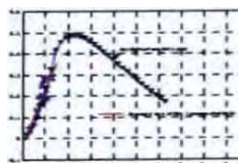
Results



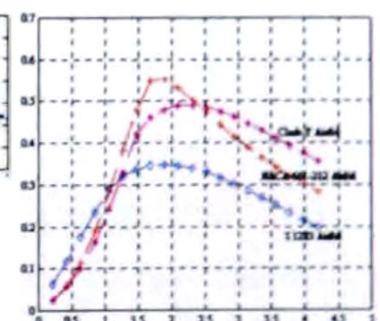
NACA661-212



S1223



Clark-Y



Analytical Model Predictions

Conclusion

NACA 661-212 was found to perform well using analytical mode 6 at high Reynolds number investigation. But it could only develop low starting torque Clark-Y airfoil showed good performance comparing with others low Re number airfoils used in the investigation. Additionally, S1223 high lift airfoil was found to perform well and showed positive results for starting behaviours. The experimental results have agreed well with the analytical prediction and supported the study. It is evident from the results of this study that the starting problem of D-rotor can be significantly reduced by careful arrangement of blade configurations. The new arrangement with careful selection of blade also improve the power coefficients of the machine by as high as 15%.

Appendix B

The performance of a Vertical Darrieus Machine with modern high lift aerofoils

By Wirachai Roynarin, M.Sc., P.S. Leung, Ph.D., Prof. P.K. Datta, Ph.D.

University of Northumbria at Newcastle, NE1 8ST, England

Paper published at *International Conference on Marine Renewable Energy 2002* organised by The Institute of Marine Engineering, Science and Technology, 11-12 September 2002, Newcastle, UK

ABSTRACT

The study of Darrieus rotor (D-rotor) Vertical Axis Wind Turbines (VAWTs) are presented in this paper. In general, VAWTs are not commonly considered for stand-alone applications, because these machines have poor starting torque behaviour resulting from blade stall conditions at high angles of wind attack. Nevertheless, Darrieus VAWTs have some significant advantages over Horizontal Axis Wind Machines (HAWTs). There are no yaw mechanisms needed to turn the rotor towards the wind direction, no power loss due to time lag tracking wind direction changes as HAWTs do. If starting behaviour of VAWTs could be improved, it would produce competitive design to HAWTs. This study aims to overcome this major disadvantage of VAWTs by investigating different blade profiles applied to this type of wind machine. Since Darrieus VAWTs operate based on lift and drag forces, and different aerofoil sections will provide various lift and drag characteristics. Therefore feasible blade profiles could develop enough starting torque for wind turbine to self-start. In this study, 20 promising aerofoils have been analysed for the purpose. The analytical models were written using Matlab packages. Lift and drag coefficients data of the 20 aerofoils were used to analyse their power coefficient at various tip speed ratios. Three feasible aerofoils were selected in order to make experimental turbine prototype. The Darrieus VAWT prototype models were tested in a wind tunnel and their performance measured. Comparison between analytical predictions and experimental results are shown in this paper. The results have indicated the most suitable aerofoil section for Darrieus VAWTs. Consequently, small but practical VAWT wind machines were constructed. Their power coefficients were investigated in the wind field at seaside environments.

Authors' Biography

All authors work at the School of Engineering, Northumbria University. W. Roynarin is currently a Ph.D. Researcher, Dr. P.S. Leung is a Senior Lecturer and Prof. P.K. Datta is Head of AMRI group.

Appendix C

Using wind turbine machine to reduce carbon dioxide emissions in shrimp farm aeration process

By Wirachai Roynarin, M.Sc., P.S. Leung, Ph.D., Prof. P.K. Datta, Ph.D., Northumbria University, NE1 8ST, England

Paper presented at Postgraduate Conference 31st January 2003, Manchester Environment Forum, Manchester, UK

Abstract

This study describes the use of renewable energy to reduce the emission of carbon dioxide, a major component of greenhouse gases, in a shrimp farm application. During the last two decades, shrimp agriculture has become increasingly important alternative to ocean-caught shrimp. Nowadays, roughly a quarter of the world's consumption of shrimp came from such farms. Therefore the reduction of pollution from a shrimp farm is an important task to achieve. The study also aims to develop a new application for a wind turbine machine as a power source for shrimp farm aeration process. A Vertical Axis Wind Turbine (VAWT) machine was designed, constructed and applied to a selected shrimp farm in southern Thailand to replace two-stroke diesel engines commonly used in the aeration process. Two-stroke diesel engines produce noise and black-smoke pollution from their exhausts to surrounding farm areas. By using the wind machine these environmental problems fairly well solved. Approximately, every litre of diesel fuel used by a typical two-stroke diesel engine in this application produces about 2.36 kg of carbon dioxide to the atmosphere per year.

This study shows that by using one wind turbine machine set in the shrimp farm aeration process for one crop cycle (4 months) reduces the use of diesel fuel by about 200 litres. This leads to a decrease of 500 kg in carbon dioxide emissions to the atmosphere every year. This study also shows the additional benefit of lower production costs for a shrimp farmer, both in terms of fuel cost and better food conversion for the shrimps (i.e. quieter environment). The study indicates that it is beneficial to use wind machines in shrimp farm production.

Authors' Biography: All authors work at the School of Engineering and Technology, Northumbria University. W. Roynarin is currently a Ph.D. Researcher, Dr. P.S. Leung is a Senior Lecturer and Prof. P.K. Datta is Head of AMRI group.

Appendix D

Wind Machine for Shrimp Farm Aeration Process

By Wirachai Roynarin, M.Sc., P.S. Leung, Ph.D., Prof. P.K. Datta, Ph.D.,

Northumbria University, School of Engineering, NE1 8ST, England

Paper published at European Wind Energy Association (EWEA) Conference 16-19th June 2003, Madrid, Spain

Abstract

This study focuses on the application of an innovative wind turbine design to reduce the levels of carbon dioxide production and noise pollution in the shrimp farm business. A novel 3m outside diameter wind machine is used as a source of energy for the *shrimp farm aeration process* and as a replacement for a polluting two-stroke diesel engine. A Vertical Axis Wind Turbines (VAWT) machine was designed, constructed and applied to a selected shrimp farm. The design is an innovative VAWT and uses a combination of the Savonius and Darrieus (S&D) types of wind machine rotors. The feasibility of the wind turbine has been investigated in Southern Thailand, which is the major area for Thai shrimp farming. The study indicates potential advantages of VAWTs over the Horizontal Axis Wind Turbines (HAWTs) machine for this type of application where average wind speeds in the range of 4 – 6 m/s can be expected.

The new wind turbine was found to be capable of replacing a small two-stroke diesel engine, which produces 2,400 kg of carbon dioxide per annum. The prototype cost of the wind machine was found to be less than the cost of purchasing 2 HP diesel engines and operating for a period of four months. The project indicates the benefit of the reduction of the production costs to a shrimp farmer, which leads to an improved food conversion ratio. The study concludes the new wind machine can be used as an energy source for the farm aeration process in a cost effective and environmentally friendly way as selected shrimp farms where there are sufficient wind resources.

Keywords: Wind energy, Turbine performance, VAWTs

Authors' Biography: All authors work at the School of Engineering and Technology, Northumbria University. W. Roynarin is currently a Ph.D. Researcher, Dr. P.S. Leung is a Senior Lecturer and Prof. P.K. Datta is Head of AMRI group.

Contact: Tel: +44 (191) 227 4618, E-mail address: w.royanarin@unn.ac.uk (Wirachai), ps.leung@unn.ac.uk (P.S. Leung)

Appendix E

The investigation of aerofoil characteristics using CFD techniques

By Wirachai Roynarin, M.Sc., P.S. Leung, Ph.D., Prof. P.K. Datta, Ph.D.,

Northumbria University, School of Engineering & Technology, NE1 8ST, England

Published in I. Mech. E. 'Up and Coming in Fluid Machinery' 9th October 2003, London, UK

Abstract

This study focuses on the investigation of aerofoil characteristics using Computational Fluid Dynamics (CFD) methods. Lift and drag forces are the essential parameters required to study the performances and behaviour of aerofoil for a wind turbine. The conventional method to study these forces is to build an experimental model and test its performance in a wind tunnel – this technique takes time and is expensive. Recently, computer technology has developed very rapidly. It can provide accurate and faster solutions to this type of problem compared to experimental tests.

In this study, a NACA 661-212 aerofoil section has been analysed and optimised by using a commercial CFD package. Essentially, CFD combines with the set of Navier-Stokes equations, continuity and additional conservation equations to solve fluid engineering problems. However, a factor influencing CFD in this application has been encountered as shown in this study. An interface mesh creation software package was introduced to solve this problem. This package provided a flexible mesh solution at localised aerofoil section and gave promising results. This study concludes that CFD combined with corrected solutions and boundaries is able to investigate and compute the physical fluid dynamics of the aerofoil more cost effectively and more rapidly than that of a usual experimental method. A comparison table showing both experimental and CFD results in the study of aerofoil characteristics is also present to validate the results of this project.

Authors' Biography: All authors work at the School of Engineering, Northumbria University. W. Roynarin is currently a Ph.D. Researcher, Dr. P.S. Leung is a Senior Lecturer and Prof. P.K. Datta is Head of AMRI group.

Contact: Tel: +44 (191) 227 4618, E-mail address: w.roynarin@unn.ac.uk, ps.leung@unn.ac.uk

Appendix F

Matlab program to predict Cp vs Tip Speed Ratio

%%(1) Main program %%

```

### Copyright 2002, University of Northumbria###

function main()
h = waitbar(0, 'Calculation is Progressing');
%H, c, N, R, b, V
%solidity=0.06
fid = fopen('dataout0.dat', 'wb');
for N = 20:20:600
h = waitbar(N/600);

[Cp(N/20), X(N/20), T(N/20), W, Cl, Cd, theta, gamma] =
power_coef(8, 0.24, N, 4, 1, 10);
fwrite(fid, Cp(N/20), 'double');
fwrite(fid, X(N/20), 'double');
fwrite(fid, T(N/20), 'double');
fwrite(fid, W, 'double');
fwrite(fid, Cl, 'double');
fwrite(fid, Cd, 'double');
fwrite(fid, theta, 'double');
fwrite(fid, gamma, 'double');
end

N = 20:20:600;
figure, plot(N(1:30), T(1:30), 'o', N(1:30), T(1:30));
title('Torque Vs RPM of NACA66, 1-212');
xlabel('RPM');
ylabel('Torque N.m');
text(200, 1000, 'pitch angle = 0 degrees');
grid;
x=X;
y=Cp;

figure, plot(x, y, 'o', x, y);
set(gcf, 'Color', [0.4 1 .6]);
axis([0 25 -0.1 0.6]);
text(5, 0.11, 'NACA 66, 1-212');
text(5, 0.25, 'No. of Blade= 1');
text(5.0, 0.22, 'Re=3.0x10^6');
text(5, 0.15, 'pitch angle = 0 degree');
title('Power Coefficient, Cp Vs Tip Speed Ratio, X of NACA 66, 1-212
aerofoil Model');
xlabel('Tip-Speed Ratio ,X');
ylabel('Power Coefficient, Cp');
grid;
close(h);
fclose(fid);

```

%%(2) Find Cl and Cd using polyfit tool%%

```
function [cl,cd] = find_clcd(theta, min_theta, max_theta, order)

load clcd1
[p1,s1] = polyfit(tmptheta, tmpcl, order);
[p2,s2] = polyfit(tmpcl1, tmpcd, order);

if theta < min_theta
    cl = 0;
else if theta > max_theta
    cl = 0;
else
    cl = polyval(p1, theta);
end
end
cd = polyval(p2, cl);
```

%%(3) Put in the database of Cl and Cd from given source %%

```
function createclcd()

%%%%%%%%%%%%%%%%%%%%%%%%%%%%%%%%%%%%%%%%%%%%%%%%%%%%%%%%%%%%%%%%%%%%%%%%%%%%%%
clear;
tmptheta = (-16:2:16)*pi/180;
tmpcl = [-0.5 -0.6 -0.9 -0.9 -0.7 -0.5 -0.3 -0.1 0.19 0.4 0.55 0.72 0.9
1.1 1.29 1.4 1.3];
tmpcl1 = (-0.9:0.1:1.3);
tmpcd = [0.016 0.013 0.012 0.015 0.0095 0.009 0.008 0.0075 0.0067
0.0052 0.0042 0.0041 0.0041 0.0043 0.008 0.0092 0.010 0.0109 0.0115
0.013 0.015 0.017 0.022];
save clcd1
```

%%(4) calculate the Power Coefficient vs Tip Speed Ratio%%

```
function [Cp, X, T, W, Cl, Cd, theta, gamma] = power_coef(H, c, N, R,
b, V);
format short;
rho=1.225;
S=c*H;
A=2*R*H;
omega=2*pi*N/60;
gamma=(0:1:360)*pi/180;
V=10;
alpha=0*pi/180;
for i=1:361
    U = R*omega;
    X1(i) = V*(cos(gamma(i)));
    Wc(i) = U+X1(i);
    Wn(i) = V*(sin(gamma(i)));
    Wc1(i) = Wc(i)^2;
    Wn1(i) = Wn(i)^2;
    W(i) = (Wc1(i)+Wn1(i))^0.5;
    thetal(i) = atan(Wn(i)/Wc(i));
    theta(i) = (thetal(i)-alpha);
```

```

[Cl(i),Cd(i)] = find_clcd(theta(i),-16*pi/180,16*pi/180, 4);
Ct(i)=(Cl(i)*sin(theta(i)+(alpha))-Cd(i)*cos(theta(i)+(alpha)));
Cn(i)=(Cl(i)*cos(theta(i)+(alpha))+Cd(i)*sin(theta(i)+(alpha)));
K(i)= (Cn(i)*sin(gamma(i)))-(Ct(i)*cos(gamma(i)));
Torque(i)=0.5*Ct(i)*rho*W(i).^2*S*R;
Wl(i)=W(i).^2;
Q(i)= Ct(i).*Wl(i);
end
SS=0:pi/180:2*pi;
sum1=trapz(SS,Q);
G1=(K.*W.^2);
sum2=trapz(SS,G1);
G=((S*b)/(8*pi*A*V^2))*sum2;
T=((0.5*rho*S*R*b)/(2*pi))*sum1;
P=(T*omega);
Pmax= 0.5*rho*A*V^3;
Pmin=(Pmax*(1+G)^3);
Cp=P/Pmin;
U=R*omega;
X=U/V;

```

%%(5) Collect the calculated parameters%%

```

function [Cp, X, T, W, Cl, Cd, theta, gamma] = readdrotor1(no);

fid = fopen('dataout1.dat','rb');
for i = 1:no
    Cp = fread(fid,1,'double');
    X = fread(fid,1,'double');
    T = fread(fid,1,'double');
    W = fread(fid,361,'double');
    Cl = fread(fid,361,'double');
    Cd = fread(fid,361,'double');
    theta = fread(fid,361,'double');
    gamma = fread(fid,361,'double');
end
fclose(fid);

```


Appendix G

Matlab program to predict Torque vs Tip Speed Ratio

%%(1) Find Cl and Cd%%

```
function [cl,cd] = find_clcd(theta, min_theta, max_theta, order)
% function [cl cd] = find_clcd(theta, min_theta, max_theta
% Copyright 2000, University of Northumbria
% cl =
% cd =
% theta =
% min_theta =
% max_theta =
% order =

% tmptheta = -16:16;
% tmpcl = [-.8 -.8 -.75 -.7 -.9 -.9 -.9 -.89 -.8 -.75 -.6 -.55 -.4 -.3
-.2 -.1 0 .1 .2 .31 .4 .55 .65 .78 .9 .9 .9 .9 .85 .82 .81 .8 .8];
% tmpcli = -.9:.1:.9;
% tmpcd = [.022 .018 .0152 .0132 .012 .011 .010 .0098 .0092 .0091
.0091 .0095 .010 .011 .012 .013 .015 .017 .021];

load clcd1
[p1,s1] = polyfit(tmptheta, tmpcl, order);
[p2,s2] = polyfit(tmpcli, tmpcd, order);

if theta < min_theta
    cl = 0;
    else if theta > max_theta
        cl = 0;
    else
        cl = polyval(p1, theta);
    end
end
cd = polyval(p2, cl);
```

%%(2)Put the Cl and Cd to the program%%

```
function createdclcd()

%NACA661-212%%
%clear;
%tmptheta = (-16:2:16)*pi/180;
%tmpcl = [-0.5 -0.6 -0.9 -0.9 -0.7 -0.5 -0.3 -0.1 0.19 0.4 0.55 0.72
0.9 1.1 1.29 1.4 1.3];
%tmpcli = (-0.9:0.1:1.3);
%tmpcd = [0.016 0.013 0.012 0.015 0.0095 0.009 0.008 0.0075 0.0067
0.0052 0.0042 0.0041 0.0041 0.0043 0.008 0.0092 0.010 0.0109 0.0115
0.013 0.015 0.017 0.022];
%save clcd1
```

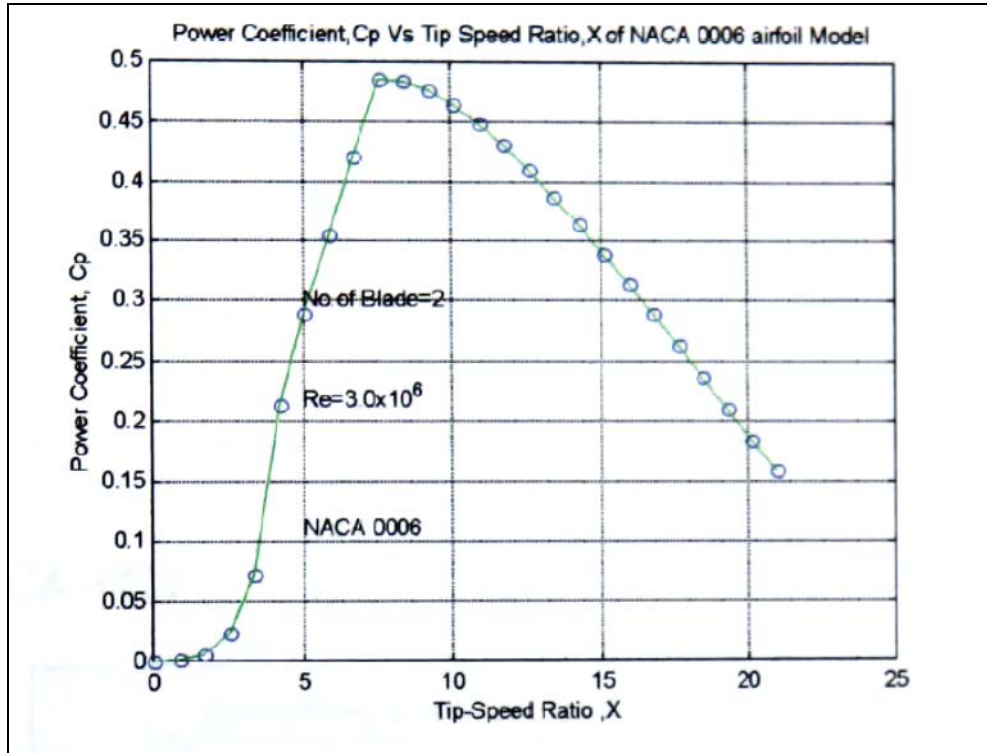
%%(3) Calculate torque at certain RPMs%%

```
function main()
clear;
format short;
rho=1.225;
c=0.2;
H=1;
S=c*H;
b=3;
N=500;
R=1;
A=2*R*H;
omega=2*pi*N/60;
alpha=0*pi/180;
gamma=(0:1:360)*pi/180;
V=10;
for i=1:361
    U = R*omega;
    Xl(i)= V*(cos(gamma(i)));
    Wc(i)=U+Xl(i);
    Wn(i)= V*(sin(gamma(i)));
    Wcl(i)= Wc(i)^2;
    Wnl(i)= Wn(i)^2;
    W(i)=(Wcl(i)+Wnl(i))^0.5;
    thetal(i)= atan(Wn(i)/Wc(i));
    theta(i) = (thetal(i)-alpha);
    [Cl(i),Cd(i)] = find_clcd(theta(i),-28*pi/180,38*pi/180,4);
    Ct(i)=(Cl(i)*sin((theta(i)+alpha))-Cd(i)*cos((theta(i)+alpha)));
    Cn(i)=(Cl(i)*cos((theta(i)+alpha))+Cd(i)*sin((theta(i)+alpha)));
    K(i)= (Cn(i)*sin(gamma(i)))-(Ct(i)*cos(gamma(i)));
    Torque(i)=0.5*Ct(i)*rho*W(i).^2*S*R;
    TT=mean(Torque);
    Wl(i)=W(i).^2;
    EE=(pi/180);
    Q(i)=Ct(i).*Wl(i);
    suml=sum(Q)*EE;
end
G1=sum(K.*W.^2)*EE;
G = ((S*b)/(8*pi*A*V^2))*G1;
T=((0.5*rho*S*R*b)/(2*pi))*suml)*2;
P = (T*omega);
Pmax= 0.5*rho*A*V^3;
Pmin=(Pmax*(1+G)^3);
Cp=P/Pmin;
U=R*omega;
X=U/V;
gammal=gamma*180/pi;
theta2=theta*180/pi;
figure, subplot(221), plot(gammal,theta2); title('Gamma
&THETA');xlabel('gamma'); ylabel('THETA');grid
subplot(222), plot(gammal,Cl);title('Gamma &Cl');
xlabel('gamma');ylabel('Lift Coeficient');grid;
subplot(223), plot(gammal,Cd); xlabel('gamma');ylabel('Drag
Coeficient');grid;
subplot(224), plot(gammal,Torque);
xlabel('gamma');ylabel('Torque');grid;
title('NACA 661-212 at Re=30e6 and 1600 rpm');
```

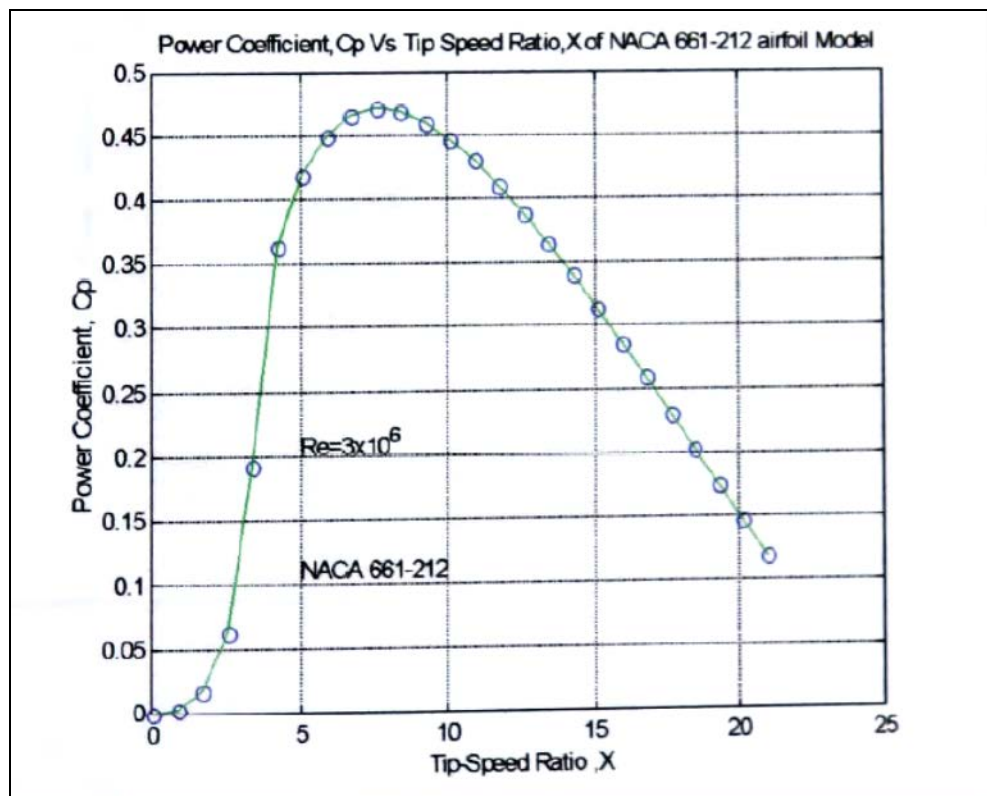
Appendix H

The Predicted Power Coefficients of 10 High Reynolds Number Aerofoils vs Tip Speed Ratio

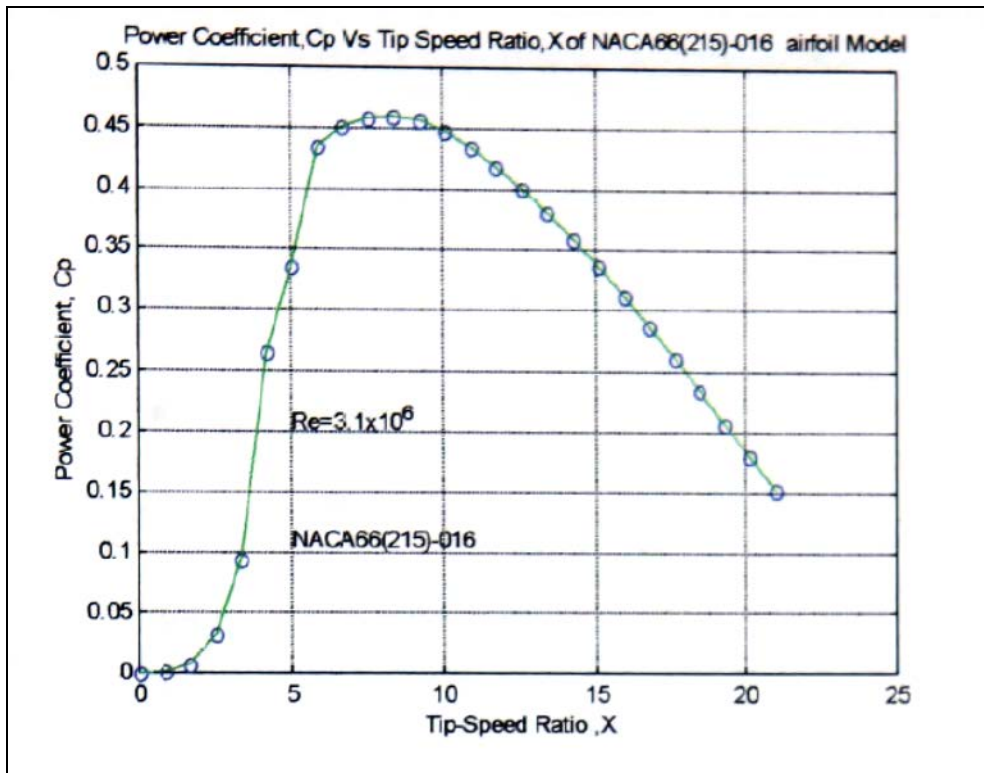
1. NACA 0006



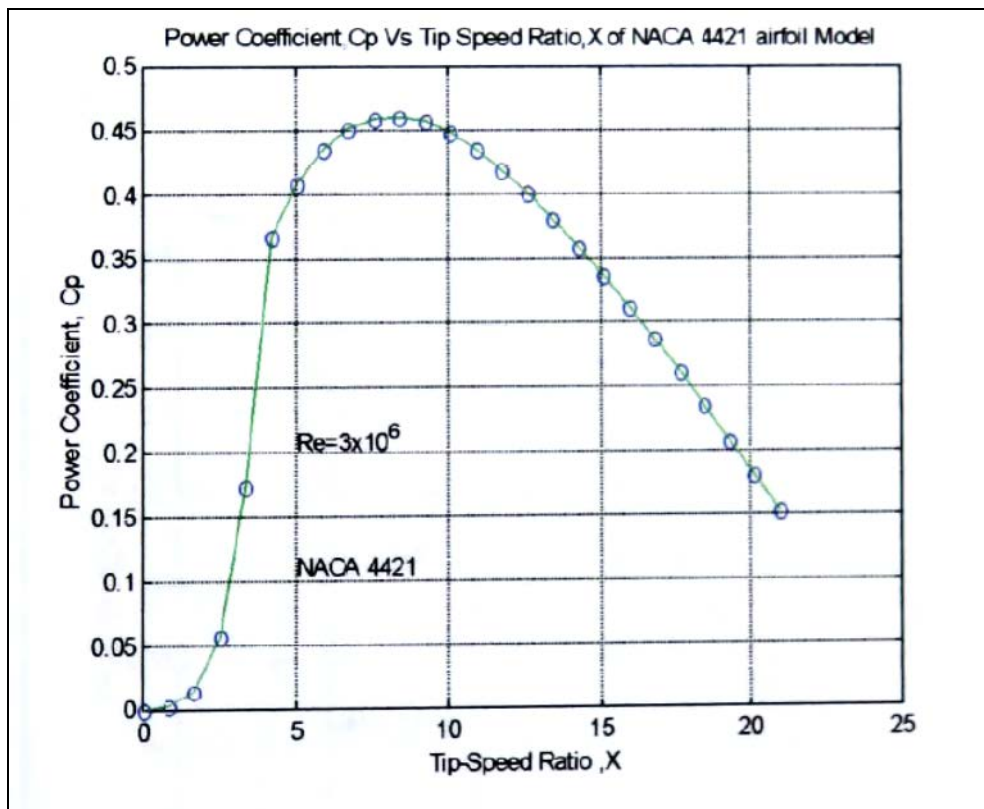
2. NACA 661-212



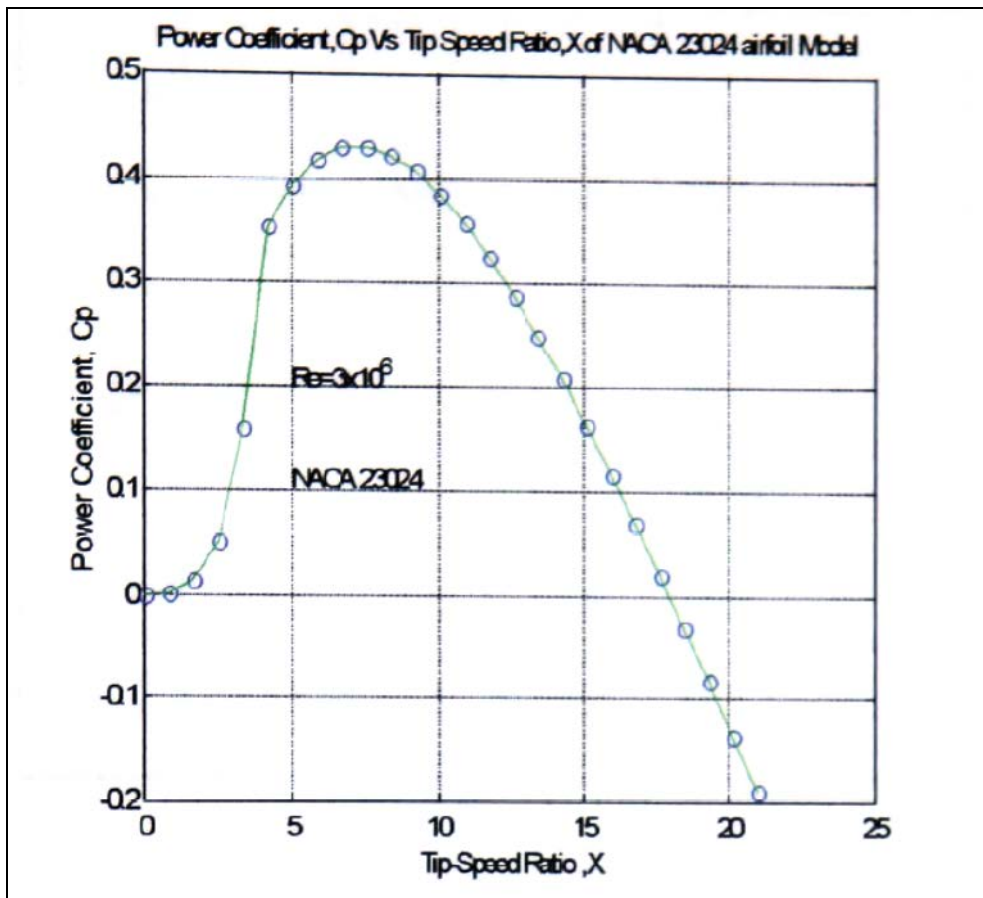
3. NACA 66(215)-016



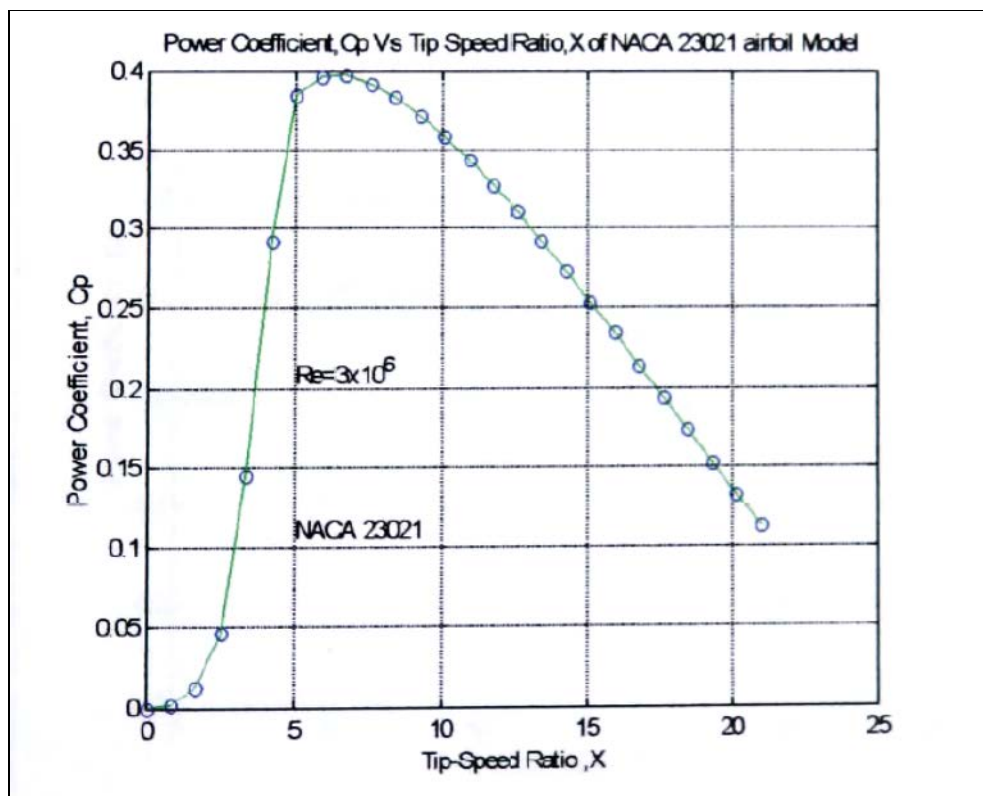
4. NACA 4421



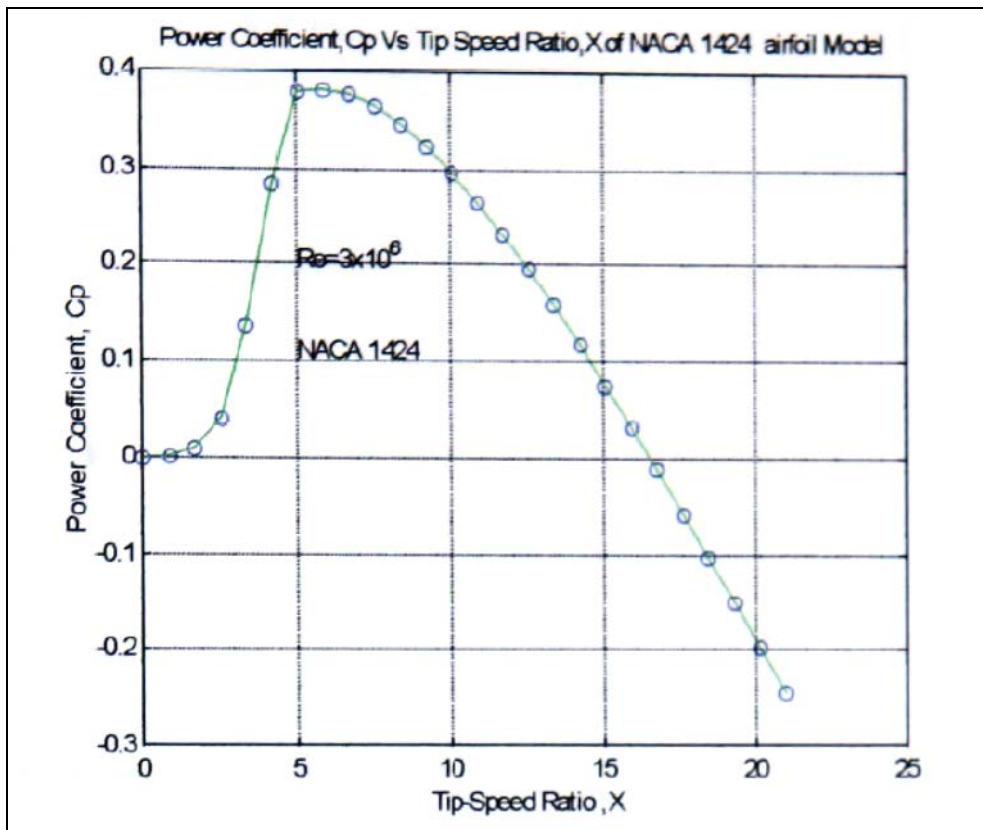
5. NACA 23024



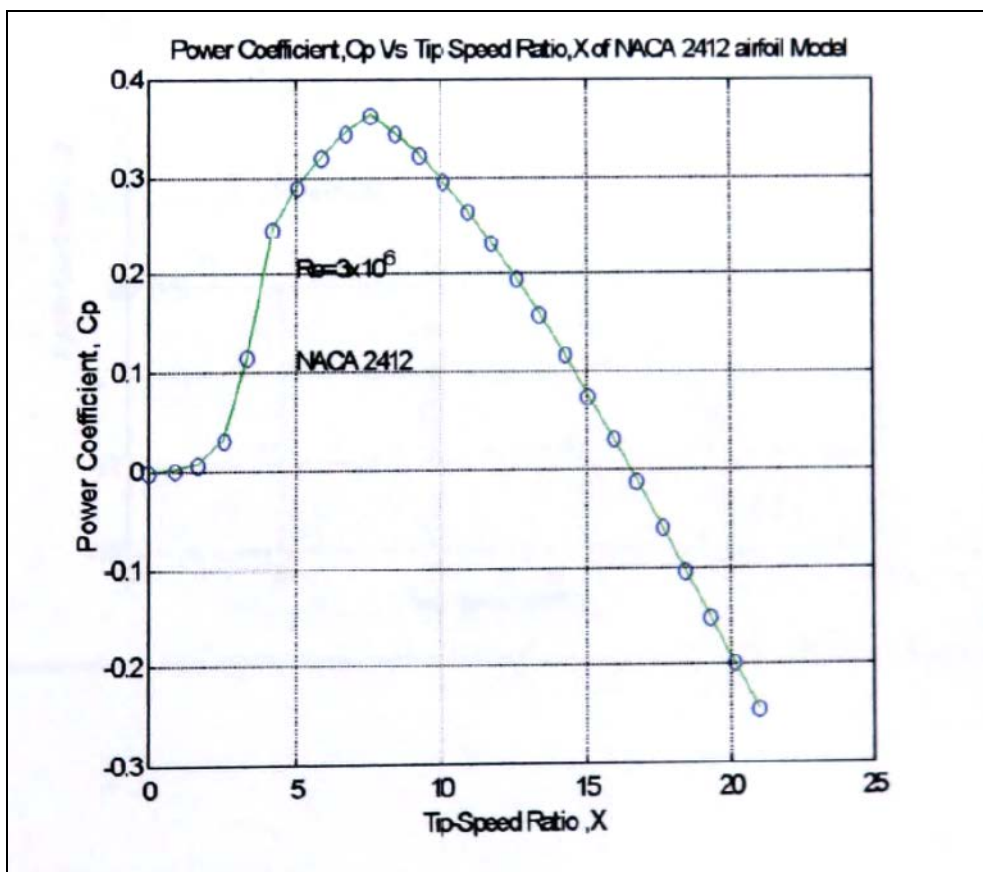
6. NACA 23021



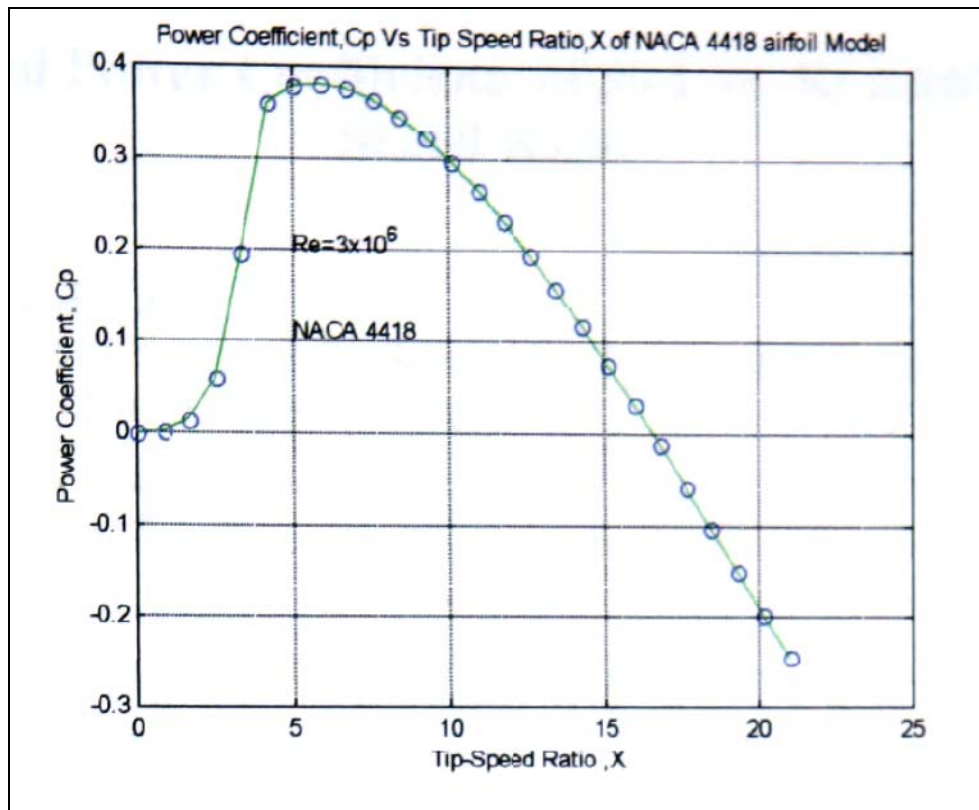
7. NACA 1424



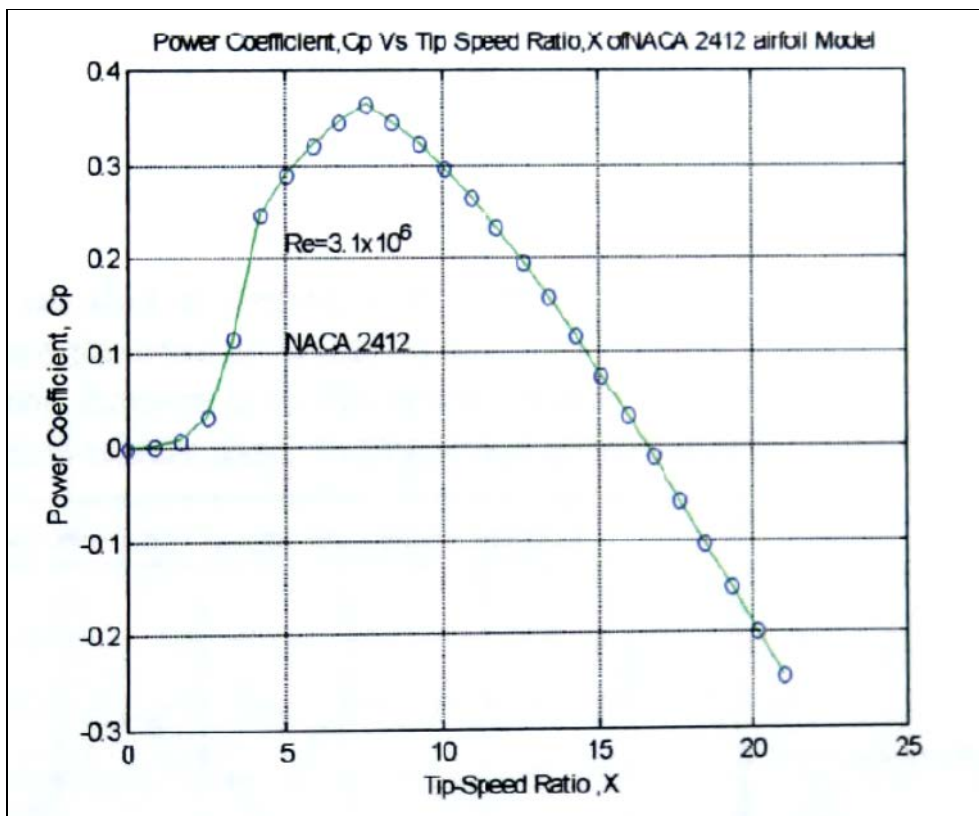
8. NACA 2412



9. NACA 4418



10. NACA 2412



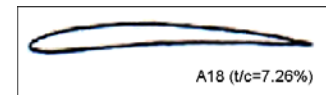
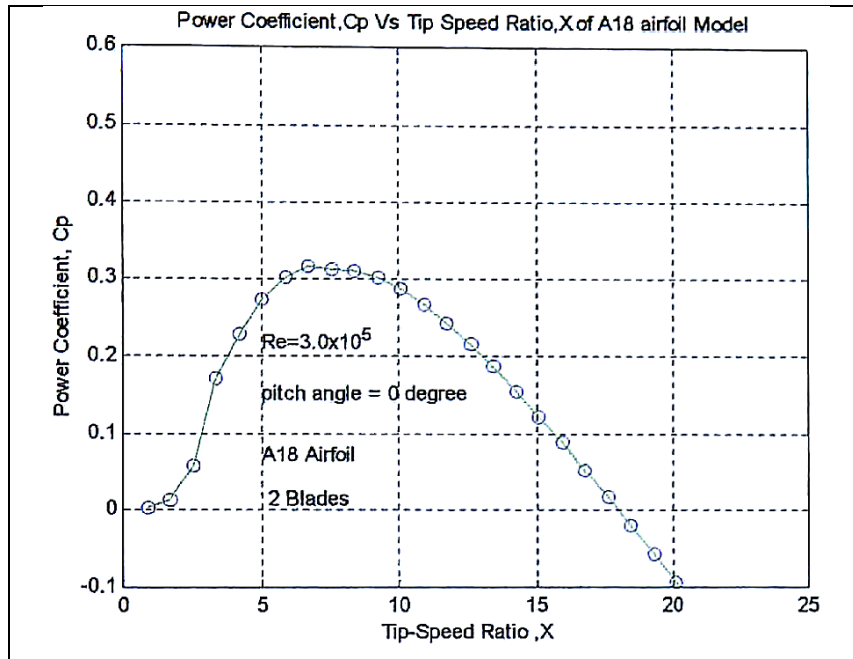
Appendix I

The Predicted Power Coefficients of 30 Low Re Aerofoils vs Tip Speed Ratio

1. A18

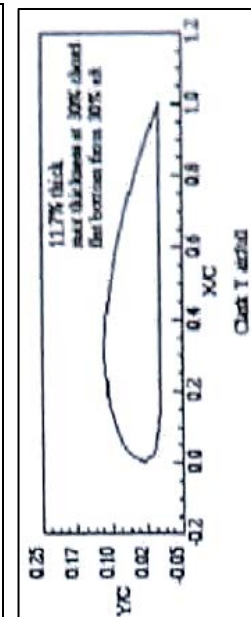
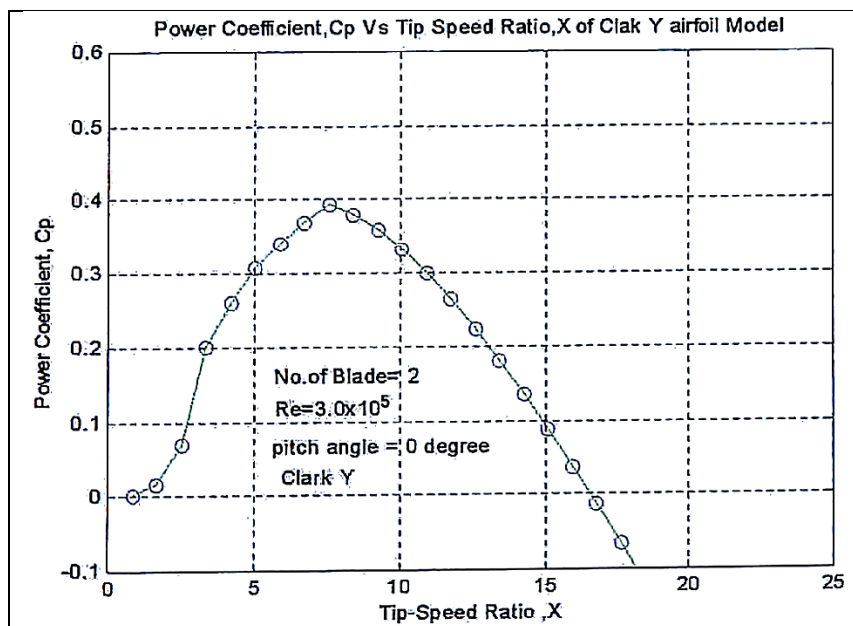
Developer: Randy Archer,

The source: M. S. Selig, J. J. Guglielmo, A. P. Broeren and P. Giguere, "Summary of Low-Speed Aerofoil Data, Volume 1, 1995"



2. Clark Y

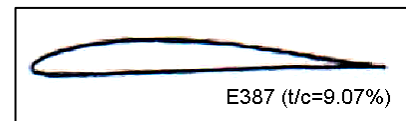
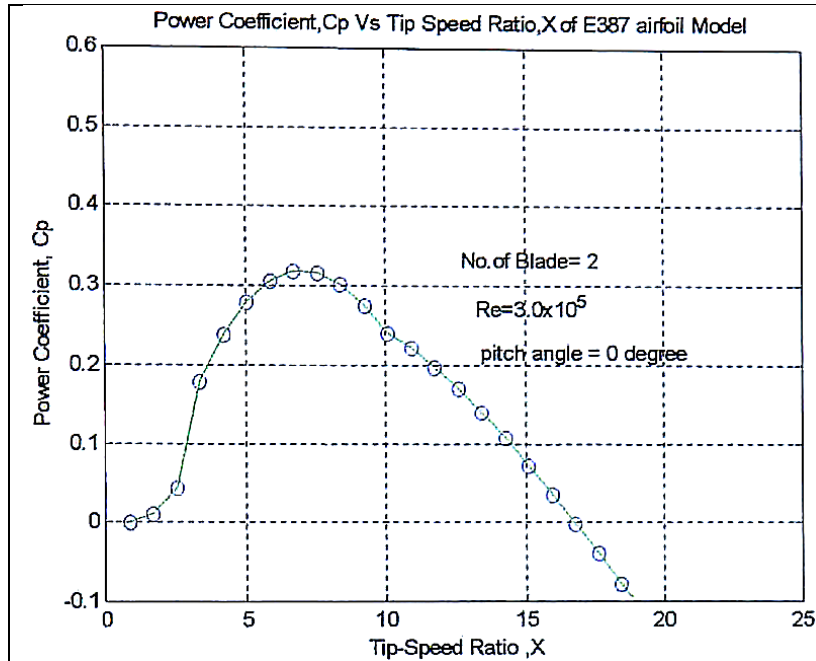
The Clark Y aerofoil is named after Col. Virginus E. Clark, who designed many aerofoils around the time of World War 1. The Clark Y was designed in 1922. One of its distinguishing features is its flat lower surface from 30% chord to the trailing edge. This aerofoil was widely used, but has been superseded by improved aerofoils today.



3. E387

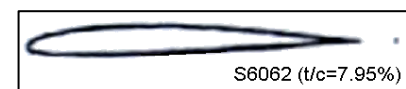
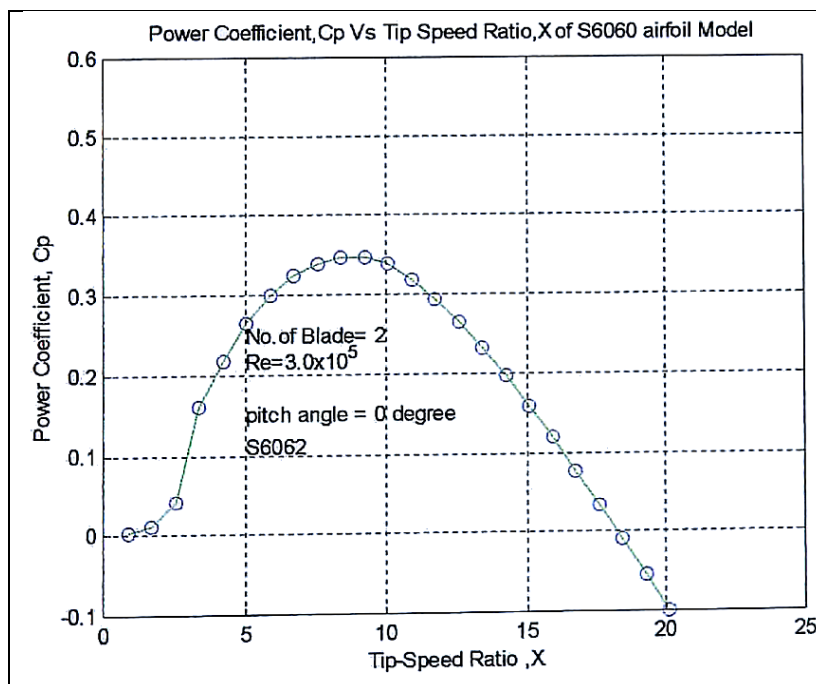
Development Group- Dr. Richard Eppler, 'Aerofoll and Data' Springer-Verlag, New York, 1990. The Source: M.S.Selig, J. F. Donovan and D. B. Fraser.

"AEROFOIL AT LOW SPEEDS", SoarTech 8,1989.



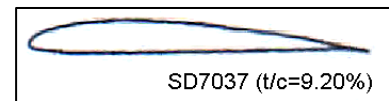
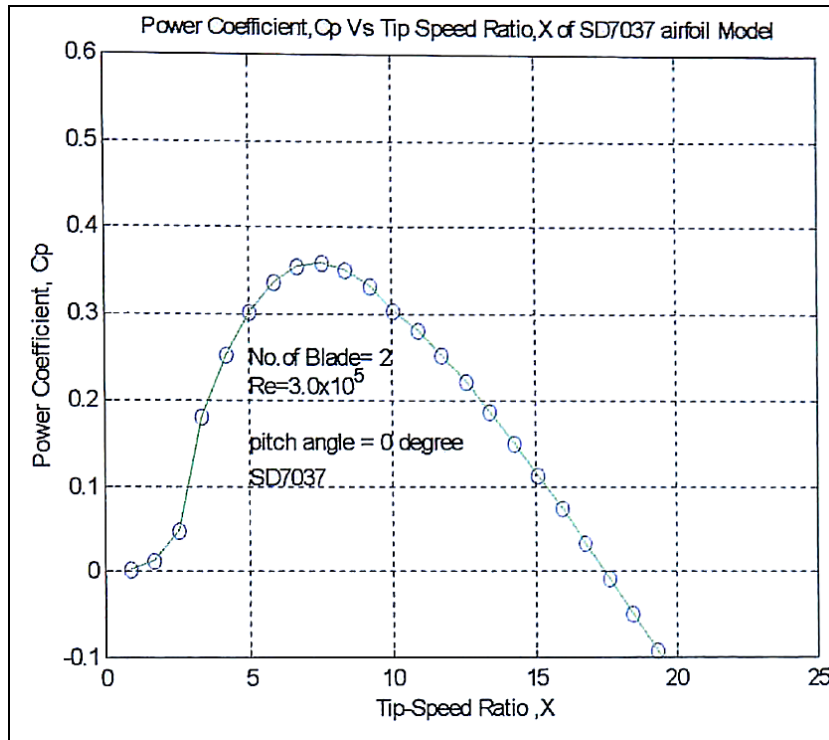
4. S6062

Source: M.S. Selig, J.J. Guglielmo, A. P. Broeren and P. Giguere. "Summary of Low-Speed Aerofoil Data, Volume 1,1995"



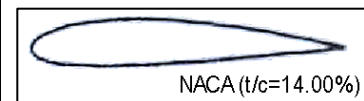
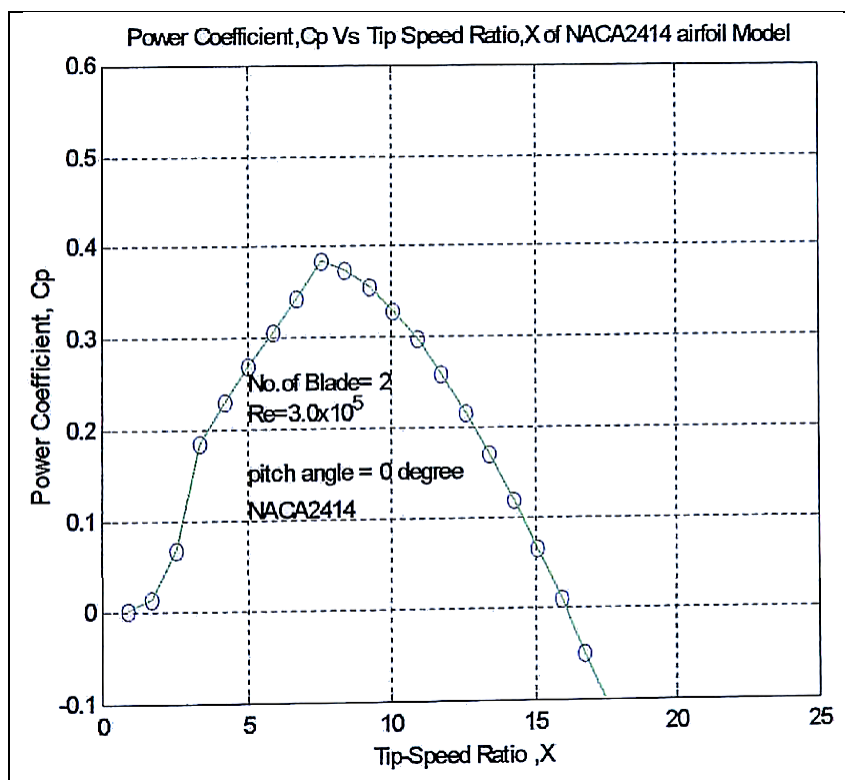
5. SD 7037

Development Group: M.S.Selig, J.F. Donovan and D.B. Fraser,
"AEROFOIL AT LOW SPEEDS", SoarTech 8,1989



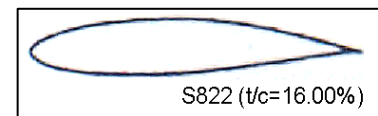
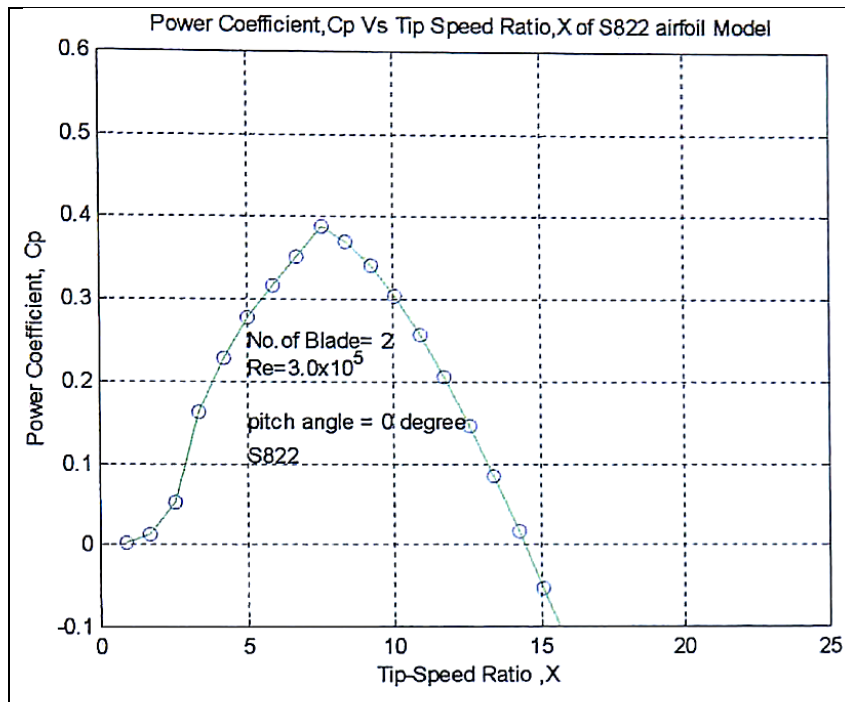
6. NACA 2414

Abbott, Ira H Von Doenhoff, Albert E. Stivers, Louis, Jr, Summary of airfoil data, NACA Report 824 NACA-ACR-L5CO5 NACA-WR-L-560,1945



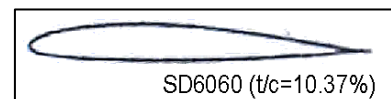
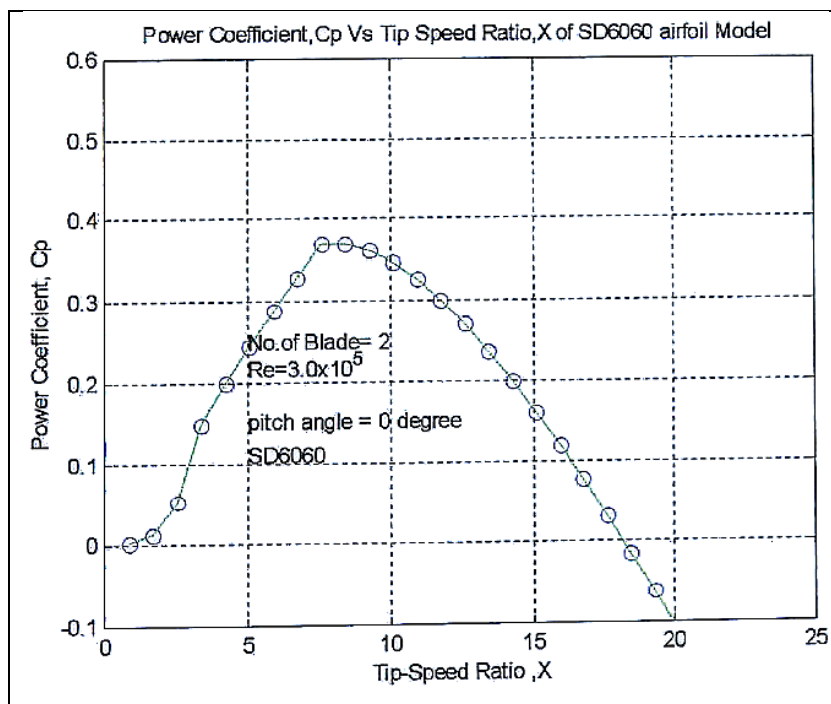
7. S822

Source: 'NREL Aerofoil Families for HAWTs' AWEA Wind Power Conference.
Washington, DC, March 1995



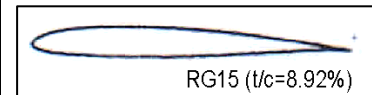
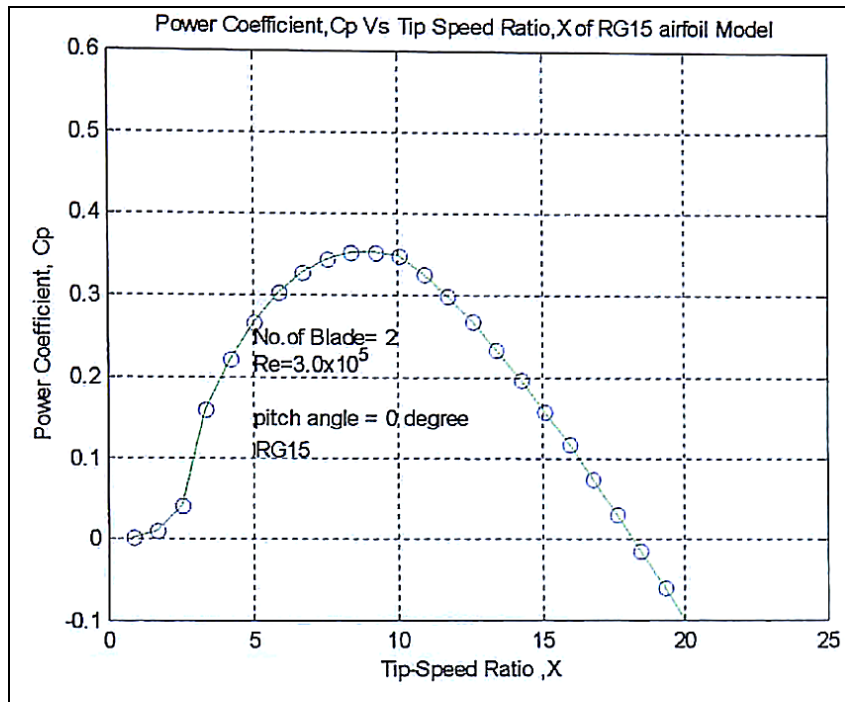
8. SD 6060

The source: Development Group: M. S. Selig, J.F. Donovan and D. B. Fraser.
"AEROFOIL AT LOW SPEEDS", SoarTech 8,1989



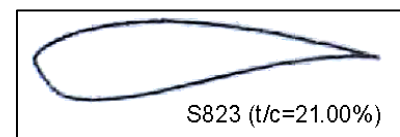
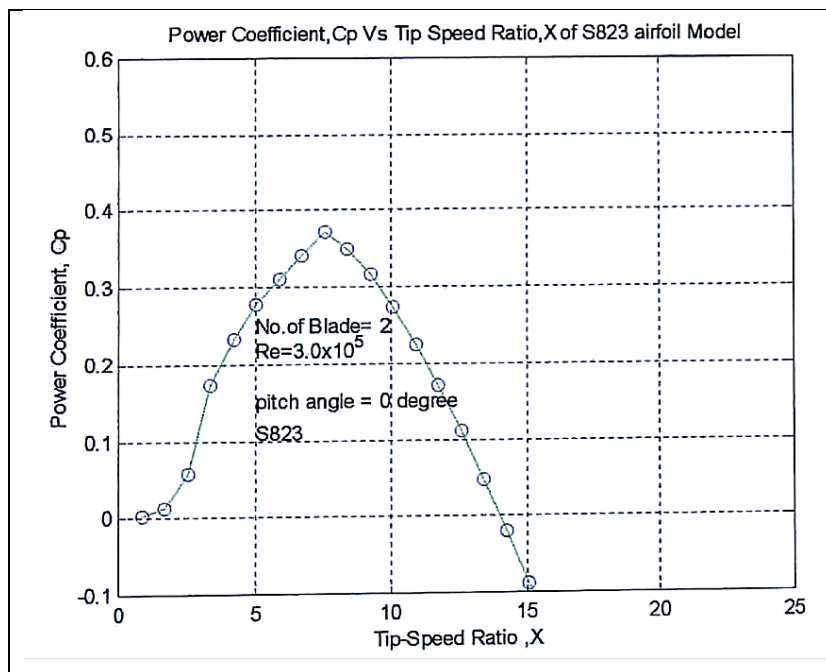
9. RG 15

First Proposed: Rolf Girsberger First reported on at the 1983 ISF-Seminar. 'Proceedings of the International RC-Segelflug Forum'. Winterthur, Switzerland, December 1983



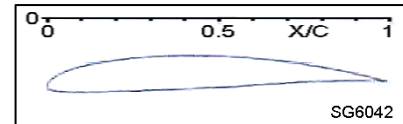
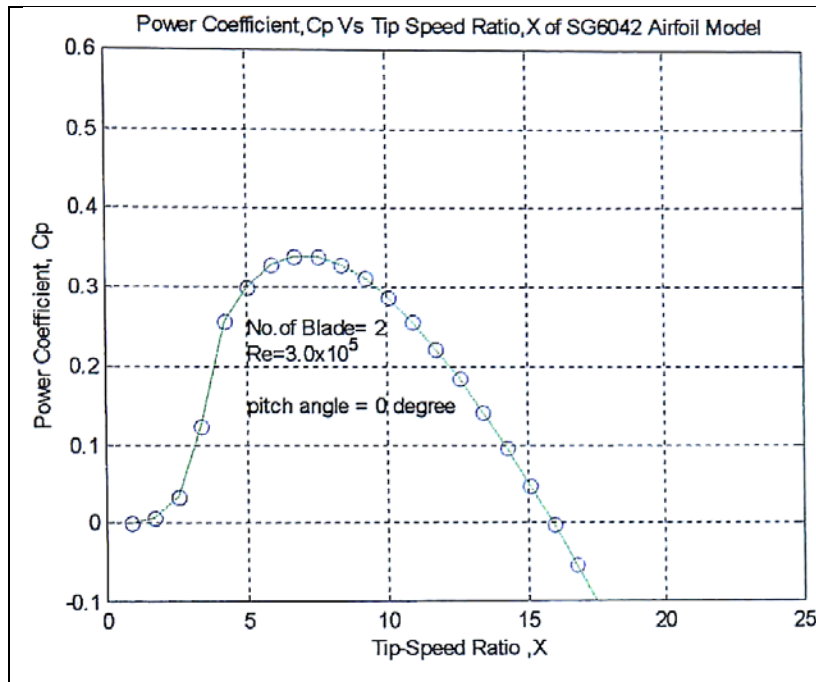
10. S823

Developer: (National Renewable Energy Laboratory), 1995, Tangler, J. L. and Somers. D.M. 'NREL Aerofoil Families for HAWTs' AWEA Wind power Conference, Washington DC, March 1995

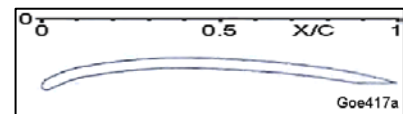
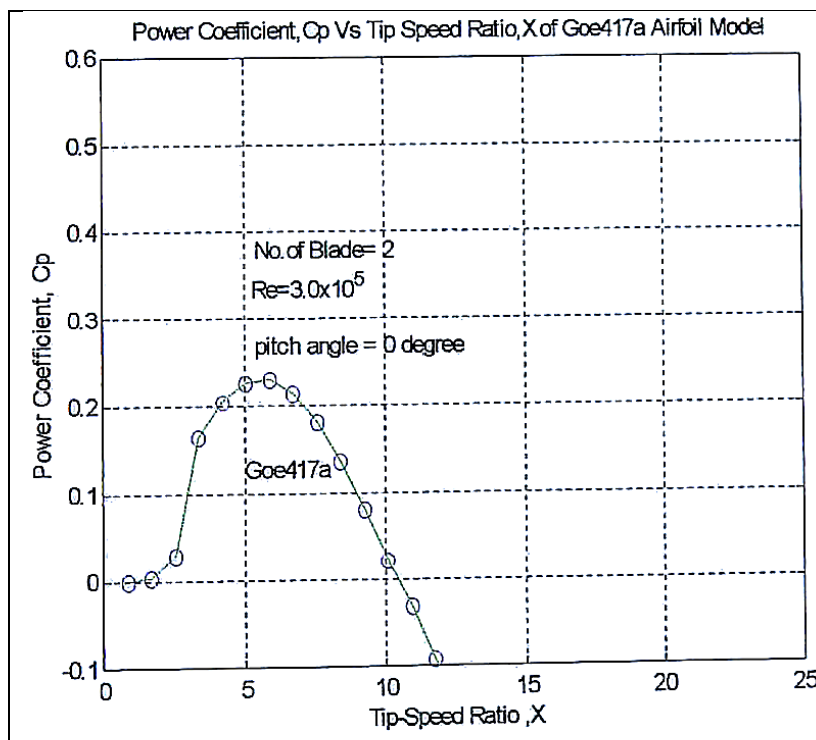


11. SG6042

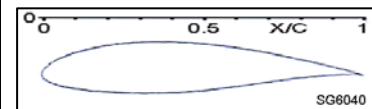
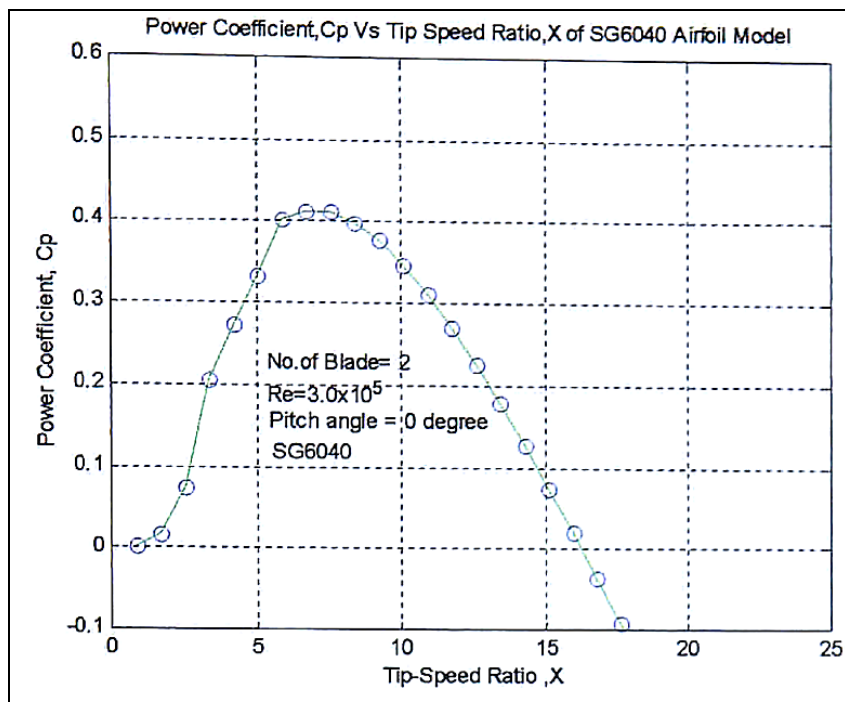
This aerofoil is usually considerable developed for HAWTs.



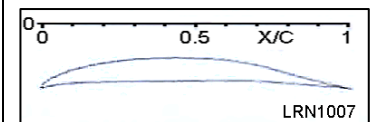
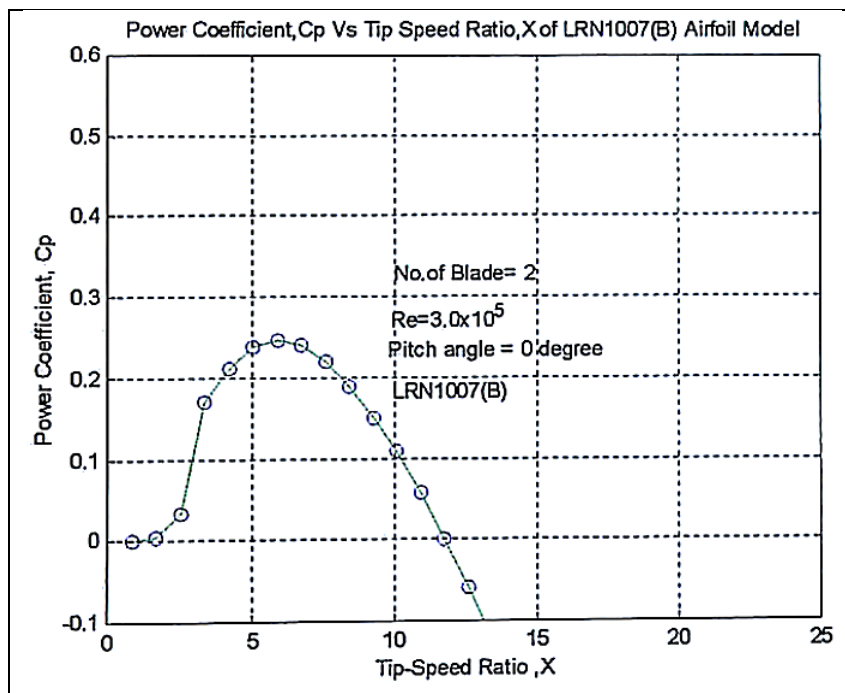
12. Goe417a



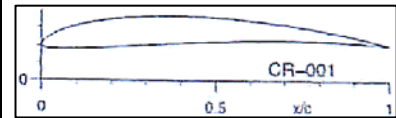
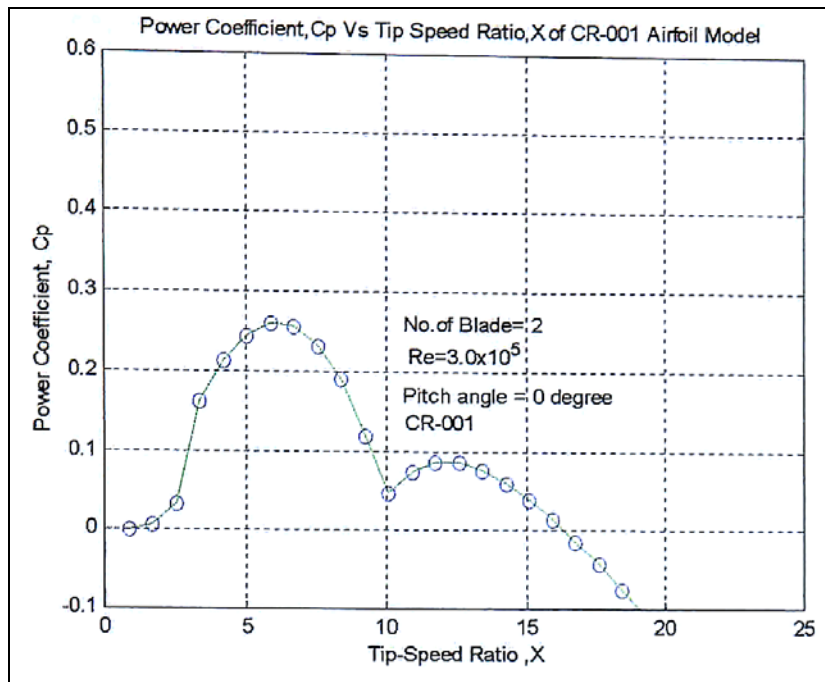
13. SG6040



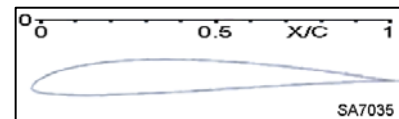
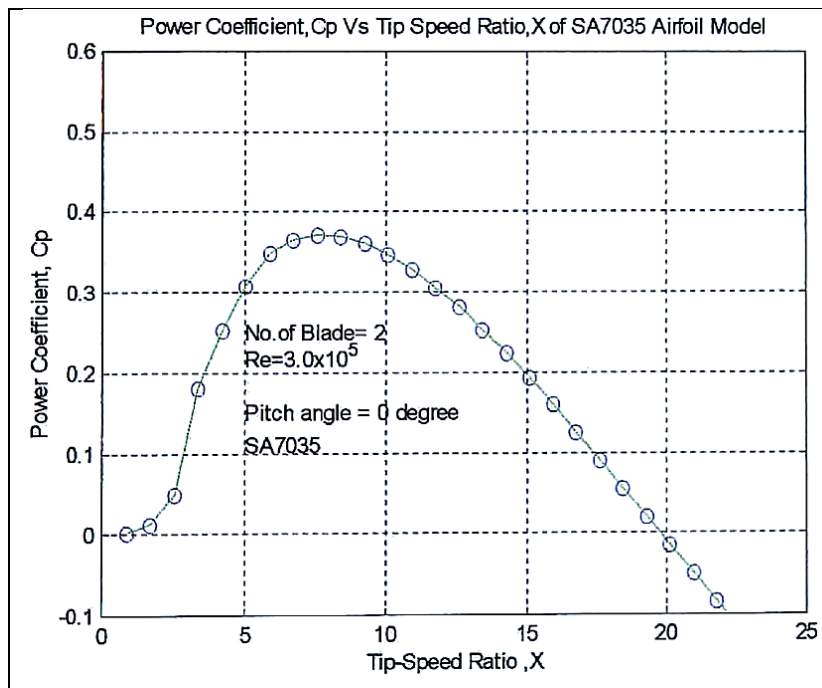
14. LRN1007 (B)



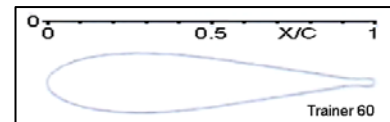
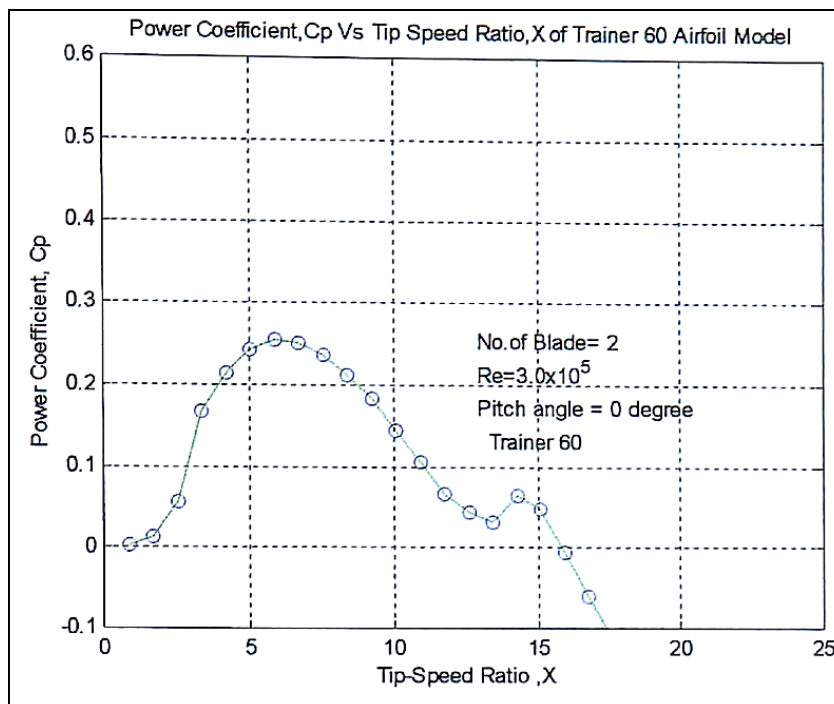
15. CR-001



16. SA7035

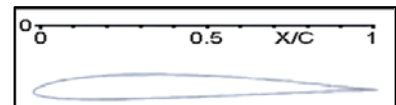
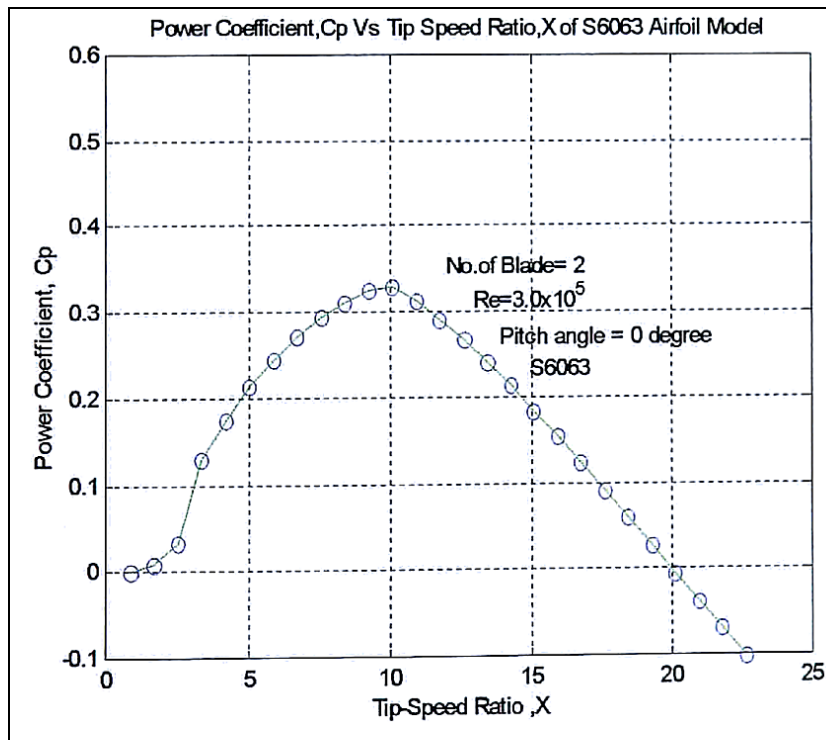


17. Trainer 60

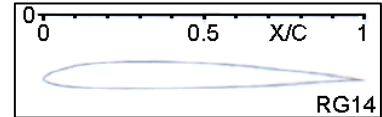
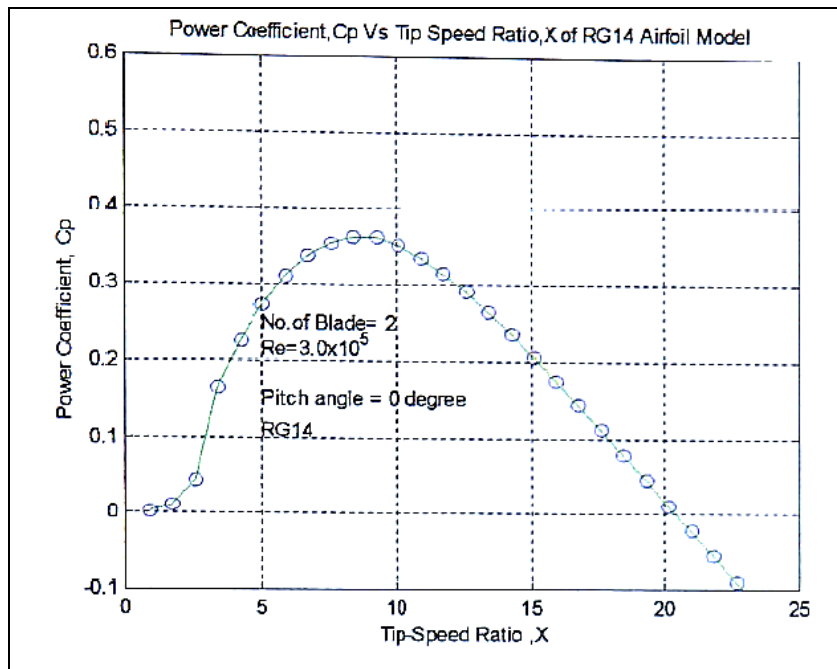


18. S6063

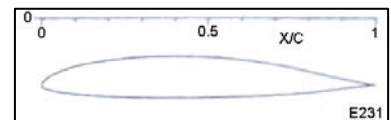
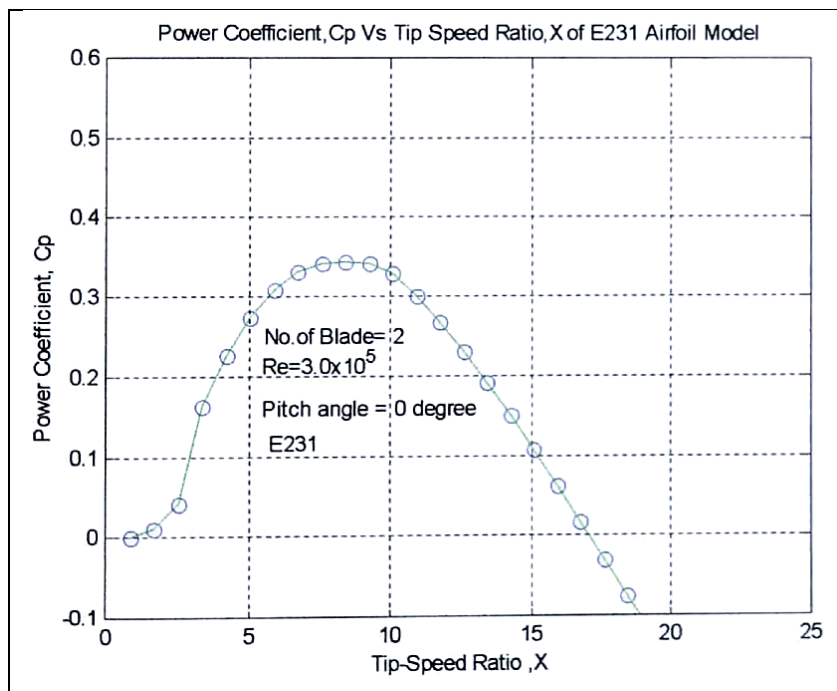
Source: M. S. Selig, J.J. Guglielmo, A. P. Broeren and P. Giguere, 'Summary of Low Speed Aerofoil Data' Vol. 1, 1995



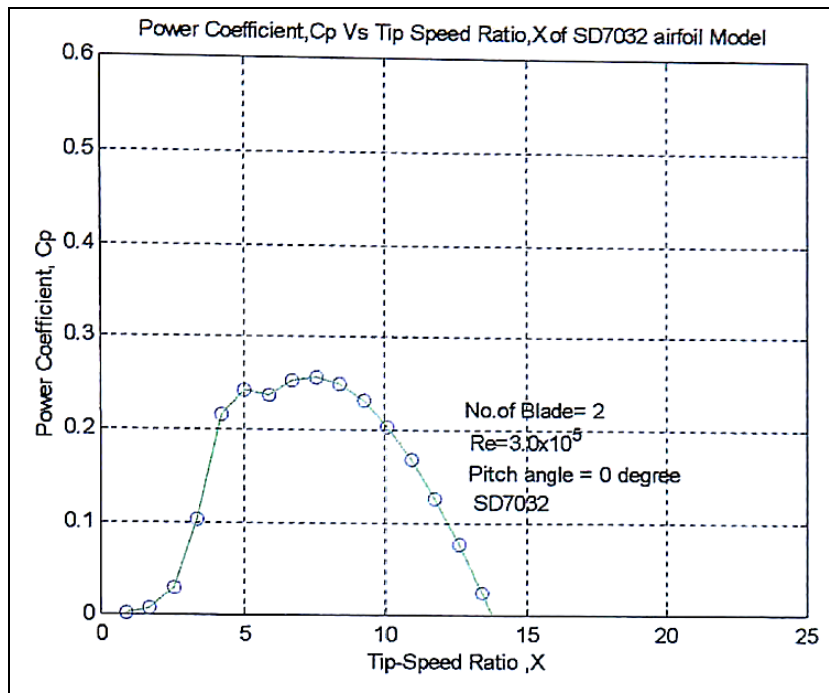
19. RG14



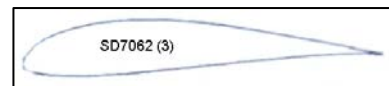
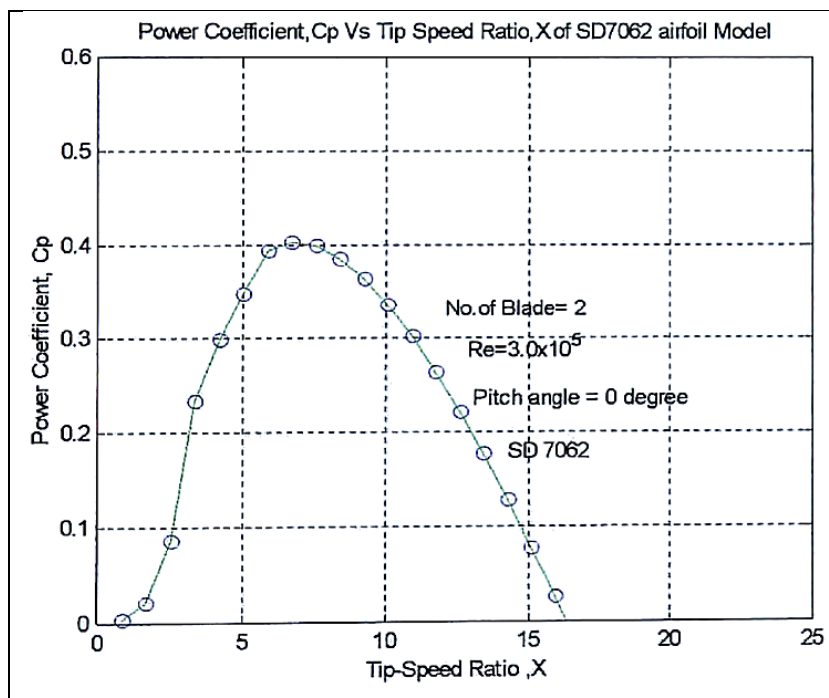
20. E231



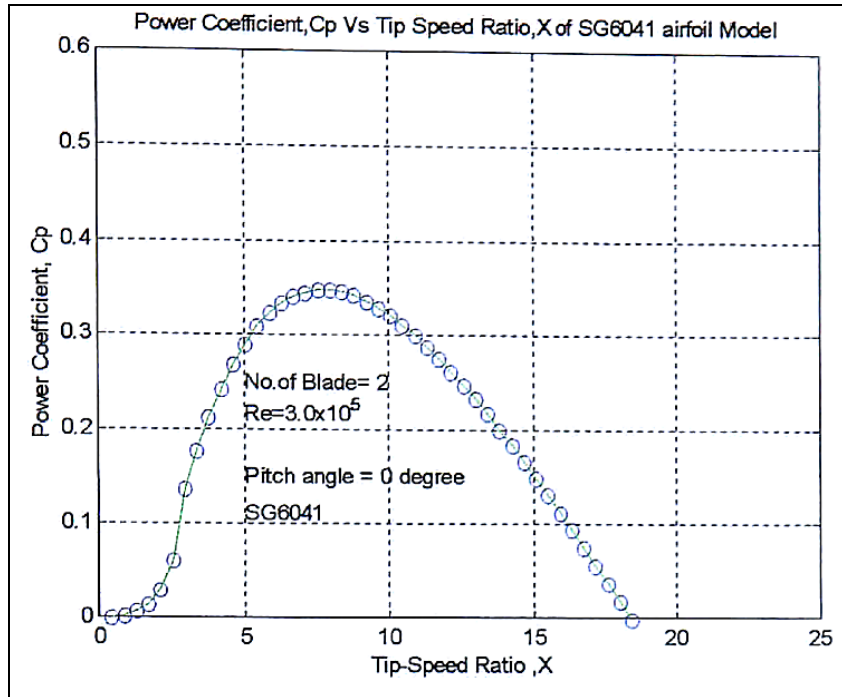
21. SD 7032



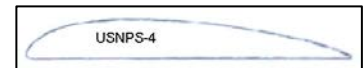
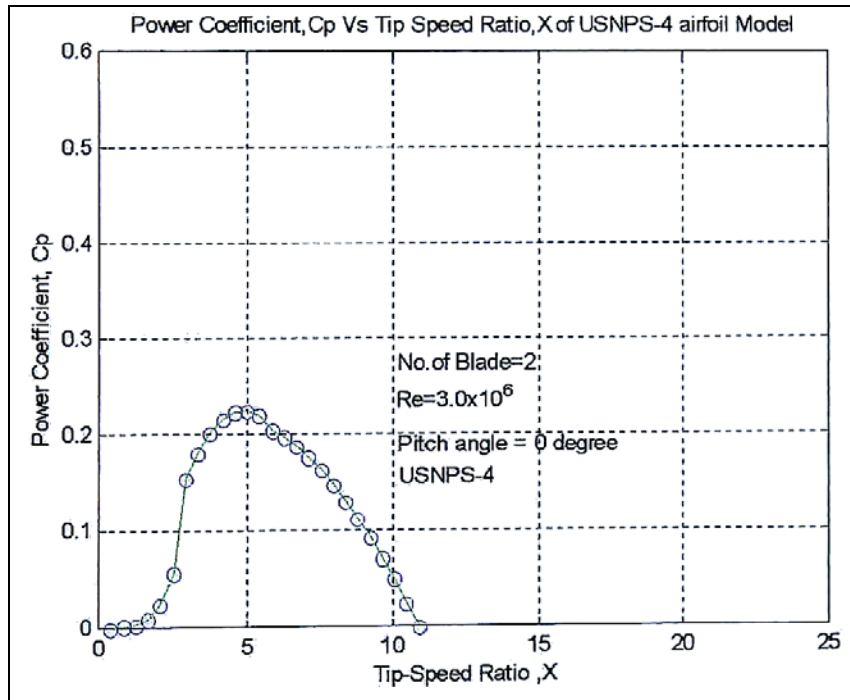
22. SD 7062



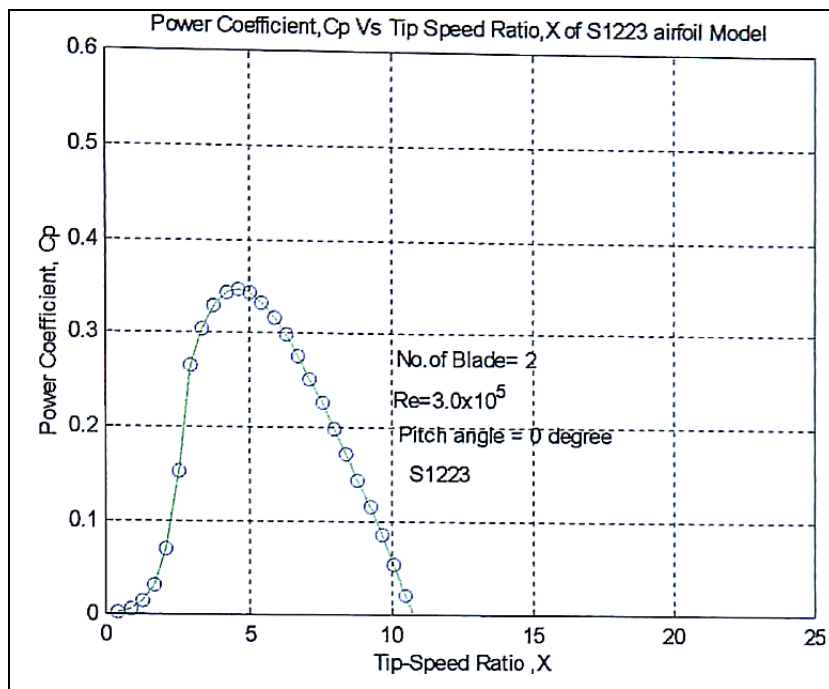
23. SG 6041



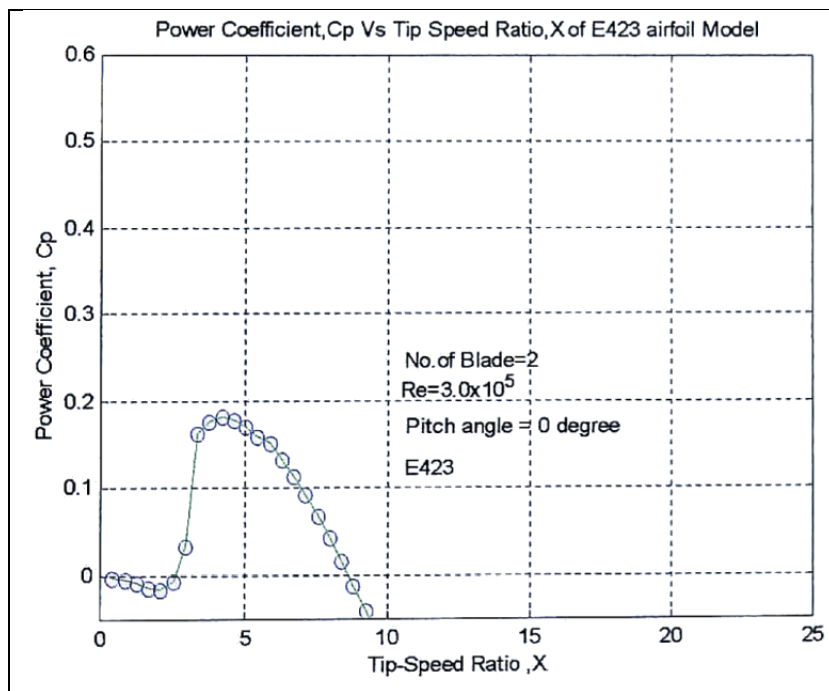
24. USNPS-4



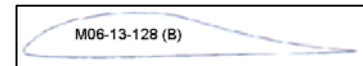
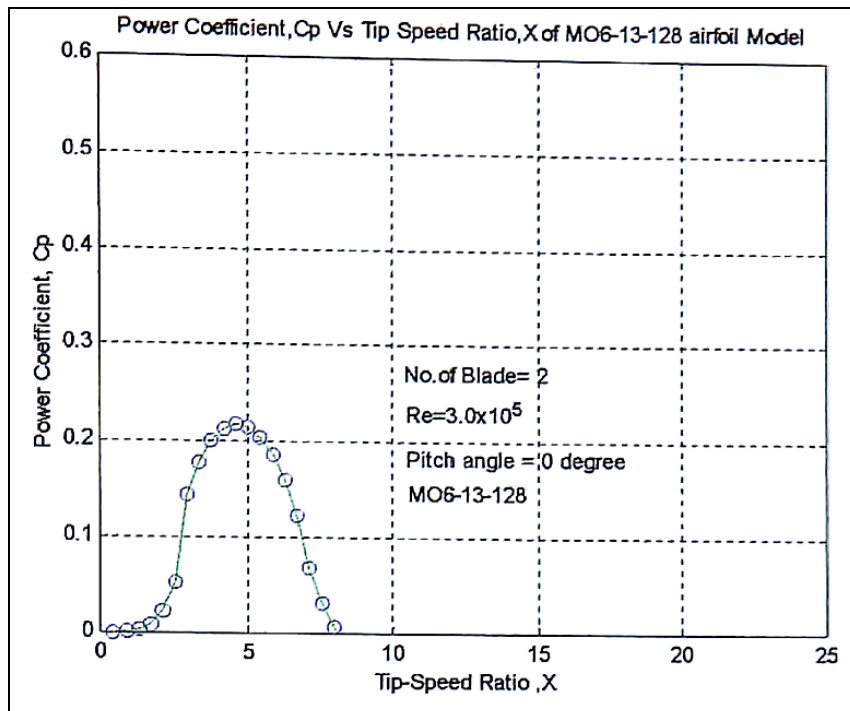
25. S1223



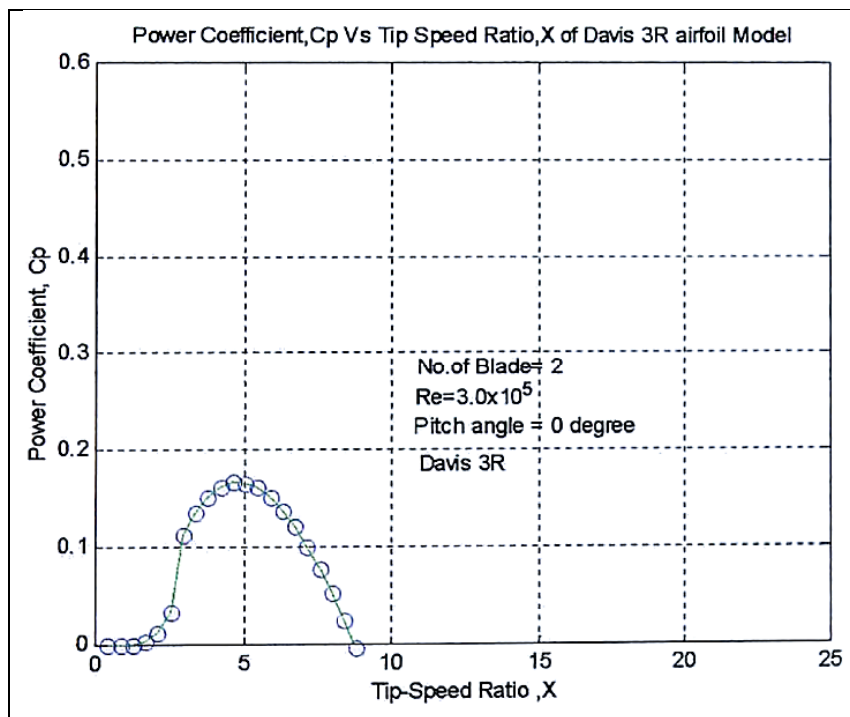
26. E423



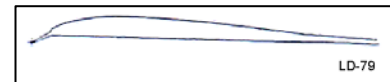
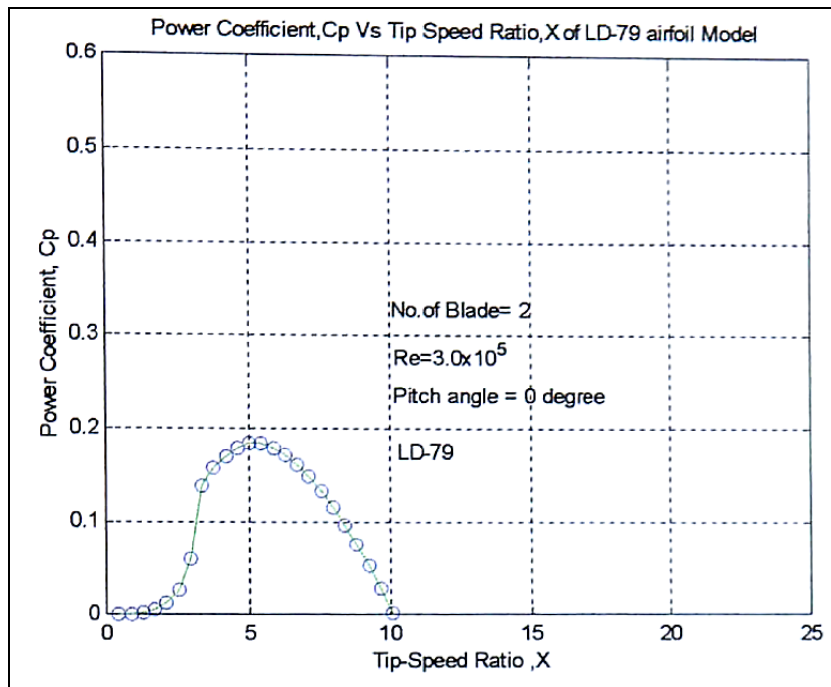
27. MO6-13-128



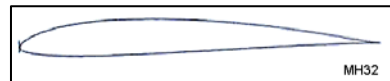
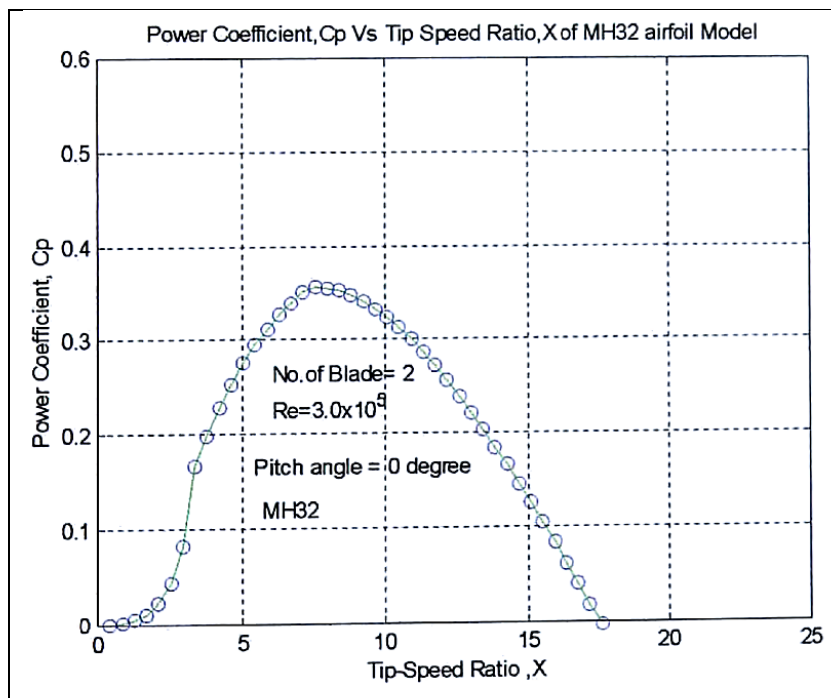
28. Davis 3R



29. LD-79



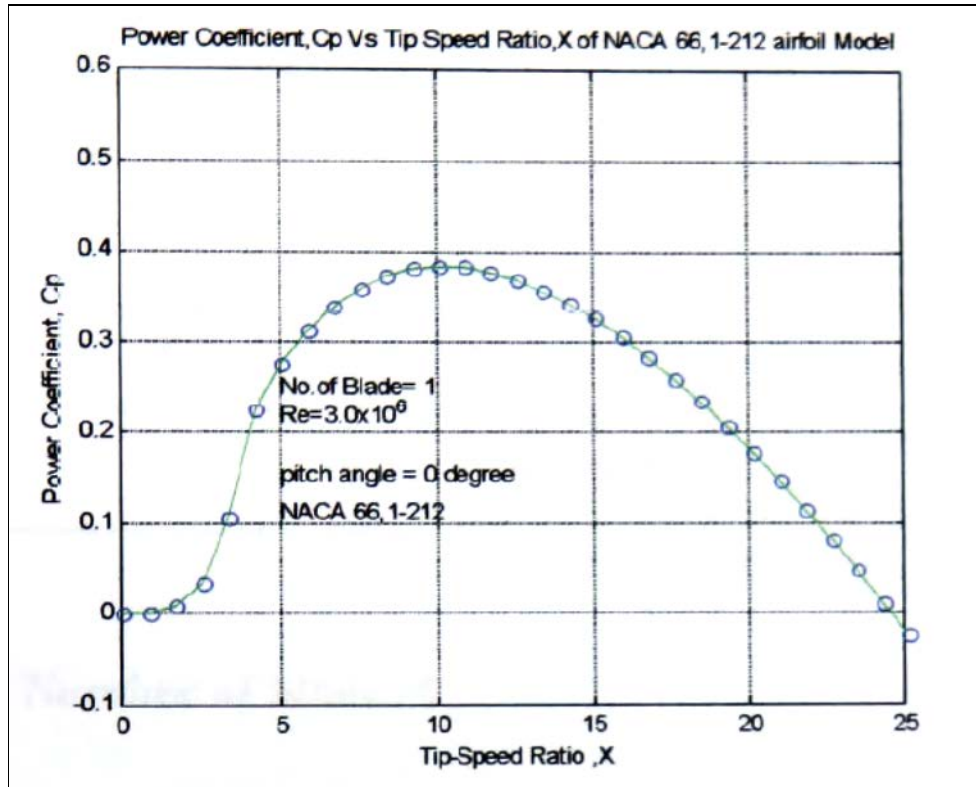
30. MH32



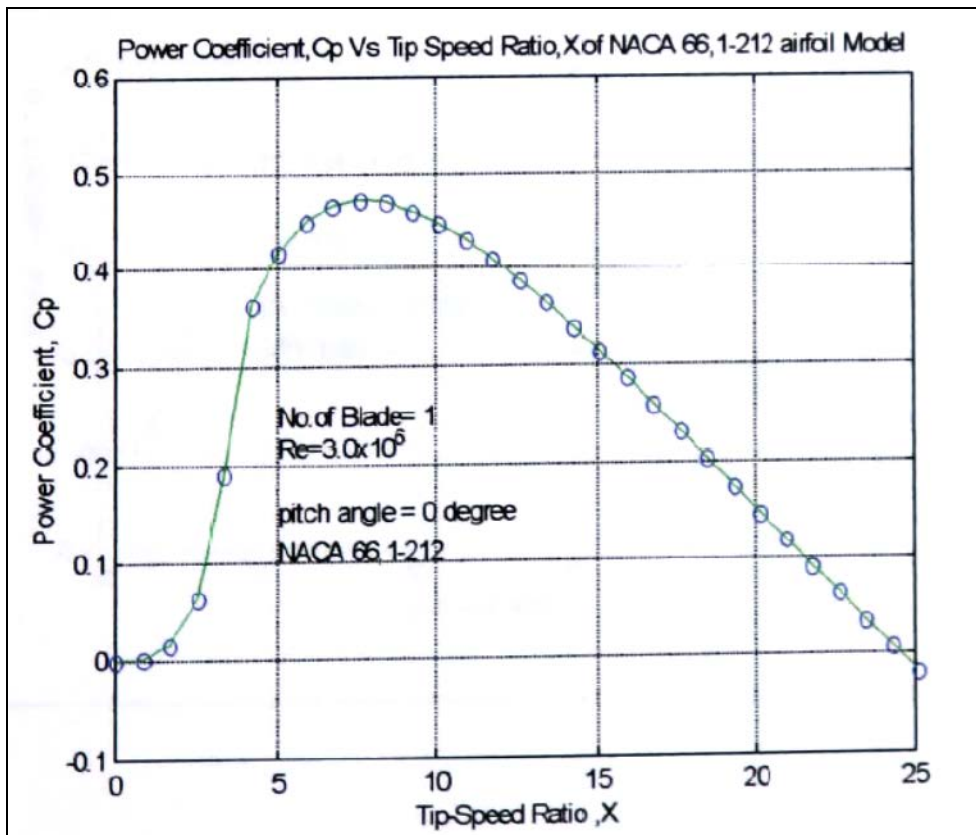
Appendix J

The Predicted Power Coefficient of NACA 661-212 with different number of blades

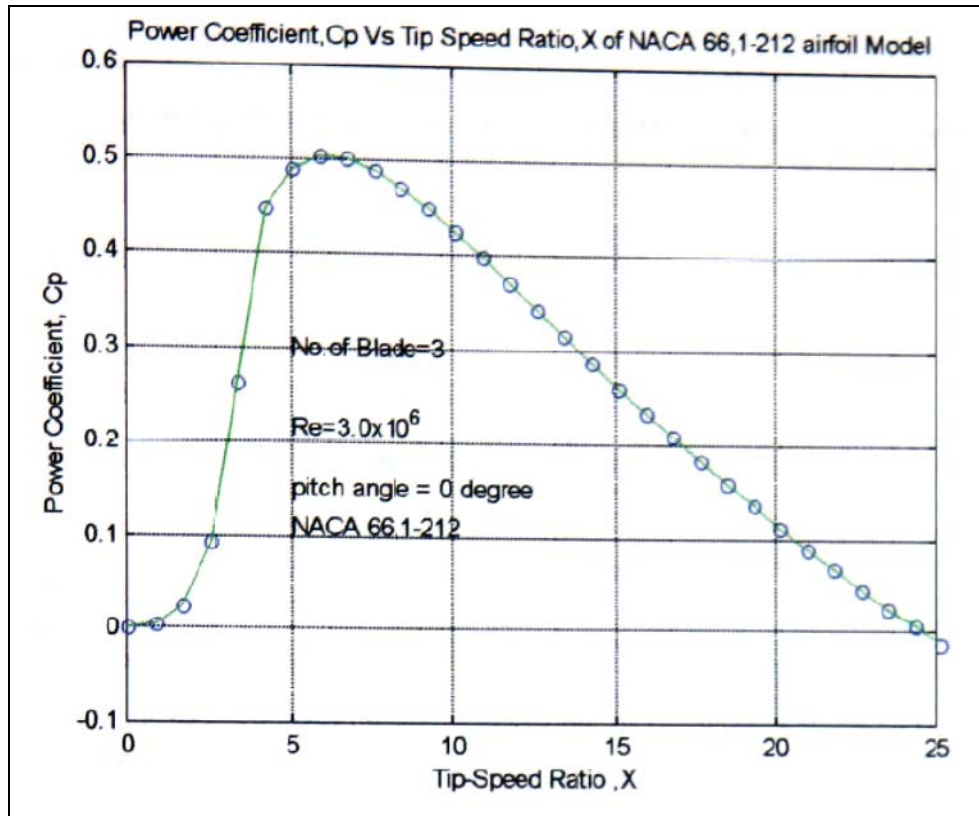
1. Number of blade = 1



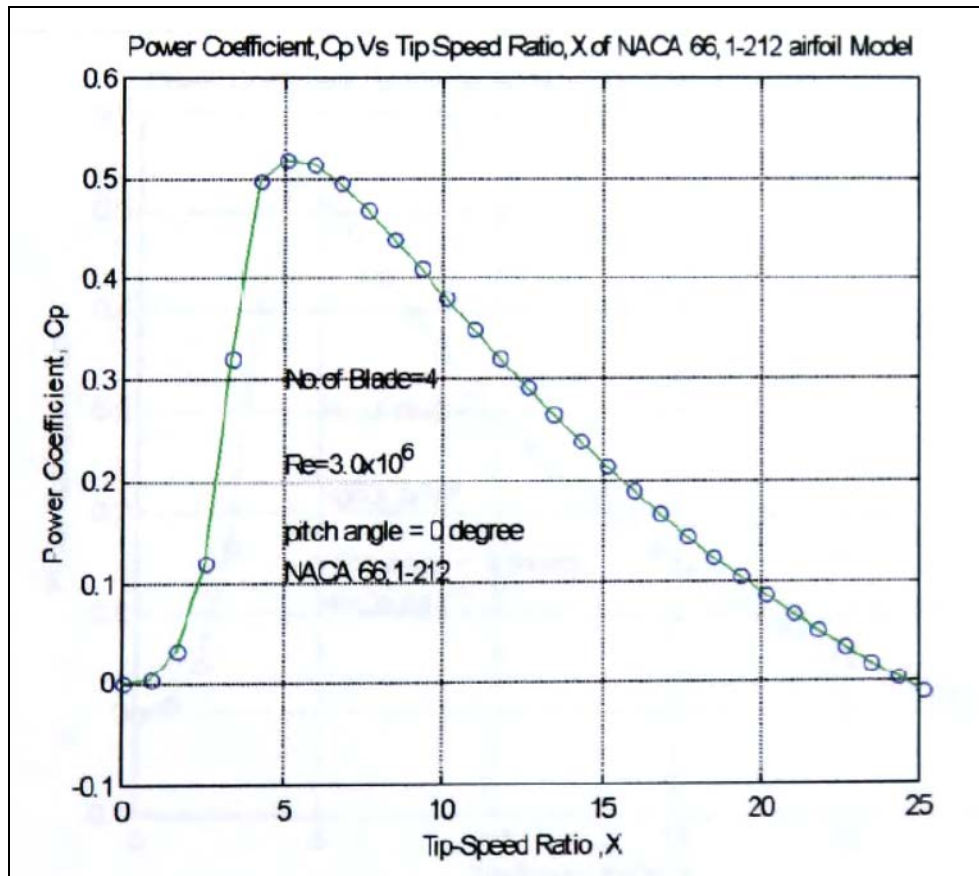
2. Number of blade = 2

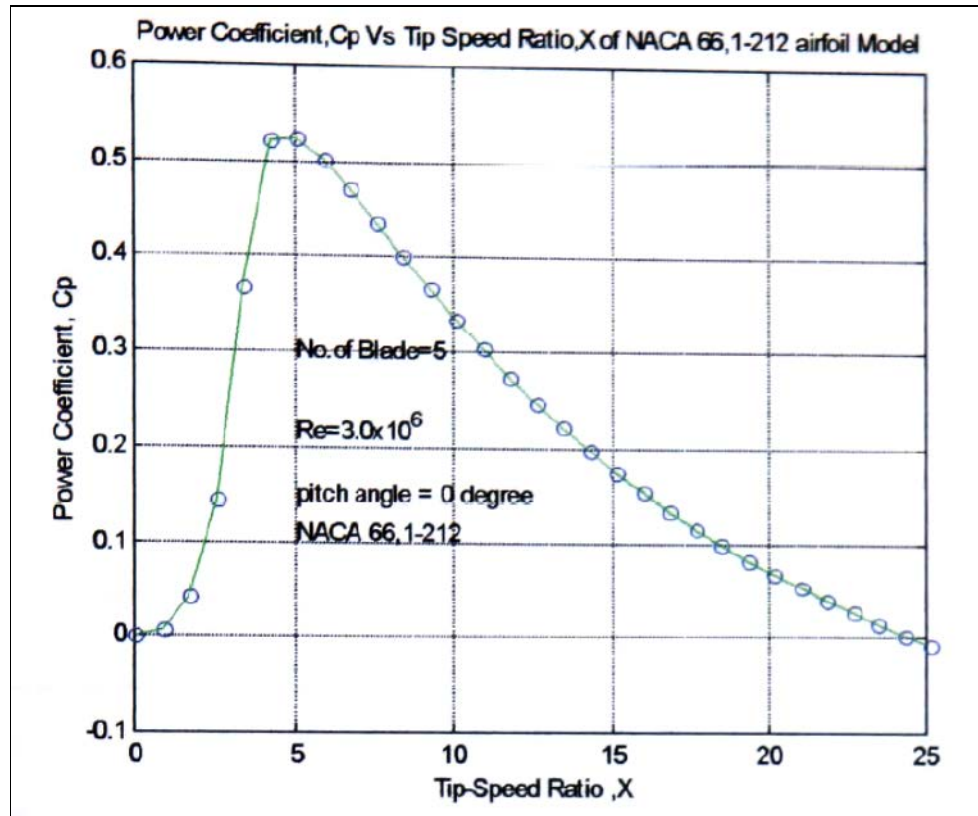
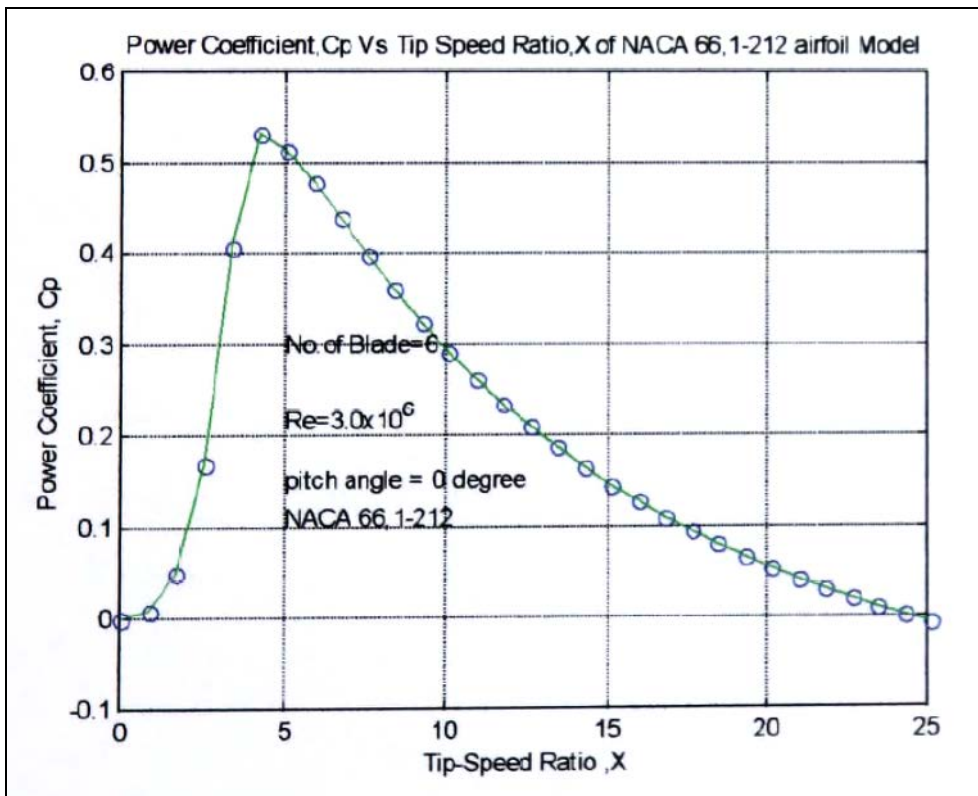


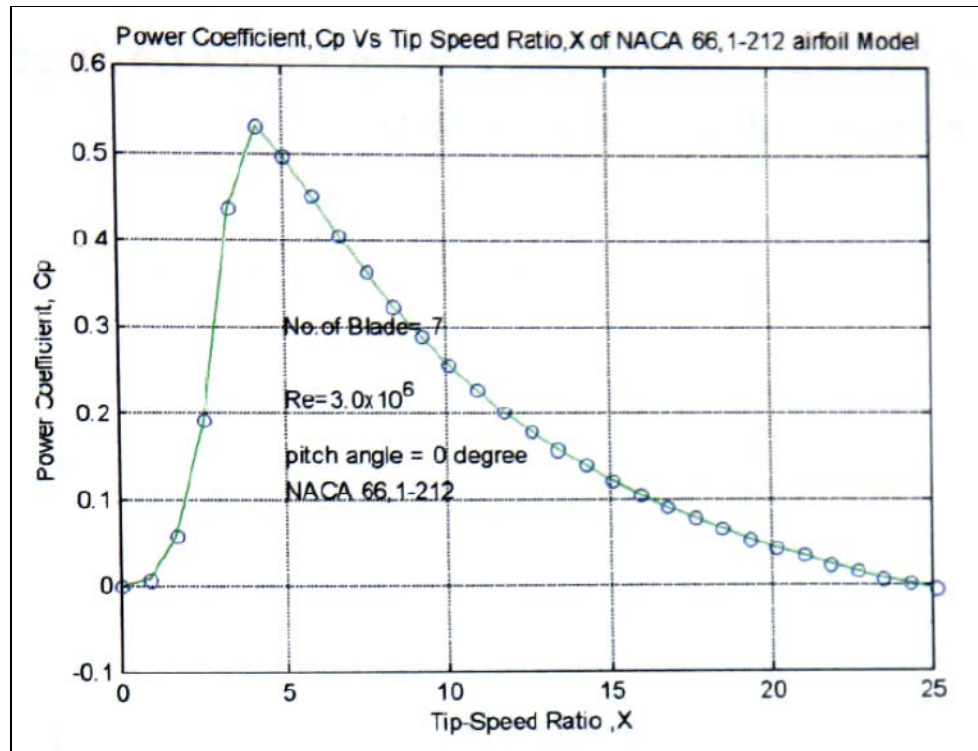
3. Number of blade = 3



4. Number of blade = 4



5. Number of blade = 5**6. Number of blade = 6**

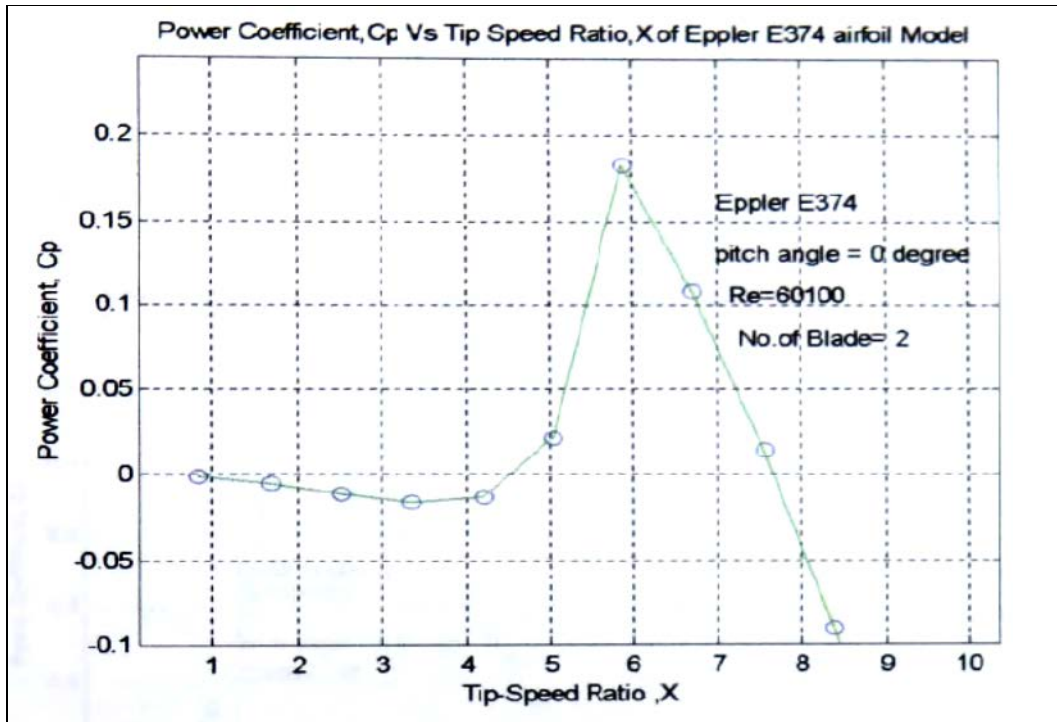
7. Number of blade = 7

Appendix K

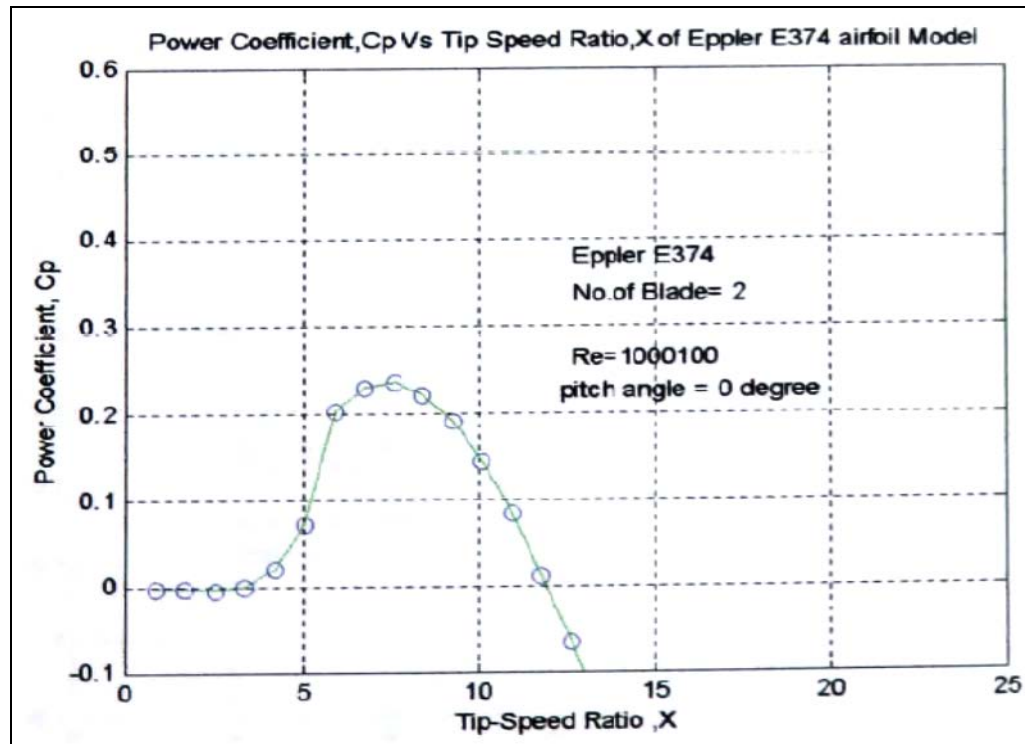
The Predicted Power Coefficients of Eppler E 374 aerofoil with different Reynolds numbers

Aerofoil: Eppler E 374 Aerofoil Geometry

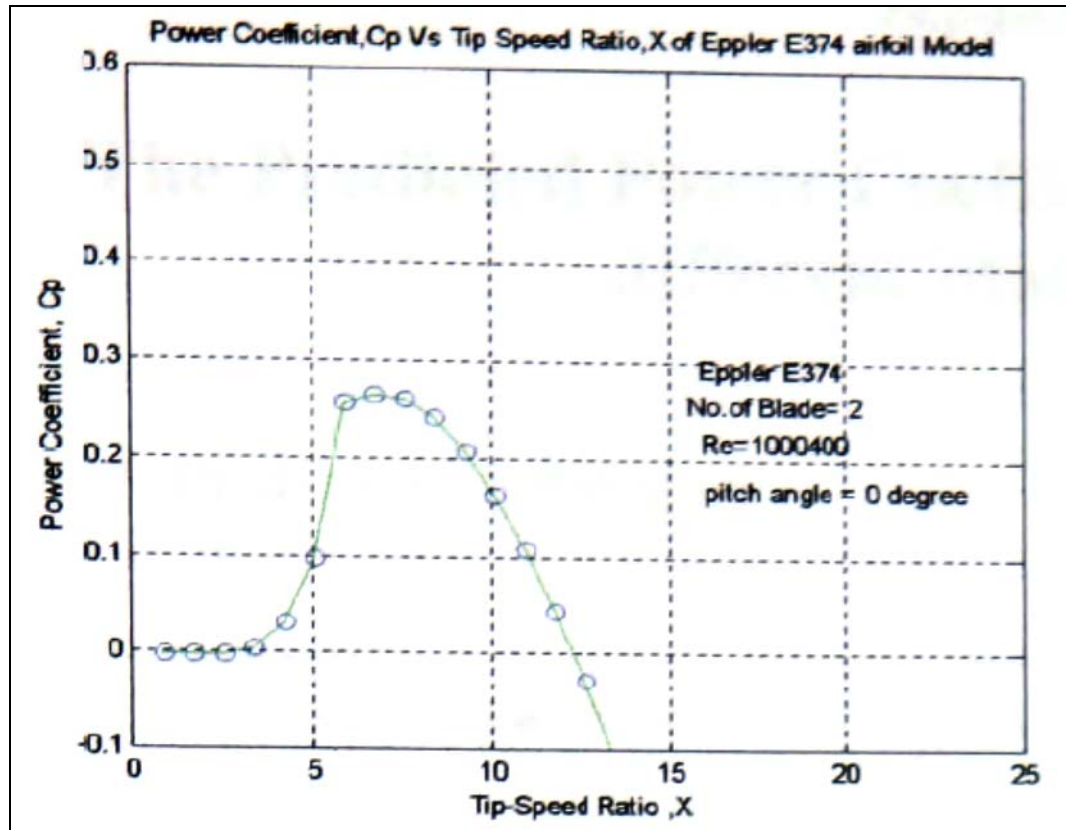
Re= 60100



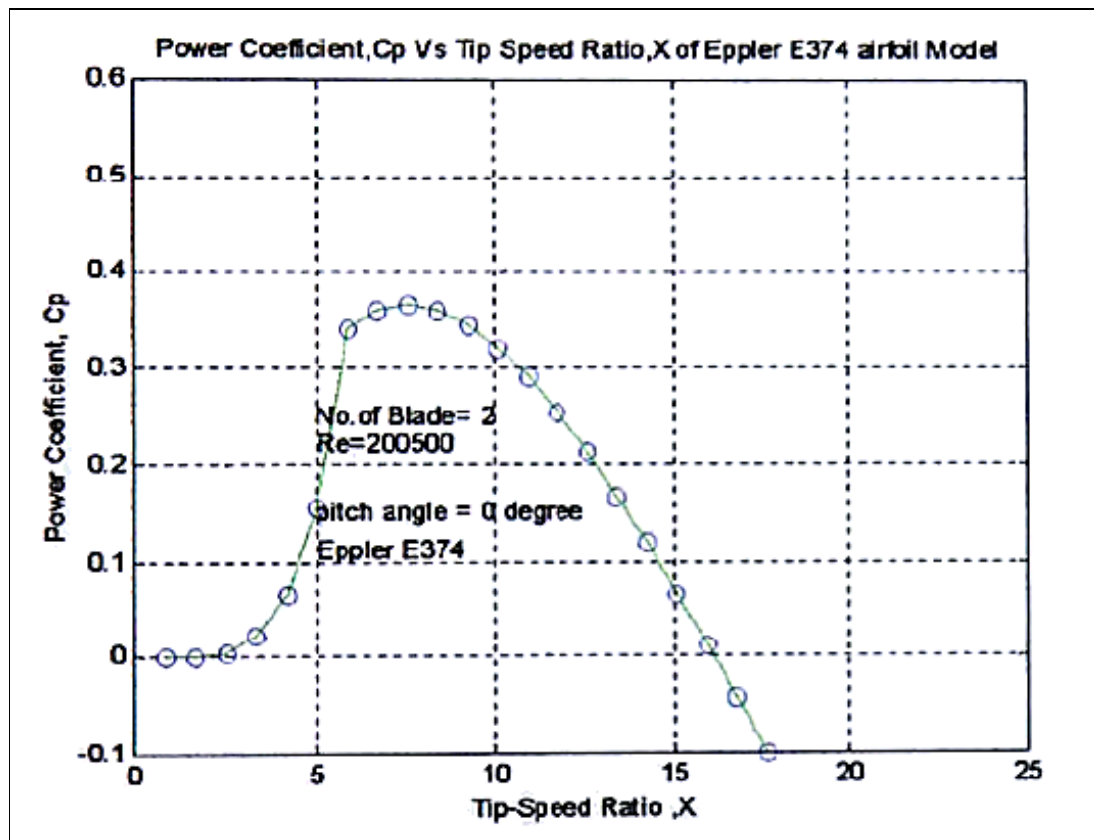
Re=100100



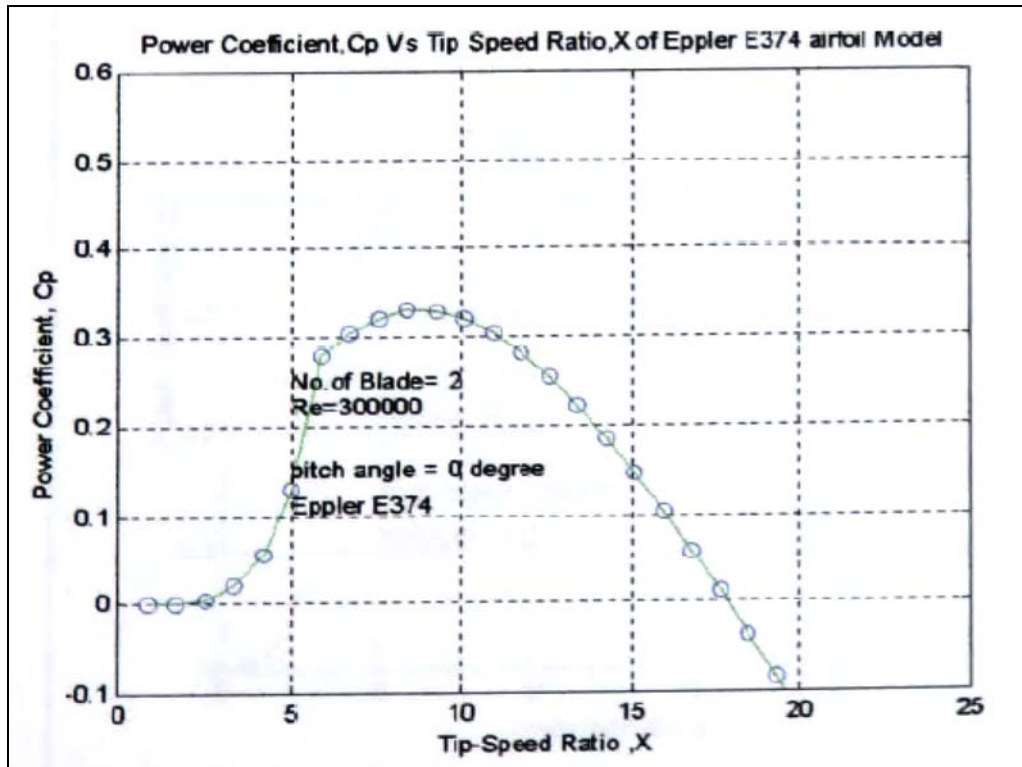
Re=100400



Re=200500



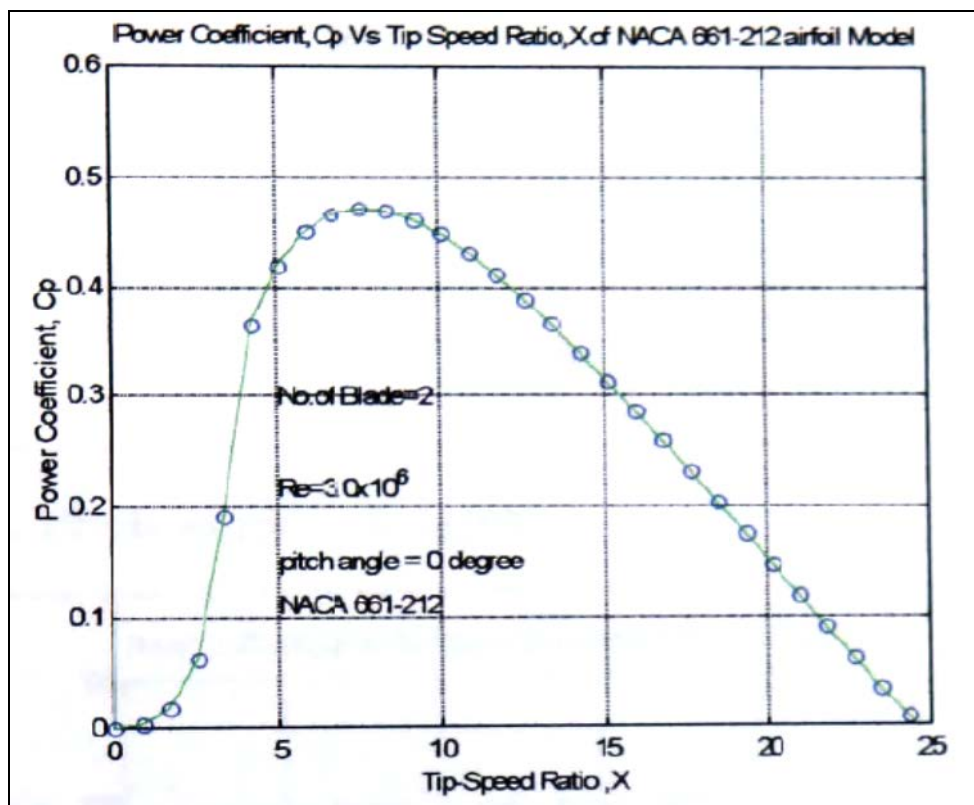
$Re=300000$



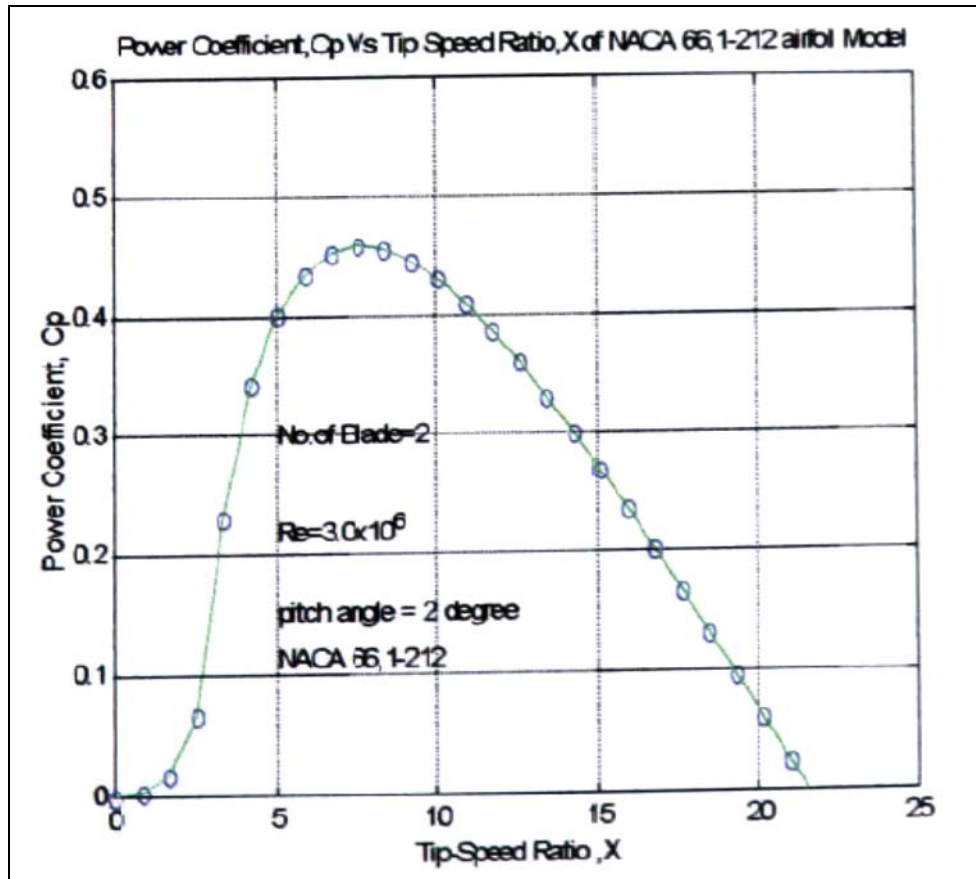
Appendix L

The Predicted Power Coefficients of NACA 661-212 with different blade pitch angles

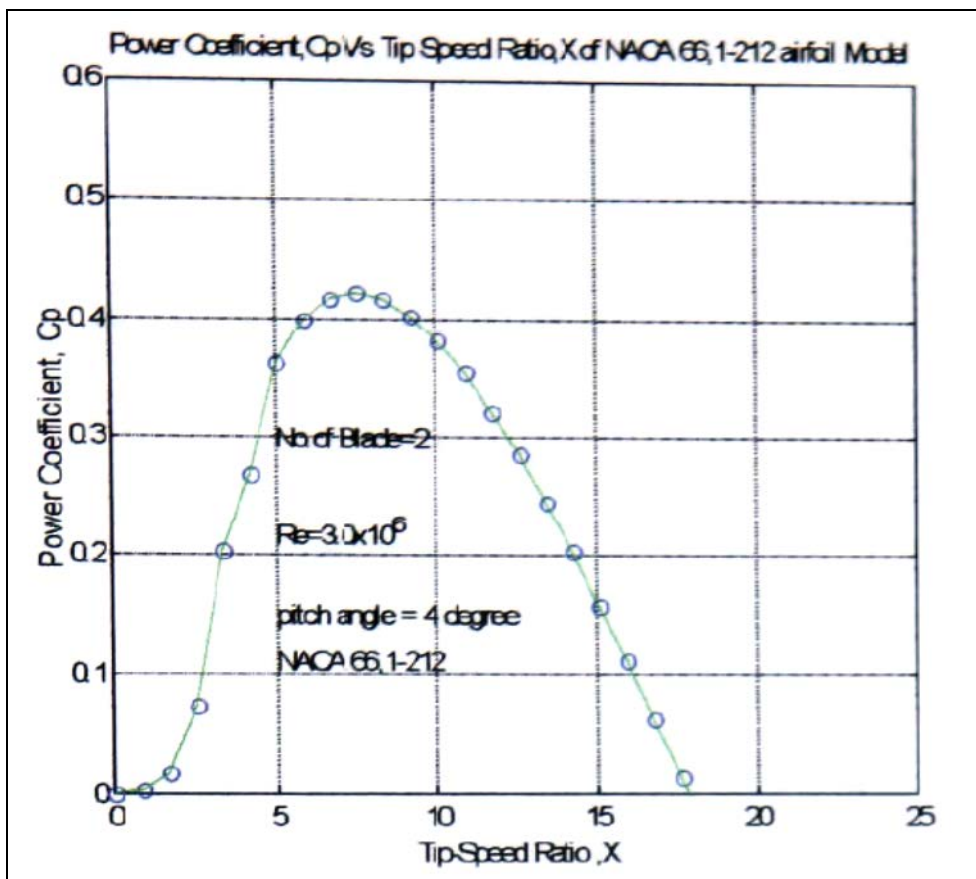
1. Pitch angle = 0 degree



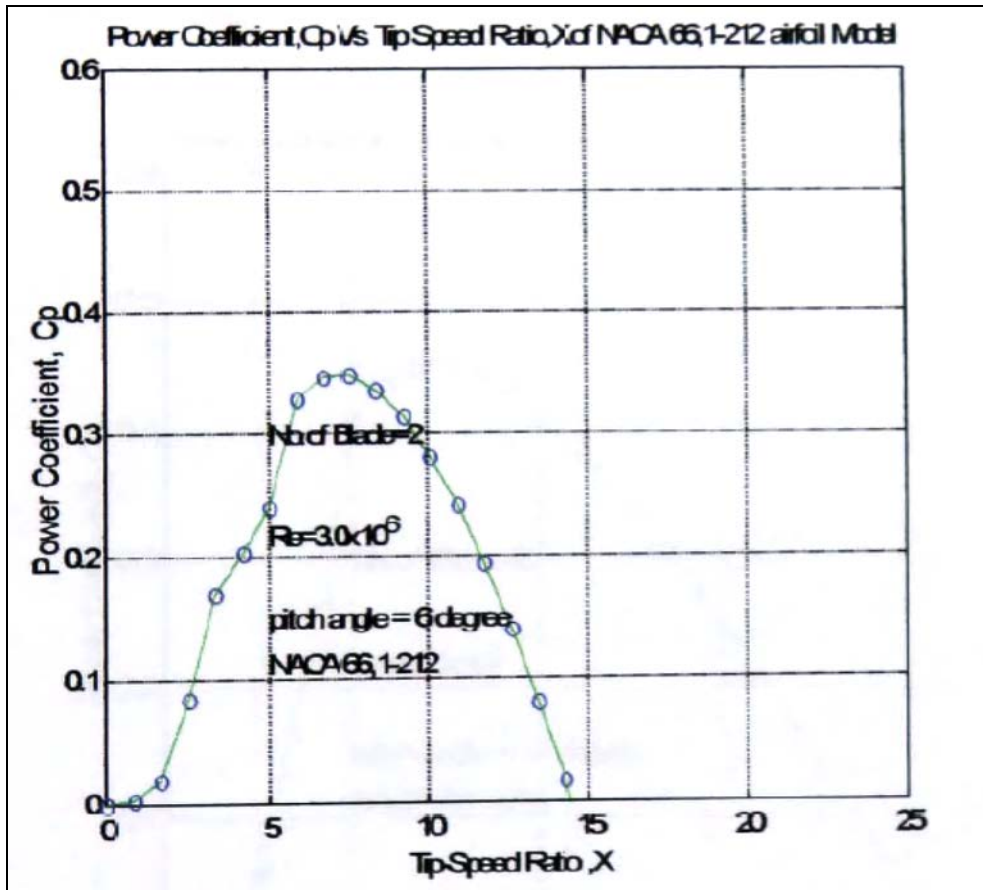
2. Pitch angle = 2 degree



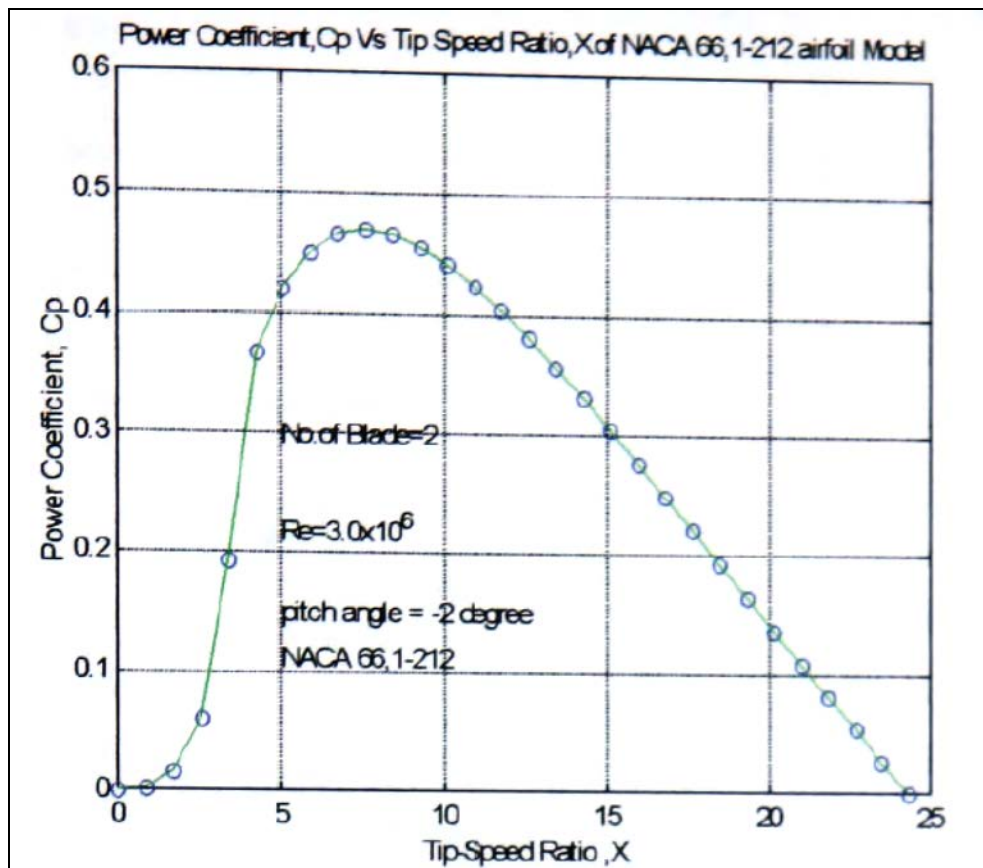
3. Pitch angle = 4 degree



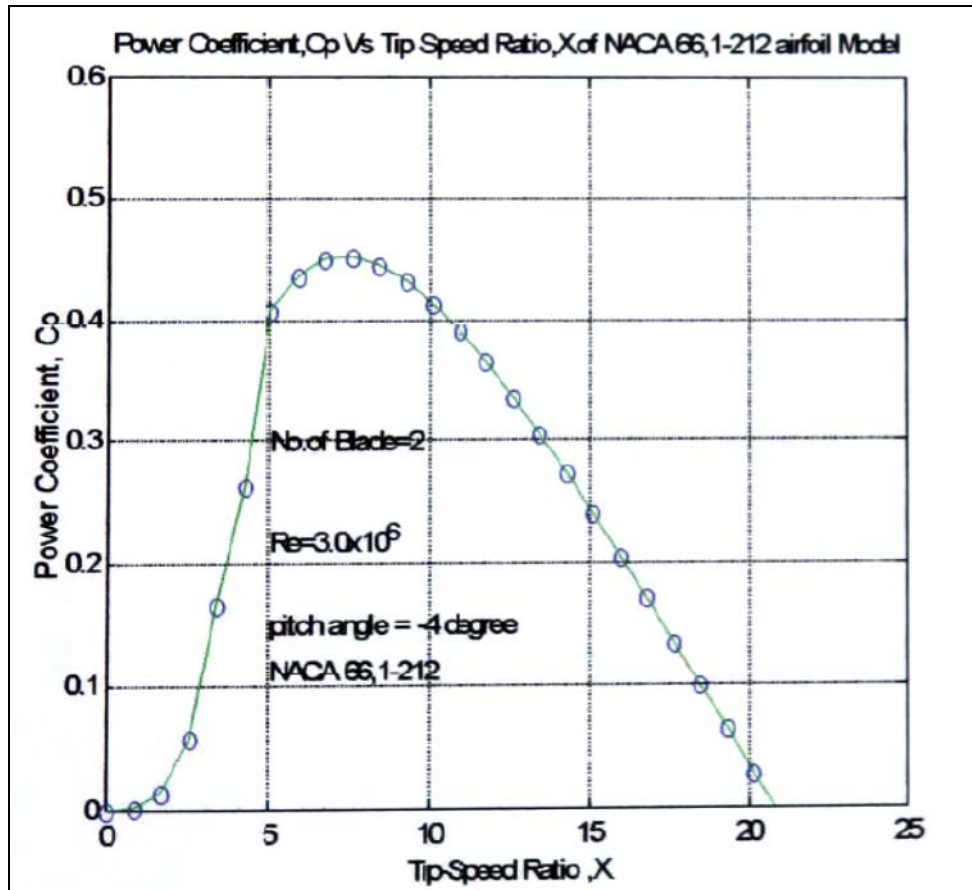
4. Pitch angle = 6 degree



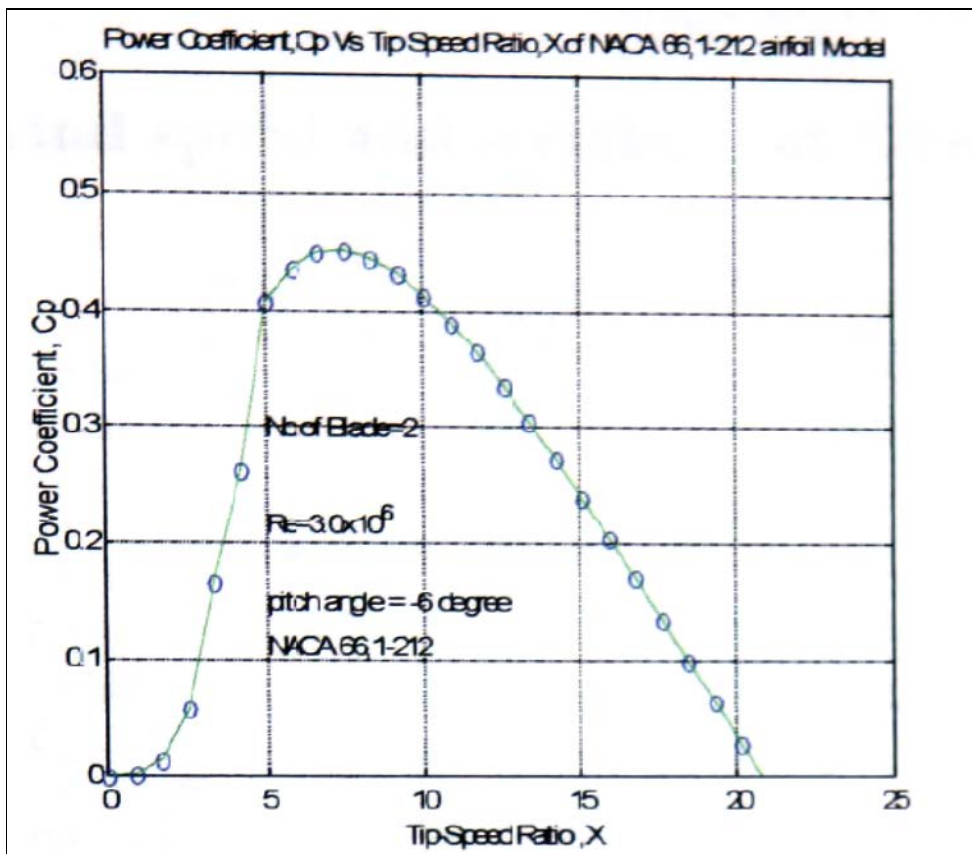
5. Pitch angle = -2 degree



6. Pitch angle = -4 degree



7. Pitch angle = -6 degree



Appendix M

The wind speed and weather conditions at Amble caravan site

Date-Time	WS	TP	WC	RH	HI	DP	WB	BP
Y-M-D-H:M:S	m/s	@C	@C	%	@C	@C	@C	Pa
2002-11-07-08:38:56	3.9	5.9	0.7	73.3	5.8	1.4	4	1008.8
2002-11-07-08:39:01	3.9	5.9	0.7	73.3	5.8	1.4	4	1008.7
2002-11-07-08:39:06	2.9	6	3	73.4	5.9	1.4	4	1008.8
2002-11-07-08:39:11	1.7	6	6	73.4	5.9	1.4	4	1008.8
2002-11-07-08:39:16	2.9	6	3	73.4	5.9	1.4	4	1008.8
2002-11-07-08:39:21	2.6	6	3.8	73.4	5.9	1.4	4	1008.8
2002-11-07-08:39:26	1.7	6	6	73.4	5.9	1.4	4	1008.8
2002-11-07-08:39:31	2	6.1	5.5	73.4	6	1.5	4.1	1008.8
2002-11-07-08:39:36	1.7	6.2	6.2	73.4	6.1	1.6	4.2	1008.8
2002-11-07-08:39:41	3.1	6.1	2.6	73.3	6	1.5	4.1	1008.8
2002-11-07-08:39:46	4.2	6	0.3	73.1	5.9	1.4	4	1008.8
2002-11-07-08:39:51	4.4	5.9	-0.2	73.1	5.8	1.4	4	1008.7
2002-11-07-08:39:56	3.1	6	2.5	73.1	5.9	1.4	4	1008.7
2002-11-07-08:40:01	1.4	6.1	6.1	73.2	6	1.5	4.1	1008.8
2002-11-07-08:40:06	1.1	6.3	6.3	73.3	6.2	1.7	4.3	1008.8
2002-11-07-08:40:11	2.1	6.3	5.4	73.3	6.2	1.7	4.3	1008.8
2002-11-07-08:40:16	2.2	6.3	5.1	73.1	6.2	1.7	4.3	1008.7
2002-11-07-08:40:21	4.2	6.2	0.5	73	6.1	1.6	4.2	1008.8
2002-11-07-08:40:26	5.3	6	-1.5	72.9	5.9	1.4	4	1008.7
2002-11-07-08:40:31	4.5	6	-0.2	72.9	5.9	1.4	4	1008.7
2002-11-07-08:40:36	3.5	6	1.7	73.1	5.9	1.4	4	1008.7
2002-11-07-08:40:41	2.8	6	3.2	73.2	5.9	1.4	4	1008.8
2002-11-07-08:40:46	2.6	6.1	3.9	73.2	6	1.5	4.1	1008.8
2002-11-07-08:40:51	2.3	6.1	4.7	73.2	6	1.5	4.1	1008.8
2002-11-07-08:40:56	3.2	6	2.3	73.1	5.9	1.4	4	1008.8
2002-11-07-08:41:01	3.8	6	1	73.1	5.9	1.4	4	1008.7
2002-11-07-08:41:06	2.9	6	3	73.1	5.9	1.4	4	1008.8
2002-11-07-08:41:11	1.2	6.1	6.1	73.1	6	1.5	4.1	1008.7
2002-11-07-08:41:16	1.7	6.2	6.2	73.2	6.1	1.6	4.2	1008.8
2002-11-07-08:41:21	4.2	6.1	0.4	73.1	6	1.5	4.1	1008.7
2002-11-07-08:41:26	3.5	6.2	1.9	73	6.1	1.6	4.2	1008.7
2002-11-07-08:41:31	3.8	6.1	1.2	73	6	1.5	4.1	1008.8
2002-11-07-08:41:36	5.4	6	-1.6	72.8	5.9	1.4	4	1008.7
2002-11-07-08:41:41	4.5	5.9	-0.3	72.7	5.8	1.4	4	1008.7
2002-11-07-08:41:46	2.2	6.1	4.9	72.8	6	1.5	4.1	1008.7
2002-11-07-08:41:51	4.6	6	-0.4	72.9	5.9	1.4	4	1008.7
2002-11-07-08:41:56	4.7	6	-0.5	72.9	5.9	1.4	4	1008.6
2002-11-07-08:42:01	4.7	5.9	-0.7	72.9	5.8	1.4	4	1008.6
2002-11-07-08:42:06	1.6	6.1	6.1	73.1	6	1.5	4.1	1008.7

Appendix N

The wind turbine field-test data of S1223 rotor blade at NaRec

T (N.m)	Rpm	Wind speed (m/s)	Omega (ω)	Power (P_w) (W)	Tip speed ratio (X)	Wind Energy (P_a)	C_p
2.5	33.45	6.5	3.501	8.75	0.54	336.42	0.026
2.8	35.61	6.4	3.727	10.44	0.58	321.13	0.032
2.3	29.36	4.1	3.073	7.07	0.75	84.43	0.084
3.8	34.2	4.2	3.580	13.60	0.85	90.76	0.150
4.5	34.1	4.4	3.569	16.06	0.81	104.35	0.154
4.8	31.2	6.7	3.266	15.67	0.49	368.43	0.043
5.8	26.3	5.3	2.753	15.97	0.52	182.37	0.088
6	28.9	5.9	3.025	18.15	0.51	251.59	0.072
4.5	34.5	4.2	3.611	16.25	0.86	90.76	0.179
4.8	31.8	5.4	3.328	15.98	0.62	192.89	0.083
5.5	35.1	4.6	3.674	20.21	0.80	119.24	0.169
7.5	34.54	4.9	3.615	27.11	0.74	144.12	0.188
7.1	31.83	5.9	3.332	23.65	0.56	251.59	0.094
4.2	41.83	5.8	4.378	18.39	0.75	239.01	0.077
3.2	32.51	4.9	3.403	10.89	0.69	144.12	0.076
4	31.71	4	3.319	13.28	0.83	78.40	0.169
3.01	42.3	4.5	4.427	13.33	0.98	111.63	0.119
4.8	47.58	5	4.980	23.90	1.00	153.13	0.156
6.6	45.23	5.9	4.734	31.24	0.80	251.59	0.124
5.3	44.73	6.9	4.682	24.81	0.68	402.42	0.062
4.7	49.35	5.8	5.165	24.28	0.89	239.01	0.102
3.5	53.2	4.5	5.568	19.49	1.24	111.63	0.175
6.9	35	5.6	3.663	25.28	0.65	215.13	0.117
3.8	40	4.8	4.187	15.91	0.87	135.48	0.117
7.6	36	5.01	3.768	28.64	0.75	154.05	0.186
7.9	31.71	5.9	3.319	26.22	0.56	251.59	0.104
8	35.63	5.6	3.729	29.83	0.67	215.13	0.139
7.5	31.25	4.8	3.271	24.53	0.68	135.48	0.181
4.6	31.5	5.2	3.297	15.17	0.63	172.24	0.088
5.6	35.61	4.6	3.727	20.87	0.81	119.24	0.175
7	34.21	5.2	3.581	25.06	0.69	172.24	0.146
4.7	35.23	4.8	3.687	17.33	0.77	135.48	0.128
7.1	33.15	5.9	3.470	24.63	0.59	251.59	0.098
3.6	31.05	4.2	3.250	11.70	0.77	90.76	0.129
7.1	31.04	5.2	3.249	23.07	0.62	172.24	0.134
7	38.15	5.9	3.993	27.95	0.68	251.59	0.111
8.5	31.83	6.3	3.332	28.32	0.53	306.31	0.092
7.1	26.3	5.4	2.753	19.54	0.51	192.89	0.101
7.5	27.2	5.9	2.847	21.35	0.48	251.59	0.085
4.2	34.1	5.9	3.569	14.99	0.60	251.59	0.060

Appendix N Continued...

4.1	38.52	4.7	4.032	16.53	0.86	127.18	0.130
4.5	26.35	5.1	2.758	12.41	0.54	162.50	0.076
4.8	19.25	4.6	2.015	9.67	0.44	119.24	0.081
6.9	36.25	8.6	3.794	26.18	0.44	779.17	0.034
4.9	36.23	7.9	3.792	18.58	0.48	603.97	0.031
6.1	37.63	5.2	3.939	24.03	0.76	172.24	0.139
4.9	36.33	5.3	3.803	18.63	0.72	182.37	0.102
6.3	26.56	4.9	2.780	17.51	0.57	144.12	0.122
3.51	36.24	3.9	3.793	13.31	0.97	72.67	0.183
4.1	38.36	4.8	4.015	16.46	0.84	135.48	0.122
3.3	35	5.6	3.663	12.09	0.65	215.13	0.056
4.8	37.23	8.7	3.897	18.70	0.45	806.67	0.023
3.9	32.15	4.5	3.365	13.12	0.75	111.63	0.118
6.6	35	5.7	3.663	24.18	0.64	226.86	0.107
4.5	32.15	5.6	3.365	15.14	0.60	215.13	0.070
4.1	35	4.6	3.663	15.02	0.80	119.24	0.126
5.7	34.14	6.8	3.573	20.37	0.53	385.18	0.053
2.8	35	6.3	3.663	10.26	0.58	306.31	0.033
3.5	33.64	5	3.521	12.32	0.70	153.13	0.080
4	34.23	5.2	3.583	14.33	0.69	172.24	0.083
4.6	35.33	5.6	3.698	17.01	0.66	215.13	0.079
8.9	31.25	6.8	3.271	29.11	0.48	385.18	0.076
7.8	35	6.9	3.663	28.57	0.53	402.42	0.071
8.8	36.51	6.4	3.821	33.63	0.60	321.13	0.105
10	36.13	6.6	3.782	37.82	0.57	352.18	0.107
3.9	35	5.1	3.663	14.29	0.72	162.50	0.088
4.8	39.21	6.8	4.104	19.70	0.60	385.18	0.051
9.5	70	7.5	7.327	69.60	0.98	516.80	0.135
3.5	31.23	3.8	3.269	11.44	0.86	67.22	0.170
4	32.09	4	3.359	13.44	0.84	78.40	0.171
3.6	34.91	5.1	3.654	13.15	0.72	162.50	0.081
5.6	31.25	5.8	3.271	18.32	0.56	239.01	0.077
5.8	31.12	5.1	3.257	18.89	0.64	162.50	0.116
4	33.03	4.5	3.457	13.83	0.77	111.63	0.124
8.9	37.21	5.6	3.895	34.66	0.70	215.13	0.161
9.6	32.03	6.4	3.352	32.18	0.52	321.13	0.100
8.91	30.03	7.2	3.143	28.01	0.44	457.23	0.061
4.8	31.54	7.5	3.301	15.85	0.44	516.80	0.031
6.6	38.51	7.9	4.031	26.60	0.51	603.97	0.044
8.23	34.25	7.1	3.585	29.50	0.50	438.44	0.067
3.85	37.05	4.2	3.878	14.93	0.92	90.76	0.165
6.5	34.02	5.2	3.561	23.14	0.68	172.24	0.134
7.88	34.06	5.6	3.565	28.09	0.64	215.13	0.131
4	35.61	6.6	3.727	14.91	0.56	352.18	0.042
7.8	39.61	5.4	4.146	32.34	0.77	192.89	0.168
8.01	36.99	5.2	3.872	31.01	0.74	172.24	0.180
4.6	38.25	5.1	4.004	18.42	0.79	162.50	0.113

Appendix N Continued...

4.8	34.63	4.7	3.625	17.40	0.77	127.18	0.137
5	23.11	4.2	2.419	12.09	0.58	90.76	0.133
4	31.25	3.9	3.271	13.08	0.84	72.67	0.180
6	35.12	4.8	3.676	22.06	0.77	135.48	0.163
5.23	21.53	5.6	2.253	11.79	0.40	215.13	0.055
4.59	32.5	5.8	3.402	15.61	0.59	239.01	0.065
5.96	21.25	4.6	2.224	13.26	0.48	119.24	0.111
4.58	18.96	5.9	1.984	9.09	0.34	251.59	0.036
4.5	35.15	4.6	3.679	16.56	0.80	119.24	0.139
4.5	35.16	5.8	3.680	16.56	0.63	239.01	0.069
8	45.21	5.6	4.732	37.86	0.84	215.13	0.176
6.6	35.9	4.8	3.758	24.80	0.78	135.48	0.183
7.1	23.45	5.1	2.454	17.43	0.48	162.50	0.107
5.5	35.61	4.6	3.727	20.50	0.81	119.24	0.172
4.3	23.54	4.9	2.464	10.59	0.50	144.12	0.074
8.5	36.98	5.6	3.871	32.90	0.69	215.13	0.153
4.6	39.15	5.9	4.098	18.85	0.69	251.59	0.075
5.3	19.25	5.3	2.015	10.68	0.38	182.37	0.059
5.6	27.89	5.1	2.919	16.35	0.57	162.50	0.101
9.4	18.56	5.8	1.943	18.26	0.33	239.01	0.076
10	16.89	5.4	1.768	17.68	0.33	192.89	0.092
3.5	26.84	5.2	2.809	9.83	0.54	172.24	0.057
7.5	36.61	5.7	3.832	28.74	0.67	226.86	0.127
5.6	26.36	5.3	2.759	15.45	0.52	182.37	0.085
7.89	25.25	6.3	2.643	20.85	0.42	306.31	0.068
3.54	39.62	4.5	4.147	14.68	0.92	111.63	0.132
7.56	40.25	5.3	4.213	31.85	0.79	182.37	0.175
4.5	30	4	3.140	14.13	0.79	78.40	0.180
4.25	35.62	5.3	3.728	15.84	0.70	182.37	0.087
4.8	33.23	5.8	3.478	16.69	0.60	239.01	0.070
6.8	32.13	5.6	3.363	22.87	0.60	215.13	0.106
8.9	35.95	6.5	3.763	33.49	0.58	336.42	0.100
7.6	45.62	8.9	4.775	36.29	0.54	863.59	0.042
9.1	31.23	8.6	3.269	29.75	0.38	779.17	0.038
9.5	39.6	6.9	4.145	39.38	0.60	402.42	0.098
6.8	39.61	5.3	4.146	28.19	0.78	182.37	0.155
8.29	35.24	5.6	3.688	30.58	0.66	215.13	0.142
4.61	30.24	5.1	3.165	14.59	0.62	162.50	0.090
3	31.58	5.8	3.305	9.92	0.57	239.01	0.041
4.8	38.96	5.5	4.078	19.57	0.74	203.81	0.096
6.9	34.56	5.8	3.617	24.96	0.62	239.01	0.104
5.5	33.15	5.1	3.470	19.08	0.68	162.50	0.117
4.8	33.25	5.6	3.480	16.70	0.62	215.13	0.078
8.2	22.03	5.6	2.306	18.91	0.41	215.13	0.088
5.3	19.54	4.6	2.045	10.84	0.44	119.24	0.091
4.5	18.47	5.9	1.933	8.70	0.33	251.59	0.035
7.9	20.13	8.9	2.107	16.64	0.24	863.59	0.019
4	12.35	5.1	1.293	5.17	0.25	162.50	0.032

Appendix N Continued...

3.8	13.25	5.4	1.387	5.27	0.26	192.89	0.027
4.2	33.21	4.1	3.476	14.60	0.85	84.43	0.173
11	33.14	5.9	3.469	38.16	0.59	251.59	0.152
8.87	33.12	6.3	3.467	30.75	0.55	306.31	0.100
5.6	12.35	5.9	1.293	7.24	0.22	251.59	0.029
4.6	18.96	6.7	1.984	9.13	0.30	368.43	0.025
3.4	12.56	6.9	1.315	4.47	0.19	402.42	0.011
4.3	23.56	5.6	2.466	10.60	0.44	215.13	0.049
8.6	34.59	8.9	3.620	31.14	0.41	863.59	0.036
4	45.25	5.1	4.736	18.94	0.93	162.50	0.117
5.54	50.21	5.7	5.255	29.11	0.92	226.86	0.128
7.8	55.12	6.9	5.769	45.00	0.84	402.42	0.112
8.95	45.23	8.6	4.734	42.37	0.55	779.17	0.054
6.8	50.21	6.1	5.255	35.74	0.86	278.05	0.129
5.9	45.23	5.3	4.734	27.93	0.89	182.37	0.153
9.1	42.35	6.2	4.433	40.34	0.71	291.95	0.138
9.8	12.35	5.3	1.293	12.67	0.24	182.37	0.069
9.5	19.56	5.2	2.047	19.45	0.39	172.24	0.113
5	20.23	5.8	2.117	10.59	0.37	239.01	0.044
7.1	50.12	6.8	5.246	37.25	0.77	385.18	0.097
5	45.23	5.2	4.734	23.67	0.91	172.24	0.137
5.86	51.23	8.5	5.362	31.42	0.63	752.30	0.042
9.84	45.12	6	4.723	46.47	0.79	264.60	0.176
9.8	12.25	5.2	1.282	12.57	0.25	172.24	0.073
4.58	35.25	6.6	3.690	16.90	0.56	352.18	0.048
7.85	55.22	5.9	5.780	45.37	0.98	251.59	0.180
4.89	45.8	5.1	4.794	23.44	0.94	162.50	0.144
10.23	23.1	7	2.418	24.73	0.35	420.18	0.059
10.5	42.3	7.1	4.427	46.49	0.62	438.44	0.106
0	0	0	0.000	0.00	0.00	0.00	0.000
2.5	10	4	1.047	2.62	0.26	78.40	0.033
5.85	5	5	0.523	3.06	0.10	153.13	0.020
4.5	6	4.8	0.628	2.83	0.13	135.48	0.021
11.5	75	7.5	7.850	90.28	1.05	516.80	0.175
9.5	80	7	8.373	79.55	1.20	420.18	0.189
9	81	7.15	8.478	76.30	1.19	447.77	0.170

Appendix O

The wind turbine field-test data of S1223+SCT at NaRec, Blyth

T (N.m)	Rpm	Wind speed (m/s)	Omega (ω)	Power (P_w) (W)	Tip speed ratio (X)	Wind Energy (P_a)	C_p
1.25	23	6	2.407	3.009	0.401	264.6	0.01
1.8	33	5.4	3.454	6.217	0.640	192.8934	0.03
1.3	28	4	2.931	3.810	0.733	78.4	0.05
1.1	33	3.4	3.454	3.799	1.016	48.1474	0.08
2.1	32	4	3.349	7.034	0.837	78.4	0.09
1.9	29.2	6	3.056	5.807	0.509	264.6	0.02
2.1	25.6	5	2.679	5.627	0.536	153.13	0.04
2.5	25.8	4.9	2.700	6.751	0.551	144.12	0.05
2.2	32.5	4.2	3.402	7.484	0.810	90.758	0.08
1.8	30.1	5.3	3.150	5.671	0.594	182.3743	0.03
2.1	34.5	4	3.611	7.583	0.903	78.4	0.10
1.9	34	3.9	3.559	6.761	0.912	72.67	0.09
2.1	31	4.9	3.245	6.814	0.662	144.12	0.05
2.1	42	5.8	3.396	9.232	0.758	239.0	0.04
1.52	32	4.8	3.349	5.091	0.968	135.5	0.04
2	30.9	4	3.234	6.468	0.809	78.4	0.08
1.5	42	3.8	4.396	6.594	1.157	67.22	0.10
2.2	46.9	5	4.909	10.800	0.982	153.13	0.07
2.2	45.8	7.8	4.794	10.546	0.615	581.33	0.02
2.3	44	6	4.605	10.592	0.768	264.6	0.04
2.1	48	5	5.024	10.550	1.005	153.13	0.07
1	52.5	4.2	5.495	5.495	1.308	90.76	0.06
2.5	35	4.9	3.663	9.158	0.748	144.12	0.06
1.8	39	6	4.082	7.348	0.680	264.6	0.03
2.1	36	4.2	3.768	7.913	0.897	90.76	0.09
2.2	31.5	5.8	3.297	7.253	0.568	239.01	0.03
2.1	35.6	5.5	3.726	7.825	0.677	203.81	0.04
1.9	31.2	4.7	3.266	6.205	0.695	127.18	0.05
1.8	30	5.12	3.140	5.652	0.613	164.42	0.03
2.5	35	4.52	3.663	9.158	0.810	113.12	0.08
2.1	34	5.2	3.559	7.473	0.684	172.24	0.04
2.4	34.5	4.5	3.611	8.666	0.802	111.63	0.08
2.2	33.5	5.7	3.506	7.714	0.615	226.86	0.03
2.4	30.5	4.1	3.192	7.662	0.779	84.43	0.09
2.5	30.85	5.1	3.229	8.072	0.633	162.50	0.05
1.5	37.96	5.7	3.973	5.960	0.967	226.86	0.03
1.8	30.23	6.1	3.164	5.695	0.519	278.05	0.02
1.9	35	5.1	2.617	4.972	0.513	162.50	0.03
2.5	35.4	5.23	3.659	6.646	0.508	175.243	0.04
1.9	33.5	5.7	3.506	6.662	0.615	226.861	0.03

Appendix O Continued...

2.1	37.8	4.5	3.956	8.308	0.879	111.628	0.07
2.2	26.35	5	2.758	6.068	0.552	153.125	0.04
2.3	19.25	4.2	2.015	4.634	0.480	90.758	0.05
2.8	35.6	7.9	3.726	10.433	0.472	603.973	0.02
2.4	33.6	7.5	3.517	8.440	0.469	516.797	0.02
0.5	36.8	5.1	3.852	1.926	0.755	162.497	0.01
0.9	35.9	5.3	3.758	3.382	0.709	182.374	0.02
0.9	25.9	4.2	2.711	2.440	0.645	90.758	0.03
1.2	35.42	3.8	3.707	4.449	0.976	67.218	0.07
1.3	37.45	4.5	3.920	5.096	0.871	111.628	0.05
1.8	31	5.1	3.245	5.840	0.636	162.497	0.04
1.4	36	8.4	3.768	5.275	0.449	726.062	0.01
0.8	32.5	4.2	3.402	2.721	0.810	90.758	0.03
1.4	34	5.9	3.559	4.982	0.603	251.589	0.02
1.25	31.2	5.5	3.266	4.082	0.594	203.809	0.02
1.8	34.5	4.5	3.611	6.500	0.802	111.628	0.06
1.5	33.4	6.7	3.496	5.244	0.522	368.435	0.01
1.6	33.6	6.2	3.517	5.627	0.567	291.952	0.02
1.7	33.4	4.1	3.496	5.943	0.853	84.428	0.07
1.8	34.23	5.2	3.583	6.449	0.689	172.245	0.04
1.5	35.33	5.4	3.698	5.547	0.685	192.893	0.03
1.6	31.25	6.8	3.271	5.233	0.481	385.179	0.01
1.9	33.9	6.5	3.548	6.742	0.546	336.416	0.02
1.4	35.62	6.3	3.728	5.220	0.592	306.308	0.02
1.5	36.5	6.1	3.820	5.731	0.626	278.052	0.02
2.1	33.4	4.1	3.496	7.341	0.853	84.428	0.09
1.9	38.9	6.2	4.072	7.736	0.657	291.592	0.03
1.5	48.6	4.2	5.087	7.630	1.211	90.758	0.08
1.6	30.2	3.5	3.161	5.057	0.903	52.522	0.10
1	32.09	4.1	3.359	3.359	0.819	84.428	0.04
1.5	34.91	5	3.654	5.481	0.731	153.125	0.04
1.8	31.25	5.7	3.271	5.888	0.574	226.861	0.03
1	31.12	5	3.257	3.257	0.651	153.125	0.02
2.9	33.03	4.5	3.457	10.026	0.768	111.628	0.09
0.6	34.5	5.1	3.611	2.167	0.708	162.497	0.01
1.2	32.5	6.2	3.402	4.082	0.549	291.952	0.01
1.5	30.1	7.1	3.150	4.726	0.444	438.441	0.01
1.8	31.54	7	3.301	5.942	0.472	420.175	0.01
2.2	38.51	7.4	4.031	8.868	0.545	496.399	0.02
1.9	34.25	6.9	3.585	6.811	0.520	402.424	0.02
0.9	37.05	4.1	3.878	3.490	0.946	84.428	0.04
0.7	34.02	5.3	3.561	2.943	0.672	182.374	0.01
0.6	33.4	5.8	3.496	2.098	0.603	239.012	0.01
1.5	35.9	6.1	3.758	5.636	0.616	278.052	0.02
1.8	39.4	5.4	4.124	7.423	0.764	192.893	0.04
1.4	36.4	5.1	3.810	5.334	0.747	162.497	0.03
2.6	38.2	4.8	3.998	10.395	0.833	135.475	0.08

Appendix O Continued...

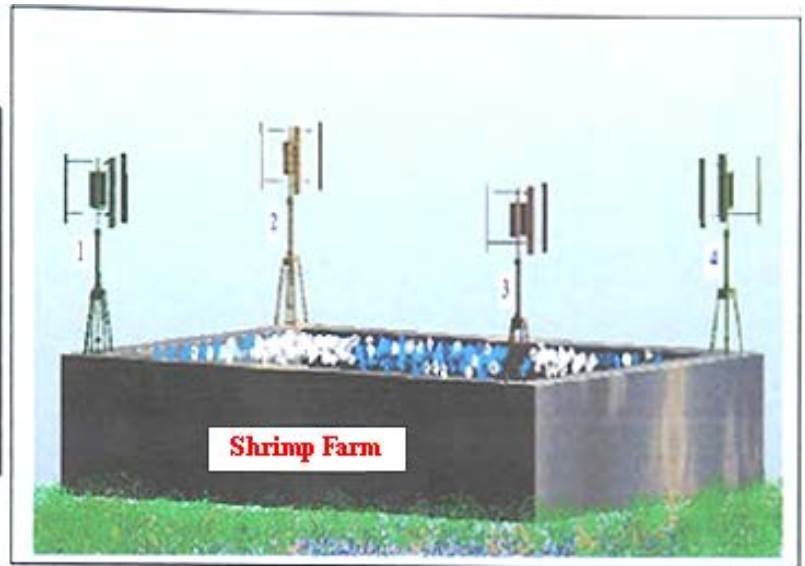
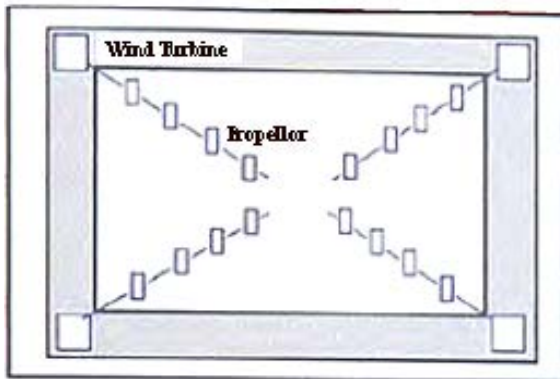
1.5	34.1	4.5	3.569	5.354	0.793	111.628	0.05
1.4	22.45	4.3	2.350	3.290	0.546	97.396	0.03
0.89	31.25	3.9	3.271	2.911	0.839	72.666	0.04
0.78	35.12	4.8	3.676	2.867	0.766	135.475	0.02
1.45	21.53	5.8	2.253	3.268	0.389	239.012	0.01
1.5	32.5	5.1	3.402	5.103	0.667	162.497	0.03
0.95	21.25	4.5	2.224	2.113	0.494	111.628	0.02
1.23	18.96	5.8	1.984	2.441	0.342	239.012	0.01
1.4	35.15	4.5	3.679	5.151	0.818	111.628	0.05
1.5	33.56	5.9	3.513	5.269	0.595	251.589	0.02
1.36	42.5	5.4	4.448	6.050	0.824	192.893	0.03
1.45	35.9	4.5	3.758	5.448	0.835	111.628	0.05
1.47	23.5	5	2.460	3.616	0.492	153.125	0.02
1.42	35.2	4.52	3.684	5.232	0.815	113.123	0.05
1.2	23.56	4.8	2.466	2.959	0.514	135.475	0.02
2.01	35.9	5.6	3.758	7.553	0.671	215.130	0.04
0.96	38.6	5.9	4.040	3.879	0.685	251.589	0.02
0.89	20.1	5.1	2.104	1.872	0.413	162.497	0.01
1.56	25	5	2.617	4.082	0.523	153.125	0.03
1.89	20	5.6	2.093	3.956	0.374	215.130	0.02
1.9	15.9	4.8	1.664	3.162	0.347	135.475	0.02
2.3	25.6	5.1	2.679	6.163	0.525	162.497	0.04
1.8	35.2	5.45	3.684	6.632	0.676	198.301	0.03
1.5	26.1	5.2	2.732	4.098	0.525	172.245	0.02
1.6	25.25	6.2	2.643	4.229	0.426	291.952	0.01
1.4	38.9	4.21	4.072	5.700	0.967	91.408	0.06
2.4	40	5.4	4.187	10.048	0.775	192.893	0.05
0.8	45	3.5	4.710	3.768	1.346	52.522	0.07
1.9	30	5.9	3.140	5.996	0.532	251.589	0.02
2.4	33	5.4	3.454	8.290	0.640	192.893	0.04
1.6	32.1	5.46	3.360	5.376	0.615	199.395	0.03
1.5	35.4	6.2	3.705	5.558	0.598	291.592	0.02
1.9	45	8.7	4.710	8.949	0.541	806.666	0.01
2.3	31	8.5	3.245	7.463	0.382	752.303	0.01
2.45	38.9	6.2	4.072	9.975	0.657	291.952	0.03
1.59	39.61	5.1	4.146	6.592	0.813	162.497	0.04
1.4	35.24	3.5	3.688	5.164	1.054	52.522	0.10
1.6	30.24	5	3.165	5.064	0.633	153.125	0.03
1.4	31.58	5.4	3.305	4.628	0.612	192.893	0.02
1.23	38.96	4.8	4.078	5.016	0.850	135.475	0.04
2.1	34.2	5.8	3.580	7.517	0.617	239.012	0.03
1.89	32.5	5.1	3.402	6.429	0.667	162.497	0.04
2.45	29.8	5.8	3.119	7.642	0.538	239.012	0.03
2.41	22.03	5.6	2.306	5.557	0.412	215.130	0.03
1.23	19.54	4.5	2.045	2.516	0.454	111.628	0.02
1.7	18.47	5.8	1.933	3.286	0.333	239.012	0.01
1.23	20.45	8.5	2.140	2.633	0.252	752.303	0.00

Appendix O Continued...

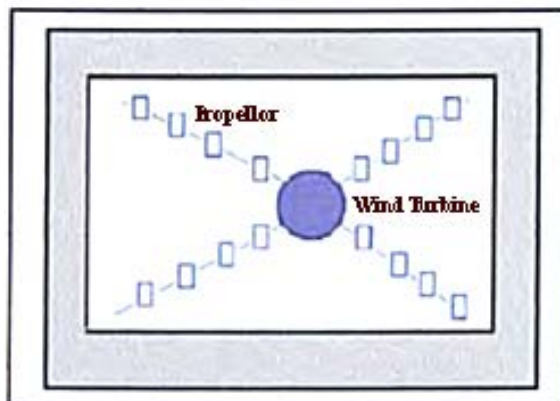
0.5	12.35	5.1	1.293	0.646	0.253	162.497	0.00
0.25	13.25	5.4	1.387	0.347	0.257	192.893	0.00
0.89	32.3	4.1	3.381	3.009	0.825	84.428	0.04
1.23	33.1	5.4	3.464	4.261	0.642	192.893	0.02
2.1	32.5	6.3	3.402	7.144	0.540	306.308	0.02
1.5	12.35	5.7	1.293	1.939	0.227	226.861	0.01
0.59	18.96	6.7	1.984	1.171	0.296	368.435	0.00
0.98	12.56	6.5	1.315	1.288	0.202	336.416	0.00
0.23	23.56	5.4	2.466	0.567	0.457	192.893	0.00
0.98	34.2	8.5	3.580	3.508	0.421	752.303	0.00
2.1	43.5	5.12	4.553	9.561	0.889	164.417	0.06
2.4	49.5	5.7	5.181	12.434	0.909	226.861	0.05
1.56	50.2	6.8	5.254	8.197	0.773	385.179	0.02
1.45	44.6	8.2	4.668	6.769	0.569	675.426	0.01
2.4	49.5	6	5.181	12.434	0.864	264.600	0.05
2.1	44.56	5.3	4.664	9.794	0.880	182.374	0.05
2.9	42.8	6.3	4.480	12.991	0.711	306.308	0.04
2.5	12.35	5.3	1.293	3.232	0.244	182.374	0.02
2.4	19.56	5.2	2.047	4.913	0.394	172.245	0.03
1.45	20.23	5.7	2.117	3.070	0.371	226.861	0.01
2.8	49.5	6.7	5.181	14.507	0.773	368.435	0.04
1.5	45.2	4.5	4.731	7.096	1.051	111.628	0.06
1.3	50.2	8.2	5.254	6.831	0.641	675.426	0.01
2.4	43.4	7	4.543	10.902	0.649	420.175	0.03
2.5	12.25	5.2	1.282	3.205	0.247	172.245	0.02
3.5	35.25	6.6	3.690	12.913	0.559	352.183	0.04
2.5	45.6	5.9	4.773	11.932	0.809	251.589	0.05
1.5	45.8	5.1	4.794	7.191	0.940	162.497	0.04
1.89	23.1	5.3	2.418	4.570	0.456	182.374	0.03
2.3	42.3	6.9	4.427	10.183	0.642	402.424	0.03
0	0	0	0.000	0.000	0.000	0.000	0.00
1.01	12	4.5	1.256	1.269	0.279	111.628	0.01
1.21	8	5.1	0.837	1.013	0.164	162.497	0.01
1.45	8.5	4.9	0.890	1.290	0.182	144.120	0.01
1.85	50	7.4	5.233	9.682	0.707	496.399	0.02
1.59	45	6.58	4.710	7.489	0.716	348.991	0.02
2.3	49	6.8	5.129	11.796	0.754	385.179	0.03
1.01	10	4.5	1.100	2.000	0.244	111.628	0.02
1.1	8	7	0.837	0.921	0.120	420.175	0.00

Appendix P

Two alternative schemes for further development for the shrimp farm industry



A: Model of four wind machines for shrimp farm



B: One unit of a wind machine for shrimp farm aeration process